



Lehrstuhl für Gießereikunde

Dissertation

**Investigation on the removal of internal sand cores from
aluminium castings**

Dipl.-Ing. Bernhard Johannes Stauder

Eidesstattliche Erklärung

Ich erkläre an Eides statt, dass ich diese Arbeit selbständig verfasst, andere als die angegebenen Quellen und Hilfsmittel nicht benutzt, und mich auch sonst keiner unerlaubten Hilfsmittel bedient habe.

Ich erkläre, dass ich die Richtlinien des Senats der Montanuniversität Leoben zu "Gute wissenschaftliche Praxis" gelesen, verstanden und befolgt habe.

Weiters erkläre ich, dass die elektronische und gedruckte Version der eingereichten wissenschaftlichen Abschlussarbeit formal und inhaltlich identisch sind.

Datum 24.10.2018

Unterschrift Verfasser

Bernhard Johannes, Stauder

Matrikelnummer: 09335207

Vorwort und Danksagung

Die Idee zur hier vorliegenden Arbeit entstand aus meiner beruflichen Tätigkeit im Bereich Aluminiumguss. Für die Bestärkung zur Durchführung danke ich den Herren Dr. Gosch und Dr. Stika sowie der Unternehmensleitung von Nematik Linz für die kontinuierliche Unterstützung des Projektes. Den Kolleginnen und Kollegen, vertretend nenne ich Herrn Rafetzeder, danke ich für die Mithilfe vor allem bei der Planung und Durchführung von Versuchen sowie Dr. Prass für die Durchsicht der abschließenden Dokumentation.

Mit den Projektpartnern in Leoben gab es einen sehr bereichernden Austausch. Meinem Betreuer, Prof. Schumacher danke ich für die vielen Stunden, die wir intensiv diskutierend verbracht haben. Ebenso danke ich Herrn Prof. Harmuth und seinem Team für die methodischen und versuchstechnischen Ansätze, durch die es gelang, den Erfahrungshorizont der Gießereitechnik wesentlich zu erweitern. Zudem danke ich dem Team des ÖGI, unter der Leitung von Herrn Schindelbacher, insbesondere Herrn Kerber für die stets offene Tür und die hervorragende prüftechnische Umsetzung neuer Ideen im Sandprüflabor.

Zahlreiche Themen wurden in Form von Praktika, Projektarbeiten und Diplomarbeiten durch Studierende bearbeitet. Ihr Interesse und Engagement für die sand- und kernbezogenen Themen war sehr wichtig für die erzielten Ergebnisse. Zahlreiche Untersuchungen und Methoden mussten erst entwickelt werden, was herausfordernd war. Mir hat die Zusammenarbeit Spaß gemacht und ich hoffe, dass die gesammelten Erfahrungen für alle von bleibendem Wert sind.

Der allergrößte Dank ergeht an meine liebe Familie, die mich in diesem Projekt über die vielen Jahre stets unterstützt hat. Vor allem bin ich dir, liebe Michaela dankbar, dass du so für unser gemeinsames Wohl gesorgt hast. So ist es gelungen, dass diese Arbeit ihren Fortschritt fand, wir aber auch auf eine gute Beziehung und viele tolle gemeinsame Erlebnisse mit unseren Kindern blicken können. Johanna und Helena, ihr habt viel gehört, was ist, „... wenn die *Diss* einmal geschafft ist.“ Danke für eure Geduld, ich bin wieder voll da!

Diese Arbeit widme ich meiner Mutter als Dank für den mir ermöglichten Bildungsweg.

Kurzfassung

Beim Gießen von Metallen in Formen werden die formgebenden Elemente durch einen ständigen Wärmeaustausch thermisch, sowie durch Strömung, Auftrieb und Bauteilwindung mechanisch beansprucht. Die Eigenschaften der Kerne, die aus gebundenem Granulat (meist Sand) bestehen, sind von den physikalischen Eigenschaften der Komponenten, der erzielten Verdichtung und der einwirkenden Belastung abhängig, wodurch sie eine ständige Veränderung während des Gießprozesses erfahren.

In der vorliegenden Arbeit wurden die Eigenschaften umgossener Kerne am Ende des Gießprozesses hinsichtlich deren Zerfallsverhalten untersucht. Es wurde besonders auf den Einfluss der granularen gebundenen Struktur der Kerne mit einem hohen freien Volumen geachtet.

Anhand gießereüblicher Dreipunkt-Biegeversuche wurden Verbesserungspotenziale für die Ermittlung mechanischer Eigenschaften von Kernen untersucht. Durch die Erfassung von Lastkurven wurden zusätzliche Parameter definiert, die Rückschlüsse auf strukturelle Veränderungen der Kerne zulassen. Der Einfluss einer thermischen Beanspruchung auf die Eigenschaften von Kernen wurde mittels unterschiedlicher Prüfverfahren nach Vorbehandlung von Proben an Luft und sauerstoffreduzierter Atmosphäre unter Anwendung realitätsnaher Temperaturprofile analysiert. Daraus konnten Parameter für ein Mohr-Coulomb-Versagensmodell, abhängig von der thermischen Vorbelastung, definiert werden. Die Keilspaltprüfmethode zur Bestimmung der spezifischen Bruchenergie ist hier erstmals an Sandkernproben angewandt worden. Die Ergebnisse haben eine indirekte Proportionalität der spezifischen Bruchenergie mit der erzielten Sandkernzerfallsrate bei sonst gleichen Randbedingungen gezeigt. Das Zerfallsratenkriterium wurde über eine Kombination aus der Entkernungs-Massenrate und dem erhaltenen Zerkleinerungsgrad des Entkerngutes definiert. Der Einfluss der Schwindung von Aluminiumguss auf die mechanische Schädigung wurde anhand von Kernen mit geringer thermischer Ausdehnung, hohen Festigkeiten nach thermischer Beanspruchung und hoher Sprödhheit nachgewiesen. Für die Untersuchung der Entkernbarkeit ist bei Verwendung unterschiedlicher Komponenten für die Kerne daher, neben den Festigkeitseigenschaften, auch deren Wechselwirkung mit dem Gussbauteil zu betrachten.

Die hier vorgestellten temperaturabhängigen Festigkeits- und Versagensparameter stellen in Kombination mit der thermisch-mechanischen Wechselwirkung zwischen einem Gussteil und umgossenen Kernen eine umfassende Informationsbasis für die Vorhersage der Entkernungseigenschaften dar.

Abstract

Casting of metals comprises filling, solidification and cooling of metal melt and causes an intensive heat exchange with the moulding parts. Mechanical loads are introduced by flow, buoyancy and casting shrinkage. Foundry cores, applied to shape internal or undercut contours, consist of a bonded granulate and are characterised by a high free volume. Their physical properties are majorly controlled by the type of granular material and binder, the realised degree of compaction and the thermal exposure, imposing a continuous property change during the casting process.

In this thesis, focus was put on the description of cast-in core properties at the end of the casting process, based on thermal conditions of cast aluminium car engine cylinder heads. The predictability of core degradation and the description of their removal behaviour from the castings was investigated based on their thermal history, with particular attention paid on the granular nature of sand cores.

Enhancements of foundry-typical mechanical property testing were presented via an improved evaluation of three-point bending tests, resulting in additional parameters allowing to evaluate structural changes of samples. The thermal impact on the mechanical properties was evaluated by standard testing methods over a set of temperature profiles in air and oxygen-reduced environment and summarised via proposed temperature dependent Mohr-Coulomb parameters for several sand core types. Evaluation of the specific fracture energy by wedge splitting tests was applied for the first time on sand core samples. The results exhibited an inverse proportionality of the specific fracture energy with the de-agglomeration rate criterion. This criterion was evaluated from the in-line acquired removed minimum core mass rate during a core removal test and the achieved de-agglomeration degree of the removed core sand. The effect of cast aluminium shrinkage on mechanical damage of cores was demonstrated with core samples of low thermal expansion, high brittleness and a low mechanical property decrease over the temperature. For the prediction of mechanical core removal of different bonded granular material types, the interdependency of cast-in cores with the casting must be considered.

The herein documented effects, mechanical properties and failure criterion parameters depending on the thermal history constitute an important information to predict mechanical core collapse.

Table of contents

1	Introduction	- 1 -
1.1	Casting process chain.....	- 1 -
1.2	Sand core removal from castings.....	- 3 -
1.3	Aim of the thesis.....	- 5 -
2	Theoretical background.....	- 6 -
2.1	Structure of sand cores.....	- 7 -
2.1.1	3D-arrangement of granular materials.....	- 8 -
2.2	Granular materials for foundry core application.....	- 10 -
2.2.1	Morphology of granular materials.....	- 12 -
2.3	Physical sand core properties.....	- 16 -
2.3.1	Thermal diffusivity.....	- 17 -
2.3.2	Thermal conductivity	- 18 -
2.3.3	Bulk density.....	- 19 -
2.3.4	Heat capacity	- 20 -
2.3.5	Thermal expansion	- 20 -
2.4	Binder systems for foundry sand cores.....	- 24 -
2.4.1	Organic sand core binders	- 25 -
2.4.2	Inorganic binders.....	- 31 -
2.4.3	Silicate-based inorganic binders.....	- 31 -
2.5	Evaluation of sand core disintegration.....	- 35 -
2.5.1	Thermo-physical investigations on sand and binder stability	- 36 -
2.5.2	Retained strength of sand core samples.....	- 37 -
2.5.3	Abrasion testing.....	- 38 -
2.5.4	Hot distortion testing	- 38 -
2.5.5	Collapsibility test under load.....	- 39 -
2.5.6	Sand core testing with melt contact.....	- 40 -

2.5.7	Core removal testing of cast-in sand cores.....	- 41 -
2.6	Material failure criteria	- 43 -
2.6.1	Comminution technologies.....	- 43 -
2.6.2	Failure criterion models.....	- 45 -
2.6.3	Wedge splitting testing of refractory and building materials	- 47 -
2.6.4	Impact testing of cemented agglomerates	- 48 -
3	Experimental methods overview	- 51 -
3.1	Core sample production	- 51 -
3.1.1	Sand and binder types for test cores	- 51 -
3.1.2	Core samples used for mechanical property testing	- 52 -
3.2	Thermal pre-conditioning of core samples	- 54 -
3.3	Mechanical property testing.....	- 56 -
3.4	Wedge splitting tests.....	- 56 -
3.5	Core removal trials.....	- 58 -
3.5.1	Ring mould for knock-out testing.....	- 58 -
3.5.2	Core removal wedge sample	- 58 -
3.5.3	Equipment for core removal testing	- 60 -
4	Results.....	- 63 -
4.1	Foundry core property assessment by 3-point bending test.....	- 64 -
4.2	Mohr-Coulomb failure criterion from unidirectional mechanical testing of sand cores after thermal exposure.....	- 74 -
4.3	De-agglomeration rate of silicate bonded sand cores during core removal	- 99 -
4.4	Specific fracture energy and de-agglomeration rate of silicate-bonded foundry sand cores	- 107 -
4.5	Core removal behaviour of silicate bonded foundry sand cores	- 118 -
5	Summary and discussion.....	- 125 -
5.1	Mechanical properties of sand cores.....	- 125 -
5.2	Fracture and de-agglomeration of foundry sand cores.....	- 131 -

5.3 Casting and core interaction..... - 134 -

6 Conclusions.....- 136 -

7 Outlook- 137 -

8 References.....- 138 -

9 Appendices- 148 -

9.1 Abbreviations..... - 148 -

9.2 List of Figures..... - 150 -

9.3 List of tables..... - 157 -

1 Introduction

1.1 Casting process chain

Casting processes are widely applied to produce complexly shaped metal parts in high quantities. Engine blocks and cylinder heads are examples of such complicated, high-volume production castings. Typical aluminium castings for the automotive industry, according to Campbell, are produced with ‘Gravity Die’, ‘Pressure Die’ and ‘High precision sand casting’ processes [1], which were historically and technically overviewed in generic literature [2], [3]. For almost all these casting processes, except the high pressurized types, hollow structures are realized by sand cores. The usual process chain to produce cast aluminium cylinder heads with semi-permanent moulding processes is illustrated in Figure 1-1.

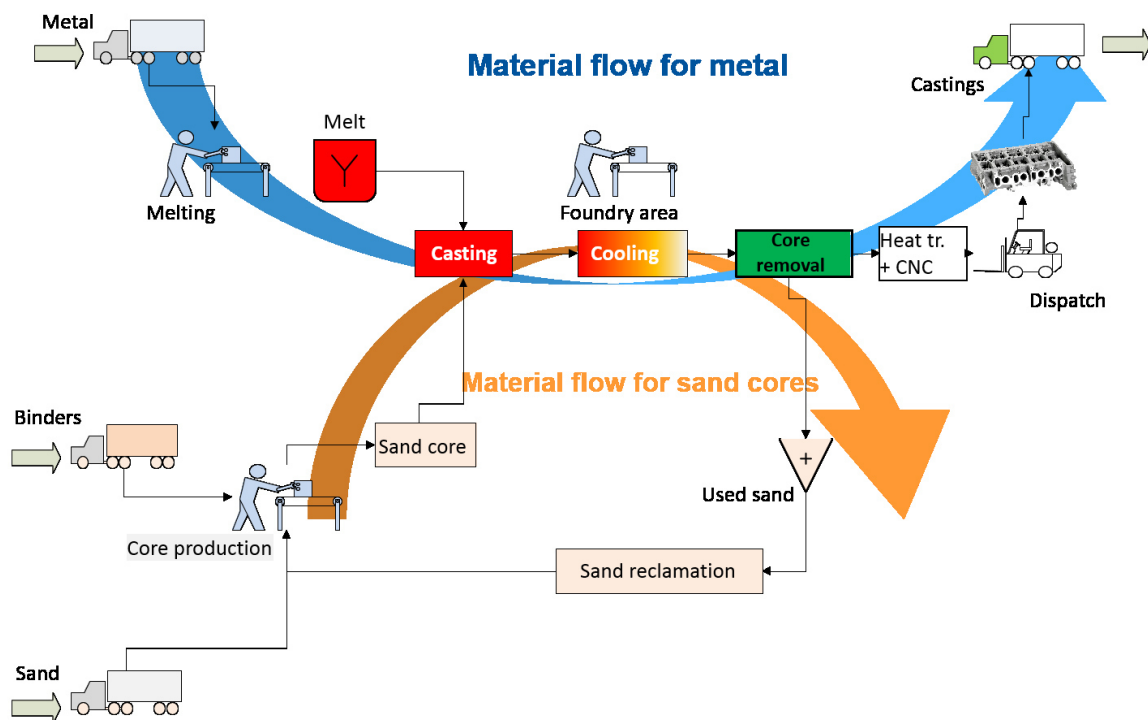


Figure 1-1: Material flow of metal and sand core at the production process chain of cast-Al cylinder heads.

During the casting process, foundry sand cores must remain dimensionally stable and may not contribute to casting defects and the shaped cast surface should be smooth and free from sand adherences. General requirements on sand cores are the following [4], [5]:

- High bonding strength to enable low binder contents for economic and ecological benefits.
- Capability to support itself and not distort after production, provide sufficient handling strength (cold strength) and resist the liquid metal pressure (hot strength).
- Low gas evolution during casting or improve the dynamic of gas evolution.

- Low hazardous product content in the used binder systems.
- Sufficient decomposition behaviour to achieve acceptable core removal and cleaning effort.
- Low sand core resistance to casting shrinkage to avoid casting cracks and to achieve an easy core removal from the solidified casting.
- Compatibility of the used core binder materials and their reaction products among each other during the reclamation process.

A crucial, but rarely investigated process step is the sand core removal at the end of the casting process chain. Cast-in cores need to be destroyed for their removal from solidified casting, which explains the terminus ‘lost cores’. In Figure 1-2 a typical sand core package for a cast aluminium cylinder head and a casting during mechanical core removal by hammering is illustrated.



Figure 1-2 (a): Example of a sand core package to shape complex internal cavities of a car engine cylinder head prepared to be placed in a steel mould. (b): Cylinder head with cast-in sand cores during hammering for core removal (Nemak, 2005).

Czerwinski et al. (2015) overviewed the currently applied high volume production processes for foundry cores [6]. They pointed out the importance of current inorganic binder developments, with an increasing volume production share, replacing established organic Coldbox- Hotbox and Warmbox systems. The different new inorganic binders are all hardened by drying using heated core boxes. The internal chemical bonding will be described in more detail in the theoretical background section 2.4. Industrial application of inorganic binders for sand cores was widely researched [7]–[11] and consequently, several high volume automotive engine production projects applying inorganic binders were ramped up in the past decade [12]–[15].

Worth mentioning is the core sand reclaiming process to achieve a closed loop for the sand usage to meet important ecological and economical goals. Intensive research on re-using sand bonded with various core binder types is ongoing [16]–[19].

1.2 Sand core removal from castings

The goal of the core removal step (see Figure 1-1) is to separate all sand from cast metal parts prior to machining and functional application. In the literature core removal is often denominated as ‘core knock-out’ or ‘de-coring’, (see ASM Handbook ‘Casting’), [20]. The process itself is defined by removing internal inorganic or organic bonded sand cores from castings. In Al-castings, due to the lower achieved thermal loads, usually more effort has to be put into the removal of sand cores from the castings. For resin bonded sands, the introduced heat during the casting process is sufficient to breakdown only the core layer closest to the metal. Core knock-out behaviour, according to Dietert (1950), is generally controlled by following influences [21, N. 16]:

- Design of casting (number and size of openings);
- Selection of core sand and binder;
- Baking (not fully hardened cores are more difficult to remove);
- Thermal exposure (more heat introduced is better for core destruction);
- Selection of favourable knock-out equipment.

Dietert highlighted main equipment types for the core removal or knock-out, which are still relevant for an up-to-date casting production. Manually or automated hammers and chisels, vibration units, wet de-coring including the wet sand recycling units, and sand blast cleaning units were described. However, advances in the mechanical engineering have led to modernisation of equipment. The most common core removal method is mechanical vibration of castings, introduced by pressurized air driven hammering tools, like chisels or bolts [20]. Examples for modern mechanical core removal equipment are shown in Figure 1-3.

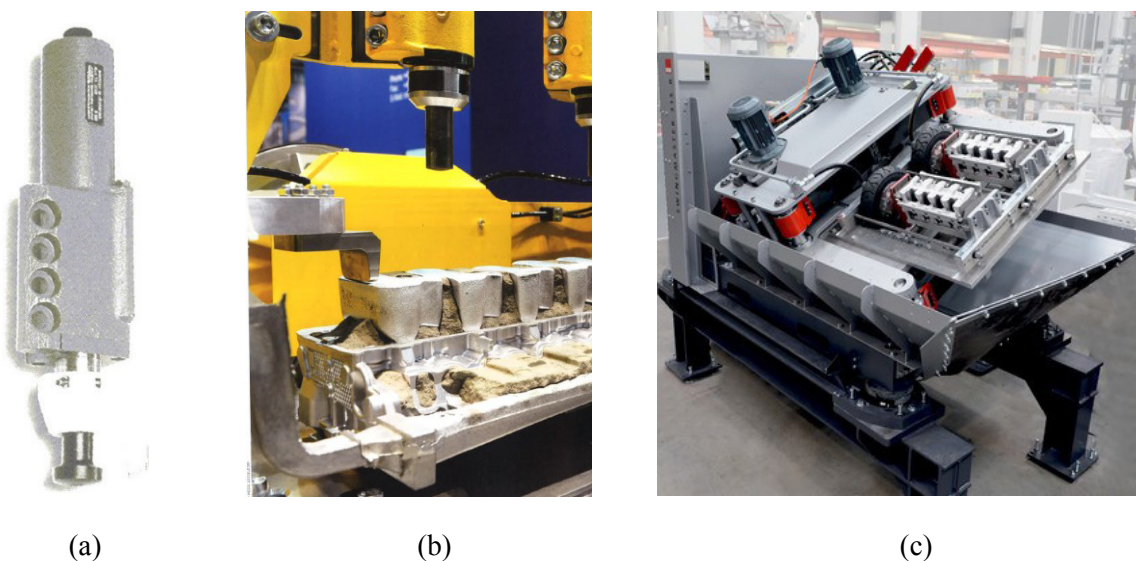


Figure 1-3: Examples of state-of-the-art mechanical core removal equipment applied for cast-Al parts. (a): Pneumatic hammer [20]; (b): Hammering station with a clamped casting containing sand cores, as exhibited on the ‘GIFA’ 2015 fair [22]; (c): Vibration shake-out unit with clamped cylinder heads [23].

High frequency vibration units, introduce accelerations between 50 and 315 m/s² at amplitudes of 5 – 10 mm with up to 60 Hz frequency. Current industrial core removal equipment for complex aluminium castings focus on avoiding high loads [24]. An initial hammering step to create fractures in the sand cores is required before applying dynamically and kinematically driven core removal methods.

Alternative methods can be shock wave application, which are applied to achieve highest cleanliness demands [25]. Moreover, an easier use of higher strength cores for fine cast channels of complex parts was enabled by shockwave core removal technology [26]. Furthermore, Zaretskiy [27] referred to Grassi [28], who patented a core removal method by ablation, applying a phosphate-modified sodium-silicate binder, which allows rapid binder dissolution and at the same time an accelerated solidification of the casting. For cast aluminium pistons mostly salt cores are applied to shape fine cast-in ring cooling channels, which subsequently are removed by water jet [29], [30]. Water soluble cores can be applied in HPDC applications with cast-Al [31, Sec. 15.1.2], but for larger and complex geometries, lost core solutions applicable in high pressure die casting processes are still under research.

Le Serve (1971) classified ‘breakdown’-properties based upon process observation of cast-in cores with usual binder systems from ‘poor’ to ‘excellent’ [32]:

- Poor breakdown was assigned to silicate bonded sand cores (CO₂- and ester hardened);
- Very good breakdown was assigned to cold set resins, oil bonded cores and shell cores;
- Excellent breakdown was uniquely assigned to organic Hotbox-bonded systems.

In contrast to the described properties of silicate-bonded cores an excellent breakdown of silicate-bonded mullite granulate cores was documented as a patented process [33]. Remarkably, such cast-in cores de-composed without external mechanical loading already during the cooling phase of the casting. From the existing knowledge about foundry core properties, this behaviour was not predictable. A picture series during the cooling phase of a casting illustrates this effect (Figure 1-4).



Figure 1-4: Picture sequence taken in 10 minute-steps starting after casting extraction from the mould (Picture 1) showing increasing, shell-wise core destruction with increasing time (Pictures 2-4) and the resulting channel after approximately 50 minutes from de-moulding¹.

¹ Bernhard Stauder, non-published documentation, VAW Mandl & Berger GmbH, 2002.

1.3 Aim of the thesis

The properties of cast-in cores at the end of the casting process, after cooling to ambient temperature were subject of this research. The goal was to improve the predictability of a mechanical core removal process.

From the described self-decomposition behaviour of silicate-bonded, mullite-based cores during cooling of the casting in the previous section (compare Figure 1-4), a lack of information to describe this effect was identified. Major assumptions about the guiding mechanism were made. Thermal-mechanical stresses between cores and the casting and the embrittlement of silicate-based binder were the most important assumptions to provide for sufficient core failure. Therefore, mechanical properties relevant for the physical situation of cast-in cores prior to mechanical core removal were investigated. Following key research topics were pursued:

- Generally identify, evaluate and develop foundry sand core testing methods to describe mechanical core properties at the end of the casting process.
- Quantitative description of core properties after various thermal loads derived from real casting situation to evaluate the sensitivity on thermal loading intensity. Failure criteria for foundry cores after the casting and cooling process should be defined.
- Identify and verify methods to quantify the specific work of fracture for foundry cores.
- Identify, evaluate or develop methods for a quantitative evaluation of core removal processes.

The core properties and core removal behaviour should be evaluated based upon various granulate and binder types. The baseline for the investigation was defined via standard sand cores from silica (quartz) sand with a silicate-solution without additives as standard binder. For comparison with industrially established conditions, evaluations were also made for several state-of-the-art organic binder systems, whose combustible nature was described more deeply in the theoretical section of this work.

The here elaborated research results should fully describe the mechanical constitution of sand cores at the end of a casting process and hence be applicable for future modelling of core removal processes.

2 Theoretical background

From a mechanical point of view sand cores used for metal casting processes must withstand all manipulation and process loads during the casting process to shape the desired geometry correctly. After the cast metal part is solidified, the cores should provide easy removal from the casting.

The used materials and their temperature dependent properties are the relevant factors influencing sand core disintegration. The applied casting process parameters and methods, mainly melt, casting method and type of cooling and core removal process define the introduced thermal and mechanical loads. In Figure 2-1 a more detailed overview on influencing factors defining sand core strength, based on casting practice and theoretical considerations is given [5].

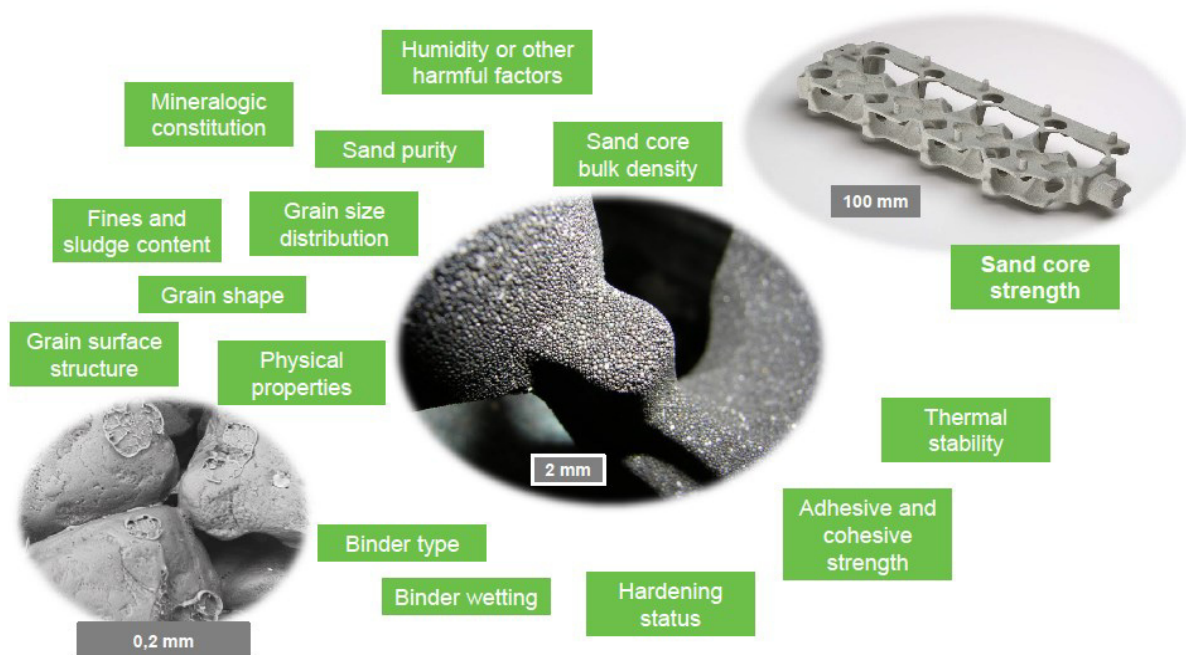


Figure 2-1: Factors influencing the achievable sand core strength in general, after Flemming & Tilch (1993), [5]. The inserts are showing inorganically bonded car-engine cylinder head sand cores² at different magnifications, illustrating the granular nature of the solid core.

The cast part geometry constitutes an important boundary condition, defining the core size and complexity and thus the local core surface modulus. For future modelling purposes additionally to adequate mechanical and physical properties also failure criterion functions are required.

² Printed with permission of Nemak.

2.1 Structure of sand cores

Foundry sand cores are built up by a bonded granular material of a defined quality, which is demonstrated in the magnified images in Figure 2-2.

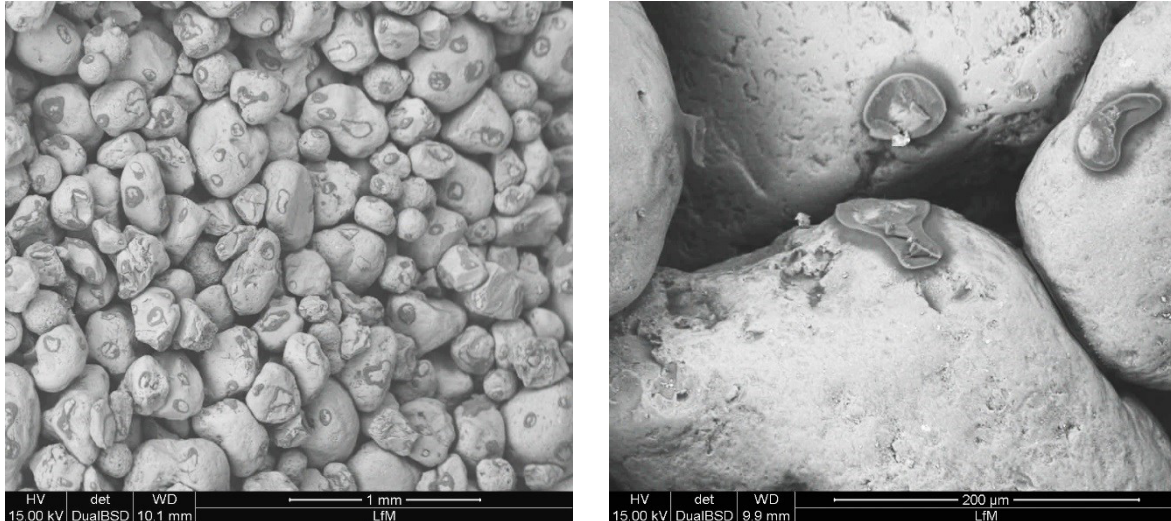


Figure 2-2: Sand core fracture surface illustrating the grains and the bonding binder patches. Silica sand and a urea-furanic based, Warmbox bonded resin were used. The sample was taken from a cast-in sand core [34].

Silica sand grains of a wide grain size range are randomly arranged. The sand appears rounded, with various grain sizes and a micro-structured surface. The void-ratio, porosity or free volume, of this example was evaluated by 45 %. A binder content of 1,4 % was used. An overview on relevant characteristics for granular forming base materials is shown in Table 2-1.

Table 2-1: Properties to evaluate technological applicability of basic forming materials [5].

Property group	Characteristic
Chemical and mineralogical constitution	<ul style="list-style-type: none"> • Chemical composition (e.g. SiO₂-content, basic components, other components). • Structure of grains. • Chemical activity of grain body and surface.
Granular and morphology parameters	<ul style="list-style-type: none"> • Grain size distribution, average grain size, fines content. • Activity of grain surface of representative grains.
Physical-technological properties	<ul style="list-style-type: none"> • Hardness of representative grains. • Density of representative grains. • Sintering properties of the sand. • Crushing resistance of grains (at mechanical and thermal load). • Thermal properties (e.g. thermal expansion, thermal conductivity).

The mineralogical constitution fundamentally defines the physical properties. The grain size distribution, grain shape, and surface morphology are major granular properties and define the specific surface. Sintering resistance, which is strongly influenced by the chemical purity and the crushing resistance accomplish the relevant property portfolio for granular materials applied in the foundry industry.

Sand cores for high volume production application are nearly completely produced by core blowing process. The compaction is achieved by fluidisation of the sand mixture by air followed by removal of air through vents and settling of the sand particles in the core box. First experiments for blowing cores can be traced back to 1903 [4, Ch. 6]. Aslanowicz et al. [35] reviewed core manufacturing, quality assurance and production technologies, where actual machine technology solutions are described. During own developments on the field of inorganic binders, relevant process and machine functions for successful binder application development important functionalities for a satisfying core blowing machine were developed and patented [36].

Simulation of the core blowing process is implemented in the casting industry to optimize sand core quality [37], [38]. The method is based on multi-phase flow and granular material physics [39]–[41]. It delivers information on the compaction and the local free volume, as shown in Figure 2-3.

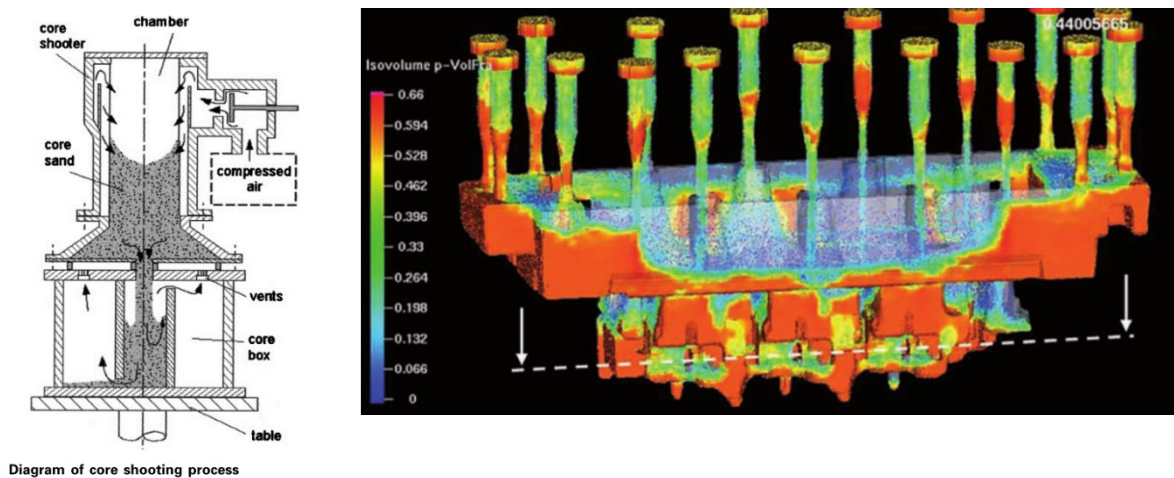


Figure 2-3 left: Cross section through a core blowing machine [40]. Right: Core blowing simulation result showing the sand volume fraction during the sand transport through the blowing nozzles on top into the core box cavity [37].

2.1.1 3D-arrangement of granular materials

In summary, strength of sand cores is influenced by the number and strength of inter-particle bonds, hence, by the grain size distribution and the compaction-degree. The average coordination number of a granular network, the adhesive and cohesive strength and thermal stability of the binder define the achieved core strength.

A typical descriptive criterion for compacted granular materials is the coordination number ‘CN’ [42], expressing the number of contact points from every particle to neighbouring particles. In bonded granular materials this allows to estimate the number of bonds per volume, when the grain-size distribution and compaction degree of a sand core are known. Another characteristic is the free volume, which is usually evaluated by the ratio of bulk to specific density, which in randomly packed granulates is not fully linked to fixed CN-values, but values decreasing with increasing intergranular friction. In Table 2-2 some basic relationships based upon regular stacking patterns of monodisperse spheres are overviewed.

Table 2-2: Coordination number for various regular packings of monodisperse spheres.

Systematic arrangement	CN	Solid volume fraction	Free volume / %
Randomly close packing [42, Ref. 10]	4,5 – 6	-	39 - 45
Simple cubic	6	$\pi/6$	47,6
BCC (orthorhombic)	8	$\pi/(3\sqrt{3})$	39,5
FCC or hexagonal	12	$\pi/(3\sqrt{2})$	26

The role of fines in the voids between regularly arranged grains has an effect on technological behaviour of foundry cores with respect to surface quality, strength and permeability [5]. Exceeded fine particle contents should be avoided and an equilibrated grain size distribution is fundamental to achieve sufficient strength. A limited maximum void size to avoid metal penetration and still maintain a satisfying core gas permeability are desired. Statistical variation of sieve analysis and the grain shape have an effect on sand core quality and sand core related casting defects [43].

DEM-simulations of granular materials of a particular size distribution allow to completely evaluate coordination numbers within particle arrangements. Brown (2014) modelled a granulate body based on spherical particles with a uniform size distribution from 1,15 mm to 2,71 mm particle radius [44]. The investigated geometry and the resulting CN per particle are shown in Figure 2-4.

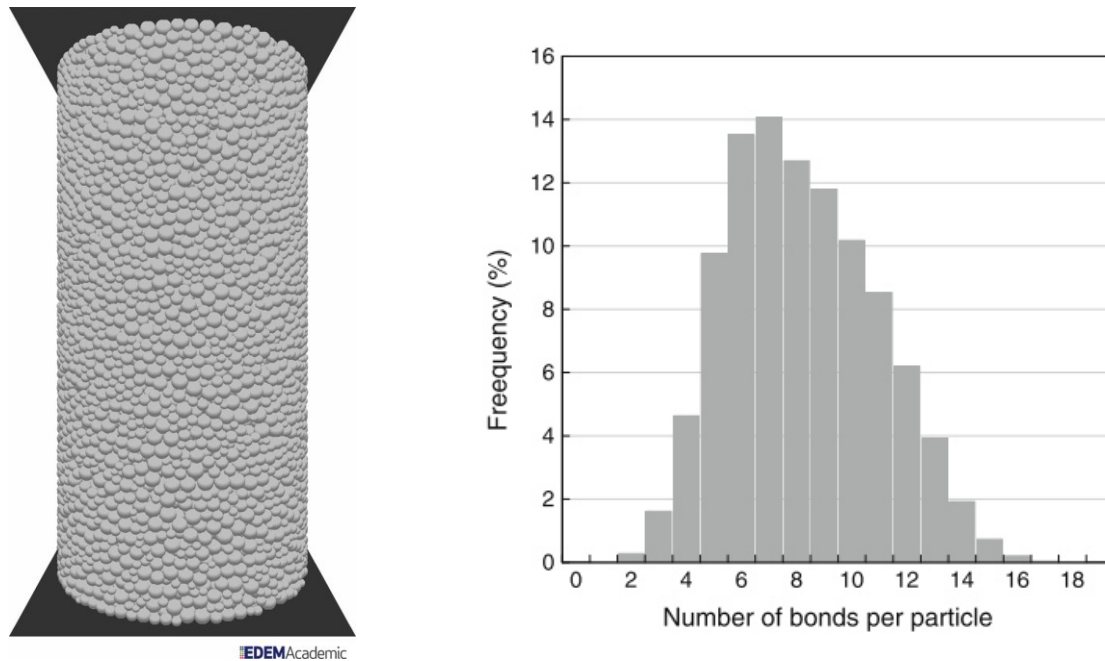


Figure 2-4: DEM-simulated cylindrical body built from a granulate with uniform spherical particle size distribution ranging from 1,15 to 2,71 mm particle radius and the evaluated coordination number distribution according to [44]. Mean coordination number is 8,2.

The CN is distributed in a range from 2-16 contacts per particle. Scaled down by a factor of ten, the size distribution is comparable to that of the granulate ‘MIN-Sand® AFS 50’ [45], which is casually applied for foundry cores. The free volume of the simulated model was 37 %, which is below that of foundry cores, where 40 % - 50 % of free volume must be expected. In summary for sand cores a mean CN ranging from six to eight is most probable.

2.2 Granular materials for foundry core application

Silica sand is the most widely applied sand type for automotive castings, with the advantages of common occurrence and abundance, ease of bonding with organic or inorganic binders, low cost, and the ability to be reclaimed for reuse by wet, dry, or thermal methods. Core practice of most foundries is directed by the properties of the local sands, which have to be used for economic reasons, determined by transport costs [4, Ch. 6]. In that context various available Mexican silica sands were benchmarked for various quality characteristics [46].

The major disadvantage of silica sand at the production of metal castings is its characteristic high thermal expansion, which can cause casting quality problems and other expansion-related defects [47]. Other minerals than silica are applied, whenever it is required by their specific thermo-physical properties or chemical inertness, e.g. for higher-melting cast metals or improved quality demands. Alternatively, the application of core coatings and washes can provide a solution [48]. In casting practice minerals like olivine ($2 [\text{Mg,Fe}]\text{O}\cdot\text{SiO}_2$), ‘zircon sand’ (zirconia mullite: $\text{ZrO}_2\text{-SiO}_2\text{-Al}_2\text{O}_3$), chrome-

ore-sand (Cr_2O_3 -FeO-spinel type with impurities) and various alumo-silicates (Al_2O_3 - SiO_2 -system) are applied, as overviewed in generic casting process literature [4], [5], [31], [32], [47], [49, Ch. 12 Sands and green sand], [50, Ch. 12 Sands and sand bonding systems], [51, Ch. 2 Formgrundstoffe], [52]. Examples of relevant sands and their main characteristics are shown in Table 2-3. Their thermal expansion is illustrated in Figure 2-5.

Table 2-3: A comparison of silica and non-silica sand properties [47].

	Silica	Olivine	Chromite	Zircon	Zircon-Aluminum Silicate
Origin	United States	United States (Washington, North Carolina), Norway	Republic of South Africa	United States, Australia	United States (Florida)
Color	White-light brown	Greenish gray	Black	White-brown	Salt and pepper
Hardness	6.0-7.0	6.5-7.0	5.5-7.0	7.0-7.5	6.5-7.0
Dry bulk density, kg/m^3	1,362-1,602	1,602-2,002	2,483-2,643	2,563-2,964	2,483-2,691
Specific gravity	2.2-2.6	3.2-3.6	4.3-4.5	4.4-4.7	3.2-4.0
Grain shape	Angular/rounded	Angular	Angular	Rounded/angular	Rounded
Thermal expansion, cm/cm	0.018	0.0083	0.005	0.003	0.005*
Apparent heat transfer	Average	Low	Very high	High	High
Fusion point	1,427°-1,760°C	1,538°-1,760°C	1,760°-1,982°C	2,038°-2,204°C	1,815°-1,982°C
High-temperature reaction	Acid	Basic	Basic	Acid	Slightly acid
Wettability with molten metal	Easily	Not generally	Resistant	Resistant	Resistant
Chemical reaction	Acid-neutral	Basic	Neutral-basic	Acid-neutral	Neutral
Grain distribution†	2-5 screens	3-4 screens	4-5 screens	2-3 screens	3 screens
AFS grain fineness number ranges	25-180	40-160	50-90	95-160	~80

Source: Kotzin 1989.

* Clay-bonded sand mixture.

† 10% or more retained on U.S. standard sieve sizes.

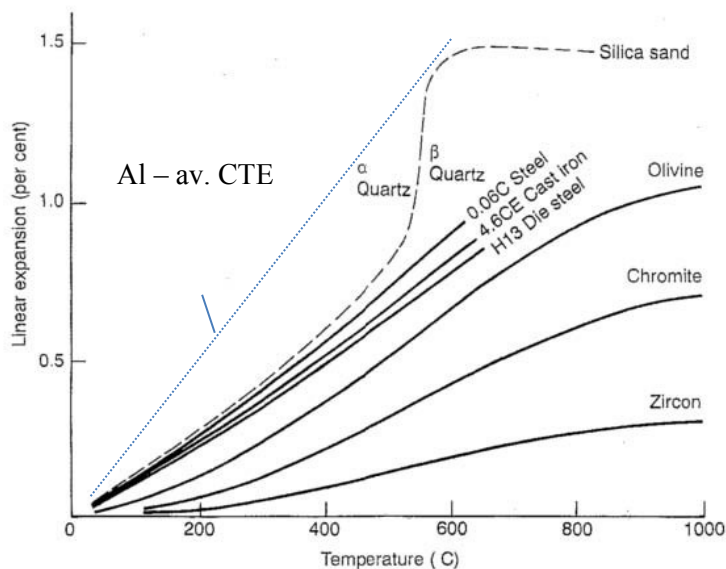


Figure 2-5: Comparison of the free expansion of non-siliceous refractory sands with high silica sand [53, Ch. 8]. In addition, a typical average thermal expansion of cast aluminium alloys of $24 \cdot 10^{-6} K^{-1}$ is indicated 'Al-av. CTE'.

Core strength is influenced by the casting process load. Due to the different thermal expansion of cast-in cores and casting metal, cores are mechanically stressed by casting shrinkage.

2.2.1 Morphology of granular materials

The diminution of quartz is a scale-invariant natural process and as such follows a fractal concept [54], introduced from Mandelbrot (1977)³. Following the fractal theory, a recursive self-similarity of shapes can be qualitatively applied in different dimensions to define grain shape and surface. Here proposed relevant size levels for foundry sand are:

- Scale of 1 mm to 10 μm : Whole grains, characterised by shape and shape factor.
- Scale of 10 μm to 1 μm : Overall grain surface structure, characterised by irregularities like roughness, steps or cleavages.
- Scale of 1 μm to 100 nm: Microstructure of surface in a sub- μm scale, characterised by surface imperfections, corrosion and phases.
- Atomistic scale: crystalline morphology, impurities and surface tension.

The different described size scales and surface structures reveal from various physical processes. Granulates can be obtained as naturally milled materials (e.g. glacial deposits, river and sea sand deposits), crushed and graded minerals, spray compacted melts or sintered slurry deposit particles. Their surface structure is influenced by, weathering, thermal and mechanical wear, corrosion and technical processes like washing, thermal-mechanical reclaiming of used sands and sand transport.

Thus, the effective specific sand grain surface can differ largely compared to calculated values based upon grain size distribution evaluations. As an overview, different methods leading to different resolution levels can be applied for specific surface investigations:

- Sieve analysis covers the level according to the applied mesh size range, typically from some 10 μm to a few mm and therefrom a theoretical specific surface can be calculated. Image analysis can improve the information by shape factor analyses, e.g. as it was presented recently by Dargai et al. (2018), [55].
- Microscopy (Light-optical or SEM) allow surface analyses and qualitative evaluation of surface irregularities and delivers qualitative information.
- Physical testing by highly wetting substances and their absorption (liquids) or adsorption (gases) are appropriate to quantitatively evaluate effective specific surface of granular materials depending on wetting/surface activity.
 - a. Water adsorption method – medium magnification; resolution of additionally the cleavages and main roughness structure
 - b. Gas adsorption method (BET) – high magnification; resolution of additionally the atomic surface structure arrangement

³ B. B. Mandelbrot, *Fractals: Form, Chance and Dimension* (W.H.Freeman & Co Ltd, 1977).

In the following paragraphs grain size, shape and morphology will be discussed in more details.

2.2.1.1 Grain size

The grain size is determined by sieving methods applying standardized mesh setups according to international (ISO), British (BS) or American (AFS) standards. Silt and fines contents are derived by additional boiling and filtering methods and constitute an important part of granulate analyses. Krukowski (2006) documented various examples for sieve analyses of different sand types [47]. Bayat (2015) evaluated several mathematical formulations of particle size distributions and prove the physical evidence of the models [56]. Based on data from Brown (1999) in Table 2-4 an overview on the grain size distribution of UK and German sands is shown [50, Ch. 12 Sands and sand bonding systems]. Brown stated: ‘*Haltern 32, 33 and Frechen 32 are commonly used, high quality German sands. German sieve gradings are based on ISO sieves. The German sands have rounder grains and are distributed on fewer sieves than UK sands, they require significantly less binder to achieve the required core strength.*’

Table 2-4: Typical UK and German foundry sands with sieve analysis [50, Ch. 12].

Sieve size		Sand type				
microns	BSS No.	UK sands		German sands		
		Chelford 50	Chelford 60	H32	H33	F32
1000	16	trace	nil			
700	22	0.7	0.4			
500	30	4.5	2.3	1.0	0.5	1.0
355	44	19.8	10.0	15.0	7.5	7.0
250	60	44.6	25.7	44.0	30.0	30.0
210	72	21.6	23.8	39.0	60.0	60.0
150	100	8.2	28.7			
100	150	2.6	7.6			
75	200	nil	1.3	1.0	2.0	2.0
75	-200	nil	0.2	nil	nil	nil
AFS grain fineness No.		46	59	51	57	57
Average grain size		0.275 mm	0.23	0.27	0.23	0.23

2.2.1.2 Grain shape

The concept of ‘true sphericity’ was first proposed by *Wadell, 1932* and further refined by *Krumbein 1941* and *Corey, 1949* and others until this century, as reviewed from *Bui (2009)*, [57]. Mathematical formulations based upon maximum, average and minimum of projected areas or representative ellipsoid dimensions are available. The author demonstrated, that *Corey’s shape factor* ‘CSF’ was sensitive for both elongated and platelet shaped particles. It is defined by the ratio of projected lengths (L: largest, S: shortest and I: intermediate) by $CSF = S/\sqrt{L \cdot I}$. A very comprehensive overview on grain shape

parameters was documented in the theoretical section of Bui (2009), as well as the fractal concept for numerical grain shape definition was presented, as shown in Figure 2-6.

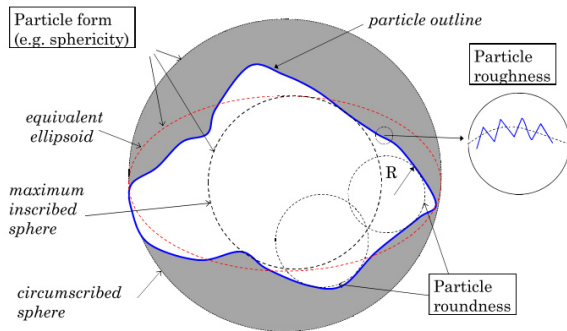
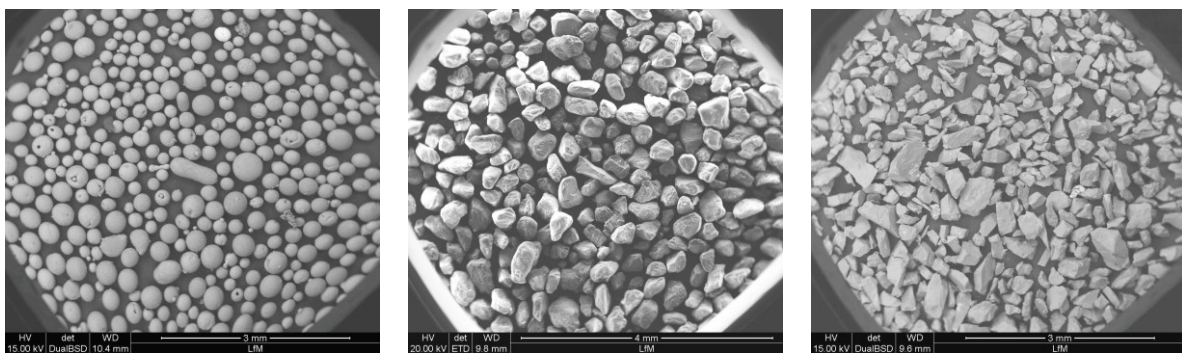


Figure 2-6: Example for applied particle shape terminology modified after Barrett, 1980, acc. to [57]. The particle roughness is schematically shown as magnified property, which demonstrates the potential to apply a fractal description concept.

Diepenbroek (1993) reviewed and investigated the Fourier-analytical description of grain shapes [58]. As a summary, a multi-fractal approach can be appropriate to describe grain shape, as the surface, the surface roughness and corrosion effects are too various to be described with only one fractal dimension. Examples of spherical, sub-angular and very angular forming materials, documented by SEM images [34], are shown in Figure 2-7.



a) spray compacted bauxite “Min-sand”

b) silica sand “H32”

c) Andalusite “Kerphalite”

Figure 2-7: Examples for foundry base forming materials with different roundness [34]. Min-sand is a spherically shaped due to spray compaction process, silica sand H32 is sub-angular rounded, due to its natural source and andalusite is faceted due to the crushing process for sand generation.

A distant similarity to foundry cores could be estimated by tests on crack propagation resistance of concrete samples [59]. The impact of different sand types (round, angular, high and low fines content) by compressive and flexural strength tests was investigated. Higher fracture energy was measured for angular sand, as well as for sand with a wider grain size distribution and with larger grain size, as intergranular fracture along the softer cement matrix occurred.

In foundry practise simplified approaches with limited complexity were introduced, e.g. as shown in Figure 2-8, with classification of sphericity and angularity [50, Ch. 12 Sands and sand bonding systems].

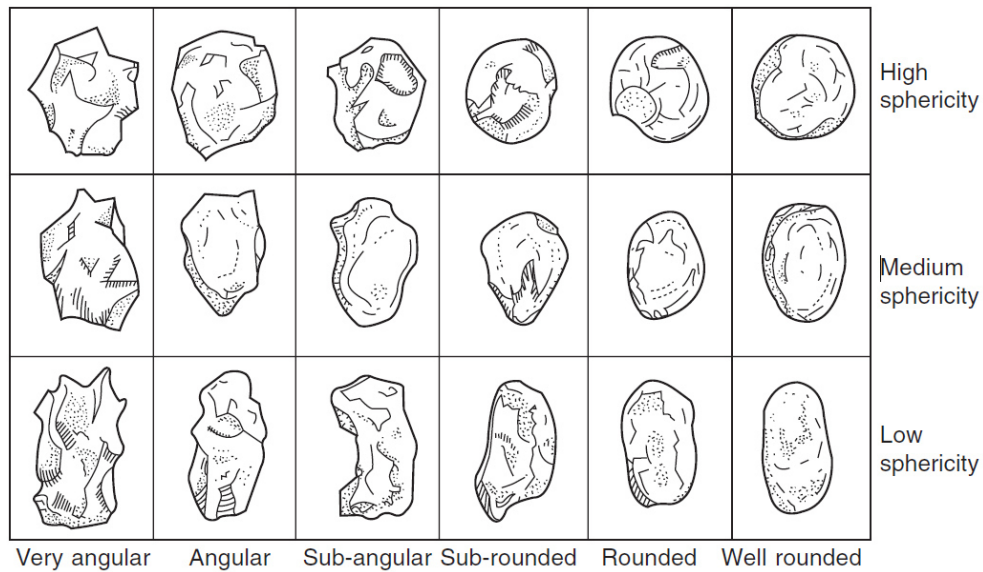


Figure 2-8: Visual grain shape classification by sphericity and angularity of individual grains [50, Ch. 12]. Sphericity is defined by the ratio of maximum to minimum projected diameter and angularity is evaluated by visual examination with low magnification microscopy in comparison to reference charts.

2.2.1.3 Grain surface

The surface structure can be categorized as smooth, rough, highly irregular and fissured. Micro-cracks in grains are potential starting points for grain de-composition, and in consequence sources of fines and dust. Reclaimed sands, due to the exposure to thermal or mechanical operations exhibit higher roundness. Flemming & Tilch (1993) published examples of possible grain surface morphology from SEM observations of silica sands [5], shown in Figure 2-9.

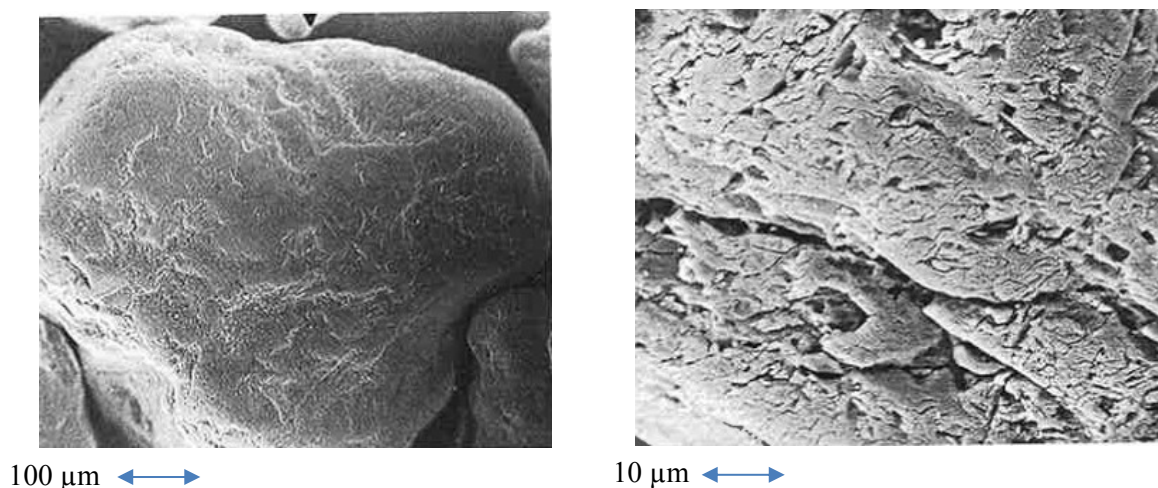


Figure 2-9: Different surface qualities of silica sands [5]. Left: sand grain with smooth surface; Right: rough and fissured sand grain surface in more detail.

The effective specific surface can be evaluated by physical measurements. For substances with very high specific surface, gas adsorption measurements (‘BET’-method) are adequate. With this method the

whole open surface including all micro-defects of the sand grains is evaluated. Beno et al. (2014) applied BET for characterisation of different silica sand types [60]. A specific surface in the range from 0,05 to 1,8 m²g⁻¹, depending on the sand source and different presence of micro-defects was reported. The *Blaine-method* is adequate, when a grain size is minimally 10 µm [61]. This method is based upon the evaluation of a pressure equilibration time of a tested granulate compared to known reference materials. Brinschwitz (2005) applied the *Blaine-method* to investigate the specific surface of various granular materials and reported values between 0,007 and 0,0225 m²g⁻¹, which are below those reported from BET measurements [62]. The difference was explained by the missing interaction of grain fissures and porosity during the Blaine-measurement. To close this gap, the surface condition and defined open porosity and cleavage contents were evaluated separately by water absorption. The ratio of evaluated to the theoretical specific surface from sieve analysis was used to define the angularity coefficient 'EK'. In Table 2-5 the angularity coefficient, the evaluated surface structure and the water absorbability are summarised for various granular materials.

Table 2-5: Angularity coefficient, visually evaluated angularity and surface condition and water absorption of different granulates investigated by Brinschwitz (2005), [62]. The angularity coefficient is defined by the ratio between physically measured and theoretical specific surface calculated from grain size analysis.

Material	angularity coefficient "EK"	observed angularity	surface condition	water absorption in mass-%
Silica H32	1,44	Angular	rough	0,77
Cerabeads	1,36	well rounded	fissured	1,11
Chamotte	2,1	very angular	fissured	1,47
Andalusite ("Kerphalite")	1,64	very angular	smooth with irregularities	0,84
Min-sand	1,63	very angular	smooth with irregularities	0,25
Zircon sand	1,15	sub-rounded	very smooth	0,18
Corundum "KKW"	1,1	well rounded	fissured	0,11

Water absorption increased for grains with more irregular grain shape and surface. Physical limits due to viscosity and surface tension were not discussed. According to the author, an eventually required increase of core binder demand due to such grain surface imperfections was identified.

2.3 Physical sand core properties

The temperature evolution of cast-in sand cores is strongly depending on the casting process type. Gravity and Rotacast® casting processes for cylinder head castings including the sand core application to shape complex cavities, as well as the Core package system (CPS®) for highly complex engine block

production are referred in the application technology handbook for Aluminium [63, Ch. 2.1]. The evolving temperature field in a cylinder head water-jacket core during solidification is exemplarily shown in (Figure 2-10), [64].

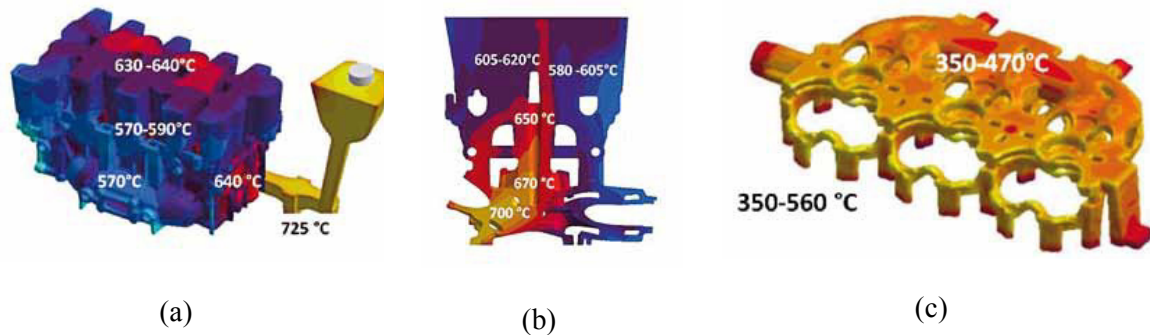


Figure 2-10: Temperature indications for a gravity cast Al-cylinder head at the end of filling. (a): Casting with filling system and feeder. (b): Cross section through the casting centre plane. (c): Water jacket core positioned in the lower casting section at the end of filling [64].

At the end of filling parts of the illustrated water jacket core were significantly heated while also cold spots resulted. A significant impact of local wall thickness and the flow distribution, which are characteristic for the casting design and the applied casting process, influences the thermal exposure of sand cores. Sobczyk evaluated cast-in cores of Al-cylinder heads based upon process simulations [10]. Depending on the core type and dimension, peak temperatures between 400 °C and 550 °C were documented for cast-in cores of cylinder heads.

However, the complex interactions of mechanical stresses between the casting and the core is not yet incorporated in casting simulation practise. Degradation by both the thermal field in the core and mechanical stresses are important contributions to core damage prior to a core removal process.

Degradation of the cores is caused by their thermal and mechanical interaction with the cast metal part. Temperature-dependent physical properties are required for heat transfer evaluations. In the next paragraphs density, thermal expansion, thermal conductivity and specific heat of sand cores will be discussed.

2.3.1 Thermal diffusivity

The spatial heat distribution velocity due to a temperature gradient is described by a fundamental heat transfer property, the thermal diffusivity a , equation (1).

$$a = \frac{\lambda}{\rho \cdot c_p} \quad (1)$$

a is directly proportional to the thermal conductivity λ and indirectly proportional to the volume related heat capacity ($\rho \cdot c_p$). Hence, the local bulk density ρ influences thermal diffusivity, which in

consequence is a result of the achieved core compaction. Please note, that λ for a heterogeneous material like a sand core is the result of different heat transport mechanisms (conduction, convection and radiation), which are as well affected by the local density. More in detail, thermal conductivity could be depending on thermal exposure, owing to structural changes of the binder.

Thermal diffusivity describes the expansion velocity of a heat wave starting from a spot-like source. Results of PU-Coldbox bonded samples from Brinschwitz (2005), applying the laser-flash measurement method are shown in Figure 2-5.

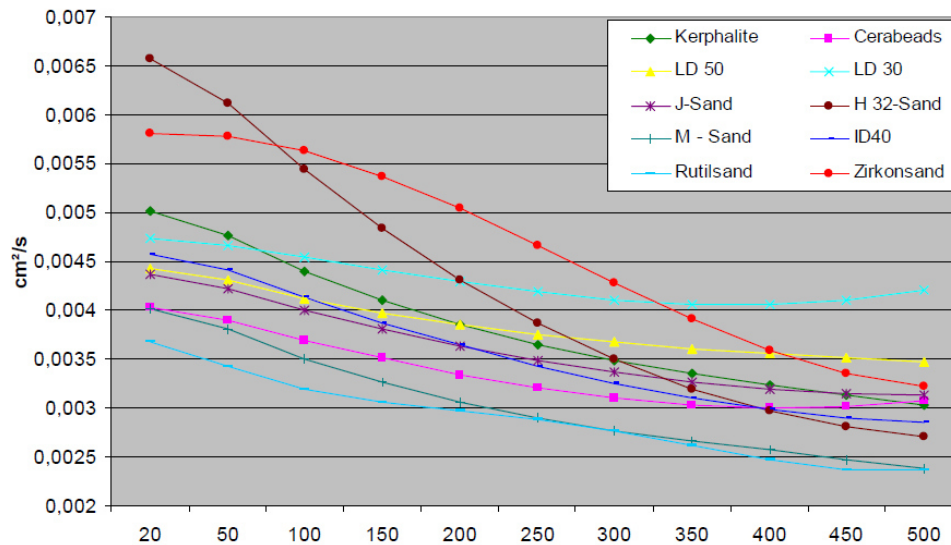


Figure 2-11: Thermal diffusivity of different granulates bonded with PU-Coldbox binder, evaluated from Brinschwitz (2005). Sand denominations are according to Table 2-5. Mineral types of additional abbreviations: J-Sand: quartz-feldspar; LD 30, LD 50 and ID 40 are sintered alumo-silicates; M-sand is molten mullite [62].

2.3.2 Thermal conductivity

Various thermal conductivity investigations of several forming base materials were reported by Recknagel & Dahlmann (2009) for minerals as well as for furan resin bonded samples [65]. From Brinschwitz (2005), applying the stationary heated wire method, the thermal conductivity of various granular materials was evaluated [62], and some results are presented in Figure 2-12.

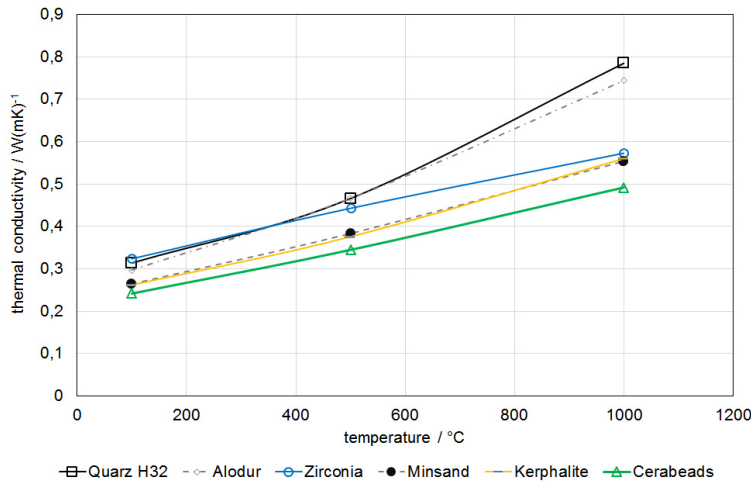


Figure 2-12: Thermal conductivity of several granular materials over temperature, evaluated by the stationary heated wire and tube - method [62].

For quartz a thermal conductivity starting at $0,3 \text{ W(mK)}^{-1}$ at $100 \text{ }^\circ\text{C}$, rising to $0,5 \text{ W(mK)}^{-1}$ at $600 \text{ }^\circ\text{C}$ was determined, which was explained by the increased contact pressure due to the high thermal expansion. Other granular materials showed a linear temperature dependency starting from $0,25 - 0,35 \text{ W(mK)}^{-1}$ at $100 \text{ }^\circ\text{C}$ and values around $0,35 - 0,45 \text{ W(mK)}^{-1}$ at $600 \text{ }^\circ\text{C}$. Granulates with a grain size above $300 \text{ }\mu\text{m}$ exhibited a higher thermal conductivity compared to those with a lower grain size, as with larger grains consequently less intergranular contacts are acting as thermal barriers. Generally it was concluded, that the grain size influenced the thermal conductivity more than the packing density of samples. A potential formation of fines was postulated for the stationary measurement principle, due to the long heating time up to $1000 \text{ }^\circ\text{C}$, which also caused changes in the mineral structure.

The thermal conductivity of foundry sands is below one W(mK)^{-1} , which compared to that of cast metals is very low. Nevertheless the differences between the single granular materials are important and are significantly influencing the heat balance during casting.

2.3.3 Bulk density

Core density values are obtained by relating core weight to the bulk volume. Interestingly, such values can be rarely found in publications. Some indications are given in commercial casting simulation software databases, but with low differentiation by granular properties. Non-compacted bulk density is usually 35 % of specific grain density and hardly more than 65 % of the specific grain density by whatever compaction applied are achievable, according to [51, Ch. 2 Formgrundstoffe]. For silica sand the specific grain density is $2,65 \text{ gcm}^{-3}$, and a typical sand core bulk density of $1,4 \text{ gcm}^{-3}$ can be expected. Increasingly applied core blowing simulations as well as computed tomography can support local density evaluations, which are comparable to results for mould compaction [66].

2.3.4 Heat capacity

The heat capacity c_p is the physically determinable amount of energy required of a substance at isobar conditions for a temperature change of one K. For sand cores, depending on the binder content, more than 95 % of the mass is defined by the granular base material. Nonetheless it is important to consider contributions by irreversible modification changes of granulate or binder and gas transport through the porous network. Irreversible phenomena can change the heat capacity during heating and cooling of a core. For silicate-bonded cores the evaporation of water, or for organic binders of solvents as well as degradation and re-combination of volatile binder constituents, are relevant heat sources and sinks [27]. Condensation zones are known for organic-bonded cores as well as for clay-bonded moulds [67]. For casting process simulation most times only the heating phase of the true heat capacity is relevant [68], (Figure 2-13).

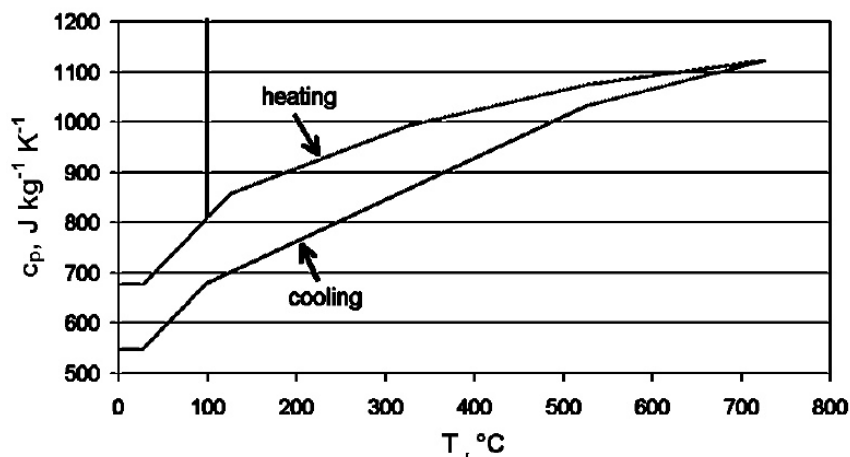


Figure 2-13: Specific true heat capacity over the temperature for a heating and cooling cycle of a clay bonded moulding sand, used for casting simulation [68]. Latent heat of evaporation at the heating cycle and a lower specific heat for the cooling cycle due to occurred irreversible effects are incorporated.

Gases contained in the core porosity are highly relevant for the heat transport. However, it was reported, that such effects often are not detected by physical measurements on small samples, whereas sophisticated simulation tools should consider such phenomena. Neves (2002) pointed out a temperature change of 40 °C in one mm and of 15 °C in 50 mm depth in a core wall, caused by the contributions from additional heat transport by gases and from specific heat changes by irreversible effects [68].

2.3.5 Thermal expansion

Thermal expansion is a source of stresses between bonded grains as well as between the core and the cast metal part. The general expansion behaviour of different material types was already shown previously in Figure 2-5. Dilatation measurement results, averaged from 20 to 300, 600 and 800 °C, published by Recknagel [52], [65], are summarised in Table 2-6.

Table 2-6: Averaged thermal expansion coefficients of forming materials for temperature ranges 20 to 300 / 20 to 600 and 20 to 800 °C [65].

	Specific density at RT in gcm ⁻³	Linear expansion coeff. α in $\mu\text{m}(\text{mK})^{-1}$		
		20-300 °C	20-600 °C	20-800 °C
Quarz (Silica-Quartz)	2,65	14	23	17
J-Sand (Quartz-Feldspar)	2,66	8,1	13,7	11,5
R-Sand (Rutile)	4,23	8,1	8,4	8,3
Bauxite sand	3,31	6,2	7,2	7,4
Chromite	4,52	7,1	7,5	7,5
Kerphalite KF (Andalusite)	3,13	5,3	6,5	7
M-Sand (molten Bauxite)	3,11	4,2	4,5	4,8
Cerabeads (sintered Mullite)	2,86	3,5	4	4,3
Zirkon (Zircon-mullite)	4,64	3,4	4,1	4,5

Silica sand exhibits the highest thermal expansion. It reveals a progressive thermal expansion until the quartz transition temperature at 573 °C, where a modification change takes place. The transformation from ‘low’ to ‘high’ quartz causes expansion in the crystal. It occurs without bond breakage, as the angle between oxygen bonds change. These stresses may fracture the crystal or induce a defect plane along the crystal c-axis [54], referring to *Smalley, 1966*⁴. For cast Al parts the quartz-modification change of lower relevancy, as the maximum sand core temperatures are rarely exceeding 600 °C, but must be considered for thin-walled or other thermally intensively loaded core sections. Above that temperature a slightly decreasing thermal expansion occurs, which is highly relevant for veining defects in iron-based castings [43]. Thermal expansion in relation to casting defects was studied by Solenicki, [69], [70]. The compressive stress formation due to quartz grain expansion is schematically shown for different grain size situations in Figure 2-14, indicating the role of contact points between fine and coarse particles.

⁴ Smalley, I., 1966. Formation of quartz sand. *Nature* 211, 476–479.

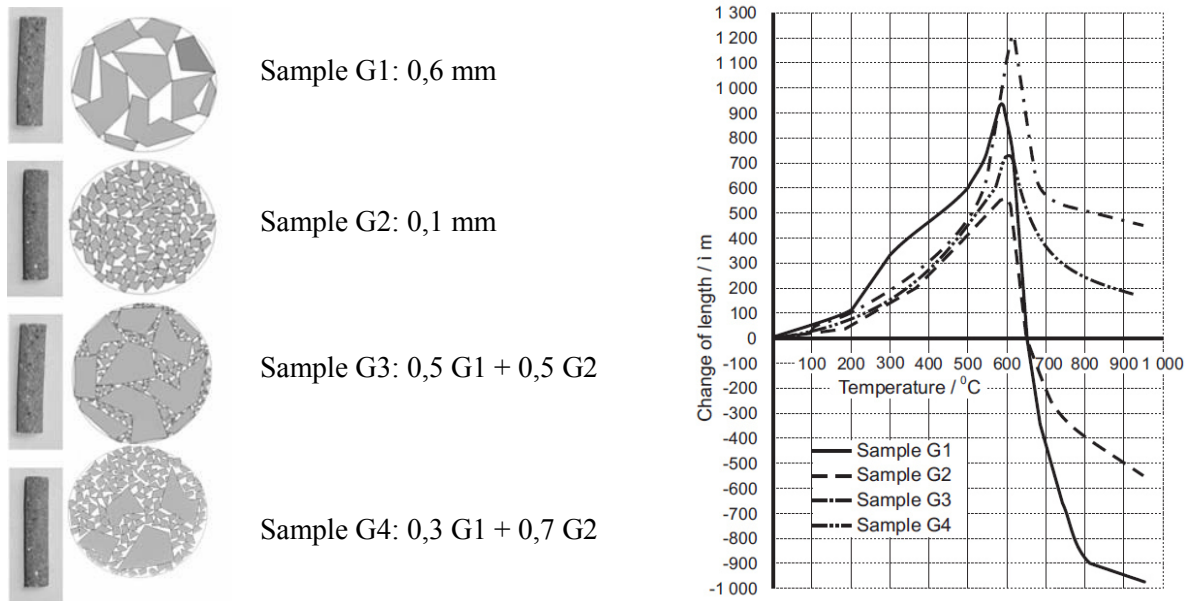


Figure 2-14: Dilatometer study (sample 50 mm length) with different amounts of a fine and a coarse grain type [69]. Samples G1-G4 are illustrated on the left hand picture and the dilatometer results are shown in the graph at the right hand side.

The effect of adjustment by grain rotation caused significant differences in the thermal expansion load transfer, with stresses not necessarily transmitted normally to the contact points. Sample G3 revealed the highest expansion, indicating a fixture of large grains by the fines and locking their rotation ability. The lowest expansion was found for the sample G2, which consisted of a multiply higher number of grain contacts compared to sample G1 and thus could better accommodate.

From Thiel et al. (2007) a very detailed study, investigating thermal expansion depending on silica sand types, grain size distribution, grain shape and on the no-bake binders PU-Coldbox, furan resin and waterglass-CO₂ was provided [71]. In summary, no big differences were revealed for different granular and purity parameters, whereas with different binder types important thermal expansion changes occurred. Some examples to demonstrate the effect of different binder types are shown in Figure 2-15.

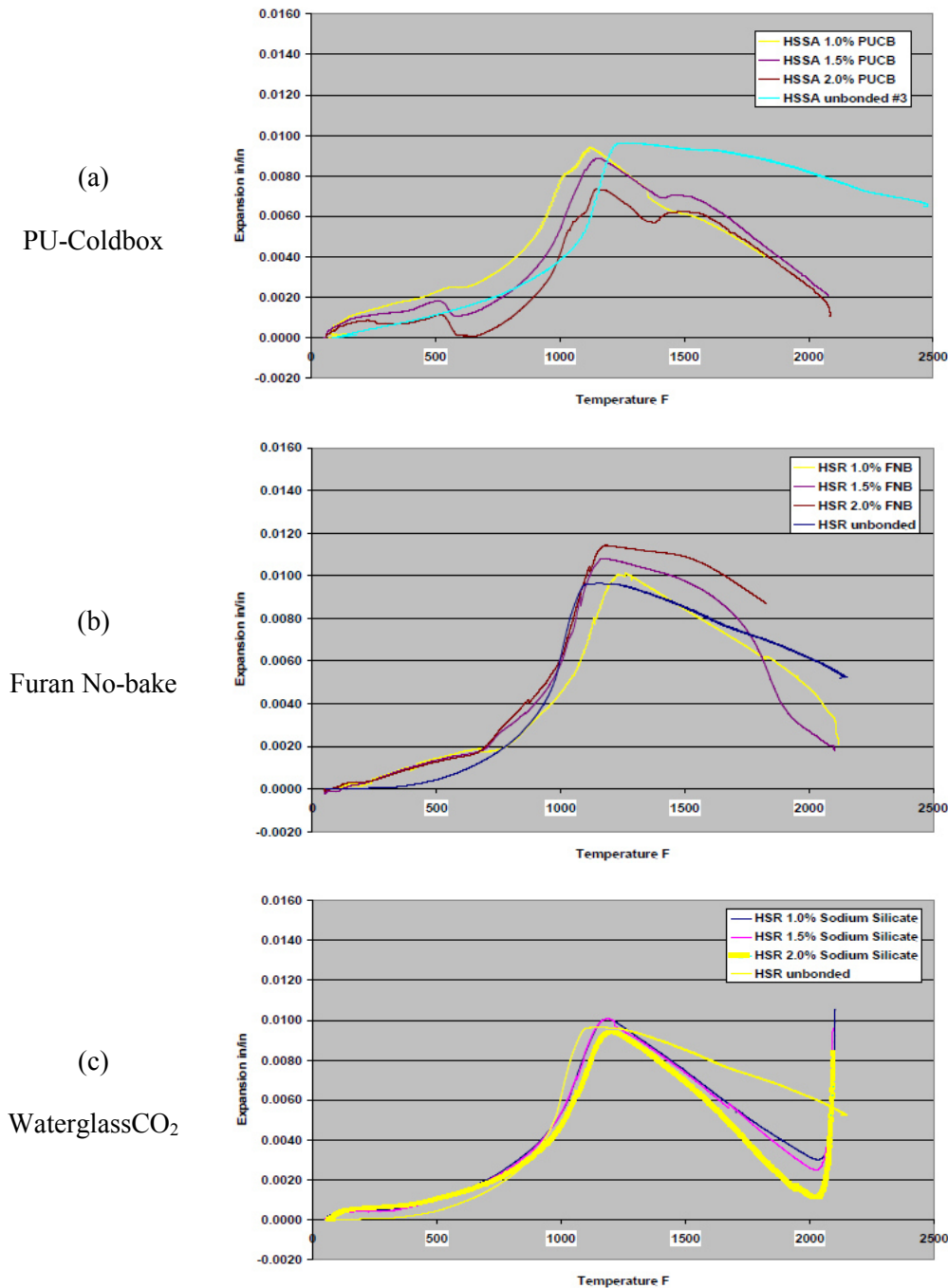


Figure 2-15: Thermal expansion of high purity silica sand samples (HSSA: sub-angular; HSR: rounded) with PUCB binder (a), FNB – Furan No-bake (b) and waterglass-CO₂-hardened – sodium silicate (c) [71]. Note relevant temperatures in °C converted from °F are: 246 °C – 500 °F; 300 °C – 512 °F; 523 °C – 1000 °F; 573 °C – 1064 °F; 600 °C – 1112 °F; 1079 °C – 2000 °F.

Effects from different binder types on thermal expansion can be summarised:

- Coldbox binder: reduced low temperature and more degressive high temperature expansion.
- Furan no-bake (FNB): Increased maximum thermal expansion with increased binder content.
- Silicate-CO₂: No change in low temperature expansion and more degressive high-temperature expansion with increased binder content.

For the temperatures below the maximum expansion level, which are most relevant for aluminium casting processes, the PU-Coldbox binder would exhibit a lower thermal expansion compared to furan and silicate bonded systems, which precisely reflected the thermal expansion profile of the used sand.

Recently, Svidró et al. (2014) evaluated the expansion behaviour of silica, chromite, olivine and zircon sand, bonded with PU-Coldbox and a furan cold setting resin for one heating and cooling cycle by dilatometry and hot distortion [73]. Here, based on these data, the heating time until the quartz transformation temperature of 573 °C was evaluated as a function of the sand sphere radius. In the centres of the 40 mm-diameter sphere, the transformation temperature was achieved after 260 s for PU-Coldbox cores and after 320 s for FNB cores. The longer time of FNB samples was due to reaction water in the cores humidity. When furan Warmbox cores would be used, less water and also a shorter heating time should be resulting. Based on their data, Figure 2-16 shows the heating time until 573 °C by direct melt contact of sand core spheres (see also section 2.5.6) over their radius.

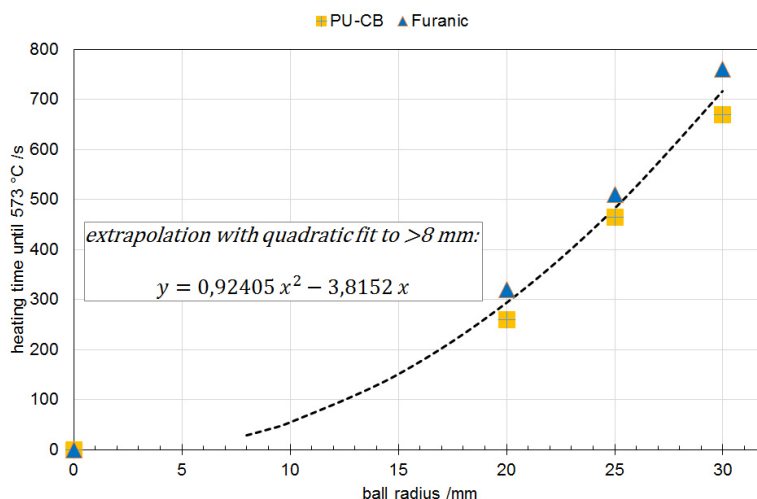


Figure 2-16: Evaluated heating time of sand spheres with PU-CB and furan no-bake hardened silica sand samples until the quartz transformation temperature, when immersed in 660 °C molten Al as function of the radius [73].

The extrapolation is valid for a radius of the spheres of above 8 mm. Transferred to aluminium cylinder heads, having a solidification time of around 200 – 300 s, equivalent situations similar or below that of the volume to surface ratio equivalent to that of a ball diameter of 20±3 mm can be prone to quartz transformation phenomena and hence, show significant dimensional changes, which is important for hot-spot regions of cast aluminium parts with thin-walled core sections.

2.4 Binder systems for foundry sand cores

The majority of foundry moulds are bonded with green-sand, hence, based on clay [74], [75]. In this thesis, sand cores positioned in moulds are considered which require chemically bonded sands, due to high strength demands. Organic, and increasingly also inorganic binders are applied and will be overviewed here.

2.4.1 Organic sand core binders

Relevant for foundry application are no-bake, chemically acid hardened, gas hardened and thermally hardened derivatives based upon phenols. Phenolic resins are applied in many industrial areas for coatings, dispersions, adhesives, moulding and foundry resins, laminates, wood bonding, composites, etc. since the early past century [76]. The basic substances for foundry application are substituted phenols and formaldehyde, used to produce phenolic resins like *Novolaks* and *Resols*.

Most relevant resin-bonding processes are self-setting and gas- or heat-triggered hardening processes [49, Ch. 13 Resin bonded sand]. The application of organic resins for foundry applications was overviewed in. In Table 2-7 a review on chemically hardening binders from 1950 up to this century is shown [77], [78]. The evolution of binder application in the German market evolved similarly [79].

Table 2-7: History of core and mould processes using synthetic resins as binders [77].

Year	Process	Resin
1950	Use of shell molding	Phenolic novolaks
1958	Furan no-bake	Furan resins (straight and modified)
1962	Hot-box	Urea, furan, and phenolic resins
1965	Alkyd oil urethanes	Alkyd drying oils
1965	Phenolic hot-box	Phenolic resoles
1968	Phenolic urethane cold-box	<i>Ortho</i> -condensed resoles
1971	Furan SO ₂	Condensed furan resins
1978	Warm-box	Modified furan resins
1981	Warm-box-vacuum	Furan or phenolic resoles
1982	Ester-cured no-bake	Alkaline phenolic resoles
1983	MF-cold-box	Alkaline phenolic resoles
1983	Cold-box plus	<i>o</i> -condensed resoles
1984	Acrylic-epoxy SO ₂	Acrylic and epoxy resins
1987	Hot-box plus	Modified phenol resins
1988	Acetal (methylal)	Resorcinol resins
1990	CO ₂ -resole cold-box	Alkaline resoles (boron modified)
1995	Biodiesel-based UCB	<i>o</i> -condensed resoles with methyl ester solvents
2001	TEOS UCB	<i>o</i> -condensed resoles with tetraethyl silicate solvents

In the second half of the past century, the importance of chemically bonded cores and moulds strongly increased [4, Ch. 6]. Oil bonded sands nearly disappeared and Polyurethane (PU) - Coldbox is the dominating high volume core production process today, which was first presented at the international casting fair "GIFA" in 1968 [51, Ch. 4 Die Formverfahren]. Shortcomings for Poly-Urethane Coldbox 'PU-CB' binders are their lower surface stability, thermoplastic binder behaviour and a high condensate level during thermal binder decomposition, leading to early clogging of mould venting systems in serial application. Often Hotbox ('HB') and Warmbox ('WB') binders found application to overcome the before mentioned deficits, especially for highly loaded cores for combustion engine castings, which also

provide good sand core decomposition properties [4], [51, Ch. 4]. In addition, in the recent decade the generative production of sand cores, termed '3D core printing', was developed and found industrial application [80].

Hot strength and brittleness are main differences between phenolic and furan resin bonded cores at casting. The cross-linked furfural polymer is of brittle nature, which allows an easy removal from the sand grain and, thus, an easier fragmentation of cores. Higher hot strength and a more elastic nature of Phenolic resins causes more difficulties in mechanical sand reclaim and sand core disintegration [77].

In Figure 2-17 a schematic picture of reaction products depending on the achieved temperature in the moulding material is shown. The effect of cast metal temperature is indicated for iron-based and aluminium-based castings, according to [51, Ch. 3 Der Formstoff].

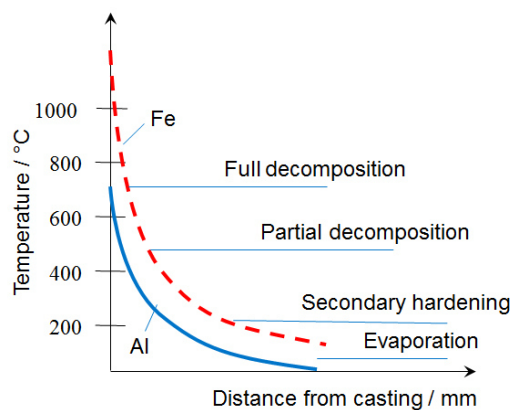


Figure 2-17: Schematic view of organic binder decomposition depending on local temperature and the core wall thickness for iron- and aluminium-based castings, redrawn from Bindernagel (1983)-fig.39, [51, Ch. 3].

For cast aluminium parts, less thermal degradation of cast-in cores is obvious, leading to less overall decomposition of the binder material. Often, prior to degradation a further strengthening of core sections, usually until approx. 300 °C due to evaporation effects without component cracking, occurs. With higher temperatures first an incomplete de-composition until 500 - 700 °C with a re-formation of components based on phenol, furan, form-aldehyde, CO₂- and water may happen, causing component dis-integration. Above these temperature range a complete dis-integration into C-H-N-containing basic molecules can be expected, which is dependent on the surrounding atmosphere. For Al-castings a complete binder disintegration is unlikely, as only the mould surface layer with melt contact may achieve 700 °C before heat dissipates into the core volume.

2.4.1.1 PU-Coldbox binder

Phenol-Formaldehyde resins are precursors of the poly-urethane Coldbox process [81], which still is the most widely applied core bonding process. The resin (part 1) is characterized by methylene and benzylic-ether bonds forming the urethane-resin. Part 2 is an isocyanate and the reaction is catalysed by amine gas, as schematically shown in Figure 2-18.

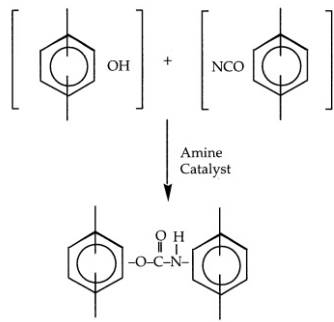


Figure 2-18: PU no-bake cold-box process – general reaction equation [81].

Due to the amine gas curing process also large sized cores and small sized cores can be hardened. Polymer- and metal-based core boxes can be applied, as no heating is required.

Thermal stability of basic phenolic resin components is decrease at temperatures above 250 °C. Decomposition continues until approximately 600 °C, resulting in poly-aromatic chars representing around 60 % of the original resin volume. In air the char ignites above 900 °C [76]. The complexity in real castings is given by the time dependent heat introduction and locally different heating rates including gas transport phenomena at real, complex shaped sand cores. Lytle et al. (1998) documented the decomposition kinetics of a commercial PU-Coldbox binder system [81], an example of a thermogravimetry analysis shown in Figure 2-19.

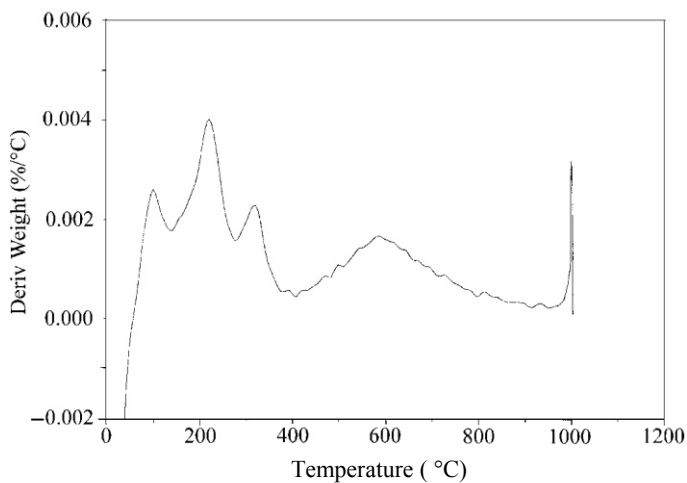


Figure 2-19: DTG analysis of a PU-Coldbox bonded sand core (with 150 °C/min), [81].

Until 500 °C they found 100 % semi-volatiles, which changed to 32 % fixed gases and 67 % light gases at 700 °C. For cast-Al applications these results evidently show the high potential of secondary strength formation by highly reactive semi-volatile constituents, relevant for cast-in and heated cores.

Bargaoui et al. (2017) investigated thermal and mechanical properties of PU-Coldbox bonded cores as well as of the pure PU-resin [82]. They described the complex nature of thermal binder cracking during the first seconds and further reactions of volatile fragments to second order components. Figure 2-20 illustrates their thermo-gravimetric and thermal analysis results with different heating rates.

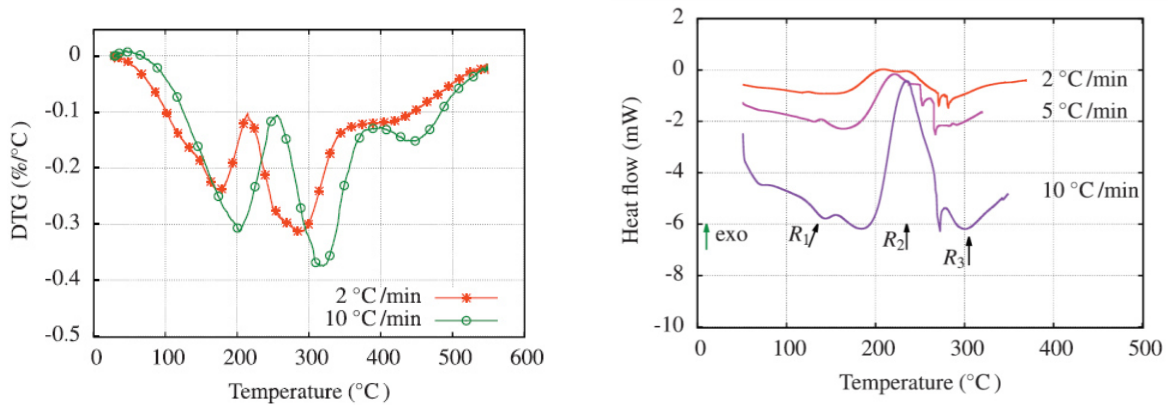


Figure 2-20 (a): DTG analysis of PU-bonded core samples. (b) Thermal analysis of the same sample types. All measurements were executed with different heating rates, according to [82].

The reactions R1, R2 and R3 of thermal analysis are:

- R1: evaporation of solvents (60 – 110 °C) along with glass transition of PU-resin
- R2: first exothermic peak (200 – 250 °C) related to further PU-crosslinking and overlapped PU-bond breakage
- R3: second exothermic reaction (~300 °C) denoted to breakdown into polymer aromatics

Additional dilatometry studies showed irreversible reactions, leading to a reduced expansion at around 250 to 350 °C. Mechanical properties revealed the lowest stiffness at 150 °C, followed by a hardening until 200 °C. At room temperature a pronounced visco-plastic behaviour was found, which disappeared at 150 °C. These data including creep data, according to the authors, allow to feed advanced material models being under development.

Holtzer et al. (2013) evaluated the gas evolution velocity and hazardous substance concentration for cast-in phenolic bond sand core specimens for low (700 °C - aluminium) and high temperature (1350 °C - iron) [83]. For the high temperature condition a seven times higher maximum gas evolution rate and a 10- to 30-fold amount of released benzylic, toluene, ethylbenzene and xylene were reported compared to the lower temperature condition.

2.4.1.2 Furan binders

Furfuryl alcohol originates from maize, as documented Dunks (1971), chap.6 [4]. The first notes on furfuryl alcohol appeared in 1873. Furan resins can be modified to a thermosetting resin, or used in combination with urea-formaldehyde or phenol-formaldehyde. These binder types are hardened by polycondensation reactions and thus form a rigid network, which is thermally stable until the resin dependent decomposition temperature. Acid catalysts are applied (phosphoric or sulphuric acids), which are typically added by 10 to 25 %-mass related to the resin. For Warmbox only the type of resin differs, which allows a lower temperature cure. However, this kind of resin is significantly more expensive

compared to those used in the hot-box process. A typical tool temperature is around 180 °C. A simplified reaction scheme is shown by equation (2) and Figure 2-21

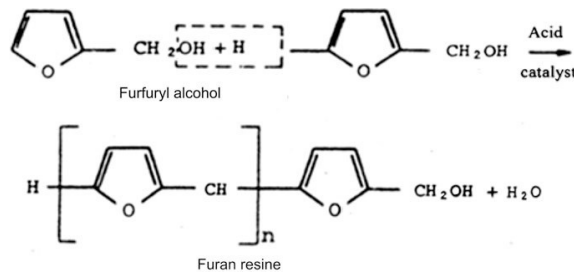
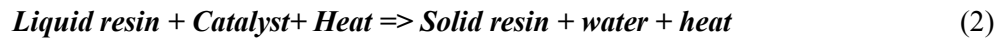


Figure 2-21: Polymerization of furfuryl alcohol monomers triggered by acid environment. A furan resin and water are formed, under generation of heat [78].

Resin types based upon urea-formaldehyde (and furfuryl alcohol) or upon urea-formaldehyde-phenol are in use [78]. Renhe (2011) overviewed thermal stability of furan resin in oxidizing and non-oxidizing environments and conditions for polymerisation (favoured by OH-groups) and poly-addition (favoured by double bonds), and described reaction types of furan resins [84]. These effects were used to modify resins and their thermal strength and were applied to design resins for high temperature steel castings.

Lucarz et al. (2014) investigated furan no-bake (FNB) cores in oxygen and oxygen-free atmosphere using TG and DTA, aiming for a further development of thermal reclaiming [85]. Characteristic decomposition profiles over the temperature on both atmospheres are shown in Figure 2-22.

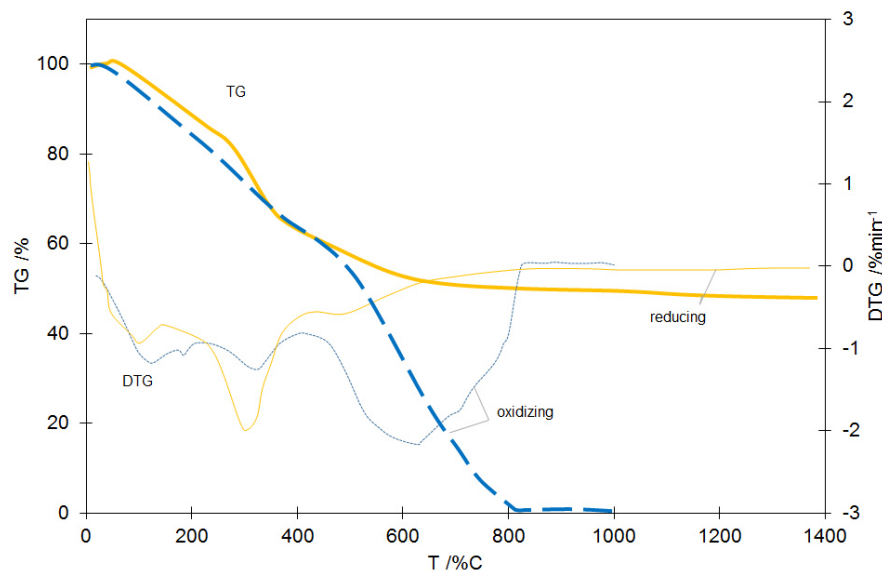


Figure 2-22: Thermogravimetric (TG and DTG) analysis of a furanic bonded moulding material in oxygen-free atmosphere (Ar) and on oxygen (air), acquired with 10 °Cs⁻¹. Redrawn from Lucarz (2014), [85].

Until 1200 °C in Ar a mass loss of 52 % was achieved, whereas in air a complete mass loss was observed until 850 °C. The DTA-result revealed an endothermal reaction on oxygen-free atmosphere and a predominantly exothermal reaction on oxygen-rich atmosphere. A significant impact of the

atmospheric conditions on the de-composition of cast-in cores is given, especially at temperatures above 400 °C. Kubecki et al. (2011), applied gas chromatography for the analysis of core samples treated at temperatures from 100 until 1300 °C and documented the volatile compounds [86]. Binder samples of 10 mg were shock-heated to the test temperature in Ar-atmosphere, and the gas collected during 3 minutes. Table 2-8 demonstrates the complex nature of organic resin de-composition above 300 °C and the even more complex mix of hazardous decomposition products from furan resin bonded moulds above 500 °C.

Table 2-8: Organic compounds generated as a result of selected temperature impact on furan resin [86]. Sand cores used for Al-castings show little portions exceeding 500 °C at casting. For them still a less complex de-composition product mix and incomplete degradation must be expected.

Compound	Retention time [min]	Process temperature [°C]					
		100	300	500	700	900	1100
Furfuryl aldehyde	2,50	o	o	o	o	o	o
Furfuryl alcohol	2,67	o	o	o	o	o	o
Phenol	4,48	o	o	o	o	o	o
Benzofuran	4,86	-	-	-	-	o	o
Indem	6,27	-	-	-	-	o	o
Cresol	6,85	-	-	o	o	o	o
2,4-dimethylphenol	11,69	-	-	o	o	o	-
3,4,5-trimethylphenol	13,64	-	-	o	o	o	-
4,7-dimethylbenzofuran	13,64	-	-	o	o	o	-
2-methylnaphthalene	15,95	-	-	-	o	o	o
2,5,6-trimethylbenzimidazole	16,46	-	-	o	o	o	o
2-vinylnaphthalene	17,85	-	-	-	-	o	o
Acenaphthalene	19,11	-	-	-	-	o	o

“o” – presence of organic compound, “-” – absence of organic compound

In practise, using such binder systems, an adequate ventilation, waste gas collection and after-treatment systems must be applied. DTG-analysis (compare section 2.5.1) and process simulation allowed to evaluate thermal exchange and gas transport for a 3D-printed furan mould [87]. The resulting local hazardous gas concentration is illustrated in (Figure 2-23).

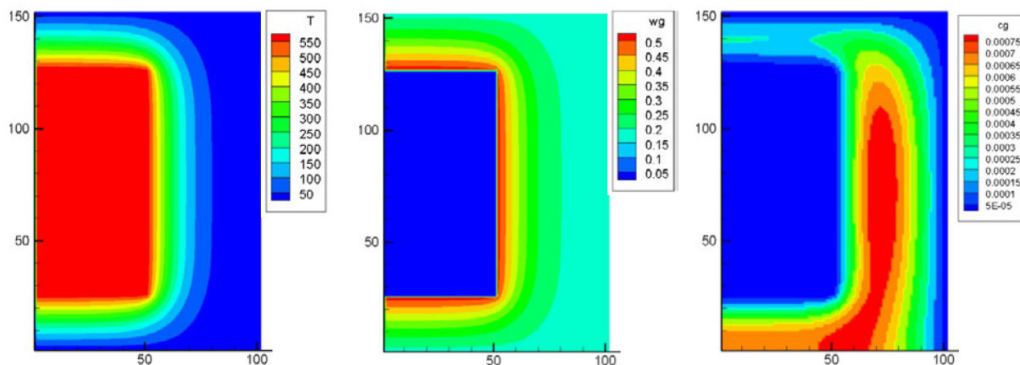


Figure 2-23: Distribution after 1000 s of a cylinder geometry cast in Aluminium, with the radius (horizontal axis) and the height indicated in mm. *Left:* temperature in °C, *Centre:* local rate of hazardous products generated in weight portion w_g of the total amount w_{tot} and *Right:* simulated hazardous product concentration c_g in kg of gas per kg of sand around a cast cylinder specimen ($x=r$; y =height) within a printed mould [87].

Such simulation results are very useful to estimate the potential outgassing of moulds and demonstrate the potential of multi-physical simulation of casting processes. Upcoming restrictions for allowed chemical substances and emissions increasingly force the casting industry to implement inorganic binder systems.

2.4.2 Inorganic binders

The absence of combustible and potentially hazardous products evolving during the casting process is a main driving force to implement inorganic binders in high volume production, e.g. in the automotive casting industry. Their shortcomings are generally owed to their non-combustible nature. These are mainly a poor thermal degradation, linked with a worse core removal ability from the castings and different reclamation processes for used core sand. Sobczyk (2008) overviewed several inorganic binder types with a potential for casting application [10]. Ongoing developments were summarised, as listed here:

- Further developments of silicate based binders (“waterglass”): mainly Na-, and more rarely, K-silicate based systems. Developments on “Geo-polymers” [88], [89], which are silicate-aluminate networks, complete this development area.
- New binder developments based upon sulphates, phosphates, borates and other inorganic constituents. Sobczyk more deeply investigated Mg-sulphate bonded sand cores for automotive cylinder head castings. Their shortcoming for serial application is their hygroscopic nature, which requires high effort for humidity control along the whole casting process chain.
- Applying salt binders based upon Na-, and K-Cl for pressurized casting processes, or gravity casting process (Al-piston production). A core removal by water dissolution is possible.

More recently, Zaretskiy (2015) overviewed all commercially applied inorganic binders in the casting industry [27]. The most widely applied systems are based upon sodium-silicate and the systems are built up from at least two components to achieve satisfying properties at process application.

2.4.3 Silicate-based inorganic binders

Sodium silicate is produced by melting silica sand and soda ash together in a furnace. The resulting glass can be dissolved in water, steam and increased pressure, to make liquid sodium silicate. Sodium silicate solutions, also denominated as ‘*waterglass*’, found application for several industrial applications, such as sealants, de-flocculants, emulsifiers and buffers in abrasive, casting industries [90].

Sodium silicate can be hardened by numerous ways [49, Ch. 14 Sodium silicate bonded sand]:

- Hardening by adding weak acids (CO₂-gas, organic esters),

- Hardening by adding various powders (di-calcium silicate, anhydrite etc.)
- Hardening by water removal operations

The typical $\text{SiO}_2/\text{Na}_2\text{O}$ molar ratio (“water glass modulus”) of industrially applied solutions ranges from 2 – 3,5. In the binary phase diagram of $\text{Na}_2\text{O} - \text{SiO}_2$ in Figure 2-24 this corresponds to a SiO_2 -mass fraction of 70-80 %. In that range the lowest glass softening temperature of approximately 800 °C also can be found.

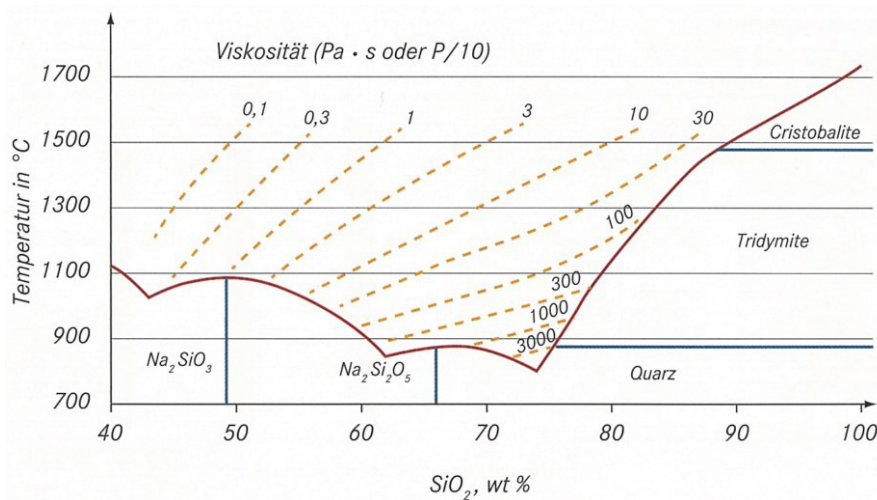


Figure 2-24: Phase diagram SiO_2 - Na_2O from 40 to 100 % SiO_2 -content, from [19]. Technically applied water glass binders are within a range of 66 to 77 % SiO_2 -content, which is corresponding to a molar $\text{SiO}_2/\text{Na}_2\text{O}$ -ratio of 2 to 3,5.

2.4.3.1 Thermal stability of silicate bonded sand cores

Thermal degradation of organic binders occurs due to pyrolysis and of the silicate binders by becoming fragile because of structural changes leading to formation of cracks and degradation of adhesive bonds with the sand grains [27]. Water glass bonded sand cores show a typical retained strength after thermal exposure of sand cores over temperature [5]. Beyond a primary strength maximum due to drying effects at around 200 °C a sand core strength decrease until 500 °C is visible, followed by an incline towards a secondary strength maximum at around 1100 °C, which is due to increasing chemical activity of the silicate binder with the silica sand, which is shown in Figure 2-25.

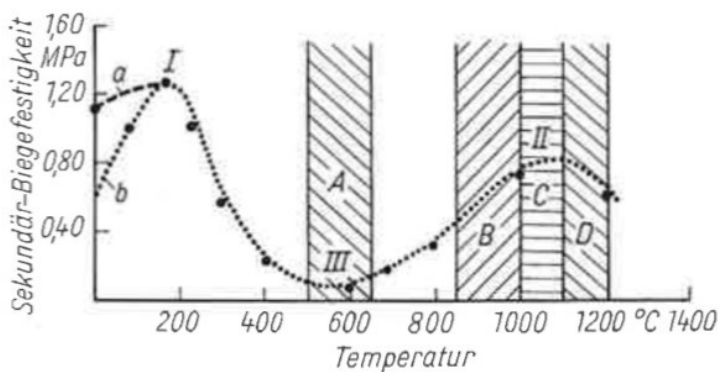


Figure 2-25: Secondary bending strength of sodium silicate bonded core samples after thermal exposure. I: primary maximum; II: secondary maximum; III: secondary minimum; A: light metal castings; B: copper based; C: Cast iron; D: Steel. [5]

Sand core temperatures of light metal castings do not easily exceed 700 °C, with exception of core surface layers situated in the melt flow areas. Thick-walled cores may even stay in maximum temperature ranges of 400 °C, with the consequence of higher retained strength.

Water is very active towards SiO₂, thus absorbed and if even chemisorbed, creating OH⁻-groups and temperatures of minimum 400 °C are required to release it from SiO₂-surfaces [61]. The solubility of SiO₂ in vapour at 500 °C and 10³ bar is 0,26 %, which may explain part of increasing bonding strength at higher temperatures due to release of crystalline bonded water. Temperature intervals of water release of inorganic substances can be best determined by DTA.

2.4.3.2 Cold hardening of silicate binders

CO₂-hardened Silicate bonded cores

In the 1950's the CO₂-bonded sodium silicate process found increasing application. In the main reaction the Na₂O is bonded to Na₂CO₃, consequently increasing the modulus and viscosity. Water is released, which is bonded into 2Na₂HCO₃ during gassing operation and de-hydrates the silica-gel. Mainly applied are silicate solutions with a modulus of two [4, Ch. 6], [91], showing best applicable strength and storage conditions. The removal of Na₂O from the silicate solution leads to an embrittlement of the silicate bonds, owed to the needle-shaped carbonates formed. The core collapsibility of sodium silicate – CO₂-hardened moulds depends on frequently added organic additives to the binder or the sand mixture [4]. Despite cold hardening is a fast method, main limits for the broader use of such bonded cores are their generally low achievable strength and the high sensitivity to humidity [92]. A process application for complex and fragile core geometries was never achieved.

Cold setting hardened silicate binders for moulds

Besides the CO₂-hardening process, other cold-setting methods are important for moulding applications, mainly applied for larger moulds but usually not for internal cores.

Bindernagel (1983) overviewed several applied cold setting methods using silicate binders [93, Ch. 4.4]: The *Nishiyama-process* is based upon the reactivity within mixtures of silicate with fine silica. *Cementing processes* are based upon Ca-silicate reactivity. The *silicate-ester process* was more recently newly investigated by Weider et al. (2012) for steel casting application [94]. The influence of different sand types on retained strength and thermal mould properties was investigated. For that process, organic esters (e.g. acetic acid esters) are added by approximately 10 % of the binder content for hardening, causing an only low amount of combustible organic products.

Generally, for all silicate cold-setting technologies, the water content of the binder solution is not removed. Therefore, gas evolution with respect to casting defects is important. When applied for outer mould parts, the additional latent heat by the water release can enhance the heat transfer.

2.4.3.3 Thermal hardening of silicate-bonded cores

To overcome shortcomings of CO₂-hardened silicate-bonded cores, Brümmer & Döpp (1997) proposed rapid drying processes to harden silicate-bonded cores [92]. Now, two decades later, this hardening principle found general application for the production of complex silicate-bonded cores.

Most widely applied inorganic binder systems are the *INOTEC* (ASK Chemicals), the *CORDIS* (Huettenes-Albertus) and *AWB* (Minelco), [27], [35]. Powders, which contain micro-silica, are added to the sand-binder mixture, except for the AWB-process, and promote hardening by the network-forming SiO₂. Hardening of inorganically bonded cores by microwave application and the required tooling materials is applicable [7], [95], [96]. For the silicate based AWB[®]-binding system, after hardening the cores in a heated core box, supported by vacuum, micro-wave drying is applied [97].

Sáenz et al. (2012) investigated the strength development of sodium silicate binders with different moduli, investigating CO₂- and thermal hardening processes, different baking temperatures and influences of ambient humidity and bench life time [98]. They concluded that with a lower modulus and higher density the higher mechanical properties can be achieved, using 2,0 – 2,5 % of sodium silicate and 120 – 150 °C curing temperature. Already after 180 °C the core properties were significantly decreasing again. Cores produced with the CO₂-hardening process were not satisfying for industrial application.

Jelínek et al. (2004) fundamentally investigated the hot hardening properties of silicate bonded cores [99]. Strength over the binder content and the waterglass-modulus after hardening for 70 s at 210 °C is shown by Figure 2-26.

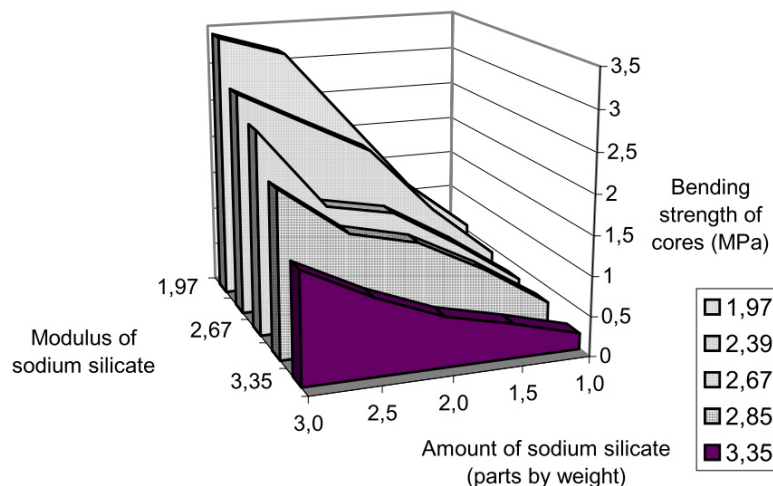


Figure 2-26: Influence of silicate modulus and binder amount in the mixture on bending strength of cores hardened by Hot-Box process (210°C, 70 sec.), [99].

Beside the positive impact of binder content up to 3 % on the strength, lower strength with higher moduli were revealed. For thermally hardened, silicate-bonded cores a high sensitivity of the resulting mechanical properties on the applied temperature and exposure time is given [100]. Strength maxima were achieved for 30 s hardening time at 150 °C already, as shown in Figure 2-27.

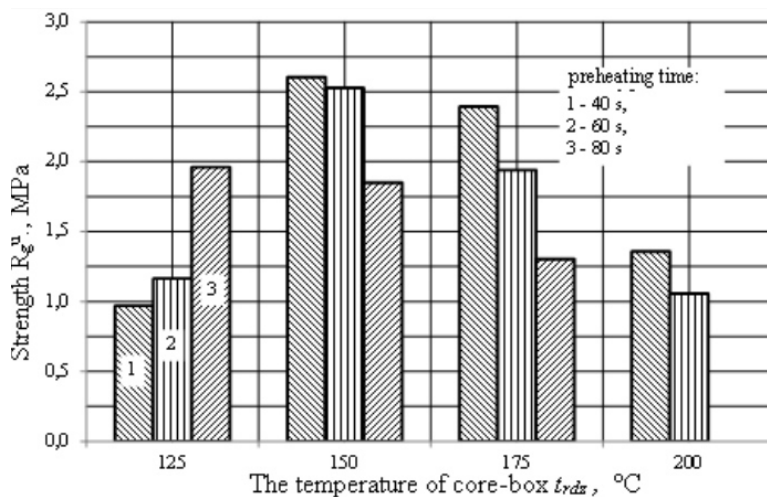


Figure 2-27: Test results for samples with Cordis binder [100].

Often, for a satisfying core manipulation, a minimum strength of 2 MPa is required. Obviously, the parameters shown in Figure 2-26 (210 °C for 70 s) presented data after a significant over-hardening and strength-decrease, at least of the binder types with higher modulus, which are more reactive.

Jelinek (2004) presented weight loss analyses over temperature to evaluate drying process of silicate-based core binders [99]. After drying at 200 °C a waterglass binder lost 59 – 62 % and after annealing at 900 °C between 60 and 64 % of mass. The low difference was due to the portion of tightly bonded water, which was released only after the 900 °C-treatment. Binder types were defined via NMR-analyses, quantifying the portions of mono-, di-, tri- and tetra-silicate. The authors evaluated microwave hardening technology positively, which would allow a further decrease of binder contents. Advantages for the core removal behaviour by application of a partially reversible de-hydration was assumed, but not verified by the authors. Similarly, Wang et al. (2009) described properties of microwave hardened sodium silicate bonded cores, and pointed out the potential to decrease binder contents [101]. It was shown, that moisture take-up can cause a significant strength decrease of sand cores within a few hours, due to bond damage.

2.5 Evaluation of sand core disintegration

In the automotive industry, the quality of a core removal process is evaluated via the amount of sticky or loose residual sand or, in the worst case, the presence of blocked passages by non-removed core parts or by early fractured core sections during casting. Besides this kind of empirical casting process control, only few fundamental research on core removal properties is available.

Flemming & Tilch (1993) proposed the evaluation of sand sticking on cast surfaces, lump size and content after the core removal station and the squeeze out load cast-in cores from a cavity as practical measures to evaluate core removal. In foundry practice, high quantities of castings need to be examined by visual inspection, endoscopy or X-ray tomography to obtain reliable results.

The ability of sand cores to be destroyed after the casting process can be evaluated by tests applied on non-cast core samples or, applying higher testing effort, on cast-in specimens.

Evaluations on non-cast binder or core specimens are:

- Thermo-physical and –chemical investigations on binder and core samples with thermal exposure.
- Retained strength or abrasion resistance evaluation of sand cores after thermal exposure.
- Mechanical testing of heated core specimens.
- Hot distortion testing during heating of core specimens.
- Collapsibility testing of heated core samples under load.

Usually applied investigations on cast-in cores are:

- Qualitative evaluation of fragmentation of removed core sand.
- Evaluation of core destruction after melt contact.
- Determination of the cumulated knocking pulse number for the removal of cast-in core specimens.
- Evaluation of the required time for the removal of cast-in core specimens on specified vibratory equipment.

These overviewed methods will be characterized in more details in the following sections.

2.5.1 Thermo-physical investigations on sand and binder stability

Characteristic decomposition temperatures and time-dependent reactions can be evaluated by thermal expansion (compare section 2.3.5.), thermo-gravimetry (TG) and thermal analysis (TA). Differential thermo-gravimetry (DTG) allows to evaluate the mass loss rate over temperature and differential thermal analysis (DTA) the difference of a thermal voltage signal between a test and a reference sample [61]. Atmosphere- and heating-rate dependent trials allow more detailed insight into binder and core stability. Examples for the method application can be found in section 2.4, supporting the description of organic binders.

2.5.2 Retained strength of sand core samples

Dietert (1950) described retained strength as a good laboratory measure to evaluate the knock-out effort of a core [21]. For testing, core samples need to be heated over a range of temperatures and their compressive strength evaluated after cooling down and allow comparison of different binder types. In summary, improving factors for good knock-out should be the use of coarse sand, low fines contents and a binder strength as low as possible.

Until present, the retained strength after thermal exposure is a usual method to characterize inorganically bonded cores [102]–[104], who evaluated the behaviour of various binder types, as illustrated in Figure 2-28.

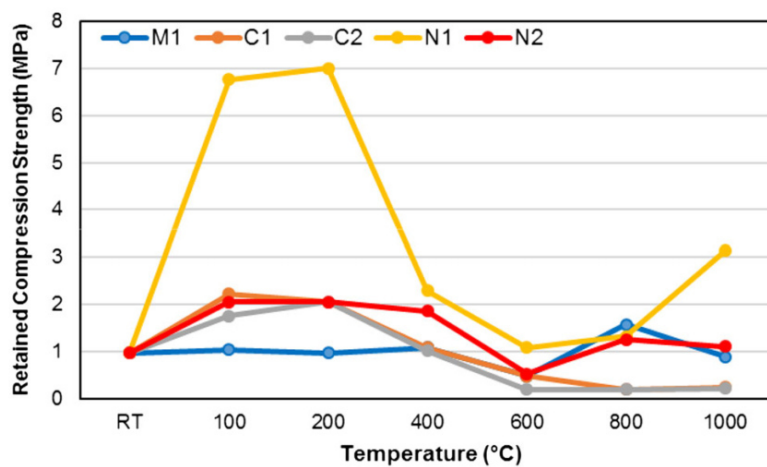


Figure 2-28: Comparison of modified (designated M1, C1, C2) and unmodified (designated N1, N2) silicate binders. Sand core retained strength [27]. Organic additives can enhance core breakdown. Inorganic additives are preferred from an ecological point of view.

Generally it is assumed that core removal should be the easier, the lower the retained strength is. Still, these basic investigations do not consider core and casting interaction by shrinkage and expansion or by overlaid surface reactions. Major-Gabryś & Dobosz (2007) discussed such effects more in details [105]. Their research was focused on castings poured with temperatures higher than 800 °C (Cu, Fe), and focused on the secondary strength maximum of silicate bonded cores. Stresses due to high thermal expansion of cast-in cores were not released and as a result, the contact pressure between casting and core remained high causing a worse knock-out behaviour [106]. Further evaluations confirmed, that around the secondary strength maximum the retained strength did not correlate with the expectable core removal properties [107].

An approach to evaluate the deformation potential of PU-Coldbox cores before and after thermal exposure was presented from Menet et al. (2017), who applied cyclic compression tests with hysteresis loops, shown in Figure 2-29 [108].

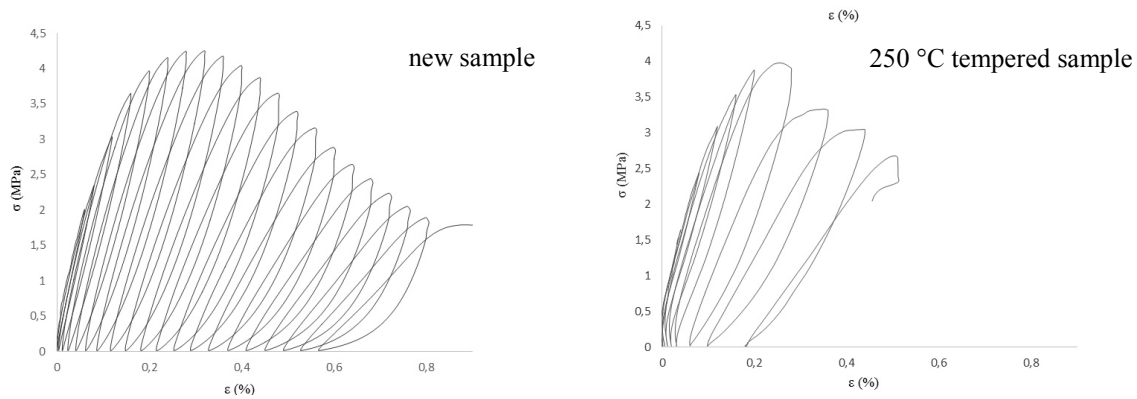


Figure 2-29: Cyclic loading and unloading during compression test of a PU-CB bonded sample in steps of 50 μm compression deformation [108].

The tempered sample exhibited higher remaining deformation per loop and consequently less cycles until failure. In casting practise no repeated cyclic loading occurs, but such investigations can be useful to evaluate the sensitivity of cores on mechanical loads. That type of investigations is more frequently applied in the field of construction materials, geo-engineering or refractory materials [109]–[111].

2.5.3 Abrasion testing

The correlation of residual strength and abrasion of thermally loaded core samples was presented by Conev et al. (2017), who aimed to provide an easy applicable method for core removal evaluation [112]. In summary they reported a decreased retained strength of inorganically bonded silica cores, but no decrease for alumo-silicate based granulates (‘MIN-sand[®]’ and ‘Cerabeads[®]’). The abrasion resistance of Min sand was high, whereas it was low for the Cerabeads. The authors postulated the most favourable core removal behaviour for inorganically bonded silica sand. An experimental verification by core removal results was not reported.

2.5.4 Hot distortion testing

The deformation of a flat sand core test bar (1/4” x 1” x 4”), which is clamped on one extremum and heated from below with defined and constant heating parameters, is evaluated. Result examples are shown in Figure 2-30.

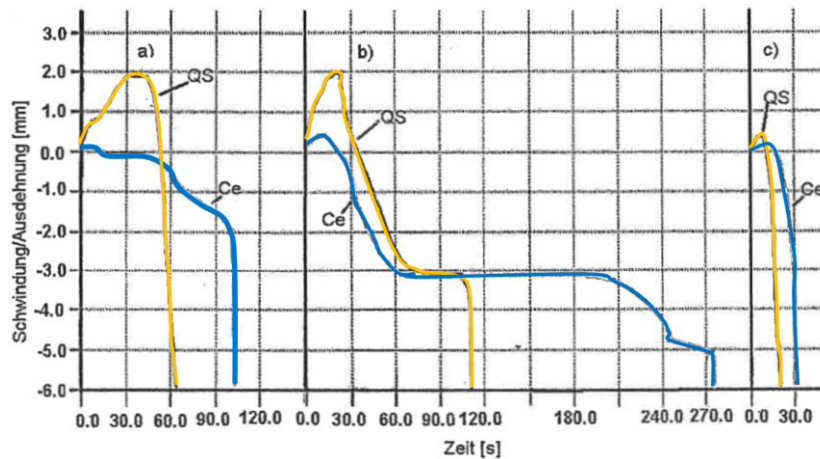


Figure 2-30: Hot distortion tests of silica (QS) and Cerabeads (Ce) samples bonded with a) Resol-CO₂; b) shell moulding material and c) PU-Coldbox [52]. x-axis: time in s and y-axis: dilatation in mm.

In general, the signal intensity is depending on thermal expansion of the materials and the thermal stability of the binder. Typical curves first show an upward bending due to thermal expansion of the heated lower side, followed by a downward bending due to thermal balancing. With increased binder de-composition an accelerated downward bending occurs. In the presented example, the lifetime of silica sand samples was generally shorter compared to that of Cerabeads-samples, which might be a consequence of different thermal stresses. Significant differences in the duration until breakdown, or thermal stability were revealed for the different binder types. The applicability of the hot distortion method to directly compare different sand core types was demonstrated. Svidró et al. (2017) reviewed the historical development and the state of the art of the hot distortion testing method [72].

Recknagel (2009) evaluated typical hot distortion investigation methods from the ceramics industry for the application on sand cores [65]. The ‘Seeger cone’ and ‘heating microscope’ methods revealed significant reactions only above 1000 °C. Therefore these methods are not relevant for Al-casting purposes.

2.5.5 Collapsibility test under load

The time under a given load until a core breakdown defines the criterion. During a core-collapsibility test core samples were loaded with a mass and held in a furnace of 1095 °C, and the time until the core breakdown acoustically determined [113]. That study investigated binder materials available in Africa, e.g. gum, starch and molasses. Reported collapsing times were in the range of 1 to 10 min. In summary, this method can be applied to directly compare different binders, but is not standardised.

2.5.6 Sand core testing with melt contact

Denis & Schrey (2006) examined the thermal stability of PU-CB binders by dipping trials of sand core samples in melt [115]. Subsequent to a defined sample exposure time in aluminium melt, the cooled samples were examined for the remaining solid core mass (Figure 2-31).

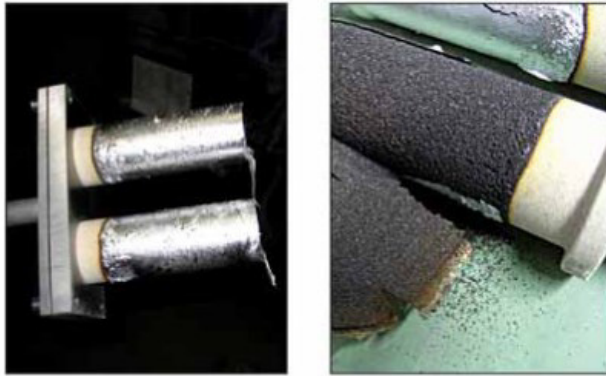


Figure 2-31: Sand core specimens after dipping in melt (left) and carefully released from the aluminium-skin before weighing (right), [115].

Svidro et al. (2014) studied the heat transfer into sand core samples dipped into aluminium melt. Temperature measurements and physical evaluations by TG and DTA (see section 2.5.1) were documented [73]. Spherical core specimens of 40, 50 and 60 mm diameter, bonded with PU-Coldbox and a furan no-bake system were examined, as shown in Figure 2-32.

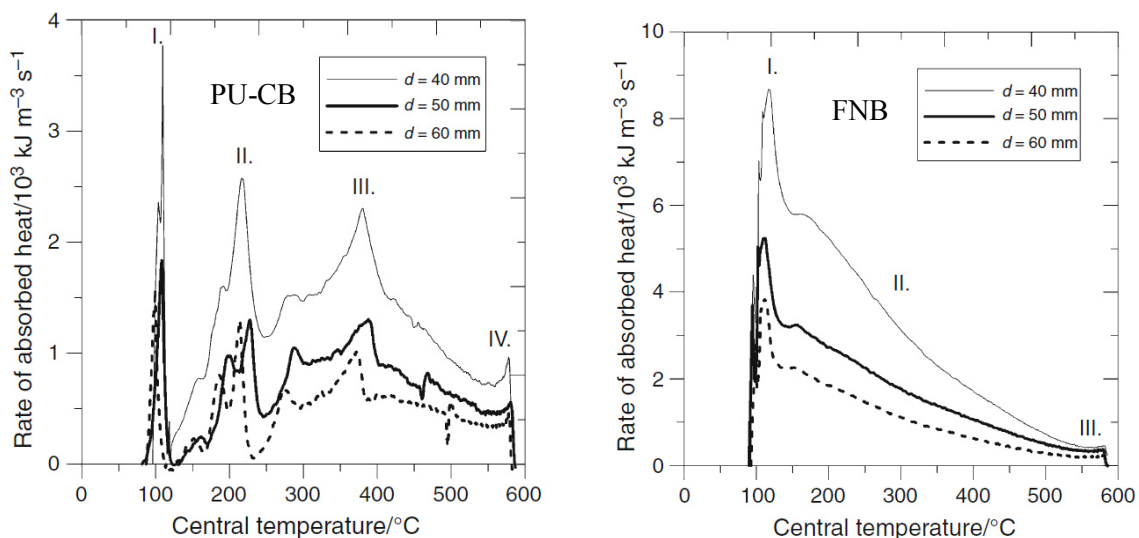


Figure 2-32: Results for absorbed heat rate from dipping trials into Al-melt of 660 °C. Spherical sand cores with diameters 40, 50 and 60 mm bonded with PU-Coldbox (left) and a furan no-bake system (right) were compared [73].

Multiple peaks over temperature were revealed for the PU-Coldbox samples. The furan resin bonded samples as result of the cold setting process only revealed a significant water evaporation peak, which extracted 40 % of the total heat. It can be assumed that using a thermal hardening process (applying the Warmbox process) no such water peak is present. In summary the importance of contained water for the heat extraction was rendered visible, which is also highly relevant for inorganically bonded cores.

2.5.7 Core removal testing of cast-in sand cores

In real castings a complex overlay of thermal, mechanical and atmospheric conditions occurs and the mechanical properties of sand cores are strongly dependent on the thermal history. To evaluate the effect of such overlaid influences requires the production and evaluation of cast-in core samples, which requires an increased experimental effort.

Since the mid of the past century a standardised knock-out test of cast in cylindrical samples (diameter and height 50 mm) is known. Flemming & Tilch (1993) documented a knocking method on cast-in sand core samples with counting the number of required knocks [116], shown in Figure 2-33. Further improvements were documented in the Polish Standard PN-85/H-11005 (1985), with a specifically developed conical knocking mass [117], which is shown in Figure 2-34. Current research work from the Polish Foundry Institute applying this device is documented [103], [104].

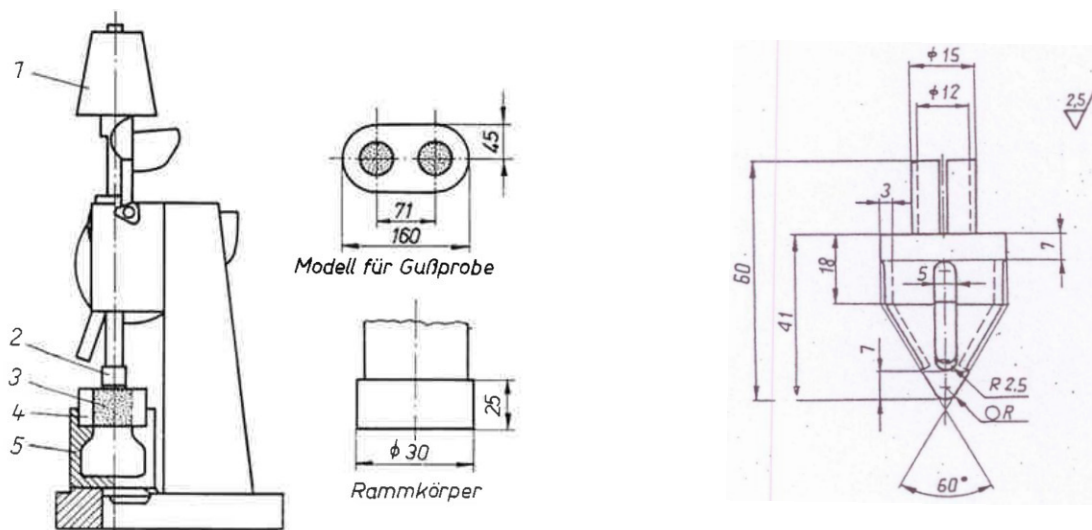


Figure 2-33: Testing device to evaluate knock-out work type LUW-C1 [116]. 1: falling mass; 2: ramming geometry; 3: test core; 4: test casting; 5: sample holder. Figure 2-34: Falling mass for knock out testing device according to a polish norm [117].

Only few setups for quantitative shake-out evaluation of samples with cast-in cores applying mechanical agitation analogue to industrially practice are documented. Tordoff & Tenaglia (1980) giving an overview about casting test moulds described samples based on cast-in tensile test cores (dog-bone shape), respectively of a cast-in disk with a diameter of seven inches [118]. This documentation was actualised by them in 2006 [119]. The respective samples are shown in Figure 2-35.

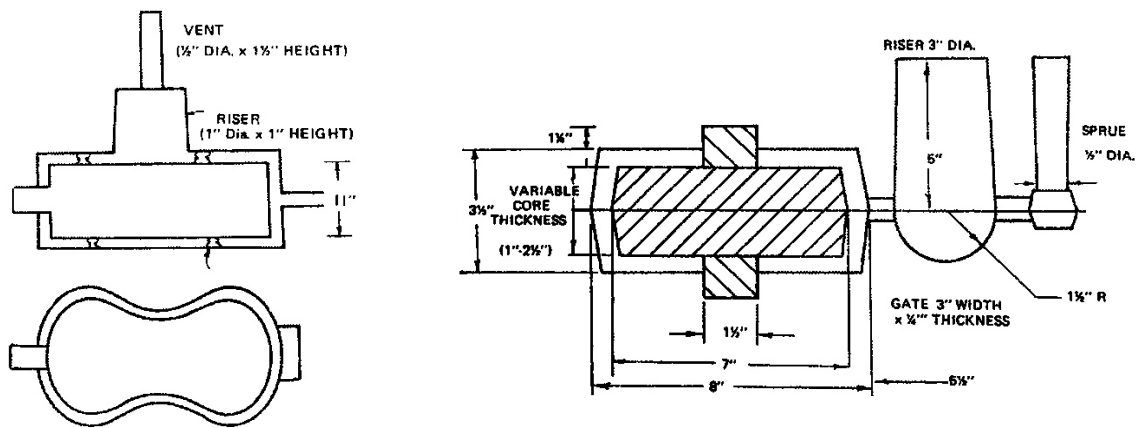


Figure 2-35: Test parts of cast-in dog bone tensile samples (1 square-inch cross-section) with chaplet support to hold constant wall thickness around the sample, gating and feeder system indicated (left) and disk test part with a mould drawing for sample production (right), [119].

The disk test was documented in several binder development patent applications of company ‘Ashland’ [120], [121]. The removed sand mass was evaluated in 30 s steps until 3 minutes shake-out time.

Henry et al. (1999) developed a wedge-shaped specimen [122]. Results for PU-CB-bonded cores applying a pressure controlled pneumatic hammer for core removal from a wedge shaped cast Al specimen, shown in Figure 2-36 (left), were presented. The method was also documented by Stancliffe (2006), who documented the shake-out performance via the percentage of removed core sand after 120 s [123]. Fennell & Crandell (2008) benchmarked different inorganic and organic binders and evaluated the average shake-out mass rate [124]. Figure 2-36 (right) shows their applied setup, which is additionally equipped with an in-line scale for a continuous acquisition of the sand mass.

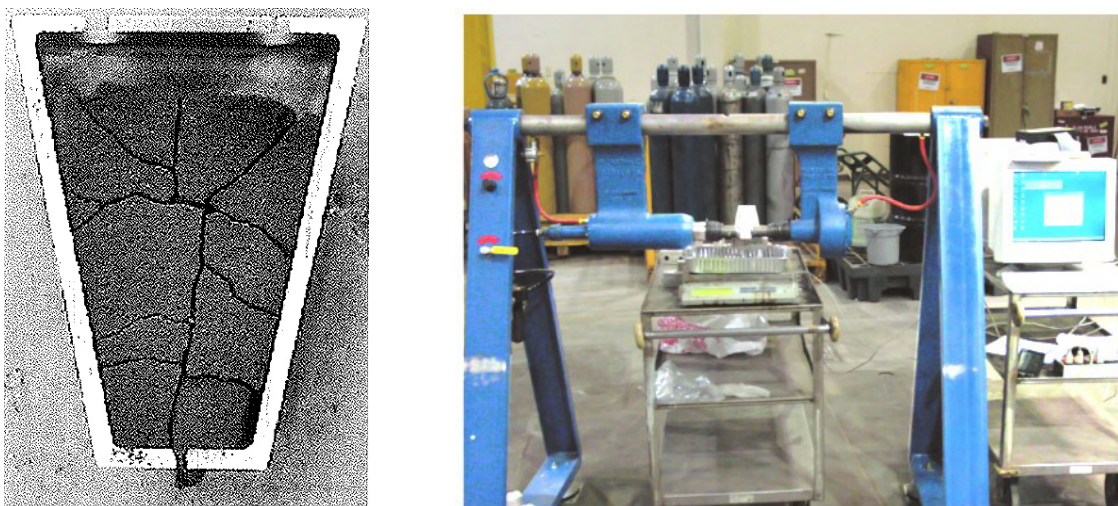


Figure 2-36 left: A cut test specimen after initial hammering, showing the fractured core [122]. Right: shake-out tests system with hammer and an in-line scale for sand collection [124].

Henry et al. (1999) characterised the mechanical core destruction with a two-phase mechanism: An initial core fracturing followed by a diminution phase by friction between loosened core fragments. The method application for other industrial castings, according to the authors, requires to customise the setup accordingly to the respective process parameters. Fennell & Crandell (2008) reported increased shake-out rates for inorganically bonded compared to organically bonded cores. The investigation was accompanied by tensile tests of sand cores after different storage conditions at room temperature. The average core removal mass rate varied by a factor of 25, which was by far not predictable by strength measurements. This underlines the importance of including the cast-in condition for a reliable core removal analysis.

2.6 Material failure criterions

The comminution of solids is a key technology in technological fields like geology, soil mechanics, construction and building materials or refractory materials. In contrast to dis-integration of solid structures, agglomeration is investigated in the fields of powder technology, food and medical production technology. Examples allowing analogous considerations with foundry cores are discussed in this section.

2.6.1 Comminution technologies

The description of rock and agglomerate comminution is based upon energy considerations for the reduction of particle size. At the end of 19th century some basic formulations for the incremental energy demand dE on a differential particle size reduction $d(d_p)$ were established. The most basic relationships are *Rittinger's* and *Kick's* laws:

- *Rittinger's law* is based upon the increased surface, leading to an inverse quadratic proportionality on the particle size:

$$dE_R \sim - \frac{d(d_p)}{d_p^2}$$

- *Kick's law* is based upon the consideration of elastic energy stored in brittle particles unless their destruction, resulting in a negative inverse proportionality on the particle size:

$$dE_K \sim - \frac{d(d_p)}{d_p}$$

For coarse material breakage and crushing, when the particle size is dominant, Kick's law is more appropriate, whereas for milling processes dealing with fine materials Rittinger's law allows a better description. To achieve a satisfying process description, practically applied equations often include

effects by plasticity, friction and particle morphology, which are documented in processing technology handbooks, e.g. [125]–[127].

Besides an energy-based consideration also fracture mechanical considerations deliver relevant approaches for fragmentation of particles or agglomerates. Fracture of particle arrangements and the analogies to *Griffith's law* for brittle defective materials were described by Einav (2007), who demonstrated the applicability of the Mohr-Coulomb failure criterion [128]. Some basic illustrations are shown Figure 2-37.

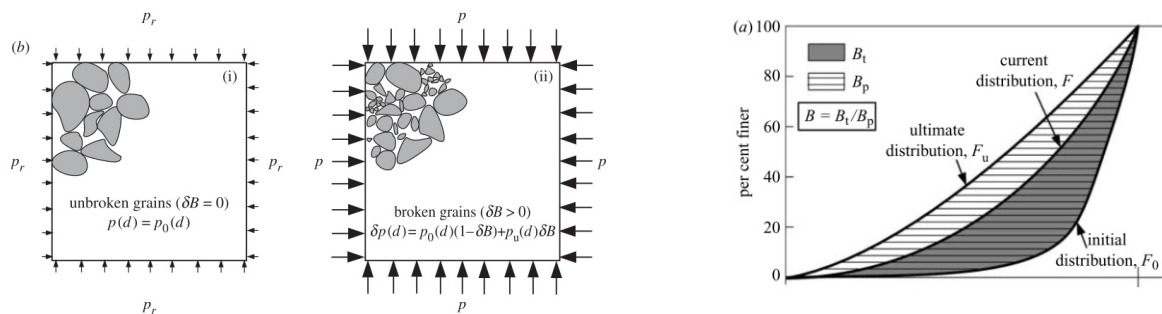


Figure 2-37: Particle fracturing model in initial state (upper left) and after being pressurized (upper right) with indicated breakage ratio ‘ B ’, respectively increment ‘ δB ’. Right: Particle size distribution function during comminution process of particle agglomerates are moving towards an ultimate distribution. B_t is the breakage fraction at time t and B_p is the breakage potential of a particle mixture, leading to the ultimate distribution F_u , where B is equal to unity [128].

A fundamental background for such statistically driven considerations is the ‘*weakest link concept*’ [129], leading to the size effect of samples according to Weibull (1951) and Bažant (2002), [130], [131]. Generally, the smaller defective samples are, the higher is their survival probability. Transferring that to foundry sand cores, every intergranular bond is such a weak link. Hence, for very thin cores walls, their destruction might be more difficult, not only due to potential surface adherence effects.

In the field of soil mechanics, the influence of granular parameters on the mechanical response was investigated applying shear modulus and damping investigations [57]. This investigation delivered useful information about the mechanical behaviour of granular systems and testing, which can be relevant also for foundry cores. In summary, higher roundness was linked with an increased normalized shear modulus and increased damping, as well as a decreased stress exponent and elastic threshold strain. An eventual cross-link to sand core destruction could be given by *Campanella 1994*⁵, who suggested that shear modulus degradation, and damping ratio are the important parameters for evaluating soil response under dynamic load such as shocks, blasting, dynamic compaction, earthquakes, pile driving, machine vibrations, vehicles, winds, waves, etc. Under these loads, effects of inertia forces are

⁵ Campanella, R.G. (1994). Field methods for dynamic geotechnical testing: An overview of capabilities and needs. In: Ebelhar, R., Drenovich, V. & L., K.B. (eds.), *Dynamic Geotechnical Testing II*, ASTM Special Technical Publication No. 1213, pp. 3–12. American Society of Testing and Materials.

accumulated and become significant, even if the shear strain is small, since the inertia forces increase proportionally to the square of vibration frequency.

This and similar works reveal a high potential by information from existing studies about the mechanical response of any type of granular material for the less intensively investigated field of foundry cores. According to Mullier et al. (1987), the particle and internal flaw size represent significant portions of the core wall thickness, which requires attention on the description of the fracture mechanical behaviour of cores [132].

2.6.2 Failure criterion models

In general, mechanical loading is multi-axial. Failure criterions are functional descriptions of the maximum achievable stress combinations before failure of the considered volumes occurs. One of the most basic and important failure criterions is the Mohr–Coulomb criterion (18th century), overviewed for application on rocks by Jones (2007), [133]. Depending on the normal stress σ_n the shear strength of the material τ is a result from the internal friction angle φ , and the cohesion strength C , as shown in equation (3):

$$\tau = C + \sigma_n \tan \varphi \quad (3)$$

For rock-engineering, and applied for various further technical applications, adapted material laws were developed, e.g. the Hoek-Brown criterion [134]. This, and the Mohr-Coulomb criterion are shown in the 2-dimensional normal-shear stress relation by Figure 2-38.

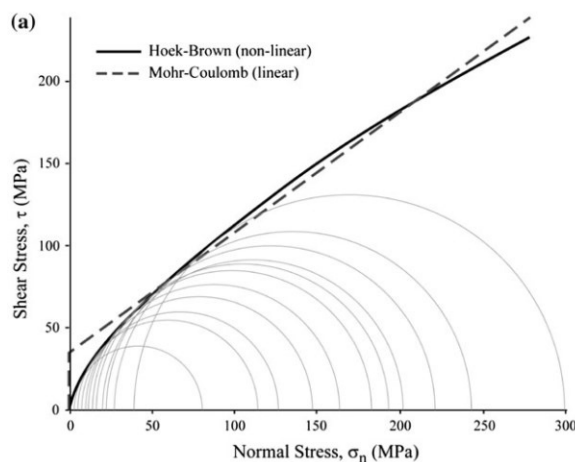


Figure 2-38: Comparison of Mohr-Coulomb versus the Hoek-Brown criterion [134].

Another important criterion is the ‘Drucker-Prager’ criterion [135], which is mostly dedicated to mining technology and is dominated by considerations about pressure dependency of the failure plane. As for foundry sand cores, failure criterion models are not yet widely applied, in this work the most basic Mohr-Coulomb criterion was used to obtain insight into the core failure behaviour (section 4.2.).

To determine the failure plane precisely, uniaxial tensile, compression and shear tests and combinations thereof, are required. A tomography picture from a foundry core sample after a compression test demonstrated a typical shear plane, which is inclined to the vertical load axis [108], as shown in a tomography picture in Figure 2-39.

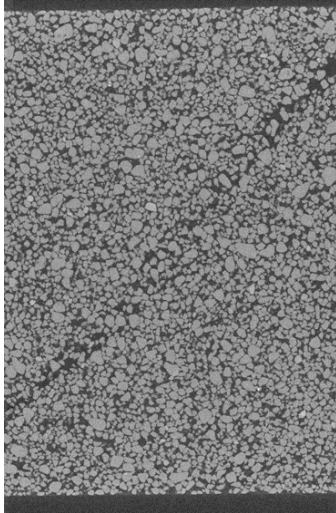


Figure 2-39: Tomography across a compression test sample showing a clear shear plane leading to failure. Sample dimensions are diameter 30 mm and height 45 mm. Loading direction was vertical [108]

A reduced solid volume fraction in the shear plane, due particle movements, is visible. Shear of granular materials is linked to particle re-orientation and requires a displacement perpendicularly to the shear plane. To initiate shear, grain motion is required. When compressive loads are present, a higher initiation shear stress unless a shear plane can evolve and a steady state shearing is achieved.

Tri-axial testing or shear cells allow such evaluations. For tri-axial testing, the cylinder surface of a compression sample is protected by an elastomer foil and pressurised, while compression loading is increased until the sample fails. Based on different settings the failure envelope is defined. Tri-axial testing is often applied for cemented materials or rock samples.

For loose granulates and soils shear cells are frequently applied. Mitarai (2006) investigated the behaviour of granular materials with different humidity concentrations applying tri-axial and direct shear testing equipment [136]. Both methods are schematically shown in Figure 2-40.

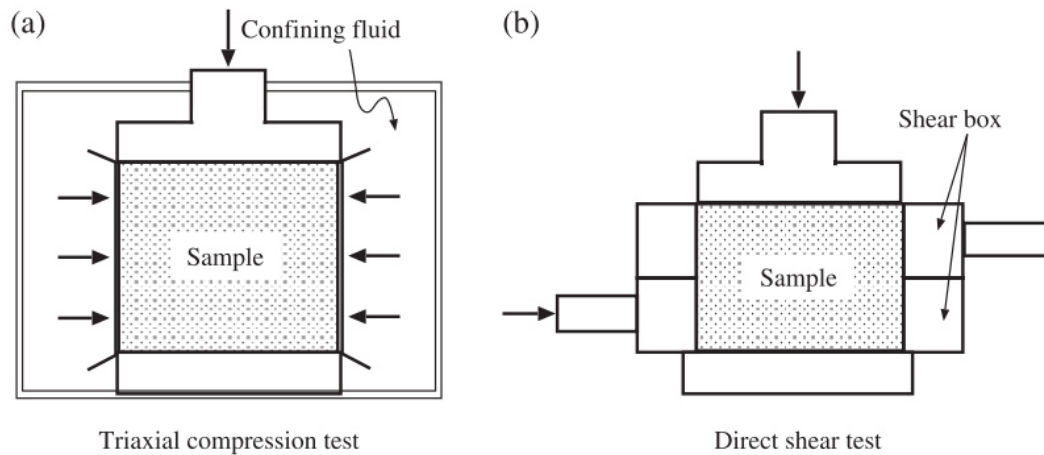


Figure 2-40: Schematic diagrams (a): tri-axial test system and (b): direct shear test system [136].

Dahlem et al. (2011) presented an adapted notched shear testing method, applying test bars with pre-defined shear planes by notches in different angles [138]. Every notch angle is related to a fixed ratio between isostatic and deviatoric stress, which was defined based upon FE-simulations. The von-Mises stress situation is illustrated by Figure 2-41 for two evaluated notch geometries.

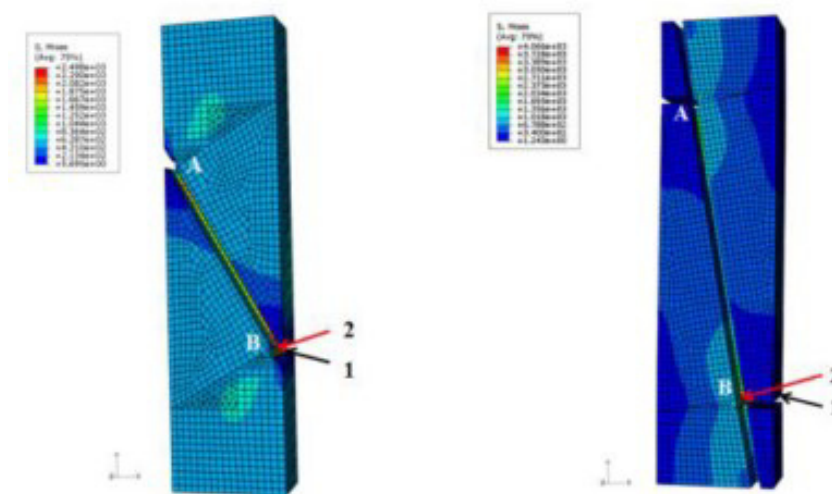


Figure 2-41: Modified shear test [137]. FE-models of applied geometries with 60° and 80° notch angle, indicating the von-Mises stress field under compression load.

2.6.3 Wedge splitting testing of refractory and building materials

Tschegg (1986) introduced the wedge splitting test for testing of cemented samples [139], based on which further developments for the application on ceramic material samples were developed [111], [140]–[142]. The test evaluation allows to determine the elastic modulus, tensile strength, specific work of fracture and to characterize brittleness based upon the characteristic length [143]. The possibility to achieve a non-critical fracture progress and to determine the specific work of fracture was firstly

transferred to foundry sand cores as part of this thesis, as documented in section 4.4. In comparison to refractory materials the sand cores show relatively low strength which is challenging for manipulation and measurement precision. Jin (2014) presented a summary about the test and the evaluation of material parameters supported by numerical simulation [141], which is schematically shown in Figure 2-42.

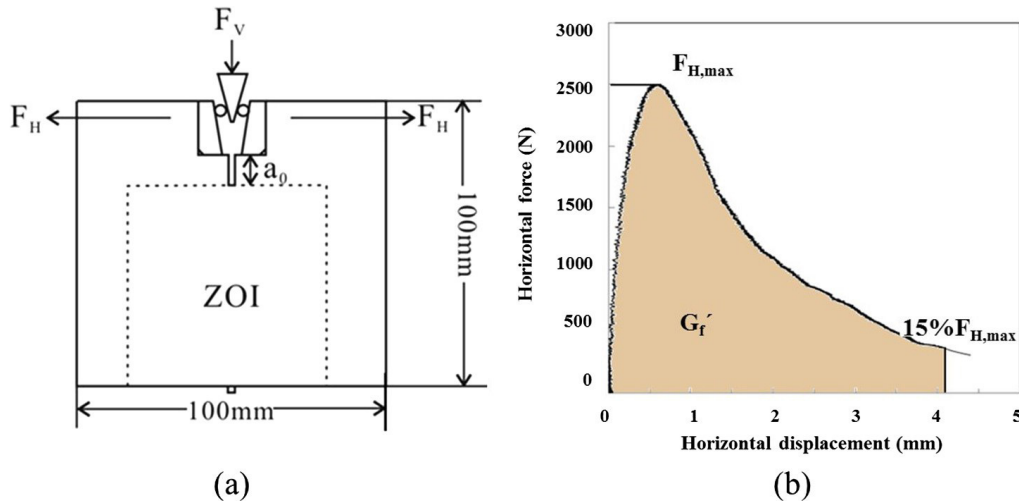


Figure 2-42: Schematic representation of the wedge splitting test (a) and a typical load/displacement curve (b), [144]. F_V : vertical load; F_H : horizontal load; a_0 : initial notch depth; ZOI: zone of interest; G_f' : specific work of fracture.

2.6.4 Impact testing of cemented agglomerates

Studies on the de-agglomeration of cemented agglomerates allow to evaluate the role of granular and bonding properties. More increasingly, such studies are supported by ‘Discrete Element Method’ (DEM) simulations, but still with a limited size of structures due to the high calculation effort. DEM-methods allow to evaluate the influence of each component and the individual properties on the mechanical behaviour, e.g. for bonded particle model simulations for varying particle and binder properties [145]. Subero et al. (1999) presented computer simulation about impact analyses of agglomerates with different specific fracture energies [146]. The size spectrum of the partly de-agglomerated body was depending on bonding energy and impact velocity. They concluded, that beyond a certain impact velocity no increased de-agglomeration can be expected as well as a significant fraction of impact energy is also not contributing to bonding fracture.

Investigations on the fracture mechanism of bonded particles, based upon silicone-bonded *LECA*-particles, highlighted the influence of particle and binder mass fraction on strength and the fracture mechanisms [147]–[149]. Figure 2-43 shows an overview about the particle breakage behaviour depending on strength relations and the matrix mass (cement or binder) fraction.

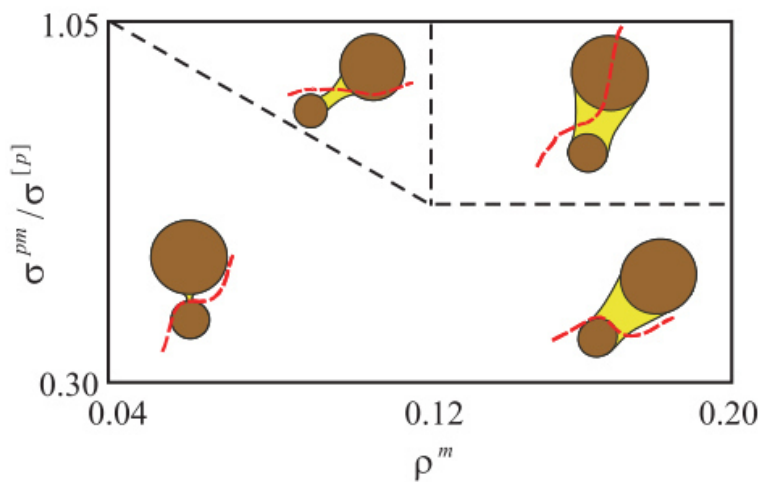


Figure 2-43: A schematic representation of cracking regimes with the ratio of particle-matrix strength related to the particle strength over the matrix volume [147].

A high matrix (cement, or binder) mass fraction and high adhesive forces would favour particle fracture. For matrix fractions up to 4 %, and with an adhesive strength below the particle strength, no particle fracture was observed.

The static and dynamic mechanical response of bonded granulates, including impact trials and computer simulations was described in the thesis of Antonyuk (2006) , and associated publications [150]–[153]. Fracture energy concepts, governing laws and industrial comminution technologies were reviewed. Some basic figures, illustrating the role of brittleness, are shown in Figure 2-44 and Figure 2-45.

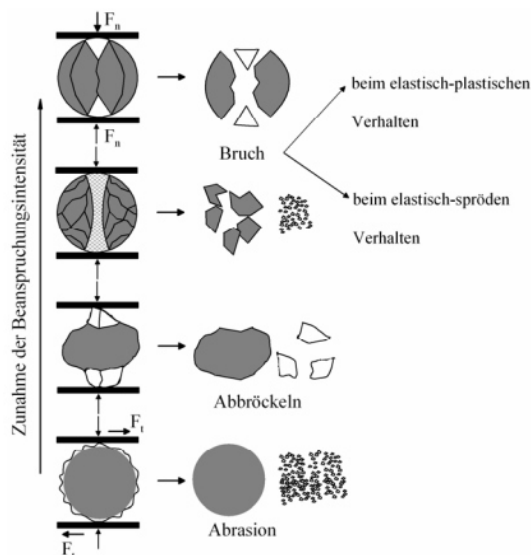


Figure 2-44: Diminution of a ball depending on the loading intensity, scheme according to Schubert (2003), [127]. Elastic-plastic and elastic-brittle fracture lead to different typical grain size distributions, also depending on the loading intensity [150].

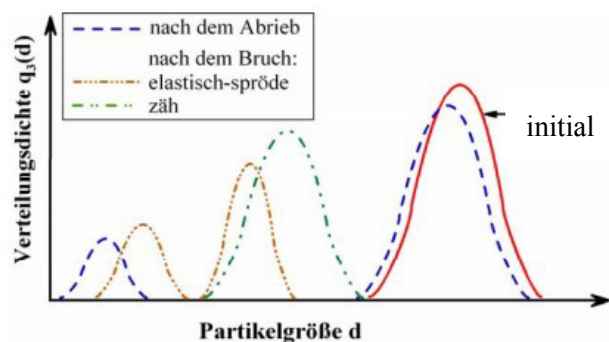


Figure 2-45: Principal illustration of the granulate grain size distribution change due to abrasion and fracture of the test body. The particle size of an initial body, after abrasion, an elastic-plastic and an elastic-brittle fracture is indicated [150]

According to that work, an elastic-brittle material behaviour enhances a bi-modal fragment size distribution, whereas an elastic-plastic behaviour leads to a more continuous fragment size distribution. Figure 2-46 illustrates the de-bonding mechanism of a particle fragment caused by a cyclic external load.

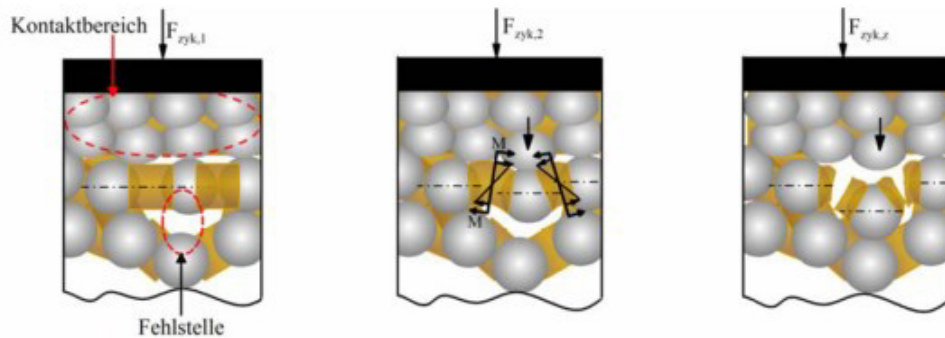


Figure 2-46: Illustration of a primary particle de-bonding and fracture of a bonded agglomerated body after multiple loading [150, Fig. 6.53]

In that schematic drawing, the load amplitude transferred by particle contacts causes a bending momentum, which exceeds the binder strength locally and results in a de-bonded particle (or agglomerate). Apart from the free volume, which is higher for foundry cores, this illustration can be valid for the situation of a cast-in foundry core during a vibration load (e.g. by hammering or shaking). The core damaging mechanism due to the contact with the metal casting wall can be the same. But eventually more complexity is given due to a potential thermal damage of the core surface layer, harming a mechanical load transfer from the beginning of a core removal process onwards.

In summary, a transfer of here presented investigation methods to foundry sand cores appears adequate, and requires following basic considerations:

- Every bond of a consolidated sand core is a weak link and, hence, a potential breakage area. Their density in a volume is defined via the grain size distribution, the compaction and the resulting (average) coordination number.
- Fragmentation of sand cores consists of intergranular bond breakage to separate sand grains from each other.
- The sand grains are not target of comminution and it is desired, that they remain undamaged during the casting and core removal process to allow a high sand reclamation rate.
- A cast-in sand core might be in a fixed contact with the solidified and cooled casting allowing a direct load transfer. In course of a core removal process, after a first fragmentation the loosened core lumps are further destroyed by wall-fragment and fragment-fragment impact and friction loads. Mechanically the interaction of multiple bodies with changing dimensions is present.

3 Experimental methods overview

In this chapter an overview on the applied experimental methods will be given. In addition to that overview relevant background information, which is not described in all details in the publications presented in chapter 4, will be presented here.

In the sections first the used sand and binder systems, the applied production tools and thermal pre-conditioning procedures of test samples are described. Secondly the different testing procedures for core samples and cast parts for core removal experiments are presented.

3.1 Core sample production

In this section the tools and samples for every previously described test type are presented and the main settings described. Precise test programs applied with each geometry are documented in the respective result sections, which will be referenced.

3.1.1 Sand and binder types for test cores

Following the sand core mixtures used for the studies are presented. For core production conditions a general parameter range is defined, which will be more precisely defined in the descriptions of the different samples.

Table 3-1: Sand core sample mixtures applied for experiments.

Sample type	Sand type	Binder type and amount in % of sand mass
Silica - Coldbox	Quartz H32 [154]	AskoCure 355/655 Phenolic resin and isocyanate solution with 0,6/0,6 % [155], [156]. Catalytic hardening applying DMEA [157].
Silica Hotbox	Quartz H32	TH 2143 / MBT. Phenol-Formaldehyde resin with ammonium-nitrate hardener [158], [159] dosed with 1,55% / 0,32%.
Silica - Warmbox 1 (WB1)	Quartz H32	HA 7022/8154 modified furanic resin hardened with a mixture of phenol-sulphonic acid its Al-salts sulphur acid and organic constituents [160], [161] dosed with 1,39% / 0,25%.
Silica - Warmbox 2 (WB2)	Quartz H32	HA 8885 / 8099 modified urea-furan-phenolic resin with aqueous sulphur acid solution [162], [163] dosed with 1,41% / 0,35%.
Silica - Sodium Silicate (WG)	Quartz H32	Betol B39 / 2,5 % sodium silicate (waterglass) solution with a molar SiO ₂ :Na ₂ O ratio of 3,2 [164].
Cerabeads - Sodium Silicate (WG)	Cerabeads 650 [165]	2,5 % of Betol B39 waterglass
Andalusite - Sodium Silicate (WG)	Kerphalite [166]	3 % of Betol B39 waterglass

Organic resin binders and sodium silicate solution were applied. The basis for binder comparisons is silica sand H32. Thermally hardened sodium silicate binder was tested with the different sand types.

To study thermal expansion effects on sand core damage, Alumo-Silicate materials, having significantly lower thermal expansion than silica sand, were chosen. They were spray compacted and sintered mullite (“Cerabeads”) and crushed rock mineral Andalusite (“Kerphalite”). Both materials also allow to study effect of grain shape (compare Figure 2-7). Their grain size distribution is indicated in Figure 3-1.

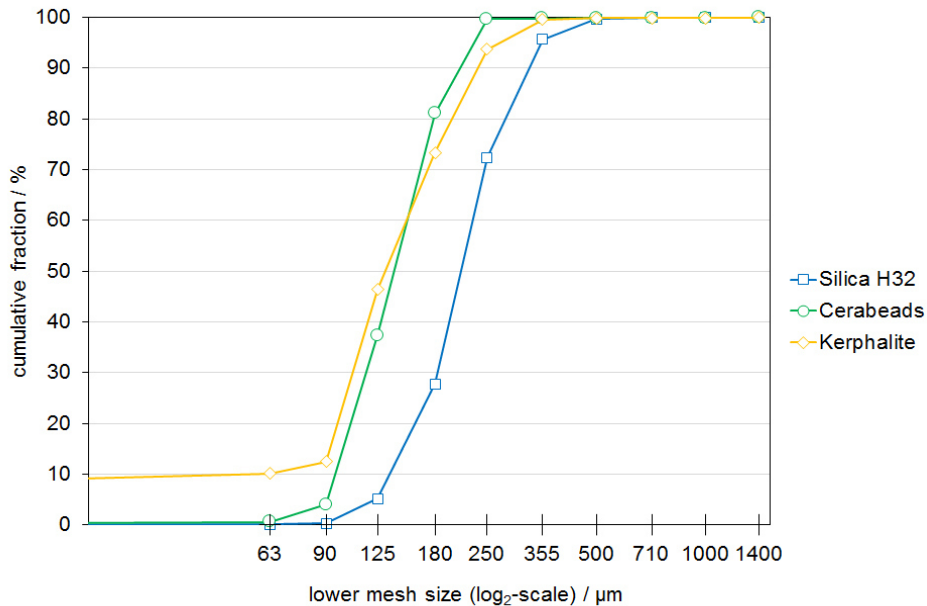


Figure 3-1: Cumulative grain size distribution arriving at a sieve of the indicated lower mesh size for the basic forming materials silica H32, Cerabeads 650 and Kerphalite. Kerphalite exhibits a high fines content of 10 % passing the 90 µm mesh. Average grain size is in the range from 125 – 200 µm. Upper grain size is limited by 0,5 mm.

Production parameters for each sample type are indicated in the respective descriptions in this chapter. Differences exist due to varying wall thickness and tooling technology.

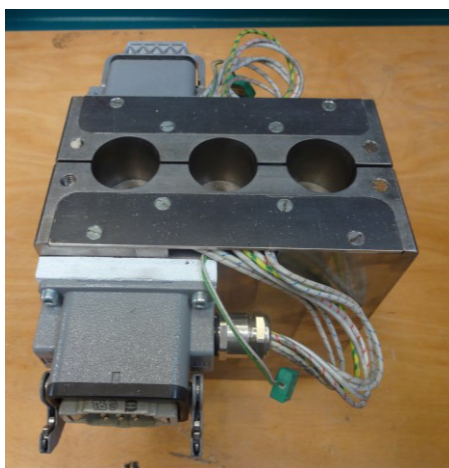
3.1.2 Core samples used for mechanical property testing

Sand core samples for mechanical property evaluation were produced at the Austrian Foundry Research Institute (OGI) on a Röper H5 core blowing machine (5 l blowing volume) using electrically heated core boxes for thermos-setting binders, and applying a gassing unit for PU-Coldbox cores, shown in Figure 3-2.



Figure 3-2: Core blowing machine of the type Röper H5 situated at the ÖGI in Leoben. (1) is a core box mounted on the machine table, (2) the gassing unit for Coldbox production and (3) a hydraulic unit for tool clamping.

The sand mixtures were prepared in 5 kg portions with at laboratory rotation stir mixer. Core blowing equipment is shown in Figure 3-3.



a



b

Figure 3-3: (a) shows the core box used for cylindrical samples and (b) the core box for bending test bars mounted on the core blowing machine [167].

Bending test bars dimensions for mechanical testing were length 180 mm (150 mm measurement section) and quadratic cross section of 22,7 mm side length. Cylindrical sample dimensions were diameter 35 mm and a 1:1 diameter to height ratio.

Berbic (2017) documented the sample production parameters in all details [167]. The core box hardening parameters for the test samples are documented in Table 3-2.

Table 3-2: Hardening parameters for mechanical test core samples.

Binder type	Hardening parameters
Coldbox	DMEA curing for 15 s with 1,5 bars with 2,2 g/s dosing rate
Hotbox	220 °C / 45 s
Warmbox	180 °C / 45
Sodium silicate	180 °C / 30 s

3.2 Thermal pre-conditioning of core samples

Thermal pre-conditioning parameters were obtained from filling and solidification simulation of a typical four-cylinder passenger car cylinder head, cast with the Rotacast®-process [168]. For the analysed casting a steel mould and seven different sand cores were modelled. Every sand core was equipped with virtual thermo-couples in central and lateral positions. The simulated temperatures of these measurement points delivered the desired temperature curves. An example of such a core and evaluated measurement points is shown in Figure 3-4.

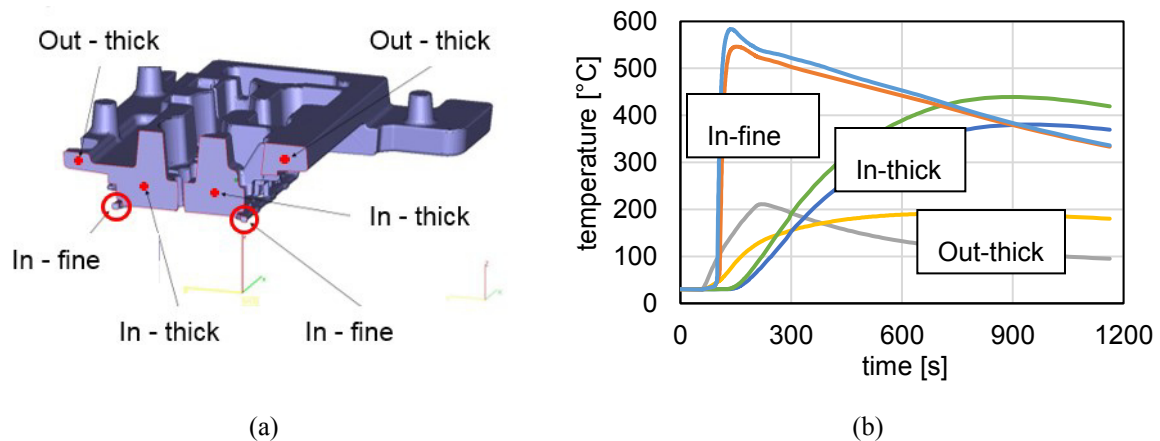


Figure 3-4: Sand core used for the upper part of a cylinder head casting with six analysed measurement positions, denominated with “In” for inner and “Out” for outer regions and “-fine” for thin and “-thick” for thick core sections (a) and the evaluated temperature profiles from the local virtual thermo-couples (b), based upon casting process simulation.

Inner positions are marked with “In-fine” for a typical thin core wall and “In-thick” for a thick one, in the same sense “Out-thick” is indicated for comparison.

For every temperature curve the individual exposure time above the maximum achieved level in 100 °C steps was evaluated.

Based on this information the typical holding time for the sand core sample pre-conditioning at every temperature step could be defined and is shown in Table 3-3, and Figure 3-5, respectively.

Temperature / °C	holding time / min
200 (+/- 5)	60
300 (+/- 5)	30
400 (+/- 5)	10
500 (+/- 5)	5

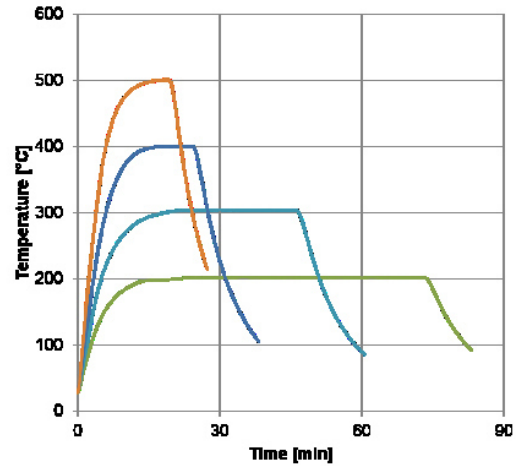


Table 3-3: Defined isothermal holding time for sand core sample thermal pre-conditioning.

Figure 3-5: Temperature profiles applied for the sand core tempering measured in test cores [167].

The pre-conditioning was chosen in two ways: in air and sealed, without air exchange. The conditioning in air served as reference. The sealed condition was chosen to evaluate the effect of a reduced oxygen offer, which approximates the situation of cast-in sand cores. During ongoing pyrolysis an intrinsic gas pressure and a changed atmosphere but reduced oxygen concentration occurs. Figure 3-6 shows bending test bars prepared for thermal pre-conditioning with air exchange (a) and under sealed conditions (b) and (c). This process was similarly executed with cylindrical samples.

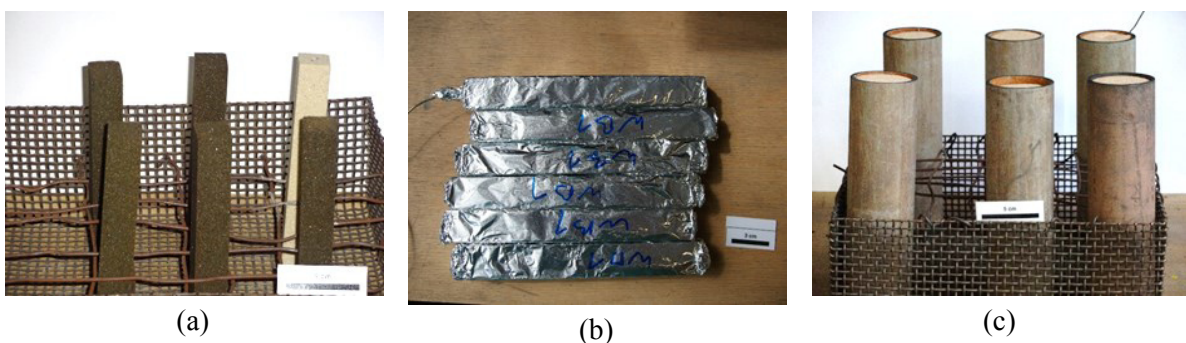


Figure 3-6: Thermal pre-conditioning of bending test samples. (a): oxidizing condition, (b): preparation of sealed samples for reducing condition and (c): prepared treatment batch for reducing condition with samples embedded in pre-heated sand; [167].

The temperature of every pre-conditioning batch was controlled with a dedicated measurement sample with a centrally positioned thermocouple. After the pre-conditioning time was finished, the samples cooled down in calm air. The sealed samples were taken out of the embedding sand immediately at the end of the conditioning time and de-wrapped in cold condition.

3.3 Mechanical property testing

Bending, compression, double shear and tensile test data were acquired applying the standard test equipment for sand core testing illustrated in Figure 3-7.

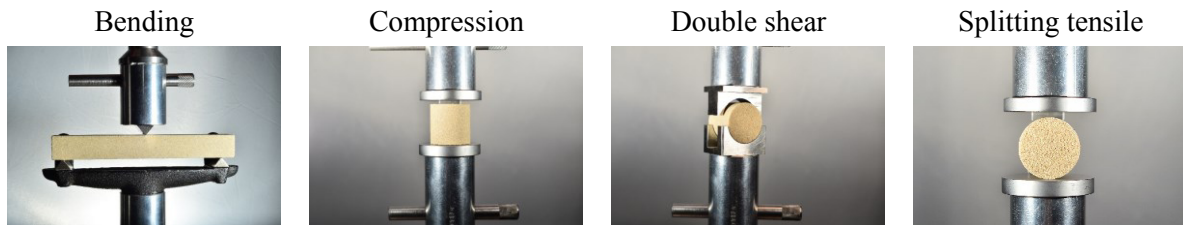


Figure 3-7: Test types applied for mechanical property assessment [167].

A universal testing machine Zwick Z005 (max 5 kN), according to publications from the Austrian Foundry Institute, OGI [169], [170], and a larger Zwick Z050 (max 50 kN) for higher loads were applied. All mechanical property testing was executed at the OGI in Leoben.

In the frame of this thesis an enhanced bending test evaluation method was developed and is documented in section 4.1, [171]. Summarized, by analysis of load-deflection curves besides the strength information also core brittleness and stiffness characteristics can be obtained.

For tensile testing a dog-bone shaped specimen was evaluated. Improvements of the specimen holder to avoid early sample fracture by local contact pressures were identified and introduced during this evaluation. In addition indirect tensile tests delivered higher result stability.

Mechanical testing of sand core specimens after various thermal loading conditions was documented in the master thesis of Berbic (2017), [167]. The results, showing the effect of thermal pre-conditioning were presented according to the Mohr-Coulomb model using compressive strength, shear strength and indirect tensile strength values. Publication therefrom is prepared according to section 4.2, [172].

3.4 Wedge splitting tests

The wedge splitting tests were all conducted at the “Institute for ceramic materials” at the University of Leoben, including using the available loading parameters and data acquisition and evaluation techniques.

Standard WST samples

For the standard wedge splitting tests (WST) samples with outer dimensions of 75x100x100 mm³ were used. The design of an electrically heated core box and a therewith produced core sample are shown in Figure 3-8.

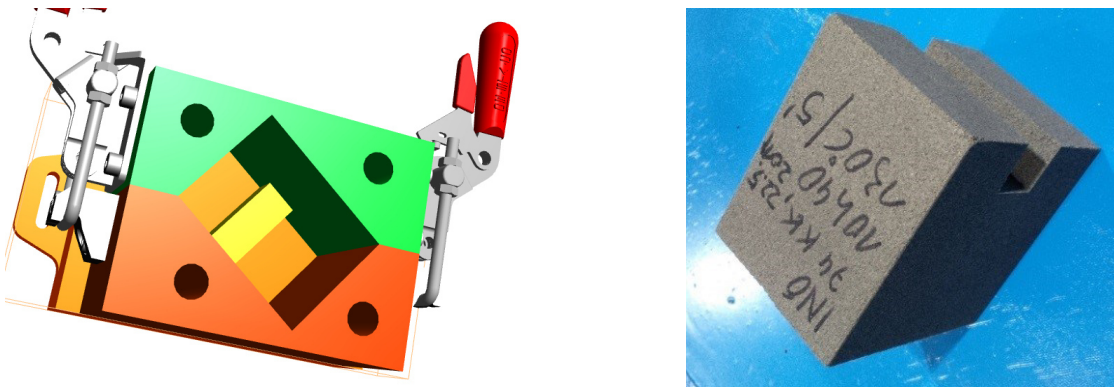


Figure 3-8 left: 3D design of the wedge split test sample core box in top view. On top of this tool is the blowing plate, which is part of the core blowing machine. Right: Sand core sample for wedge split testing.

To avoid overheating of the outer core surface and strong thermal gradients by the thermal hardening, temperature was reduced to 160 °C for Warmbox and 150 °C for sodium silicate bonded samples and the hardening time set to 5 minutes. The sodium silicate bonded cores were dried for additional 10 minutes at 120 °C after their removal from the core box.

By help additional inserts the thickness of the sample can be reduced to 50 mm or 25 mm. To produce those samples, the hardening time has to be adequately reduced. With unchanged temperatures, 2 min hardening time for 25 mm core wall thickness was found to be adequate. With thinner samples it is possible to adjust the hardening parameters similar to any practically applied value for individual sand core systems.

Miniaturized WST samples

To enable in-situ observation of wedge splitting experiments, a miniaturized sample dimension was realized [173]. The sample is designed to precisely observe the crack initiation and propagation by high resolution imaging. For the splitting test additional load transfer elements are laterally glued on the sample. During test the load displacement curves can be recorded and allow the work of fracture evaluation. The sample dimensions and a sand core specimen are shown in Figure 3-9.

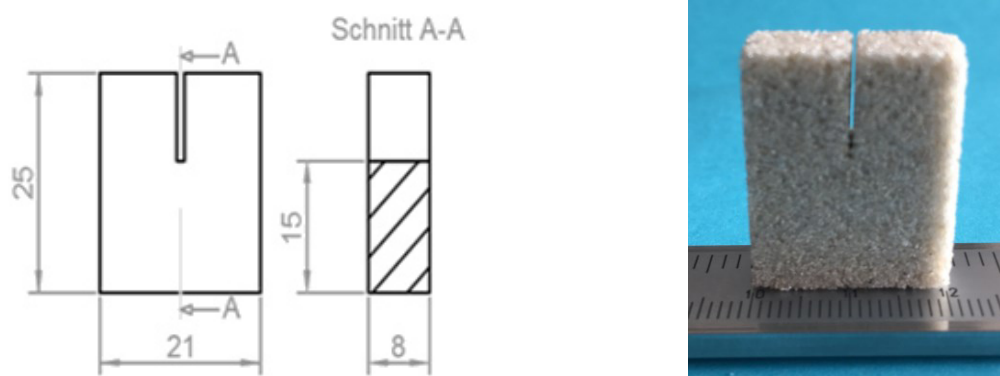


Figure 3-9: Drawing for miniaturized wedge split test specimen [173] and a first realized test core.

3.5 Core removal trials

3.5.1 Ring mould for knock-out testing

The knock-out testing, actively used at the Polish Foundry Institute (see section 2.5.7) was initially foreseen for investigations. A metallic mould with a conical shape was designed which allowed to cast in a cylindrical sample with 50 mm diameter and height. The mould has been evaluated during the master thesis of Wang (2014), who documented heating curves of several therewith cast-in core types [34].

During production of castings to evaluate the knock-out procedure it was observed that all cast in cores are damaged on their front ends due to the Al-shrinkage, independent of the used core type. In case of organic Warmbox bonded samples, the cast-in cores even slipped out of the casting which was due to thermal damage of the surface sand layer. As consequence of these preliminary results the knock-out testing was not pursued any more.

3.5.2 Core removal wedge sample

The samples for core removal trials were produced with a *Röper H1 – 11* core blowing machine at Nemak Linz, having the same principal construction compared to the *H5* machine used at the OGI, except the gassing equipment for PU-Coldbox curing. The test core dimensions are shown in Figure 3-10.

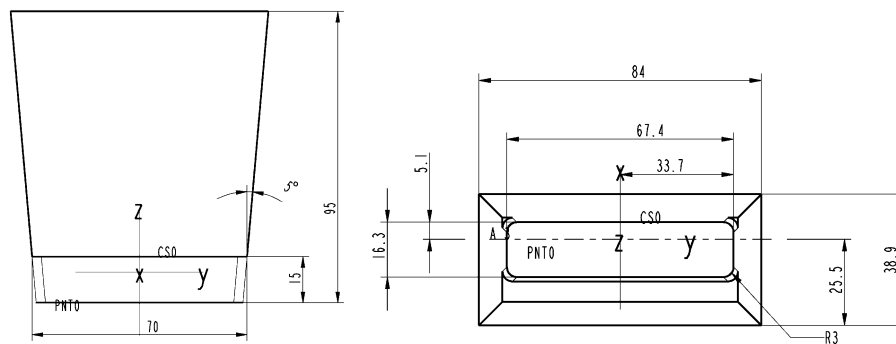


Figure 3-10: (a): Test core main dimensions. The asymmetric core print allows wall thickness variation in the mould by rotation of the core. The increase of width and core thickness along the core height is 14 mm.

The sand core hardening parameters were set to 2 minutes hardening time and a temperature of 180 °C for Warmbox and 160 °C for sodium silicate cores. The core take-out time was 10 s due to the required partial core box disassembly. After removal from the core box the silicate bonded sand cores

were additionally dried in a chamber furnace with 120 °C for 5 – 10 minutes. The core box and a produced test core are shown in Figure 3-11.

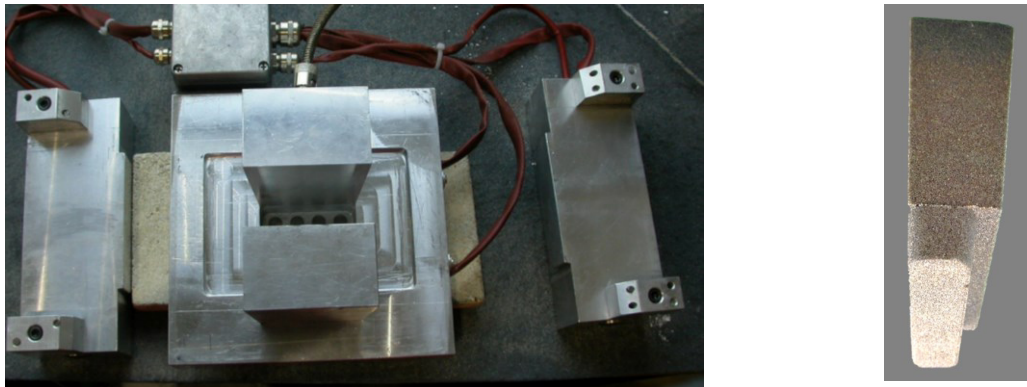


Figure 3-11: The core box for the core removal test cores with opened side parts (left) and a therewith realized sand core (right).

The test casting using this removal test core is performed using a steel mould setup. The test core is positioned on a mould base plate and the outer shape of the test casting is moulded by a steel part. The trial evaluation of this casting setup and the core removal trials was described in the results section 4.3. Figure 3-12 shows the testing setup schematically and during the casting process.

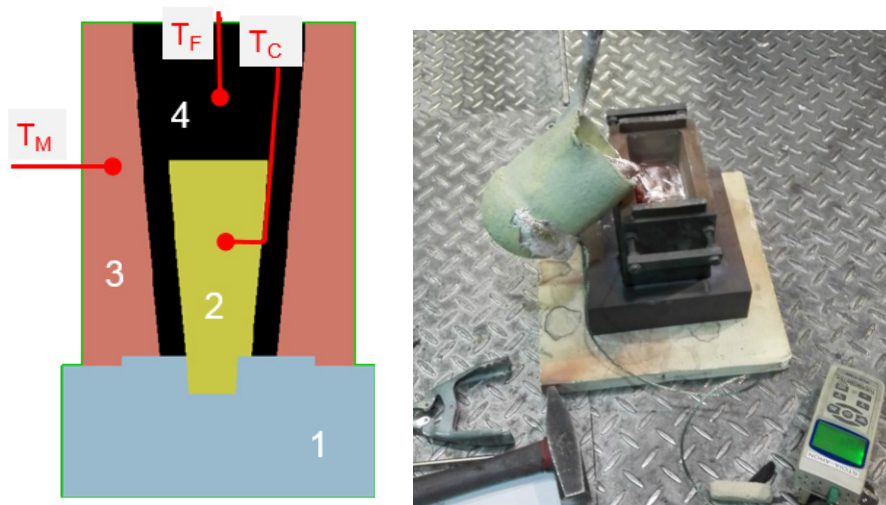


Figure 3-12 left: Schematic cross section through the mould setup consisting of (1) a base plate, (2) a core, and (3) the upper mould part. The casting is formed in the cavity (4). The thermocouple positions are: T_M in the mould, T_C in the core centre, and T_F in the feeder centre. Right: Casting of a test part.

The different cooling processes of the castings were measured in the casting feeder and the core centres.

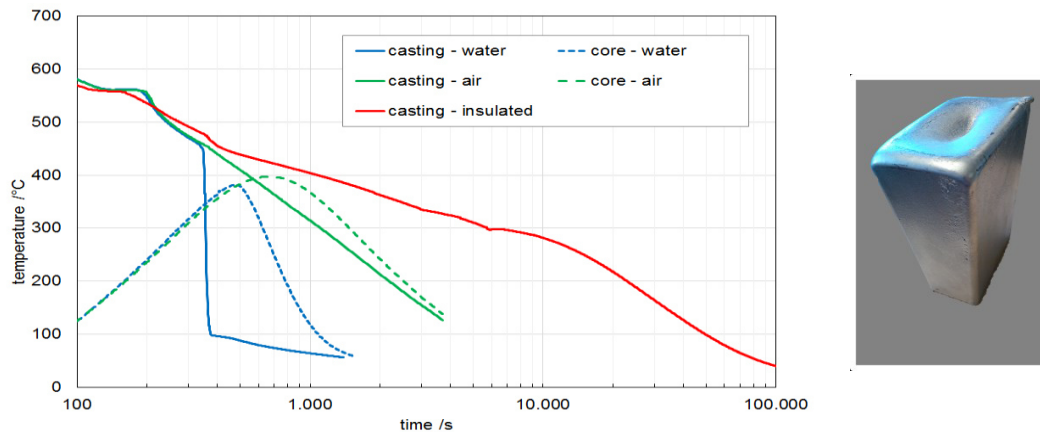


Figure 3-13: temperature curves of the cast in cores and the feeder temperatures with the cooling methods on air, in water and insulated (without core temperature), starting 100 s after pouring start. The simple wedge shaped cast part is shown to the right hand side.

The delayed heating of the sand cores and limited cooling at the water cooling type is obvious. Significantly different thermal exposure intensities could be realized with this setup.

3.5.3 Equipment for core removal testing

For core removal experiments a vibratory device and a hammering station were applied. In the framework of the internal study from [174], acceleration measurements were conducted to characterize the devices. In addition the experimental setup consisting of the core removal equipment, an in-line attached electronic scale and the data-acquisition were introduced. The developed evaluation method was published [175], as included in the results section 4.3.

3.5.3.1 Vibratory core removal equipment

The sample was clamped into the vertically sliding sample holder (Figure 3-14), which was fixed in the vibration device. The effect on the vibration device was evaluated by acceleration measurements, which were documented by Wurm (2016), [174].

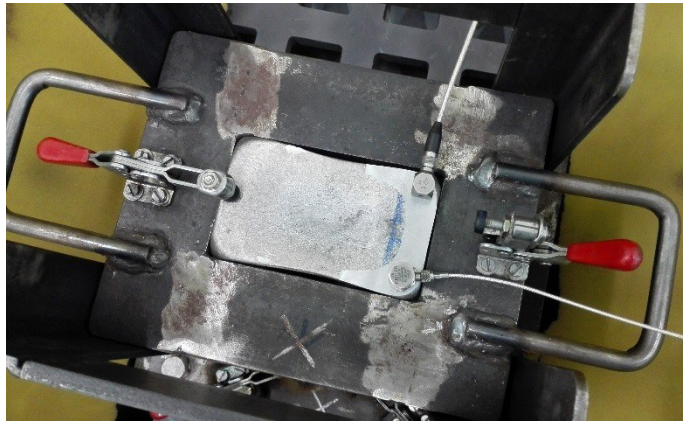


Figure 3-14: Top view on test casting clamped in the sliding sample holder with attached vibration measurement sensors [174]. The sample holder guidance and the base grid of the vibration device can be seen, also.

3.5.3.2 Sand mass data acquisition

An electronic scale type *Kern PBJ 6200 2M* with 0,1 g precision and 0,01 g readability was used for sand mass acquisition. At the vibration device the scale was placed below the hopper outlet on damping plates. Data were transmitted with 1 Hz to the data acquisition software *DASYLab* version 11.

3.5.3.3 Hammering core removal equipment

A hammering station, also used for industrial core removal of cylinder heads, was applied for hammering tests. The hammering station was set to a 2 s hammering interval. Effectively by acceleration measurements a slope in and fade out was observed with a total time of 2,5 – 2,6 s. The sand mass was evaluated manually after each interval. In Figure 3-15 the equipment is overviewed.

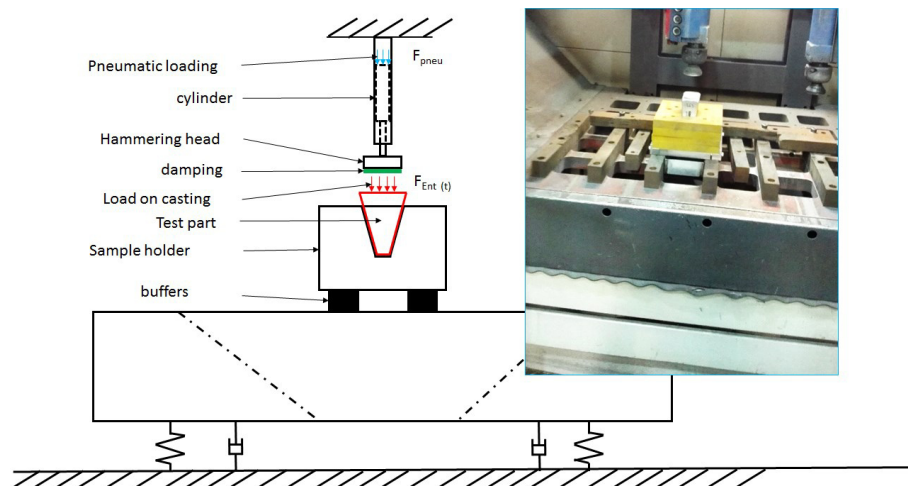


Figure 3-15: Schematic description of the pneumatic hammer used for core removal [174]. The PP-sample holder and upper part of test casting are put on the core removal station. Below the sample holder the sand collecting tray is positioned.

To limit maximum acceleration additional damping was realized by rubber plates on the hammering heads. Various acceleration measurements using the setup shown in Figure 3-14 and Figure 3-15 have

been conducted to characterize the testing setup in multiple functional modes. In Figure 3-16 a comparison between the vibration unit and the hammer station is shown.

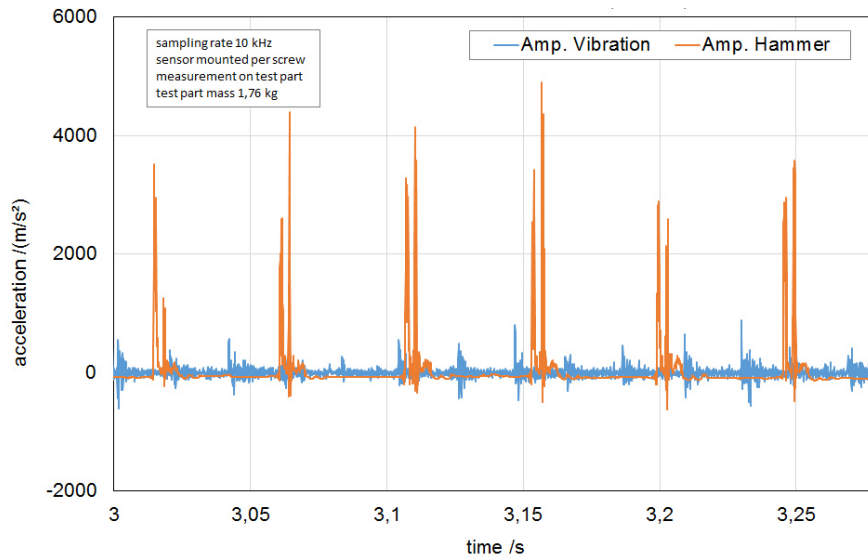


Figure 3-16: Vertical acceleration measured on the sample positioned in the vibration device and in the hammer station including a rubber damping on the hammer head [174] measured over a period of 0,25 s.

The 20 Hz knocking frequency of the hammer as well as the 50 Hz agitation of the vibration device is reflected in the graphs. The maximum acceleration of the vibration device is limited with 400 m/s², whereas 5000 m/s² were measured during hammering. At technical implementation higher accelerations are acting which requires a high investment into the adequate measurement equipment.

4 Results

The results were published and re-prints of the publications are presented following their content depending relationship. The published results are listed in Table 4-1:

Table 4-1: List of resulting publications from this thesis.

Publication	Reference
Stauder, B. J.; Kerber, H.; Schumacher, P. (2016). Foundry sand core property assessment by 3-point bending test evaluation, <i>Journal of Materials Processing Technology</i> , Vol. 237, 188–196. doi:10.1016/j.jmatprotec.2016.06.010	[171]
Stauder, B. J.; Berbic, M.; Schumacher, P. (accepted for review in July 2018). Mohr-Coulomb failure criterion from unidirectional mechanical testing of sand cores after thermal exposure, submitted to: <i>Journal of Materials Processing Technology</i> .	Acceptance for production pending
Stauder, B. J.; Harmuth, H.; Schumacher, P. (2018). De-agglomeration rate of silicate bonded sand cores during core removal, <i>Journal of Materials Processing Technology</i> , Vol. 252, 652–658. doi:10.1016/j.jmatprotec.2017.10.027	[175]
Stauder, B. J.; Gruber, D.; Schumacher, P. (2018). Specific fracture energy and de-agglomeration rate of silicate-bonded foundry sand cores, <i>Production Engineering</i> , 10. doi:https://doi.org/10.1007/s11740-018-0854-8	[176]
Stauder, B. J.; Schumacher, P.; Harmuth, H. (2017). Core removal behaviour of silicate bonded foundry sand cores, <i>International Conference on Frontiers in Materials Processing, Applications, Research & Technology - FIMPART'17</i> , Springer, Bordeaux, 6	[177] Production pending

4.1 Foundry core property assessment by 3-point bending test

Authors	B.J. Stauder (Nemak Linz); H. Kerber (ÖGI); P. Schumacher (MUL)
Journal	Elsevier - Journal of Materials Processing Technology DOI: 10.1016/j.jmatprotec.2016.06.010 © 2016 Elsevier B.V. All rights reserved.
Individual author contributions	70 %: B.J. Stauder: sample planning; evaluation method; corresponding author; Presentation at 56 th int. foundry conference in Portoroz, SLO, Sept. 2016. 20 %: H. Kerber: bending tests and load data acquisition. 10 %: P. Schumacher: scientific context.

Abstract

Improved understanding of foundry sand core properties is a key requirement for high precision casting process development. The present work demonstrates the potential to evaluate mechanical and functional sand core properties using precisely acquired 3-point bending test load curve data applying standard bending test geometries.

Four organic binder systems have been investigated. Further to bending strength and the elastic modulus, which can be directly derived from the load curves, a load curve pre-treatment to eliminate sample settlement effects was applied for a corrected deflection and stiffness analysis. The consumed mechanical work shows characteristic elastic and plastic work portions until fracture, which are specific for different sand cores, respectively their condition. Dimensionless indicators to quantify core brittleness have been developed based on curve and on work parameters.

In general for mechanical evaluations of resin bonded sand cores, visco-plastic effects need to be considered, as for not fully hardened binder systems decreased strength, deflection and work of fracture were observed at lower load speeds.

The benchmark results show that the load curve evaluation concept is a suitable tool to analyse foundry sand core properties more sensitively.



Foundry sand core property assessment by 3-point bending test evaluation



Bernhard J. Stauder^{a,*}, Hubert Kerber^b, Peter Schumacher^c

^a Nemak Linz GmbH, A-4030 Linz, Zeppelinstraße 24, Austria

^b Austrian Foundry Research Institute—ÖGI, A-8700 Leoben, Parkstraße 21, Austria

^c Montanuniversität Leoben, Chair of Casting Research, A-8700 Leoben, Franz-Josef-Str. 18, Austria

ARTICLE INFO

Article history:

Received 25 September 2015

Received in revised form 1 June 2016

Accepted 4 June 2016

Keywords:

Casting

Sand core testing

Load curve evaluation

Work of fracture

Core deformation

Quality control

ABSTRACT

Improved understanding of foundry sand core properties is a key requirement for high precision casting process development. The present work demonstrates the potential to evaluate mechanical and functional sand core properties using precisely acquired 3-point bending test load curve data applying standard bending test geometries.

Four organic binder systems have been investigated. Further to bending strength and the elastic modulus, which can be directly derived from the load curves, a load curve pre-treatment to eliminate sample settlement effects was applied for a corrected deflection and stiffness analysis. The consumed mechanical work shows characteristic elastic and plastic work portions until fracture, which are specific for different sand cores, respectively their condition. Dimensionless indicators to quantify core brittleness have been developed based on curve and on work parameters.

In general for mechanical evaluations of resin bonded sand cores, visco-plastic effects need to be considered, as for not fully hardened binder systems decreased strength, deflection and work of fracture were observed at lower load speeds.

The benchmark results show that the load curve evaluation concept is a suitable tool to analyse foundry sand core properties more sensitively.

© 2016 Elsevier B.V. All rights reserved.

1. Introduction

Metal casting using sand cores allows to produce complex components with internal geometries in high volumes, typical examples are combustion engine cylinder heads and blocks. Fig. 1 shows a cylinder head casting from Al and the required sand cores for the internal surfaces, while in Fig. 2 a preassembled sand core package is shown prior to casting.

The influence of technology, materials and process parameters on dimensional accuracy of near-net-shaped casting products has been systematically compiled by Campbell (2000). The foundry industry is forced to steadily improve process capabilities to facilitate light-weight, respectively thin walled castings, to contribute to ever tightening emission legislation requirements (Lellig et al., 2010). The importance of sand core technology development is highlighted.

1.1. Foundry sand core technology and developments

The development of new binder systems, such as chemically bonded sand cores was intensively characterized by Bindernagel (1983). A comprehensive collection of sand and binder systems was given by Flemming and Tilch (1993). Mechanical properties of sand cores are mainly qualitatively described and no property related material laws are proposed.

In automotive foundries the most widely applied core manufacturing processes are the organic Coldbox, Warmbox, and Hotbox core production processes. Process descriptions are given by Langer and Dunnivant (2011) and Brown (2010). Currently a substitution process of organic by inorganic binders having less odour development is ongoing. However, because of different properties, process relationships for such new binder types require increased attention on the process control (Weissenbek et al., 2011). Recently Czerwinski et al. (2015) reviewed the state of the art of foundry core technology for several relevant organic and inorganic binder systems used in various foundry applications.

Summarized, fundamental requirements into sand core properties are:

* Corresponding author.

E-mail addresses: bernhard.stauder@nemak.com, bernhard.stauder@aon.at (B.J. Stauder).

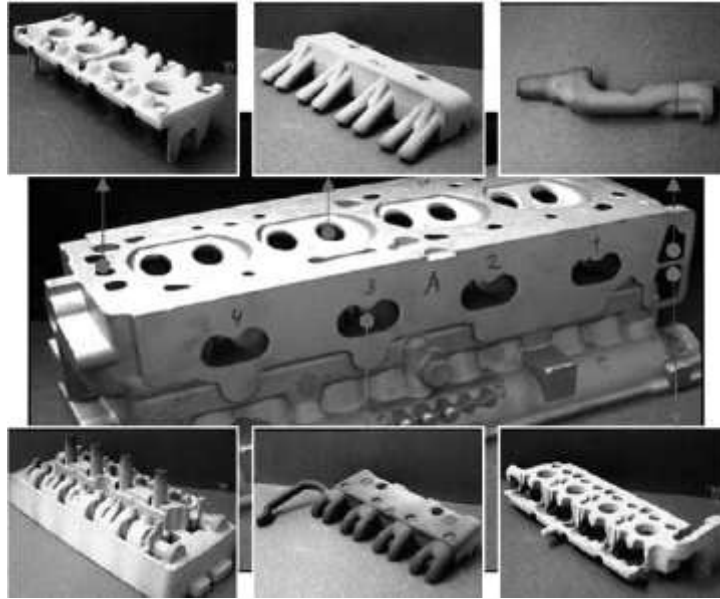


Fig. 1. Illustration of a medium complexity car cylinder head in cast Al and the required sand cores to shape its cavities (Sobczyk, 2008).

- Sufficient strength to allow handling and manipulation operations;
- High resistance against humidity during core storage.
- High erosion and penetration resistance and no chemical interaction with the cast metal to deliver a good casting surface quality.
- Low gas evolution and high gas permeability to avoid casting defects.
- High bending strength: bending is the most critical load type for sand cores under casting conditions. It can be imposed by clamping forces, thermal load, flow drag and buoyancy loads.
- Easy shake-out after casting to obtain sand-free cast parts.
- A good recycling ability of used foundry sand.
- Environmentally friendly core systems with low odour development.

1.2. Research on sand cores under thermal load

Generally only little research on sand core behaviour under casting conditions can be found in the literature. Some examples of foundry sand core investigations under realistic loading conditions and the applied types of modelling data are given here.

The deformation of a complex cylinder head water-jacket core has been studied by Dong et al. (2010). Their used material data were based upon bending tests and upon validations using a cup type core for casting trials. Critical regions in the casting due to core bending could be predicted. Motoyama et al. (2013) investigated residual stresses of castings influenced by counter forces from furanic moulds applying specifically developed in-situ measurement of the transmitted loads. The material properties for modelling were obtained by compressive tests.

Stachowicz et al. (2011) have described cohesive and adhesive fracture mechanisms of inorganically bonded cores. Even sand grain cracking was observed, but not below a thermal load of 1100 °C. High temperature bending tests to describe the properties of a novel starch binder for foundries were performed by Zhou et al. (2009). They observed sand core damage through binder cracking and delamination.



Fig. 2. Sand core package for an intricately shaped cylinder head prepared for casting by the Rotacast process (Gosch and Stika, 2005).

1.3. Testing of sand cores and other bonded granular materials

Testing methods for foundry sand cores and other relevant material types with low plastic deformation will be discussed in the following.

Within the foundry industry the standards of sand core testing were established in the middle of the last century, as documented by American Foundrymen's Society – AFS – (Dieter, 1950). Bending tests are the most widely applied quality control for foundry sand cores, described by AFS (1962) and similarly by the German standard (VDG, 1999). In both, no load curve acquisition is required and the beam deflection can be manually driven. The loading velocity is not quantified, but should be constant and smoothly applied. The bending strength is calculated from the maximum load based upon linear elastic continuum mechanical relations.

To enable sand core deformation studies additional information from load-deflection curves is required. (Kerber et al., 2014) reviewed the conventional testing methods and standards

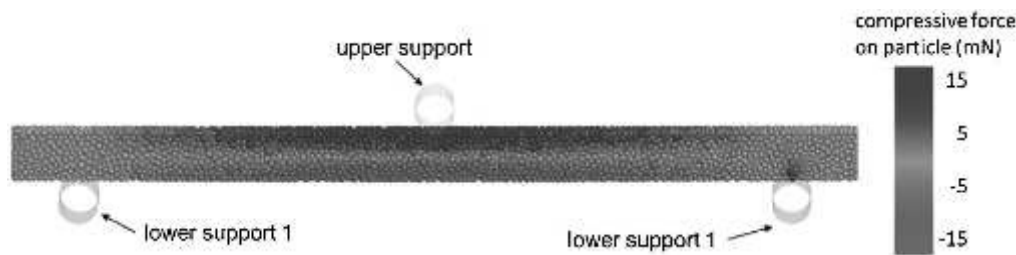


Fig. 3. Tensile and compressive forces on particles during 3-point bending (Wolff et al., 2013).

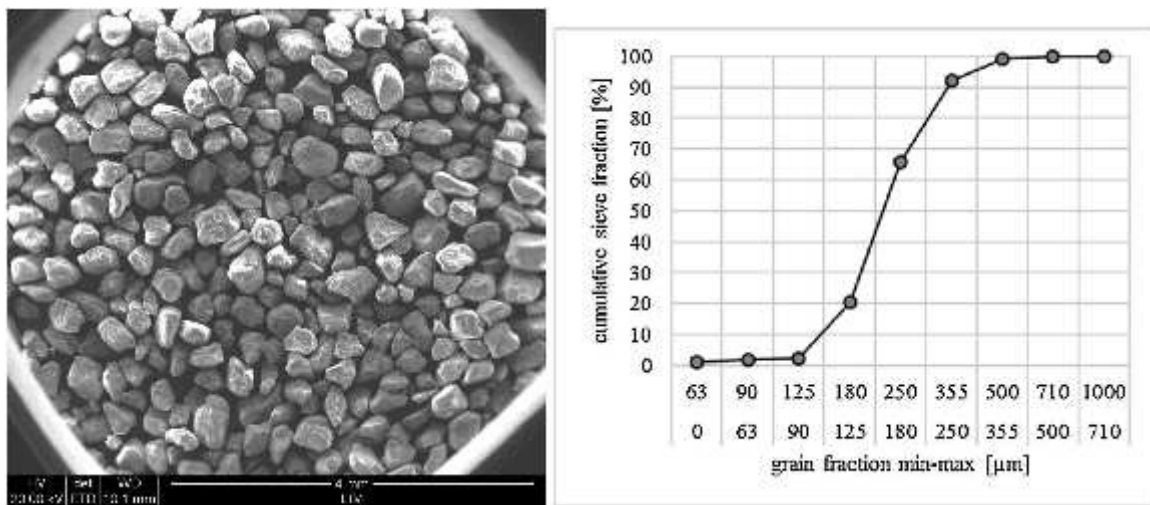


Fig. 4. Sand grain morphology of the used H32 silica sand and the according sieve analysis.

Table 1

Used binder systems for the experiments and main hardening parameters.

Binder System	Mixture ratios	Hardening parameters
Coldbox (CB)	Phenolic resin and isocyanate solution in 1:1 ratio. Di-Methyl-Ethyl-Amine (DMEA)	DMEA vapour gassing 15 s
Hotbox (HB)	Phenol formaldehyde resin and aqueous ammonium nitrate solution in 5:1 ratio.	Heated tool: 220 °C/30 s
Warmbox type 1 (WB1)	Furanic resin and aqueous phenol-sulfonic acid solution, its Al-salts and sulphuric acid in 5.5:1 ratio.	Heated tool: 220 °C/30 s
Warmbox type 2 (WB2)	Modified urea-furanic resin and aqueous phenol-sulfonic acid solution and its Al-salts in 4:1 ratio.	Heated tool: 220 °C/30 s

for foundry sand cores. They demonstrated the improvement potentials by applying modern testing technology with precise load-displacement acquisition. A load velocity of 5 mm/min has been determined to achieve comparable conditions to existing bending test practice.

Ratke and Brück (2006) analysed load displacement curves from bending and compression tests to investigate the influence of granulometry and binder content on silica-Aerogel bond composites. Thole and Beckermann (2009) researched the deformation of phenolic-urethane no-bake self-setting cores applying three-point bending test standards from metal testing. Elastic moduli close to 4 GPa in the as-produced samples and about 1 GPa after thermal exposure were determined.

(Schacht, 2004; chap. Schacht&Hayes, Silica brick material properties) described the load-displacement curve evaluation for compression tests on refractory silica bricks. The relation between the maximum slope tangent and the secant from zero to the maximum load point was presented as a suitable criteria to describe plasticity. (Schacht, 2004; chap. Bradt, Fracture of Refractories)

pointed out the limitation of using linear continuum mechanics for bonded granular materials when having plasticity. Improvements were shown by Wolff et al. (2013), applying “Discrete Element Method (DEM)” – simulations for a ceramic-polymer composite material under different bending test conditions. For small loads they have shown that visco-elastic effects could be neglected for the used acrylic binder. Moreover, initial settling against the load points are important and must be considered. They illustrated the performance of DEM simulations to investigate bonded particle compounds. A three-point bending DEM-setup is shown in Fig. 3.

Tarokh and Fakhimi (2014) compared measured and simulated bending test curves of silt stones. A satisfyingly good agreement was given identifying the initial deformation of the physical specimen. The early portion of the curve was influenced by closure of the space between the specimen and the loading platen and furthermore a postulated closure of micro-cracks in the specimen.

Further to load curves, the introduced work into the sample can be analysed also. Rice (1968) presented the “J-integral”-method to describe crack tip plasticity. An adoption of that principle will

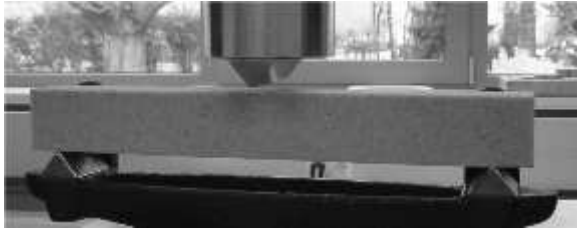


Fig. 5. Foundry sand core sample at bending test. The three supports are line supports with a top radius of 3 mm according to the German Foundrymen's Standards.

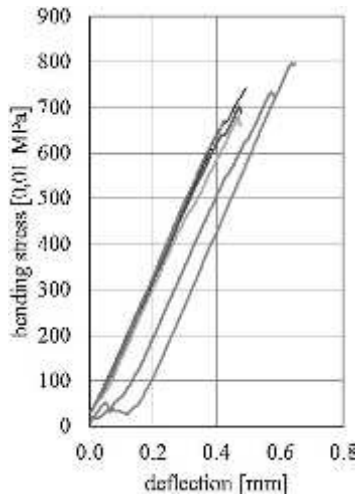


Fig. 6. Untreated high resolution stress – deflection curves. Core binder WB1 tested after 4 h storage time.

be used in this work. The goal is to quantify the introduced work from the testing machine and evaluate the elastic and plastic work portions.

2. Experimental methods

2.1. Used materials

The sand used for all samples was silica sand “H32” according to the technical datasheet (Quarzwerke, 2009), being a widely used reference for binder testing purposes. Fig. 4 shows its grain morphology and the grain size distribution.

Experiments are based upon one sand type and four different organic binder additions ranging from 1.2–1.9 wt.%. Table 1 defines the used binder systems and the hardening parameters, which are similar to typical serial applications used for Al-castings.

2.2. Sample production

The sand-binder mixtures were prepared in 5 kg batches using a laboratory stir mixer and then immediately used for core production. A conventional 51 core blowing machine (Roeper H5) and a core box for three test bars per shot according to (VDG, 1974) were used. The effectively obtained test bar dimensions were $22,7 \times 22,7 \times 180 \text{ mm}^3$. The samples were stored and tested in standard room conditions with 30–50% relative humidity.

Bending tests were conducted after storage times of 0, 1, 4 and 24 h. The storage times were chosen as they are representative for high volume engine casting production. The “0 h”-condition

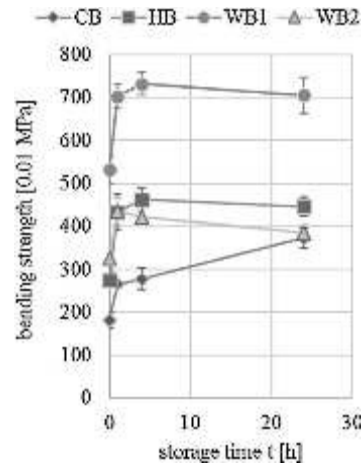


Fig. 7. Bending strength results for all tested cores over storage time.

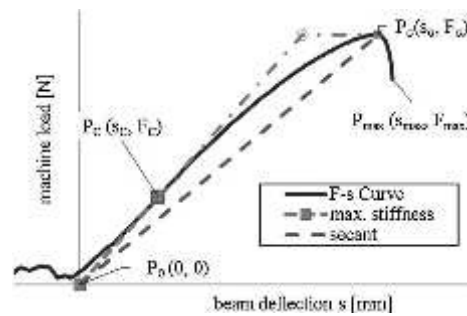


Fig. 8. Illustration of the load curve settlement correction pre-treatment method based upon the maximum stiffness tangent. Additionally the secant to the maximum strength is indicated.

describes the handling strength of the sand cores, which is important for their first manipulation after the core production. Testing was performed 5 min after core production. The results after 1 and 24 h represent the core properties at the beginning and end of a typical core usage in foundry practice.

Mean values and standard deviations were determined for a minimum of three samples.

2.3. Three-point-bending-tests

The bending tests were performed on a 5 kN universal testing machine (Zwick.Roell, 2015) with a precise load-displacement measurement. A load velocity of 5 mm/min and a data acquisition rate of 10 Hz were set for the benchmarking.

The lower support distance l is 150 mm and the cross section side length a is 22.7 mm. The bending stress calculation from the measured load F [N] according to continuum mechanics is shown by Eq. (1).

$$\sigma = F \times \frac{3l}{2a^3} \quad (1)$$

A three-point bending test sample put on the machine supports according to the VDG-testing standard is shown in Fig. 5.

3. Results

The result section is structured to show the novel data acquisition and the subsequent evaluation method leading to evaluation

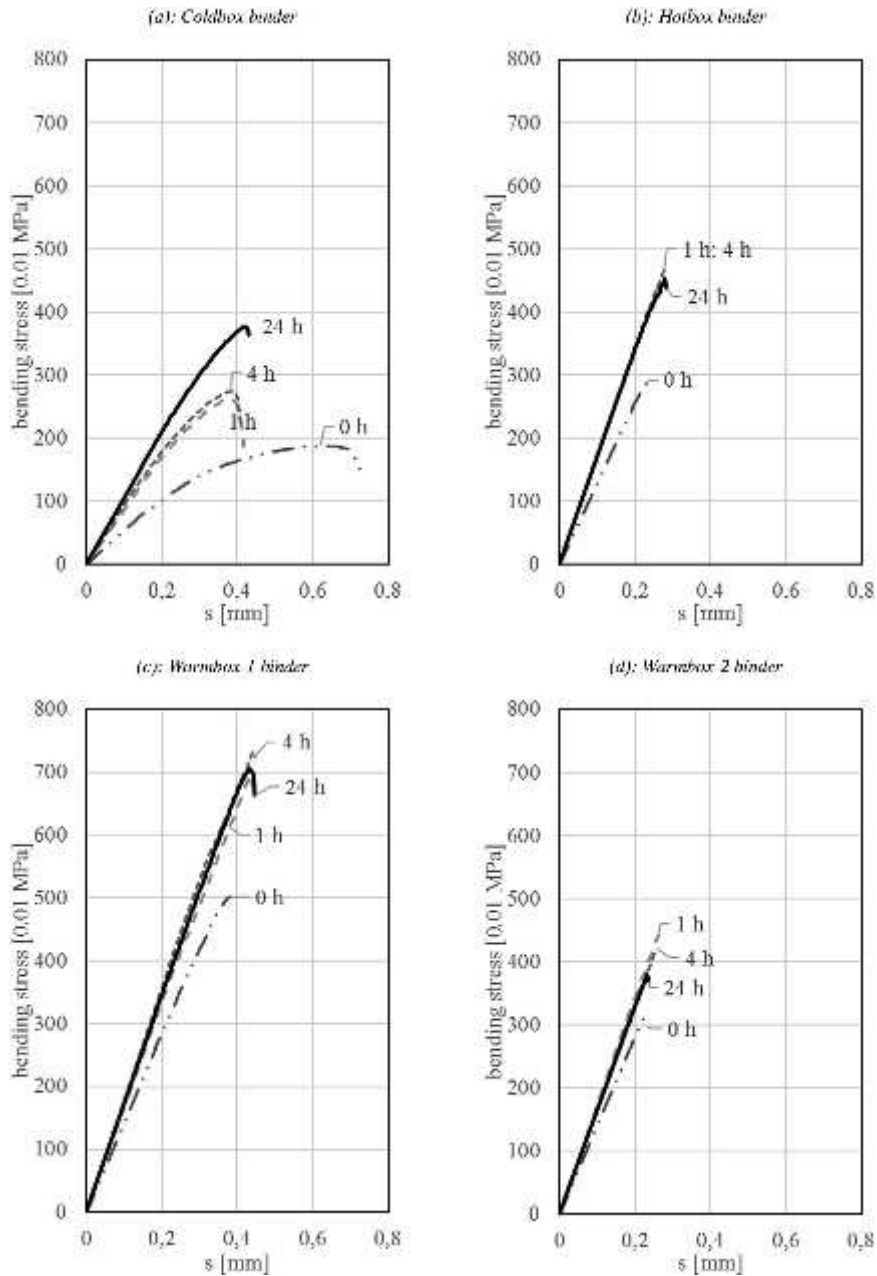


Fig. 9. Bending stress curves as function of beam deflection after 0h, 1h, 4h and 24h storage time. The binder systems are: (a): Coldbox–CB; (b): Hotbox–HB; (c): Warmbox-1–WB1; (d): Warmbox-2–WB2.

of the sample brittleness. A final sequence will show the influence of load velocity on the properties.

3.1. Data acquisition and bending strength evaluation

A typical example of acquired load curves is shown in Fig. 6 (WB1 binder system after 4 h storage time). The acquired bending strength results are visualized for all tested conditions in Fig. 7.

The different curve onsets in Fig. 6 are caused by settlement effects at the start of loading. However, the inclining curve shape is similar for all tested samples, and highly linear. Some irregular-

ities due to the granular nature of the sand cores can be observed. Sample fracture occurs spontaneously after reaching the maximum strength.

From Fig. 7 it can be seen, that HB- and WB-cores reach their maximum bending strength at 1–4 h. After 24 h of storage, the bending strength of WB1- and HB-cores is decreased by about 3%, and for WB2-cores more significant, by 12%. The effect is generally associated to humidity take-up after the samples are cooled down, leading to softened bonds.

In contrast to that, CB cores show much lower bending strength but a continuous increase over time due to ongoing polymerisation.

Table 2
Bending strength average values and standard deviation.

t [h]	CB			HB			WB1			WB2		
	σ_B [0.01 MPa]	s	s/ σ_B [%]	σ_B [0.01 MPa]	s	s/ σ_B [%]	σ_B [0.01 MPa]	s	s/ σ_B [%]	σ_B [0.01 MPa]	s	s/ σ_B [%]
0	182	18.9	10	275	16.5	6	532	32.6	6	326	22.3	7
1	265	9.7	4	434	41.6	10	703	27.7	4	435	30.6	7
4	278	24.2	9	462	27.6	6	732	25.4	3	421	12.0	3
24	372	22.6	6	446	21.7	5	705	42.1	6	385	17.9	5

However, after 24 h the strength of CB cores is only similar to that of WB2. A summary of the bending strength results is presented by Table 2, including absolute and relative standard deviations.

The typical standard deviation is 6% of the bending strength. Testing 10 samples for CB and HB-cores at the 24 h storage condition could confirm this typical scatter.

3.2. Load curve stiffness and deformation

To permit further evaluations, a load curve pre-treatment to eliminate the observed initial settling effects is required. Characteristic curve points are the point of maximum strength P_σ with the condition $\frac{d\sigma}{ds} = 0$, the point of maximum stiffness P_C with the condition $\frac{d^2\sigma}{ds^2} = 0$ and the curve end point P_{max} . The load curve correction is conducted by shifting the curve with the intersection of the maximum stiffness tangent through P_C and the horizontal axis through the origin (Fig. 8).

Typical pre-treated load-deformation curves for all binder systems with one representative example for each storage time (0/1/4/24 h) are shown in Fig. 9(a–d).

Generally, the CB-system shows a pronounced curvature and a lower stiffness compared to all other hot hardening systems. The curves for CB also show a distinct time dependency of the load-deflection curve shape up to 24 h storage time. All hot setting systems show a rather linear loading characteristic. Their stiffness is comparable and unchanged from 1 h storage time onward, despite their different bending strength levels.

Quantitative curve parameters are deflection at maximum load and the compliance (compare Fig. 8). In the initial load phase the introduced work is elastically stored in the sample volume. It is postulated that until P_C is reached no fracture energy is consumed. Based upon linear elastic continuum mechanical relations the elastic modulus can be evaluated using the maximum stiffness $C_{max} = \frac{F_C}{s_C}$ according to Eq. (2):

$$E = \frac{\sigma_b}{\epsilon} = \frac{l^3}{4a^4} C_{max} \quad (2)$$

Fig. 10 shows beam deflection results at the maximum load level (s_σ) and Fig. 11 the elastic modulus results.

Beam deflection from pre-treated load-curves can be used as a first indicator for core deformability. For hot hardening systems the deflection results are significantly below that of CB-cores, except for WB1-cores, developing the highest strength.

Interestingly, the elastic moduli of the different HB- and WB-systems are very similar to each other. After 1 h storage time E is about 2.7 GPa. The CB-cores exhibit about 30–50% lower elastic moduli. After 24 h the CB-samples obtained a level of 1.7 GPa. All systems exhibited 20% lower values at the 0 h condition compared to the 1 h results. This, combined with initially higher deformability underlines the importance of proper handling and storage conditions for newly produced sand cores.

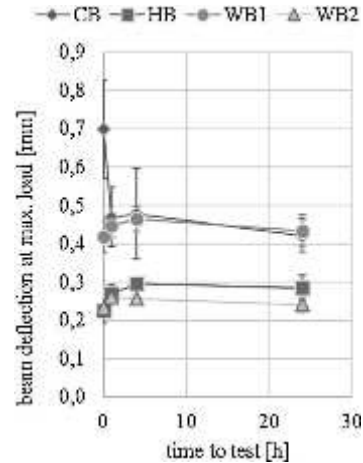


Fig. 10. Total beam deflection results for all tested cores over storage time.

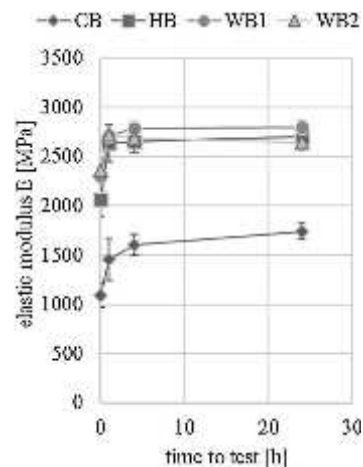


Fig. 11. Elastic modulus results for all tested cores over storage time.

3.3. Mechanical work evaluations

The totally introduced work W_M into the testing setup is displayed by the area below the untreated load-displacement curve. In Fig. 12 an exemplary pre-treated load curve is shown. The characteristic points and the distinguishable elastic and plastic work areas I, II, III and IV are illustrated.

Work area I (W_{pl}^i : initial plastic work) defines the area above the maximum stiffness tangent (P_0 to P_C) and the load curve. This area is dedicated to settlement effects of the sample towards the supports. This work portion is not contributing to the sample fracture.

Work area II (W_{pl}^σ : plastic work until max. stress) defines the area between the corrected load curve and the linear incline to P_σ

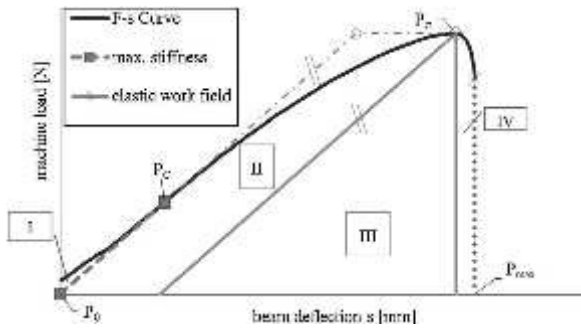


Fig. 12. Graphical definition of the regions I–IV used for the mechanical work evaluation upon an exemplary bending test stress-deflection curve.

with the maximum stiffness slope. It represents the plastic work portion until the maximum load.

Work area III (W_{el}^{σ} : elastic work until max. stress) defines the area below the maximum stiffness incline to P_{σ} and thus describes the elastic work stored in the sample volume at the maximum stress. It depends on the geometric relations and the mechanical properties. At fracture W_{el}^{σ} is released. It is transformed to fracture surface energy and into non-measured kinetic spring back energy at the moment of sample fracture.

Work area IV (W_{pl}^f : plastic work until final breakage) defines the area below the load curve from P_{σ} until sample breakage. This work portion, if measurable at all, reflects the crack propagation work. Typically for three point bending tests of rather brittle sand cores an overcritical crack propagation can be observed, resulting in very low values of W_{pl}^f .

Table 3 gives the terms for the work-regions I–IV applied to evaluate the acquired load-displacement curves.

The whole irreversible energy input is defined by the regions II and IV: $W_{pl} = W_{pl}^{\sigma} + W_{pl}^f$. The irreversible, or plastic, work acts on the highest stressed regions. Having discrete load-displacement data points from a testing machine, W_S has to be evaluated according to Eq. (3):

$$W_S = W_M - W_{pl}^i = W_{el}^{\sigma} + W_{pl} = \frac{F_C \times s_C}{2} + \sum_{s=s_C}^{s_{max}} F \Delta s \quad (3)$$

Eq. (3) shows the importance of a precise maximum stiffness point definition in order to obtain F_C and s_C properly.

In summary the entire fracture energy can only be evaluated from continuously acquired load curves until all load bearing points broke. For the given standard foundry sand core bending test setup this was not achievable due to the observed non-stable fracturing.

Fig. 13 displays the results for the mechanical work W_S of the tested core binder systems split into the different work contributions.

It can be seen, that the CB-samples consume the highest plastic work portions. They show a plastic deformability with a decreasing trend over time. For HB and WB-bond cores the majority of work is elastically stored in the sample. Moreover, a distinct final plastic work portion is not visible. Compared to HB- and WB2-cores, CB-cores present lower bending strength but exhibit higher work consumption due to significantly higher plastic work portions. This can be an advantage to avoid core breakage but also implies a higher plastic deformation risk.

The absolute numbers reflect, that the WB1 samples take up the highest total work. The second highest work consumption is given by CB-cores, with their higher plastic work portions. HB and WB2-samples show lower consumed work than CB-cores.

3.4. Sample brittleness evaluation

Two approaches, one based on load curve shape and the other on the work evaluation, to describe sand core brittleness are presented.

For the load curve approach, stiffness and deformability are correlated. As illustrated in Fig. 8, the relation between the secant stiffness $C_{sec} = \frac{F_{\sigma}}{s_{\sigma}}$ and the maximum stiffness C_{max} leads to the modulus based brittleness index B_M (Eq. (4)):

$$B_M = \frac{C_{sec}}{C_{max}} \quad (4)$$

For the work based evaluation, the elastic work (Region III in Fig. 12) related to the total work defines the work-based elasticity index B_W (Eq. (5)):

$$B_W = \frac{W_{el}^{\sigma}}{W_S} \quad (5)$$

Both, B_M and B_W , are dimensionless and independent from the absolute strength level. Results may be compared among similar

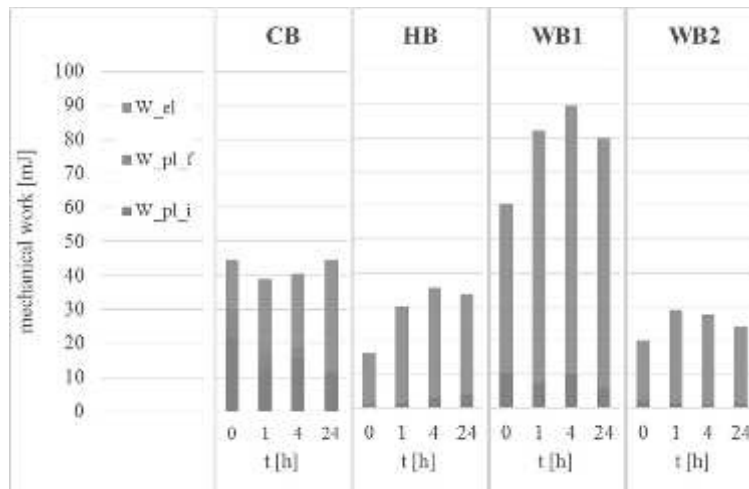


Fig. 13. Mechanical work of bending test samples. Initial and final plastic work and elastic work are separately indicated for each binder type over the storage time t.

Table 3
Mathematical definition of the mechanical work regions I–IV.

Totally introduced work by the testing machine (W_M)	$W_M = \int_0^{s_{max}} F(s) ds \approx \sum_{s=0}^{s_{max}} F \Delta s$			
Region:	I	II	III	IV
Denomination:	W_{pl}^i	W_{pl}^σ	W_{el}^σ	W_{pl}^f
Curve energy portion:	$\int_0^{s_c} F(s) ds$	$\int_{s_c}^{s_\sigma} F(s) ds$	–	$\int_{s_\sigma}^{s_{max}} F(s) ds$
Added (+) or subtracted (–) elastic energy terms:	$-\frac{F_c \cdot s_c}{2}$	$+\frac{F_c \cdot s_c}{2} - \frac{F_{max}^2}{2C_{max}}$	$+\frac{F_{max}^2}{2C_{max}}$	–
			W_S	

Table 4
Dependence of CB properties on the load velocity (low: 0.5 mm/min and high: 50 mm/min). Values are given as percentage of the 5 mm/min – reference results. Values for 0, 1 and 24 h storage time were evaluated for a minimum of 5 samples per data point.

Results in [%] of 0.5 mm/min – values	bending strength		deflection		elastic modulus		total work at fracture		mod. based br. index		work based br. index	
	Load vel.											
	low		high		low		high		low		high	
Storage time												
0 h	78	114	93	109	97	116	77	113	99	112	102	115
1 h	80	112	90	90	95	110	75	108	94	111	92	109
24 h	83	100	87	91	100	107	76	99	97	106	97	96

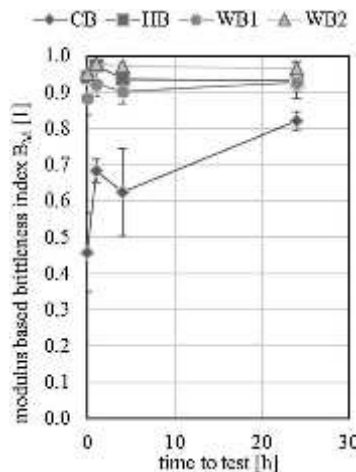


Fig. 14. Modulus based brittleness index results for all tested cores over storage time.

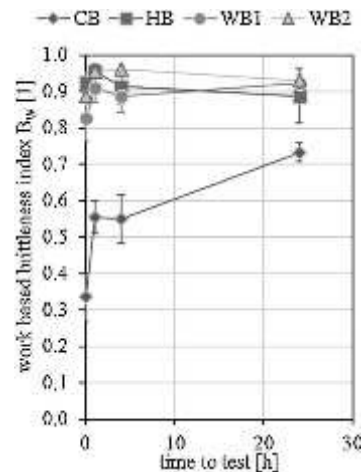


Fig. 15. Energy based brittleness index results for all tested cores over storage time.

bending test setups only, because sample stiffness and elastic work are size dependent parameters.

Generally, the more a load curve is bowed, the lower is the brittleness index. For a completely linear load curve it would reach unity. Results for B_M are shown in Fig. 14 and for B_W in Fig. 15.

The work based brittleness indices are slightly lower than the modulus based ones. high brittleness indices of above 0.85 are given for HB- and WB-cores. The most brittle system from both evaluations is the WB2-system. The bent curve shape and the higher plastic work fraction lead to lower brittleness indices for the CB-system. Especially at the 0h-condition the values are below 0.5, giving evidence for a high deformability of those cores. Practically the need of a careful core manipulation to avoid deformations is obvious also from these evaluations.

For CB-cores the final plastic work portion W_{pl}^f (Fig. 13) contributes significantly to W_S . The work based brittleness indices are

generally below the modulus based ones, more distinct for the CB-cores than for the hot hardened core systems. Investigating materials with some plasticity, the work based approach should be chosen, to include the final curve section also into the evaluation. The modulus based evaluation reflects curve relations until the maximum strength level only.

3.5. Influence of load velocity

Due to their high plasticity and time dependency of the results, CB cores have been chosen to study the influence of load velocity. Load rates of 0.5–5 and 50 mm/min have been applied. In Table 4 the results are shown in relation to 0.5 mm/min load velocity, which was constant for the previously shown results.

For the low load velocity of 0.5 mm/min, resulting in about 1 min bending test time, strength and total work are significantly decreased by 20–25% related to the nominal load velocity of

5 mm/min. Deflection is decreased by about 10%. However, the elastic modulus and the brittleness indices are close to the reference values.

For the high load velocity of 50 mm/min, resulting in a testing time below 1 s, mean values of bending strength, elastic modulus, work of fracture and the brittleness are above 100% and average deflection is slightly decreased.

Summarized, very low load velocities permit plastic deformation over time of binder bridges and thereby permits a degree of plasticity in sand cores. This leads to decreased strength and work of fracture.

Such viscous effects are expected to have less effect for more brittle sand cores with fully hardened Hotbox and Warmbox binder systems.

4. Conclusions

The here presented study has demonstrated the potential to significantly enhance the evaluation of standard foundry sand core bending tests. Benchmarking of Coldbox-, Hotbox- and Warmbox bonded sand cores proved the successful application of this concept.

- Bending strength and elastic modulus can be directly evaluated from non-treated load curves.
- A load curve pre-treatment is essential to eliminate initial settling effects of the samples towards the testing supports prior to further analyses in particular for soft bonded granular materials like sand cores.
- Elastic and plastic mechanical work and deflection can be evaluated from pre-treated load curves.
- Brittleness has been expressed by a modulus based- and a work based concept. Both deliver comparable relationships.
- For materials with higher plasticity the work based approach should be preferably applied.
- At low load rates strength and deformability may be reduced due to visco-plastic effects.

Limitations of the concept are given by the overcritical sample fracture of samples at bending test setups according to foundry standards, promoting instable crack propagation. Therefore it is proposed to investigate the specific work of fracture, e.g. by wedge split tests as developed by (Harmuth and Tschegg, 1997). This has been proven as a suitable concept to characterize heterogeneous materials like refractory bricks or concrete samples, due to an improved ratio of fracture surface to sample volume.

Future research should address sand core properties during the casting process, investigating the impact of thermal exposure and the resulting high temperature properties. Moreover, focus should also be put on inorganically bonded cores. These require a more complex process control while giving environmental and work hazard benefits.

Acknowledgements

The authors thank the Austrian Research Promotion Agency for supporting this work within projects FFG 844552 and FFG 849486. We also acknowledge the given industrial partner contributions by company Nematik supporting with valuable process information and the Austrian Foundry Research Institute for applying new measurement approaches, which highly upgraded the present work content.

References

- AFS, 1962. *Molding Methods and Materials*, 1st ed. American Foundrymen's Society, Des Plaines, Illinois.
- Bindernagel, I., 1983. *Formstoffe und Formverfahren in der Gießereitechnik*, VDG-Taschenbuch. Verein Deutscher Gießereifachleute, Giesserei-Verlag GmbH, Düsseldorf.
- Brown, J.R. (Ed.), 2010. *Foseco Non-Ferrous Foundryman's Handbook*, 11th ed. Butterworth-Heinemann, <http://dx.doi.org/10.1016/B978-075064284-2/50001-6>.
- Campbell, J., 2000. The concept of net shape for castings. *Mater. Des.* 21, 373–380, [http://dx.doi.org/10.1016/S0261-3069\(99\)00072-2](http://dx.doi.org/10.1016/S0261-3069(99)00072-2).
- Czervinski, F., Mir, M., Kasprzak, W., 2015. Application of cores and binders in metalcasting. *Int. J. Cast Met. Res.* 28, 129–139, <http://dx.doi.org/10.1179/1743133614Y.0000000140>.
- Dieter, H.W., 1950. *Foundry Core Practice*. American Foundrymen's Society, Chicago, IL.
- Dong, S., Iwata, Y., Hohjo, H., Iwahori, H., Yamashita, T., Hirano, H., 2010. Shell mold cracking and its prediction during casting of AC4C aluminum alloy. *Mater. Trans.* 51, 1420–1427, <http://dx.doi.org/10.2320/matertrans.F-M2010815>.
- Flemming, E., Tilch, W., 1993. *Formstoffe und Formverfahren*, 1st ed. Deutscher Verlag für Grundstoffindustrie, Leipzig, Stuttgart.
- Gosch, R., Stika, P., 2005. Das ROTACAST-Gießverfahren – millionenfach für Aluminiumzylinderköpfe in der Serie bewährt. *Giesserei-Rundschau* 52, 170–173.
- Harmuth, H., Tschegg, E.K., 1997. A Fracture mechanics approach for the development of refractory materials with reduced brittleness. *Fatigue Fract. Eng. Mater. Struct.* 20, 1585–1603, <http://dx.doi.org/10.1111/j.1460-2695.1997.tb01513.x>.
- Kerber, H., Riegler, M., Schindelbacher, G., Schumacher, P., 2014. New possibilities with improved green sand testing facilities. In: Jan-Blažič, M. (Ed.), 54th International Foundry Conference. Slovenian Foundrymen Society, Portoroz, Slovenia, p. 10.
- Langer, H.J., Dunnavant, W.R., 2011. Foundry resins. *Polym. Sci. Technol.*
- Lellig, K., Nolte, M., Kube, D., Gosch, R., Gröschel, A., Ragus, D., 2010. Neue Leichtbaukonzepte in Motorenkonstruktion und -bau: Antworten auf die veränderten Herausforderungen im modernen Fahrzeugbau. In: 37. Internationales Wiener Motorensymposium, Verein Deutscher Gießereifachleute, Giesserei-Verlag GmbH, pp. 213–231.
- Motoyama, Y., Inoue, Y., Saito, G., Yoshida, M., 2013. A verification of the thermal stress analysis, including the furan sand mold, used to predict the thermal stress in castings. *J. Mater. Process. Technol.* 213, 2270–2277, <http://dx.doi.org/10.1016/j.jmatprotec.2013.06.024>.
- Quarzwerte, 2009. *Quarzsand Haltern H 31 bis H 35, Quarzwerte Stoffdaten*. D-50207 Frechen.
- Ratke, L., Brück, S., 2006. Mechanical properties of aerogel composites for casting purposes. *J. Mater. Sci.* 41, 1019–1024, <http://dx.doi.org/10.1007/s10853-005-3152-8>.
- Rice, J.R., 1968. A path independent integral and the approximate analysis of strain concentration by notches and cracks. *J. Appl. Mech.* 35, 379–386.
- Schacht, C.A. (Ed.), 2004. *Refractories Handbook*. Marcel Dekker, Inc., New York, Basel.
- Sobczyk, M., 2008. Untersuchung zur Nutzung der Vakuumtrocknungshärtung für die Herstellung und den Einsatz magnesiumsulfatgebundener Kerne für den Leichtmetallguss. Otto-von-Guericke-Universität Magdeburg.
- Stachowicz, M., Granat, K., Nowak, D., 2011. Influence of water-glass grade and quantity on residual strength of microwave-hardened moulding sands. Part 2 11, 93–98.
- Tarokh, A., Fakhimi, A., 2014. Discrete element simulation of the effect of particle size on the size of fracture process zone in quasi-brittle materials. *Comput. Geotech.* 62, 51–60, <http://dx.doi.org/10.1016/j.compgeo.2014.07.002>.
- Thole, J., Beckermann, C., 2009. Measurement of elastic modulus of PUNB bonded sand as a function of temperature. In: 63rd SFSA Technical and Operating Conference, Steel Founders Society of America, Chicago, IL, p. 22.
- VDG-Merkblatt M 11, 1974. *Beheizbares Formwerkzeug für die Herstellung von Biegestäben VDG*. Düsseldorf.
- VDG-Merkblatt P 71, 1999. *Biegefestigkeit von warmhärtenden, kunstharzgebundenen feuchten Formstoffen*. VDG, Düsseldorf.
- Weissenbek, E., Kautz, T., Brotzki, J., Müller, J., 2011. Zylinderkopffertigung der Zukunft – Ökologie, Ökonomie und Werkstoffoptimierung im Einklang. *Mot. Zeitschrift* 72, 484–489.
- Wolff, M.F.H., Salikov, V., Antonyuk, S., Heinrich, S., Schneider, G. a., 2013. Three-dimensional discrete element modeling of micromechanical bending tests of ceramic-polymer composite materials. *Powder Technol.* 248, 77–83, <http://dx.doi.org/10.1016/j.powtec.2013.07.009>.
- Zhou, X., Yang, J., Su, D., Qu, G., 2009. The high-temperature resistant mechanism of α -starch composite binder for foundry. *J. Mater. Process. Technol.* 209, 5394–5398, <http://dx.doi.org/10.1016/j.jmatprotec.2009.04.010>.
- Zwick, Roell, 2015. *ProLine Tischprüfmaschinen 2005 bis Z100*, Produktinformationen.

4.2 Mohr-Coulomb failure criterion from unidirectional mechanical testing of sand cores after thermal exposure

Authors	B.J. Stauder (Nemak Linz); M. Berbic (ÖGI); P. Schumacher (MUL)
Journal	Elsevier - Journal of Materials Processing Technology Manuscript re-submitted after corrections and accepted for review (July, 2018). © Elsevier B.V. All rights reserved – valid after acceptance.
Individual author contributions	60 %: B.J. Stauder: sample planning and sample conditioning parameters; data evaluation methodology, corresponding author. 30 %: M. Berbic: Sample testing, data acquisition and statistical evaluation. 10 %: P. Schumacher: scientific context and failure model definition.

Abstract

Thermal exposure by the melt and overlaid mechanical loads by shrinkage counteracting the core expansion define the major boundary conditions for cast-in sand cores.

Four different sand core compositions were mechanically tested after defined thermal exposure profiles with and without air exchange, to better approach the atmosphere of cast-in cores. The bending modulus drop indicated temperatures of starting core integrity degradation, which were effectively similar to temperatures for achieving half of the initial strength as retained strength. Sealed atmosphere shifted the strength drop of furanic Warmbox by 20 °C and the one of PU-Coldbox by 50 – 100 °C upwards and the ones of Na-silicate bonded samples to 20 °C lower values. Silicate bonded cores with spherical sintered mullite granulate kept high retained properties up to highest exposure temperatures. Silicate bonded silica sand were thermally degraded due to micro-cracks in the bonds introduced by thermal strains.

A Mohr-Coulomb failure criterion was presented for the shear - compression stress room, applicable to describe cast-in cores in thermal-mechanical interaction with the casting. The internal friction angle was > 40 ° for spherical sintered mullite and < 30 ° for sub-angular shaped silica sand. High hydrostatic pressures seemed not probable and were not evaluated.

For future numerical simulation the use of a master failure criterion function scaled with relative strength evolution based on evaluated properties is proposed. Subsequent to such describable initial core damage, studies of the de-agglomeration kinetics might require the application of adapted material comminution methods.

Mohr-Coulomb failure criterion from unidirectional mechanical testing of sand cores after thermal exposure

Bernhard J. Stauder ^{a,*}, Mirnes Berbic ^b, Peter Schumacher ^c

^a *Nemak Linz GmbH; A-4030 Linz Austria*

^b *Austrian Foundry Research Centre; A-8700 Leoben Austria*

^c *Chair of Casting Research, Montanuniversität Leoben; A-8700 Leoben Austria*

Abstract

Sand core samples were subjected to thermal pre-conditioning profiles between 200 and 500 °C both in ambient air and under sealed conditions. These were customised similar to an industrial cast aluminium cylinder head. The samples were investigated via unconfined compression, splitting tensile, shear, and bending tests. The suitability of the data to parametrise a Mohr–Coulomb failure criterion model was evaluated.

Four core types were examined more closely. The relative retained strength evolution was largely independent of the test type. Structural changes such as hardening or degradation were indicated by changes of the elastic bending modulus. In particular, polyurethane-coldbox-bonded sand cores after 400 °C pre-conditioning without air exchange retained 40% of the initial strength compared to 20% after treatment in air. Less atmospheric influence was revealed by furan warmbox-bonded cores, showing a decrease to 30% of the initial strength up to a 300 °C pre-conditioning temperature. Inorganic silicate-bonded

* Corresponding author: phone: +43 732 300103 5261; Email: bernhard.stauder@nemak.com,
bernhard.stauder@aon.at (B. Stauder)

cores using quartz sand exhibited a decrease in strength to 10% up to a 400 °C pre-conditioning temperature. In contrast using a silicate-bonded sintered mullite granulate, more than 50% of the initial strength was retained up to a 500 °C pre-conditioning temperature.

Based on position-dependent temperature profiles, evolving during casting within the insulating sand cores, the mechanical behaviour until failure can be predicted and assigned, further allowing the evaluation of the mechanical core removal.

Keywords: Casting; sand core; thermal exposure; mechanical properties; failure criterion

I. Introduction

Sand cores are utilised to shape and preserve complex cavities in cast metal parts. During the casting process, the cores must withstand manipulation and melt flow loads under thermal exposure until the core removal step at the end of the process chain. The granular structure and the high free volume of sand cores should facilitate satisfactory fragmentation of the core for enhanced mechanical core removal.

Owing to their insulating properties, the flow of heat into sand cores is rather slow and they continue to expand whilst the cast metal section solidifies and further cools. Campbell (2011) in the examination of dimensional accuracy has documented a reduced casting contraction for parts with high-volume cavities. For automotive castings, the ‘casting envelope density’, defined as the ratio of metal mass per casting envelope volume, is $\sim 1000 \text{ kgm}^{-3}$ using aluminium alloys with a density of approximately 2700 kgm^{-3} , which means that 60% of the volume is hollow space shaped by sand cores. A significant mechanical interaction of cast-in sand cores with the cast metal section became evident owing to the decreased casting contraction from 1.3% to 1.0%.

According to Krukowski's (2006) overview on minerals used for foundry cores, silica sand is the most widely used core sand type. Silica sand exhibits high thermal expansion with a distinctly non-linear characteristic. Thiel et al. (2007) provided multiple dilatometry results of pure and bonded silica sand

qualities, and Recknagel and Dahlmann (2009) have outlined the physical properties for various granular materials.

Casting process simulations can indicate the evolving thermal fields during a casting process.

Regrettably, thermal-mechanically coupled simulations, including stress evaluation, are not state of the art because time-dependent material properties of sand core materials are inadequately understood and documented.

With limited binder stability, site-specific core degradation and collapse of core sections are distinct possibilities. Denis and Schrey (2006) have documented a method to investigate thermal degradation of polyurethane coldbox cores after dipping trials of cores into melt followed by an evaluation of the thermally deteriorated core volume. Stauder et al. (2018) investigated the kinetics of a core removal process of cast-in sodium-silicate-bonded sand cores. A significant impact of the casting process and subsequent thermal exposure on core disintegration was observed, indicating thermal-mechanically overlaid core damage during the casting process. The application of inorganic binders, which provide ecological benefits, was reviewed by Zaretskiy (2015), who specifically highlighted the challenge of mechanical core removal. Thermally induced binder bridge embrittlement was surmised as a major contributing factor to the failure of inorganic cores. The residual strength of core samples after thermal exposure is a common method to evaluate thermal stability. Döpp et al. (1985) determined the typical secondary strength maximum of silicate-based binders attained at 800–900 °C. These determinations are particularly pertinent with high-temperature melting cast metals.

According to foundry standards, mechanical strength of foundry cores is evaluated by uniaxial testing methods such as tensile, bending, and compression. To address the need for enhanced foundry core material characterisation, Stauder et al. (2016) described the load curve analysis of bending tests based on thermally non-conditioned samples. In another study, Menet et al. (2017) provided data for compression and shear strength after thermal exposure for a polyurethane coldbox system, and a thermo-physical evaluation of such a system was presented by Bargaoui et al. (2017).

Presently, there are few specific investigations on the deformation or fracture of sand cores.

Motoyama et al. (2012) developed an in situ measurement method and device to evaluate the

contraction resistance of a mould against casting shrinkage. Applying this method, results for furan moulding materials were subsequently presented by Motoyama et al. (2013) and for green sand moulds in combination with simulation by Inoue et al. (2013). In their simulation approach, constant material parameters were applied, which were adequate for the insignificantly heated massive mould. Dong et al. (2010) successfully predicted core cracking of hollow cylindrical and notched cores filled with Al-melt. Thermally deteriorating core strength was introduced based on material data from bending tests to predict mould deformation and cracking tendency. The authors also considered the size effect according to Weibull (1951), which postulates a decreasing strength with increasing sample volume. In that study, a purely tensile-strength-based failure criterion was applied, whereas for cast-in cores, compressive loads must also be considered.

Failure criterion functions for materials under compressive stress conditions are implemented in the engineering of rock and soil mechanics, building and refractory material research, and powder materials technology. Overviews on the most relevant failure criterion functions were presented by Labuz and Zang (2012) for the *Mohr–Coulomb* criterion, by Alejano and Bobet (2012) for the *Drucker–Prager* criterion and by Eberhardt (2012) for the *Hoek–Brown* criterion.

Multi-axial testing methods are required to determine the upper limits of hydrostatic pressure conditions. In the field of cemented sandy soils, Consoli (2014) determined the failure envelope inclination, or internal friction angle, for a Mohr–Coulomb model from both multi-axial testing and from uniaxial compression and splitting tensile testing. Galles and Beckermann (2017) applied the Drucker-Prager failure criterion to evaluate the deformation of a cylindrical sand core during iron casting, thus representing one of the first documented applications of tri-axial testing for foundry cores. The cast-in sand core was considered to be essentially free of cohesion owing to binder degradation by the high casting temperature, so that data obtained from room temperature tri-axial testing of pure sands could be applied. It was reported that in addition to thermal expansion, grain rotation effects contributed significantly to the volume growth. Generally, during Al-casting, significant sections of a core are only partly degraded compared to high-melting-point metals.

The subject of this work is the field of mechanical properties of sand cores after the casting process of aluminium parts prior to core removal. The sand core strength after representative thermal exposure will be evaluated for all relevant temperature ranges up to 500 °C for different sand core types.

Thermal exposure following industrially relevant temperature profiles was performed with and without air exchange to mirror the atmospheric conditions of cores more realistically. The property changes were evaluated for bending, splitting tensile, shear, and compression tests. Additionally, the visualisation by the Mohr–Coulomb (MC) failure criterion was used to demonstrate the retained mechanical properties after casting, which represents the situation prior to core removal.

II. Experimental method

The materials used for core sample production, the thermal pre-conditioning procedures, and the material testing types will be characterised here.

Sand core types

Silica sand type ‘H32’ (Quarzwerke, 2009), termed as ‘Si’, was used as reference material with all binders. Additionally, a ceramic granulate termed as ‘Ce’, which is a spherical sintered mullite according to Itochu’s datasheet (2010), was used with the waterglass binder.

Applied organic binders were the furan warmbox (termed ‘FW’) and polyurethane coldbox (termed ‘CB’) binders (the same as used in Stauder et al. (2016)), and additive-free Na-silicate solution (waterglass, termed ‘WG’), which was applied by Stauder et al. (2018), was used as inorganic binder. In Table 1, the individual sand core types are overviewed.

Table 1: Sand core sample designations.

Sand	% of sand mass binder	Hardening	Sample designation
Silica	1.6% furan warmbox	180 °C / 30 s	Si-FW
Silica	1.2% polyurethane coldbox	Amine gassing	Si-CB
Silica	2.5% Na-silicate (waterglass)	160 °C / 30 s	Si-WG
Ceramic granulate	2.5% Na-silicate (waterglass)	160 °C / 30 s	Ce-WG

Sand cores were characterised by applying light-optical microscopy (Zeiss ‘SteREO Discovery’) and scanning electron microscopy (SEM Jeol ‘JSM-IT300 LV’) utilising a low-vacuum modus. Figure 1 illustrates both granulates bonded with Na-silicate, the appearance of a sand core surface, and the grain morphology.

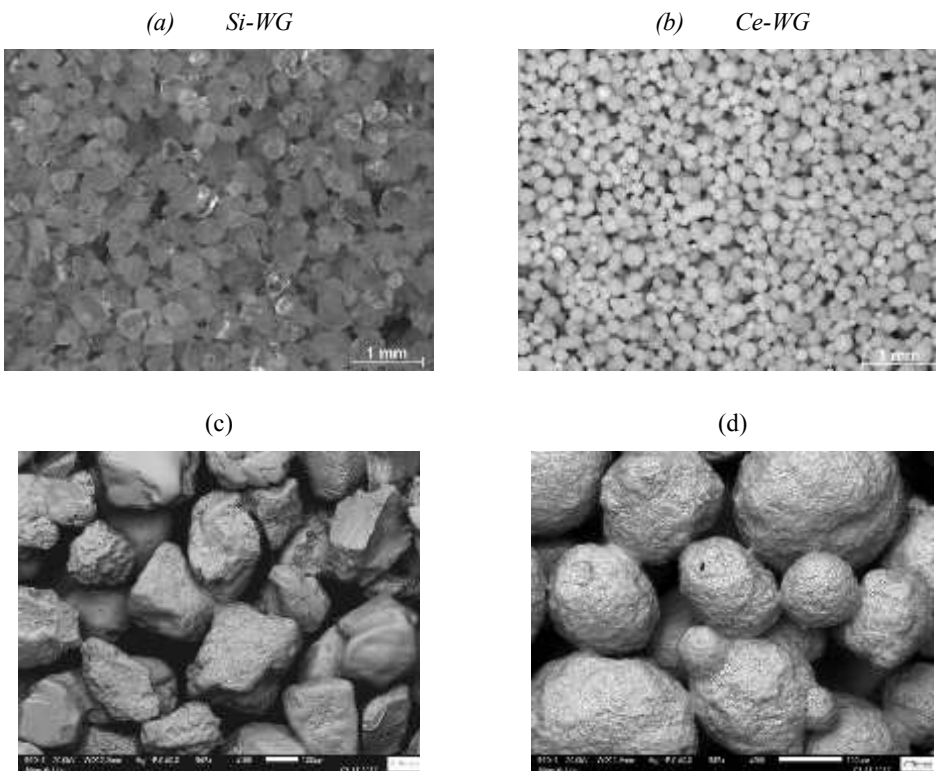


Figure 1: Silica sand (a, c) and ceramic granulate (b, d) bonded with Na-silicate. A thermally and mechanically unloaded core surface is shown. Light-optical microscopy pictures (above) and SEM pictures (below) illustrate the surface appearance and the grain shape.

Thermal pre-conditioning of core samples

All tests were performed after a thermal loading collectively derived from casting process simulation of an aluminium engine cylinder head. The heating curves of all cast-in cores were evaluated at different core wall thicknesses at peripheral and central positions in the casting. The resulting pre-conditioning parameters are graphically shown in Figure 2.

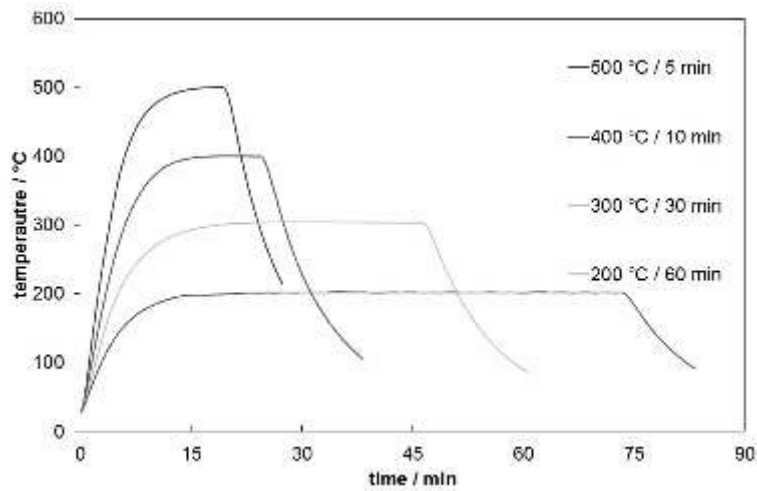


Figure 2: Temperature profiles measured in test cores during pre-conditioning from 200 to 500 °C with a target temperature tolerance of ± 5 °C.

The thermal exposure was performed in air (abbrev. 'A') and without air exchange (sealed, abbrev. 'S'). The exposure in air served as a reference, because most available retained strength studies were performed in ambient atmospheric conditions. The sealed condition was chosen to approximate the situation of cast-in sand cores. Therefore, samples were wrapped in Al foil and embedded in pre-heated sand during thermal exposure. For organically bonded materials, the sealed condition causes a partly reducing atmosphere and for inorganically bonded samples a diminished drying owing to hindered steam percolation. Figure 3 illustrates bending test bars prepared for thermal pre-conditioning at both atmospheric conditions. This procedure was executed similarly with cylindrical samples (not pictured).

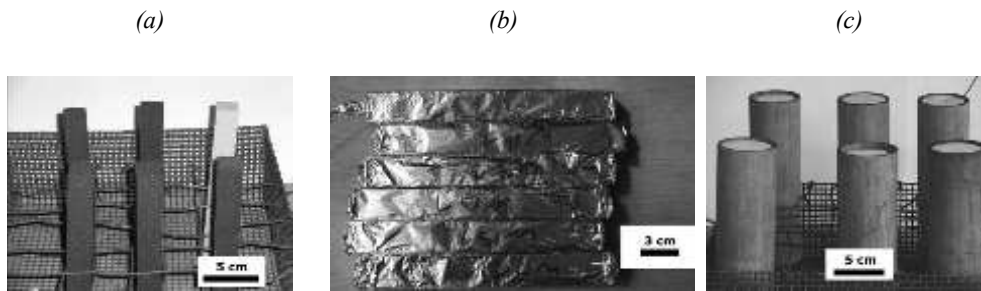


Figure 3: Thermal pre-conditioning of bending test samples. (a): in air (b): sealed samples wrapped in Al foil and (c): prepared treatment batch for the sealed condition with samples embedded in pre-heated sand.

Each pre-conditioning batch was controlled by an instrumented measurement sample. All samples were cooled in calm ambient air after pre-conditioning. Careful unwrapping of the sealed samples was performed in a cool environment before testing to avoid damage.

Mechanical core testing

The testing queries and formulas for strength evaluation are illustrated in Figure 4.





Bending	Compression	Double shear	Splitting tensile
			
$\sigma_B = \frac{3Fl}{2bh^2}$	$\sigma_c = \frac{4F}{d^2\pi}$	$\sigma_s = \frac{2F}{d^2\pi}$	$\sigma_T = \frac{2F}{d\pi l}$

Figure 4: Test types applied for mechanical property assessment and the respective strength evaluation equations. F : maximum load / N; l : loaded sample length / mm; b : sample width / mm; h : sample height / mm; d : sample diameter / mm.

Universal testing machines with 5 and 50 kN maximal loads ('Zwick/Roell Z005' and 'Z050') were used to determine the load curves. The loading velocity was 10 mm/min for bending tests and

20 mm/min for compression, shear, and tensile tests. In addition to bending tests, the elastic modulus was further evaluated following the method documented by Stauder et al. (2016). After pre-conditioning, the elastic modulus is expected to reflect any altered adhesive and cohesive strength by eventual structural changes of bonds.

Cylindrical samples 35 mm in diameter and height were used for the splitting tensile, shear, and compression tests. This sample size was chosen to achieve improved homogeneity and reduced temperature gradients during sample production and pre-conditioning compared to normally applied 50-mm compression test samples used for bentonite-bonded 'green sand' testing.

Mohr-Coulomb failure criterion

Based on the obtained tensile, shear, and compression stress data, the MC failure envelope was constructed according to the schematic diagram shown in Figure 5.

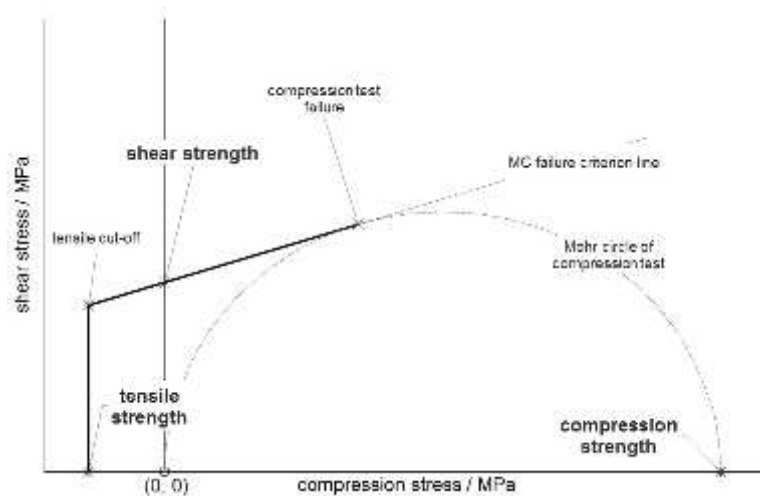


Figure 5: Schematic illustration of the Mohr–Coulomb figure construction based on compression, shear and tensile strength showing all relevant characteristics.

The tangent from shear strength touching the indicated Mohr circle of the unconfined compression test defines the MC failure envelope incline and consequently the internal friction angle. The compression test stress–failure condition is defined by the coordinates of the tangential point.

The linear elongation of the failure envelope into the compressive stress room and the Mohr circle representing the unconfined compression test are indicated by dashed lines. It can be assumed that, owing to the high free volume, sand cores could withstand only moderately increased hydrostatic pressures until they would collapse. The precise shape of the failure envelope at higher compressive stresses would require multi-axial testing procedures, which were not applied here.

The failure envelope was linearly extended via the shear strength point into the tensile stress direction (indicated by negative compression stress). It was cut off at the tensile strength level. Alternatively, a direct connection from the shear to the tensile strength points was chosen in case the elongated failure envelope intersected with the tensile stress axis already below the tensile strength. Such cases reflected errors due to the delicate measurements. Generally, the precise failure envelope shape presumably is a curved shape below that area.

III. Results

Room-temperature reference results and the effect of thermal pre-conditioning on the elastic modulus and mechanical strength will be presented. Following that, an equivalent evaluation with the Mohr–Coulomb failure criterion model will be presented.

Room-temperature results

At room temperature ‘RT’ (ambient atmosphere with 23 ± 3 °C and 20-40% rel. humidity), furan warmbox samples (Si-FW) revealed the highest strength and stiffness. The other silica sand-based samples Si-WG and Si-CB showed lower mechanical properties, whereas waterglass-bonded ceramic sintered mullite cores (Ce-WG) demonstrated the lowest strength. The highest elastic modulus was evaluated for Si-FW, whereas with Si-CB samples 70% of that level was achieved. This corresponds well with the existing data of Stauder et al. (2016). For both waterglass-bonded core types, Si-WG and Ce-WG, a 16% lower elastic modulus compared to Si-FW was determined.

In Table 2, all room-temperature results and the standard deviation from a minimum of ten tested samples per method and material combinations are presented.

Table 2: Mechanical properties from shear, compression, splitting tensile, and bending tests. Tested after 24 h storage at room temperature. Average values and standard deviation s are indicated.

Sample type	Shear strength / MPa	Compression strength / MPa	Splitting tensile strength / MPa	Bending strength / MPa	Bending elastic modulus / MPa
Si-FW	2.1 s: 0.1	8.2 s: 0.58	1.8 s: 0.05	4.6 s: 0.63	2508 s: 143
Si-CB	1.7 s: 0.11	4.6 s: 0.94	0.6 s: 0.06	3.9 s: 0.44	1738 s: 160
Si-WG	1.8 s: 0.17	5.7 s: 0.68	1.0 s: 0.18	4 s: 0.26	2158 s: 120
Ce-WG	0.8 s: 0.1	3.3 s: 0.39	0.8 s: 0.1	2.5 s: 0.15	2068 s: 145

Elastic modulus after thermal exposure

In Figure 6, the change of the elastic bending modulus relative to room temperature values is shown for all binder types in both ambient and sealed conditions.

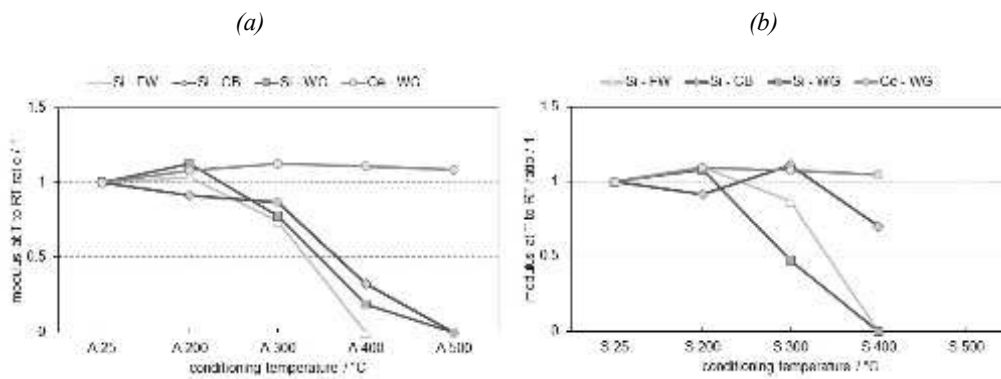


Figure 6: Elastic bending modulus of the different binder systems after pre-conditioning in air (a) and under sealed conditions (b).

There are significant differences in the elastic modulus for samples treated in ambient and under sealed conditions. All silica-based samples conditioned in air showed a similar decline over temperature, whereas Ce-WG exhibited no decrease. Under sealed conditions, the organic binder types — predominantly the Si-CB samples — exhibited higher thermal stability. After pre-conditioning at temperatures greater than 300 °C, only the Ce-WG samples showed an elastic modulus similar to room temperature values, in contrast to Si-WG type.

Strength after thermal exposure

To test the strength development after thermal exposure in relation to RT-values, a minimum of five samples for each data point were tested. A standard deviation of approximately 20% of the nominal value was determined. The results for all mechanical tests are presented in Figure 7, with each tested core type and both atmospheric conditions in separate figures.

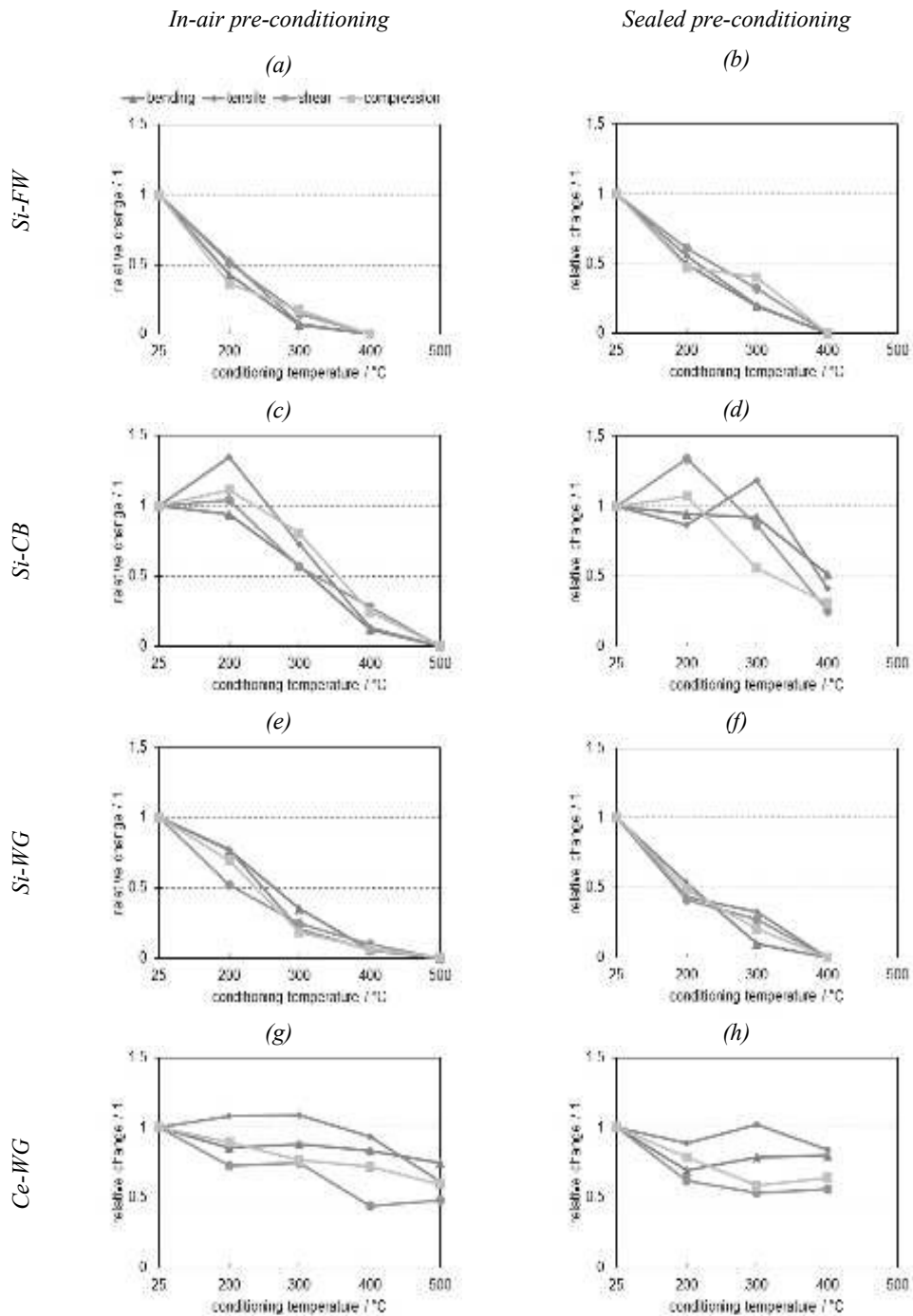


Figure 7: Temperature-dependent strength relative to room temperature for bending, indirect tensile, shear, and compression testing. Results after pre-conditioning in air and under sealed conditions are presented for silica-furan warmbox: (a, b), silica-polyurethane coldbox: (c, d), silica-waterglass: (e, f) and waterglass-bonded ceramic granulate cores: (g, h).

Principal differences between the core types and the atmospheric conditions were observed, although a significant degree of scatter in the relative change of strength to room temperature values was present.

The sealed condition of the Si-CB cores resulted in elevated retained strength compared to the in-air condition, which corresponds to the development of the elastic modulus after thermal exposure.

Among the silica sand samples, the Si-CB cores revealed the highest thermal stability. The lowest temperature-dependent property decrease was observed for Ce-WG. After any pre-conditioning, at least 50–80% of initial strength was maintained by the samples.

Waterglass-bonded samples behaved significantly differently depending on the sand type. With silica sand, the temperature for a property decrease by 50% occurred at approximately 240 °C in air and at 200 °C under sealed conditions. In contrast to the Si-WG samples, Ce-WG samples revealed a low sensitivity on thermal pre-conditioning, and all properties were retained at a high level up to a 500 °C exposure temperature.

Mohr–Coulomb failure criterion

Figure 8 illustrates the MC failure criterion functions for the RT condition of all tested core types.

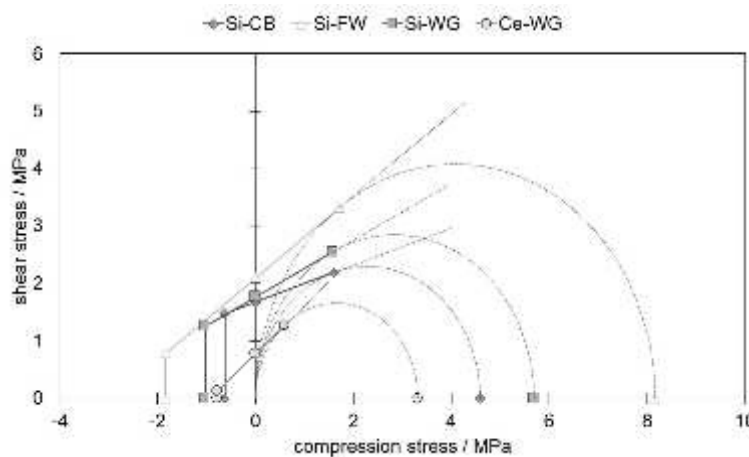


Figure 8: Mohr–Coulomb criterion figures for the four investigated sand core types based on room-temperature tensile, shear, and compression test results from Table 2.

The overview at room temperature reflects the strength relations already discussed in context with Table 2. A typical incline of the failure envelope appeared. In Figure 9 the results after thermal preconditioning are shown for all sand core types and atmospheric conditions in individual diagrams. To avoid confusion, only selected Mohr circles are indicated.

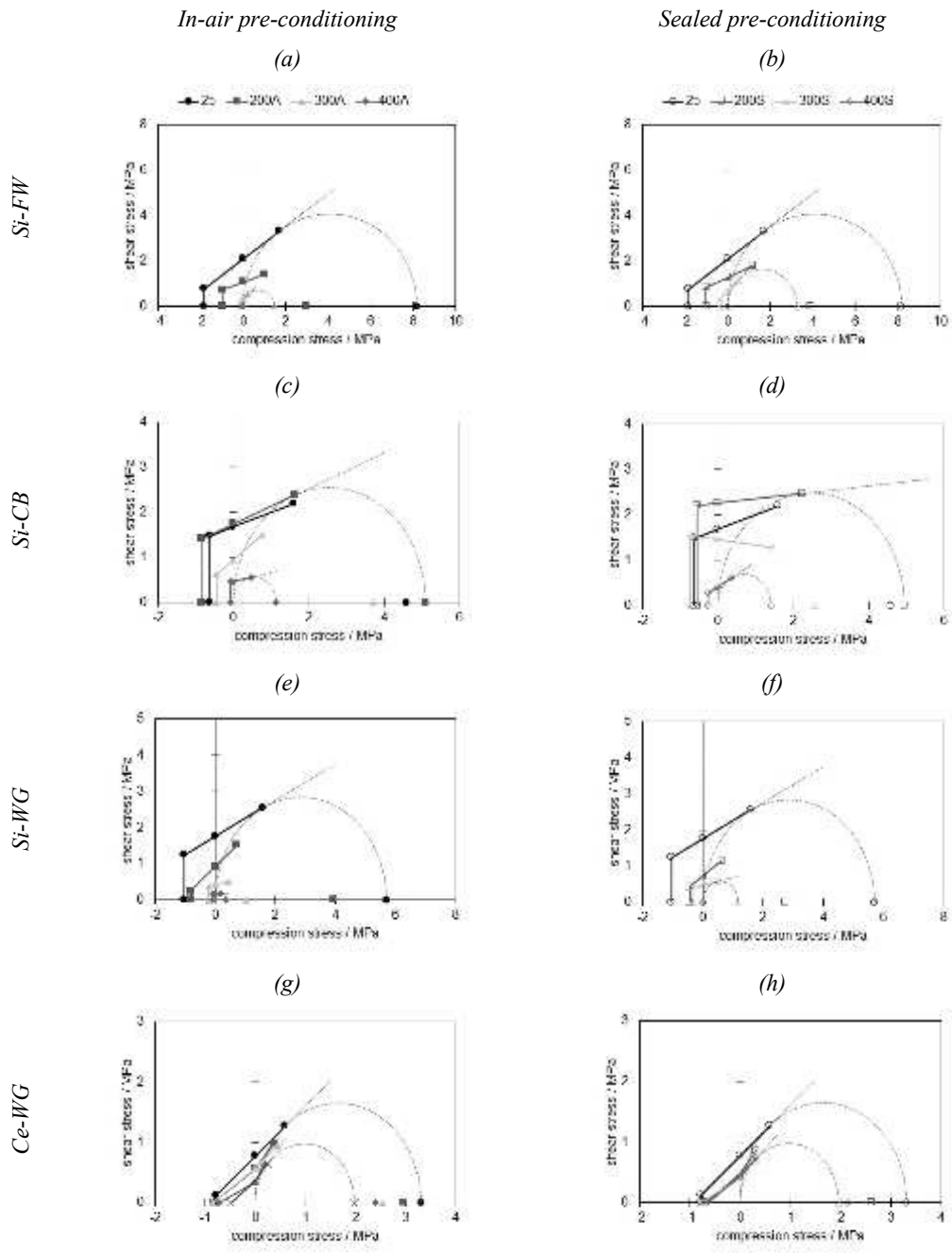


Figure 9: Mohr–Coulomb figures illustrating the temperature dependency of the investigated binder systems after pre-conditioning in air and under sealed conditions. Silica-furan warmbox: (a, b), silica-polyurethane coldbox: (c, d), silica-waterglass: (e, f) and synthetic-sintered mullite-waterglass-bonded cores: (g, h).

The data clearly reflect the temperature dependency of the mechanical properties. This was discussed for the relative changes of the single test types in the previous section. Based on the given data, a typical failure envelope shape could be obtained for all tested conditions except for the Si-CB samples pre-conditioned at 300 °C under sealed conditions. Here, a clear evaluation of the failure envelope was hindered by the high degree of scatter potentially caused by the deteriorated surface quality of the sample contact area during mechanical testing.

The tensile cut-off of the failure envelope was evident for all testing conditions, except the Ce-WG results shown in Figure 9 (e) and (f). For those samples, after analysing the original load–displacement curves, a high sensitivity on local contact pressure of the double shear testing supports was reflected by erratic curve shapes.

IV. Discussion

Compared to the initial core properties, a decreased strength of furan warmbox and silica-waterglass samples is evident. Polyurethane coldbox cores retained more strength, and ceramic granulate-waterglass samples remained approximately unchanged and can be ranked as the second-strongest material after pre-conditioning.

Figure 10 shows the decreased sand core properties for all tested core types after thermal pre-conditioning at 300 °C in air. Note that the axes are scaled down by a factor of two relative to the room-temperature values shown in Figure 8.

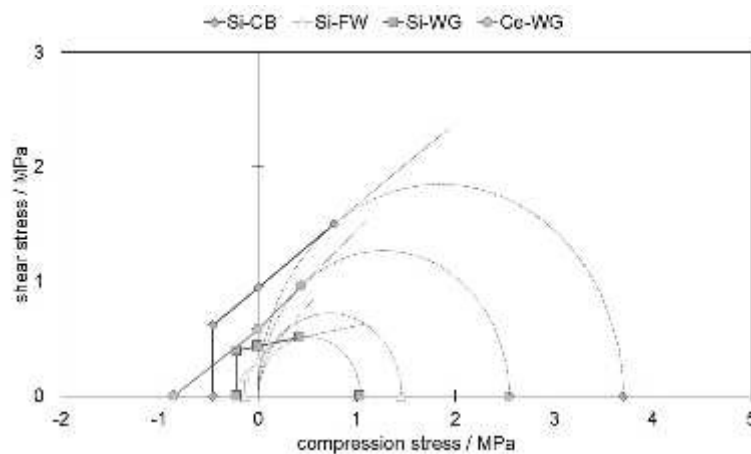


Figure 10: Mohr–Coulomb criterion function of all tested sand core types pre-conditioned at 300 °C in air.

The highest impact of sealed versus in-air treated samples was given by the complex strength development of the polyurethane coldbox system, which demonstrably reflected effects due to recombination of volatile binder components, as discussed by Bargaoui et al. (2017). After sealed pre-conditioning at 400 °C, an average of 40% of the initial strength versus 20% after in-air pre-conditioning was evaluated.

Generally, the furan warmbox system exhibited a property decrease at lower temperatures compared to polyurethane coldbox cores and, effectively, at pre-conditioning temperatures above 300 °C, no complete property evaluation was possible. These test results reflected the rigid bonding nature of furan resin systems and their limited thermal stability without any significant secondary network-forming ability.

The behaviour of the inorganic waterglass-bonded samples with silica and ceramic granulates was markedly different. Up to 200 °C, an additional hardening was observed. The retained strength of waterglass-bonded silica sand core samples decreased at temperatures up to 50 °C higher compared to the Si-FW samples. The retained strength properties of sealed waterglass-bonded samples were slightly below those of air-treated ones, which reflects the reduced drying capacity possible under

sealed conditions. However, after the 400 °C pre-conditioning, the evaluated retained properties of the Si-WG samples were generally on a very low level.

In contrast, waterglass-bonded samples produced with ceramic granulate presented an overall low temperature dependency on the retained properties. Furthermore, after the highest exposure temperatures, at least half the initial strength was retained. No elastic modulus decrease below the initial values was observed. Therefore, no thermally induced binder damage is assumed. In summary, for Ce-WG core samples, the only structural binder change up to 500 °C consisted of the secondary hardening by drying.

In casting practise, the different mechanical responses of individual core systems by thermal exposure has led to an empirical selection of cores for individual tasks. A selection which, although not fully understood, nevertheless reflects the behaviour discussed in this paper. Organic thermally cured (hotbox or warmbox) resins are preferably used for filigree, cast-in cores that are difficult to remove from the casting. Today's known most efficient core production is realised with polyurethane coldbox cores, which in application are showing some drawbacks due to thermally induced deformation and worse core removal. New challenges arise with an ongoing replacement of organic by inorganic bonded cores, which are not damaged by the same temperature-dependent mechanisms and with upcoming application of 3D-printed cores for volume production. Thus, increased emphasis must be given to the mechanical properties of such new core systems and their interaction with the casting to facilitate mechanical core removal.

V. Conclusions

For known atmospheric conditions, temperature profile, and a given binder, the local mechanical properties can be assessed using the method presented herein.

- The property evolution after thermal exposure was largely independent of the applied testing method. The elastic modulus from the bending tests clearly signalled structural core bonding changes.

- The Mohr–Coulomb failure criterion can be applied further to assess the presence of damaged core volumes by a numerical analysis of the mechanical stresses acting on cast-in cores. The implementation is recommended by scaling an original room-temperature criterion function with temperature-dependent factors, both of which were presented in this work.
- Atmospheric conditions were important for the characteristic degradation temperatures of the cores:
 - Polyurethane coldbox-bonded cores up to 400 °C revealed higher retained strength after pre-conditioning without air exchange (sealed condition) compared to in-air exchange.
 - The furan warmbox-bonded samples after thermal exposure up to 300 °C revealed a significant strength decrease and reflected a slight increase in the retained properties under the sealed versus the in-air conditions.
 - The waterglass-bonded silica samples exhibited a more important temperature-dependent strength decrease under the sealed conditions owing to diminished drying.
 - The waterglass-bonded ceramic granulate samples revealed a low temperature sensitivity and thereby high retained strength over the whole pre-conditioning temperature range.

More investigations are recommended to obtain a complete high-pressure failure envelope region using multi-axial core testing and in situ hot strength testing to enable future thermal-mechanically coupled casting process simulations.

Acknowledgements

The authors acknowledge the Austrian Research Promotion Agency (FFG) for supporting the projects *FFG 844552* and *FFG 849486*, on which all mechanical property evaluations were based. We furthermore appreciate the support given by the Austrian Foundry Research Institute and Nematik. We also thank T.A. Vacca for the valuable proofreading support.

References

- Alejano, L.R., Bobet, A., 2012. Drucker-Prager criterion. *Rock Mech. Rock Eng.* 45, 995–999. doi:10.1007/s00603-012-0278-2
- Bargaoui, H., Azzouz, F., Thibault, D., Cailletaud, G., 2017. Thermomechanical behavior of resin bonded foundry sand cores during casting. *J. Mater. Process. Tech.* 246, 30–41. doi:10.1016/j.jmatprotec.2017.03.002
- Campbell, J., 2011. *Complete Casting Handbook Metal Casting Processes, Metallurgy, Techniques and Design*, 1st ed. Elsevier Ltd.
- Consoli, N.C., 2014. A method proposed for the assessment of failure envelopes of cemented sandy soils. *Eng. Geol.* 169, 61–68. doi:10.1016/j.enggeo.2013.11.016
- Denis, J.M., Schrey, A., 2006. Fortschrittliche Polyurethan-Cold-Box- Binder für Aluminiumguss mit verbessertem thermischen Zerfall und geringerer Umweltbelastung (Progressive PU Cold box binder for aluminum casting with improved thermal decay and of smaller environmental impact). *Giesserei* 93, 26–31.
- Dong, S., Iwata, Y., Hohjo, H., Iwahori, H., Yamashita, T., Hirano, H., 2010. Shell Mold Cracking and Its Prediction during Casting of AC4C Aluminum Alloy. *Mater. Trans.* 51, 1420–1427. doi:10.2320/matertrans.F-M2010815
- Döpp, R., Deike, R., Gettwert, G., 1985. Beitrag zum Wasserglas-CO₂-Verfahren. *Giesserei* 72, 626–635.
- Eberhardt, E., 2012. The Hoek–Brown Failure Criterion. *Rock Mech. Rock Eng.* 45, 981–988. doi:10.1007/s00603-012-0276-4
- Galles, D., Beckermann, C., 2017. Effect of sand dilation on distortions and pattern allowances during steel sand casting. *Int. J. Cast Met. Res.* 30, 257–275. doi:10.1080/13640461.2017.1290909
- Inoue, Y., Motoyama, Y., Takahashi, H., Shinji, K., Yoshida, M., 2013. Effect of sand mold models on the simulated mold restraint force and the contraction of the casting during cooling in green sand molds. *J. Mater. Process. Technol.* 213, 1157–1165. doi:10.1016/j.jmatprotec.2013.01.011
- Itochu, 2010. Spherical Ceramic Sand for Foundry Naigai CERABEADS 60 for Any Kind of Metal.
- Krukowski, S.T., 2006. Foundry Sands, in: Kogel, J.E., Trivedi, N.C., Barker, J.M., Krukowski, S.T. (Eds.), *Industrial Minerals and Rocks*. Society for Mining, Metallurgy, and Exploration, Inc. (SME), Littleton, Colorado, USA 80127, pp. 1433–1440.
- Labuz, J.F., Zang, A., 2012. Mohr-Coulomb failure criterion. *Rock Mech. Rock Eng.* 45, 975–979. doi:10.1007/s00603-012-0281-7
- Menet, C., Reynaud, P., Fantozzi, G., Thibault, D., Laforêt, A., 2017. Thermomechanical properties and fracture of resin-bonded-sand cores – Experimental study and application in aluminium foundry, in: *Powders and Grains 2017 – 8th International Conference on Micromechanics on Granular Media*. pp. 8–11.
- Motoyama, Y., Inoue, Y., Saito, G., Yoshida, M., 2013. A verification of the thermal stress analysis, including the furan sand mold, used to predict the thermal stress in castings. *J. Mater. Process. Technol.* 213, 2270–2277. doi:10.1016/j.jmatprotec.2013.06.024
- Motoyama, Y., Takahashi, H., Inoue, Y., Shinji, K., Yoshida, M., 2012. Development of a device for dynamical measurement of the load on casting and the contraction of the casting in a sand mold during cooling. *J. Mater. Process. Technol.* 212, 1399–1405. doi:10.1016/j.jmatprotec.2012.02.007
- Quarzwerke, 2009. Quarzsand Haltern H 31 bis H 35, Quarzwerke Stoffdaten. D-50207 Frechen.
- Recknagel, U., Dahlmann, M., 2009. *Spezialsande - Formgrundstoffe für die moderne Kern- und*

Formherstellung / Special Sands - Base Materials for modern Core and Mould Making.
Giesserei-Rundschau 56, 6–17.

- Stauder, B.J., Harmuth, H., Schumacher, P., 2018. De-agglomeration rate of silicate bonded sand cores during core removal. *J. Mater. Process. Technol.* 252, 652–658.
doi:10.1016/j.jmatprotec.2017.10.027
- Stauder, B.J., Kerber, H., Schumacher, P., 2016. Foundry sand core property assessment by 3-point bending test evaluation. *J. Mater. Process. Technol.* 237, 188–196.
doi:10.1016/j.jmatprotec.2016.06.010
- Thiel, J., Ziegler, M., Dziekonski, P., Joyce, S., 2007. Investigation into the Technical Limitations of Silica Sand Due to Thermal Expansion. *AFS Trans.* 07-145, 18.
- Weibull, W., 1951. A statistical distribution function of wide applicability. *J. Appl. Mech.*
doi:citeulike-article-id:8491543
- Zaretskiy, L., 2015. Modified Silicate Binders New Developments and Applications. *Int. J. Met.* 12.
doi:10.1007/s40962-015-0005-3

4.3 De-agglomeration rate of silicate bonded sand cores during core removal

Authors	B.J. Stauder (Nemak Linz); H. Harmuth (MUL); P. Schumacher (MUL)
Journal	Elsevier - Journal of Materials Processing Technology DOI: 10.1016/j.jmatprotec.2017.10.027 © 2017 Elsevier B.V. All rights reserved.
Individual author contributions	80 %: B.J. Stauder: Experimental method, sample planning and evaluation, corresponding author. Presentations at the 2 nd “Formstoff-Forum” in Aachen in March 2018 and “A-D-CH Gießereitagung” in Salzburg in April 2018. 10 %: H. Harmuth: Material technology and statistical evaluation. 10 %: P. Schumacher: Casting process related scientific context.

Abstract

The here presented criterion describes the disintegration kinetics of cast in sand cores, which is influenced by transient thermal and mechanical casting process loads.

A semi-permanent mould setup allowing for various thermal exposure intensities was developed and used with wedge shaped, hot hardened silicate bonded sand cores. During defined mechanical agitation of such produced castings the minimum core removal mass rate was identified and combined with the de-agglomeration degree of the collected core sand. The de-agglomeration degree was evaluated from particle size analysis with specifically adapted sieving parameters and a modelling approach for the size distribution. The retained mass on the top mesh constituted the lump mass.

Cast-in cores generally exhibited higher de-agglomeration rates compared to non-cast-in reference cores, which confirmed a deteriorating influence of a casting process on the sand core. Increased de-agglomeration rates and more disintegrated core lumps were observed for the samples with longer thermal exposure. Avoiding ambient humidity resulted in a significantly increased de-agglomeration rate compared to openly stored samples.



Contents lists available at ScienceDirect

Journal of Materials Processing Tech.

journal homepage: www.elsevier.com/locate/jmatprotec

De-agglomeration rate of silicate bonded sand cores during core removal

Bernhard J. Stauder^{a,*}, Harald Harmuth^b, Peter Schumacher^b^a *Nemak Linz GmbH, A-4030 Linz, Austria*^b *Montanuniversitaet Leoben, A-8700 Leoben, Austria*

ARTICLE INFO

Keywords:

Casting
 Foundry sand core
 Core removal
 Particle size
 Testing

ABSTRACT

The here presented criterion describes the disintegration kinetics of cast in sand cores, which is influenced by transient thermal and mechanical casting process loads.

A semi-permanent mould setup allowing for various thermal exposure intensities was developed and used with wedge shaped, hot hardened silicate bonded sand cores. During defined mechanical agitation of such produced castings the minimum core removal mass rate was identified and combined with the de-agglomeration degree of the collected core sand. The de-agglomeration degree was evaluated from particle size analysis with specifically adapted sieving parameters and a modelling approach for the size distribution. The retained mass on the top mesh constituted the lump mass.

Cast-in cores generally exhibited higher de-agglomeration rates compared to non-cast-in reference cores, which confirmed a deteriorating influence of a casting process on the sand core. Increased de-agglomeration rates and more disintegrated core lumps were observed for the samples with longer thermal exposure. Avoiding ambient humidity resulted in a significantly increased de-agglomeration rate compared to openly stored samples.

1. Introduction

Sand cores are used in numerous metal casting technologies to shape complex internal contours and undercut sections. After the solidification and cooling of a casting, a sand core removal process is required to obtain a sand-free casting. Czerwinski et al. (2015) recently reviewed the state of the art in sand core technology. Over the past century, demands by the automotive casting industry for higher productivity and complex cores have led to the replacement of inorganic binders with organic binders. Due to of more restrictive health and safety guidelines and emissions regulations, inorganic core production technologies are once again being implemented, because these technologies are odourless and nearly emission free. According to Izdebska-Szanda et al. (2012) thermal degradation during casting affects core removal less in inorganic bonded cores than in organic binder systems. Therefore, applying inorganic core binder systems requires special attention to core removal properties.

Gamisch (2002) reviewed existing industrial solutions for core removal. Mechanical core removal processes usually consist of hammering and shaking steps. Fig. 1 shows a typical setup applied for an aluminium cylinder head with inorganically bonded sand cores.

Quantitative evaluation methods for core removal properties are rarely available. Henry (Ashland) et al. (1999) studied the shake-out

behaviour of wedge shaped Coldbox test cores cast in aluminium. Using a pressure-controlled pneumatic hammer, they documented the shaken-out sand mass at specific times and the required shake-out time for complete sand core removal. According to them, binder properties influenced core removal more than casting process variations. To transfer their method to foundry applications, they recommended customising a trial setup for given process conditions. Fennell and Crandell (2008) used a similar setup with an in-line scale for sand collection, and evaluated the average shake-out mass rates of different inorganically and organically bonded sand core types. Inorganically bonded samples had a higher shake-out mass rate than organically bonded cores.

At the Polish Foundry Institute, several investigations have been performed using knock-out testing, according to standard (PN-85/H-11005, 1985). In such tests, strokes with a defined energy are placed directly onto a cast-in test core. Izdebska-Szanda et al. (2012) presented the residual strengths of different binders after thermal exposure and using parallel knock out tests. Different organically and inorganically bonded samples were cast in copper and aluminium. The knock-out work remained similar, in contrast with the different retained strength levels after pre-conditioning to equivalent temperature exposures. Subsequent investigations by Major-Gabryś et al. (2014) demonstrated that retained strength measurements could not be used as the criterion for the knock-out properties of silicate bonded cores, once a secondary

* Corresponding author.

E-mail address: bernhard.stauder@nemak.com (B.J. Stauder).<http://dx.doi.org/10.1016/j.jmatprotec.2017.10.027>

Received 3 July 2017; Received in revised form 15 October 2017; Accepted 16 October 2017

Available online 19 October 2017

0924-0136/ © 2017 Elsevier B.V. All rights reserved.



Fig. 1. Cylinder head with inorganic test cores during (a) hammering process and (b) shaking process (Nemak, 2005).

hardening maximum above 600 °C was attained. The authors postulated a high degree of mechanical interaction by casting contraction counteracting the expansion of the cast-in core. They proposed high temperature thermal expansion as a more significant criterion for predicting knock-out properties.

In the present study, the kinetics of sand core de-agglomeration are investigated; no contributions to such research could be found in the available literature. Therefore, the field of mineral processing has been evaluated in greater depth, as the fragmentation properties (e.g. of ores or rocks) are central to this field. Rosin and Rammler (1933) developed a basis for investigating coal dust particle size distributions. Based on their work, the Rosin-Rammler-Sperling-Bennet (RRSB) approach was used to describe the particle sizes of dusts, soils, and crushed materials. Note that the RRSB approach represents a specific case of the later-established, widely known Weibull probability distribution (Weibull, 1951). This was applied by Paluszny et al. (2016) to describe the particle size distributions of crushed rocks. Bayat et al. (2015) reviewed the fitting accuracy of several particle size distributions. The physical evidence of various functional approaches for describing particle size distributions was demonstrated by Brown and Wohletz (1995).

In summary, the RRSB approach is widely accepted, and is generally documented in mineral processing handbooks (Fuerstenau and Han, 2003; Zogg, 1993). It is a convenient and approved approach for describing de-agglomeration process results. In this study, this approach will be applied for the first time to a foundry application, to model the achieved particle size distributions of raw sand and removed core sand.

2. Material and methods

Sample production for core removal trials are presented. These include the different applied cooling conditions, the core removal setup, and the particle size evaluation method.

2.1. Test casting production

Silica sand H32 (Quarzweser, 2009) bonded with 2,5% mass of sodium silicate binder with a molar $\text{SiO}_2:\text{Na}_2\text{O}$ ratio of 325 was used. The sand cores were produced using an electrically heated core box on a Roeper H1 core blowing machine. The cores were hardened in the core box at 160 °C for 2 min, followed by drying in a 120 °C chamber furnace for 5 min. After cooling, the sand cores were sealed in foil to avoid air exchange and intensive humidity condensation during storage.

For casting the test core was placed in a steel mould and liquid Al (alloy AlSi7Cu0,5Mg) at a temperature of 745 ± 10 °C was poured in. Fig. 2 illustrates (a) the schematic mould setup, (b) the test core dimensions, and (c) the core.

The steel mould was operated based on the mould side wall temperature T_M according to Fig. 2a. The mould temperature at the start of pouring was 400 °C. After T_M exceeded its maximum, the casting was

gently demoulded at 450 °C. Overall, a cycle time of approximately 7 min was obtained.

Four different thermal exposure scenarios were defined. The following colour coding applies throughout the text and figures:

Hardened reference: non cast-in cores, realised by re-filling the empty cavities of test castings with virgin core sand mixture hardened therein (yellow).

- Water cooling: realised by setting the casting with the feeder 40 mm deep into a water bath of 60 – 70 °C (blue).
- Air cooling: cooling the cast samples at non-agitated air ambience (green).
- Insulation: completely embedding the cast part between 30 mm thick ceramic fibre mats (red).

Table 1 summarises the evaluated thermal exposure time for the casting and cast-in cores, and the time and value of the achieved sand core peak temperatures after the start of pouring. It is not applicable for the hardened reference sample.

Times of thermal exposure of the sand cores are significantly different with the different cooling types. Because the sand cores have low thermal conductivity, they show long heating delays relative to the short pouring time of < 10 s. For the water-cooled case, the sand cores reach their peak temperature even after the casting has been cooled by water quenching. For air and insulation cooled cases, the cooling of the cores is fully linked to that of the castings.

2.2. Core removal trials

A vibration unit equipped with two electrical imbalance drives rotating at 50 Hz has been used for the shake-out trials. The shaken-out sand was directly funnelled onto a balance, and the removed sand mass was recorded with 1 Hz resolution. The test castings were clamped into a vertically guided sample holder, which is shown in Fig. 3.

On top of the sample, a knocking mass has been placed. Both the sample and mass are freely movable in the vertical direction. The maximum vertical acceleration of the vibration unit was measured as 6 g. On the sample, a maximum vertical acceleration was measured as 40 g for 99 % of the values, with peaks of up to 100 g.

2.3. Particle size analyses

A Retsch AS200 digit sieve machine with meshes of 0 (tray), 63, 90, 125, 180, 250, 355, 500, 710, 1000 and 1400 μm width was used for the particle size analysis, according to the standard sieving procedure (ISO, 2016).

The removed core sand from castings also contains larger agglomerates and core lumps. To avoid their excessive breakdown during sieve analysis, the sieving amplitude was reduced from 1,5 to 0,2 mm, and

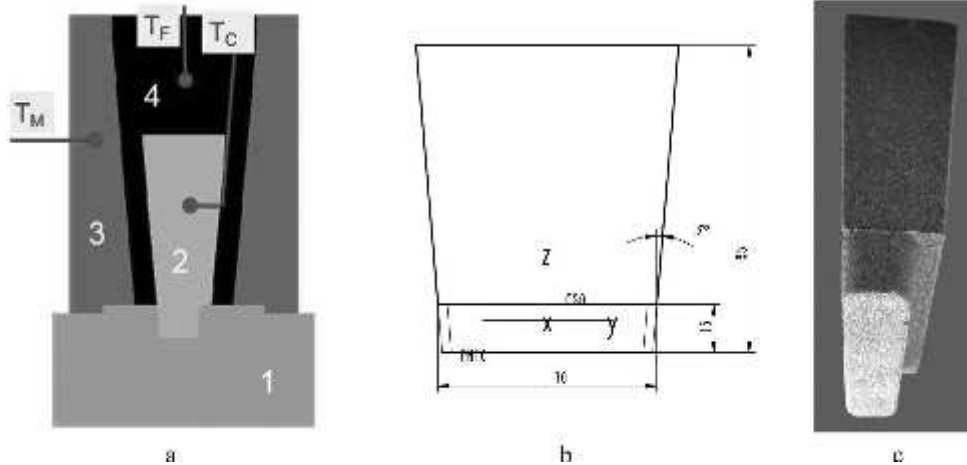


Fig. 2. Test core geometry and mould setup. (a): Schematic cross section through the mould setup consisting of (1) a base plate, (2) a core, and (3) the upper mould part. The casting is formed in the cavity (4). The thermocouple positions are: T_M in the mould, T_C in the core centre, and T_F in the feeder centre. (b): Test core main dimensions and (c) realised core.

Table 1
Main thermal characteristics of test castings and cast-in cores.

Condition	Casting cooling time below 120 °C in s	Sand core exposure time above 120 °C in s	Sand core peak temperature time in s	Sand core peak temperature in °C
Water	400	900	480	380
Air	4000	4000	700	400
Insulation	40000	40000	900	410

the sieving time was reduced from 600 to 60 s. The whole retained sand portion for the largest mesh (1,4 mm) was defined as the lump mass fraction m_l .

3. Results and discussion

3.1. Core removal experiments

Curves for removed mass over time (obtained from the vibration test bench) are presented for the different sample conditions, followed by mass rate and particle size evaluations.

Fig. 4 illustrates the typical visual appearance of the collected removed core sand. The hardened sample yielded finely de-agglomerated sand and a large single core lump. The water – cooled sample revealed very few and small core lumps. In contrast, the air and insulation cooled samples exhibited a significantly higher number of core lumps. Higher initial damage was observed for longer thermal exposure times.

Fig. 5 shows mass curves over time for the four different thermal exposure scenarios. The curve sections with the lowest mass-over-time incline are indicated. The removed core mass curves all have a characteristic shape. An initial transient phase is followed by a steady state

phase with a typically lower mass rate; this reflects the maximum sand core resistance. At the end of the process, a final transient phase is observed, where most of the removed sand core is yielded as lumps. Core removal at the end of the process is dominated by the casting geometry and controlled by the size of the opening of the casting. The required time for core removal was typically 5–20 min for the hardened and water-cooled variants and 1–2 min for the air and insulation cooled variants.

To improve manual minimum mass rate evaluation, an objective criterion is required. The minimum core removal mass rate R_{min} can best be described by the quarter mass rate R_{25} , which can be defined as the longest time segment t_Q on a mass-time curve for obtaining 25 % of the total removed core mass m_{tot} (Eq. (1)):

$$R_{25} = \frac{m_{tot}}{4 \cdot t_Q} \tag{1}$$

Fig. 6 illustrates such identified R_{25} -segments for one example of each sample condition. Fig. 7 shows the high correlation between the manually obtained minimum mass rate and R_{25} -criterion. Fig. 8 summarises the obtained quarter mass rate results.

From Fig. 8, it is clear that thermal exposure leads to an increased core removal rate for silicate bonded samples. The slowest core removal was observed for the hardened condition. The water-cooled condition exhibited a 2–3 times larger core removal rate. Significantly higher core removal rates were found for the air and insulation cooled conditions. In particular, the air-cooled condition revealed high scatter, which required deeper investigations into process sensitivity and storage conditions.

In this study, three castings were sealed against air exchange during the cooling phase at a still-elevated casting temperature. This was done to eliminate humidity condensation. For a direct comparison, two more castings were openly stored in ambient air. After 10 h of overnight

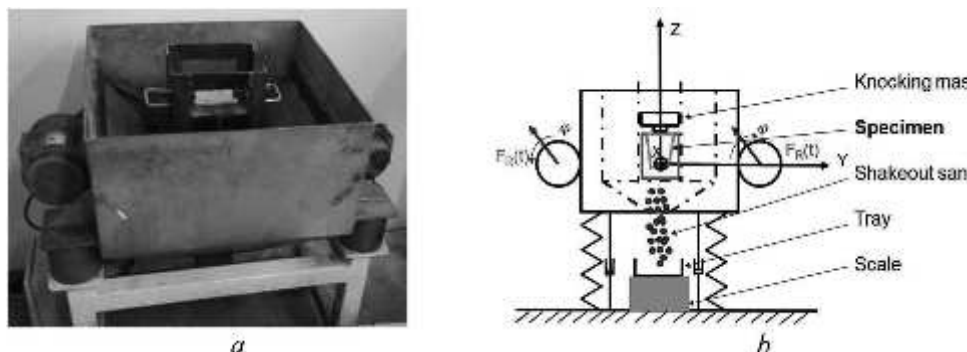


Fig. 3. Vibration unit for shake-out trials. (a) Setup, and (b) Schematic view of the functional elements. The cross section of the hopper opening is $0,8 \times 0,8 \text{ m}^2$.

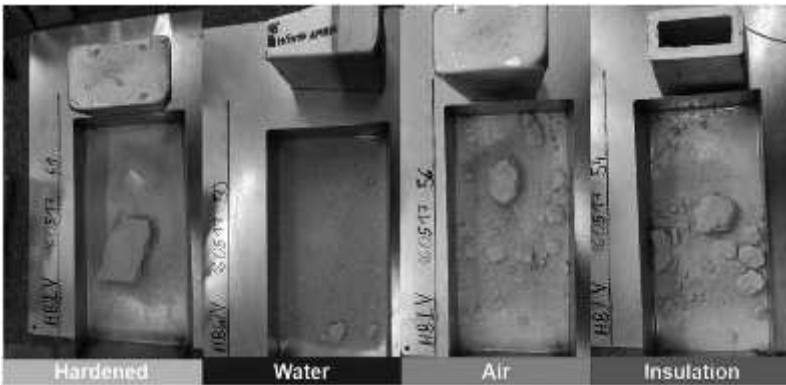


Fig. 4. Results of core removal trials for silicate bonded sand core samples with different thermal exposure conditions. The empty castings are positioned beside the core sand tray.

storage at 25 °C and a relative humidity of 40–50 %, the cores were removed. The resulting mass over time curves are shown in Fig. 9.

The results demonstrate a significant deceleration in core removal for the unsealed samples compared to the sealed samples. The core removal mass-time curves for the unsealed samples are similar to the initial curves presented in Fig. 5(c) and (d). In contrast, the sealed samples had both low scatter and the shortest measured core removal times of all studies.

The silicate bonded sand cores had a propensity to absorb humidity. This prolongs the core removal rate, which is potentially overlaid to all results.

3.2. Particle size evaluation

This section presents an analysis of particle size modelling, and the deduction of the de-agglomeration degree and rate. The achieved results for the different conditions are summarised and discussed.

To apply an extended analysis of the obtained sieve fraction after core removal, a particle analysis according to the RRSB approach was performed. The RRSB function of the retained mass portion R_{RRSB} of the total mass for a particle diameter d_p is shown by Eq. (2).

$$R_{RRSB} = e^{-\left(\frac{d_p}{d_p^*}\right)^k} \tag{2}$$

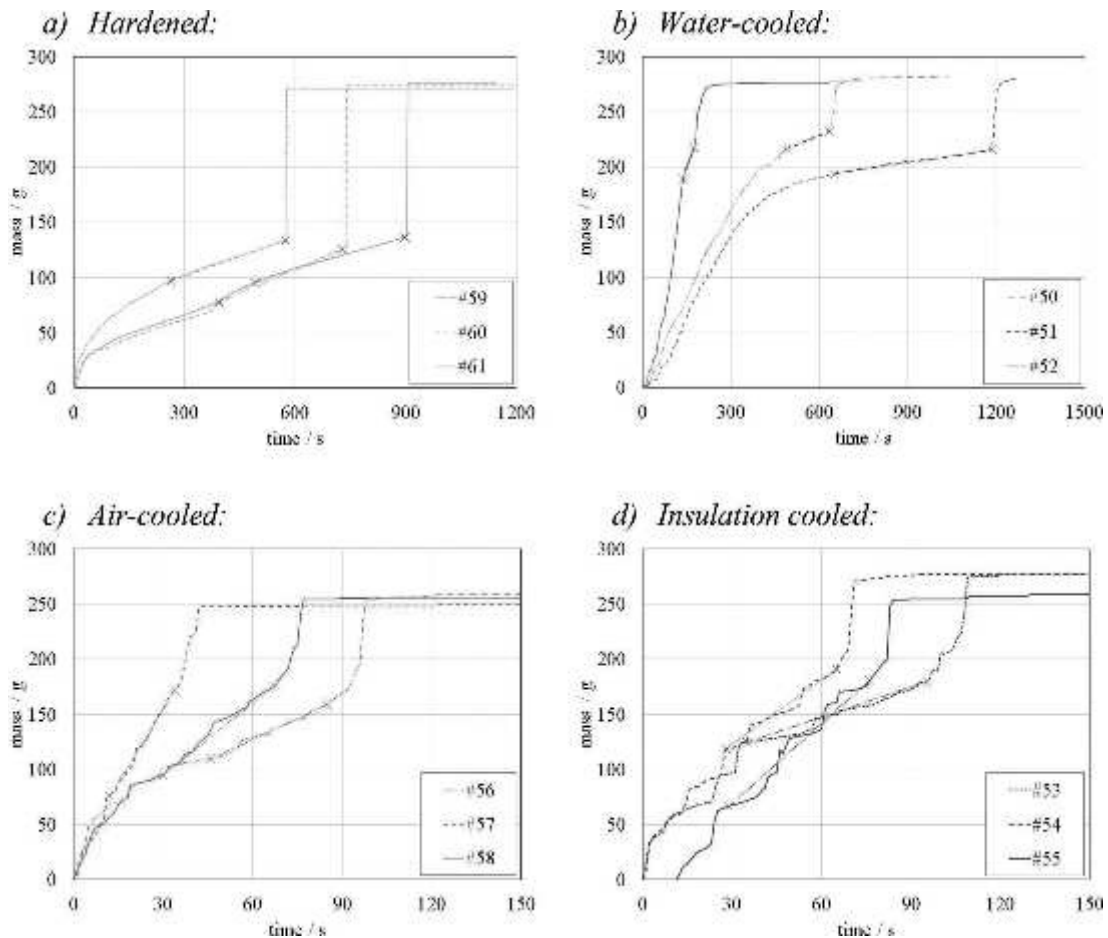


Fig. 5. Mass over time curves for the differently treated samples (# given in Table 3). The manually identified steady state range showing a minimum slope is indicated by X to X.

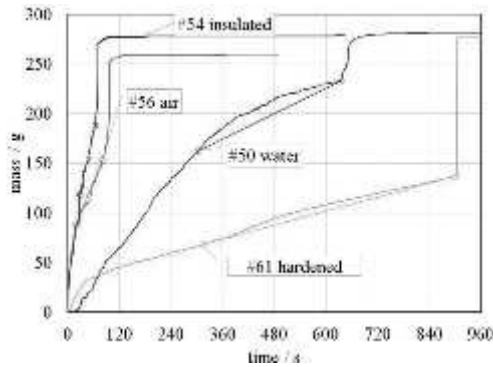


Fig. 6. Typical shake-out mass increase curves for silica bonded samples. One example of every cooling condition including the quarter mass evaluation range is shown.

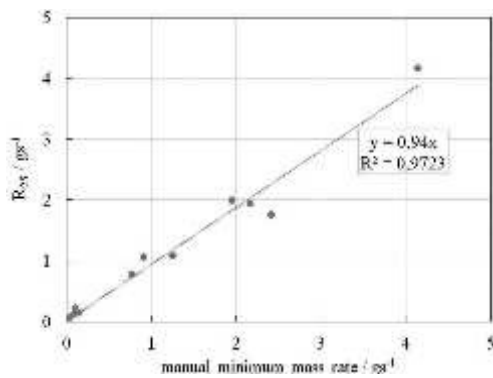


Fig. 7. Correlation of manually evaluated minimum mass rate with quarter mass shake-out rate R_{25} .

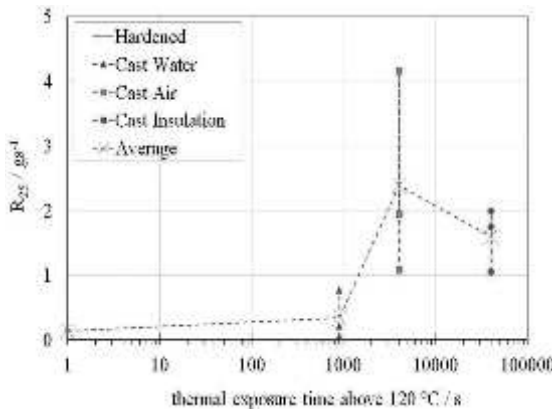


Fig. 8. Minimum core removal mass rate, defined by quarter mass rate. Single measurement results and group average results are shown over thermal exposure time.

k : distribution parameter; d_p^i : grain size parameter.

$$s^2 = \frac{\sum_{i=1}^n (R_m^i - R_{RRSB}^i)^2}{n - 1} \quad (3)$$

During experimental evaluation, the RRSB parameters are obtained by minimising the variance of s^2 the modelled versus the measured particle size distribution curves (Eq. (3)). R_m^i : measured retained mass fraction on mesh i , R_{RRSB}^i : RRSB-modelled retained mass fraction on mesh i

The relevant retained mass fractions for the RRSB fit are those on $n = 9$ meshes from 63 to 1000 μm . Excluded are the collecting tray, which always contains 100 %, and the 1400 μm mesh, which by

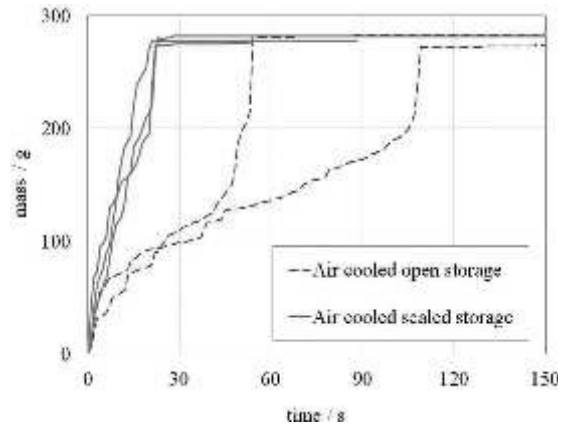


Fig. 9. Mass over time curves of silicate bonded cores with dry storage (solid line) and open storage in ambient air (dashed line).

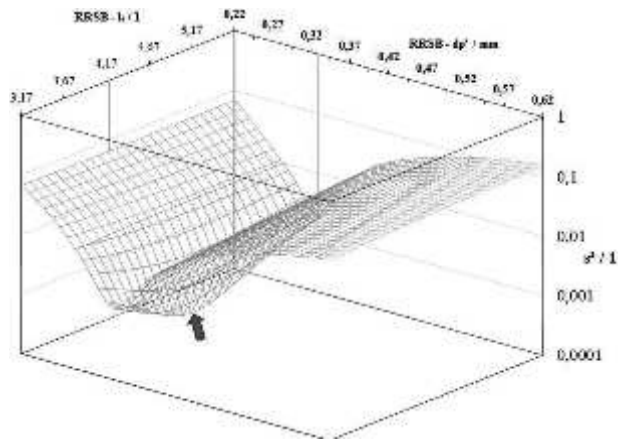


Fig. 10. Variance in RRSB fit for silica raw sand over RRSB-parameters showing a distinct minimum, indicated by the arrow.

Table 2

Sieve analysis of the used silica sand. Lower and upper meshes, measured mass fractions, and the RRSB-modelled retained mass fractions are listed.

Lower mesh in μm	Upper mesh in μm	Sieved mass fraction in %	Retained mass fraction R_m in %	RRSB modelled mass fraction R_{RRSB} in %
0	63	0	100	99,9
63	90	0	100	99,6
90	125	0,3	99,7	98,3
125	180	4,9	94,8	92,5
180	250	22,9	71,9	73,4
250	355	45,4	26,4	26,2
355	500	22,5	3,9	0,4
500	710	3,6	0,3	0
710	1000	0,3	0	0
1000	1400	0	0	0
1400		0	0	0

definition contains m_L . The parameters were fitted with three-digit accuracy.

Assuming spherical particles, the specific surface S_M^{RRSB} can be approximated with an error below 2,5 %, as documented by Eq. (4) (Zogg, 1993).

$$S_M^{RRSB} = \frac{A_K}{\rho \cdot V} = \frac{6,39}{\rho \cdot d_p^i} \cdot e^{\left(\frac{1,795}{k^2}\right)} \quad (4)$$

A_K : granulate surface; ρ : density; V : volume.

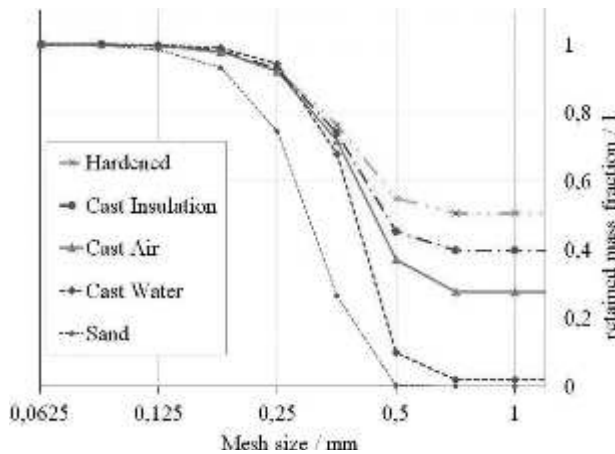


Fig. 11. Retained mass fraction from sieve analysis for removed core sand from all thermal exposure conditions compared to the raw sand.

Because of its low specific surface contribution, the lump mass fraction will be excluded from the specific surface evaluation of core sand S_M^{sand} , leading to Eq. (5):

$$S_M^{coresand} = S_M^{RRSB} \cdot (1 - m_l) \tag{5}$$

The researched de-agglomeration degree is defined by the quotient $S_M^{coresand} : S_M^{rawsand}$. Any presence of agglomerated sand particles results in a de-agglomeration degree < 1.

To assess time dependency, an identified minimum core removal rate R_{min} is linked with the created specific surface results in the de-agglomeration rate R_S (Eq. (6)).

$$R_S = R_{min} \cdot S_M^{coresand}$$

This criterion reflects the rate at which sand particle bonds are broken up. The de-agglomeration rate predominantly refers to the sand core bonding strength properties. Any pre-damage to the core is reflected (e.g. by different thermal loads or casting contraction stresses), along with the residual core strength and brittleness.

Based upon the measured grain size analysis and the retained mass fraction, all mesh sizes have been obtained. Subsequently, the optimum RRSB distribution was evaluated. Fig. 10 illustrates the variance plot over the field of RRSB parameters that serves to find the optimum RRSB

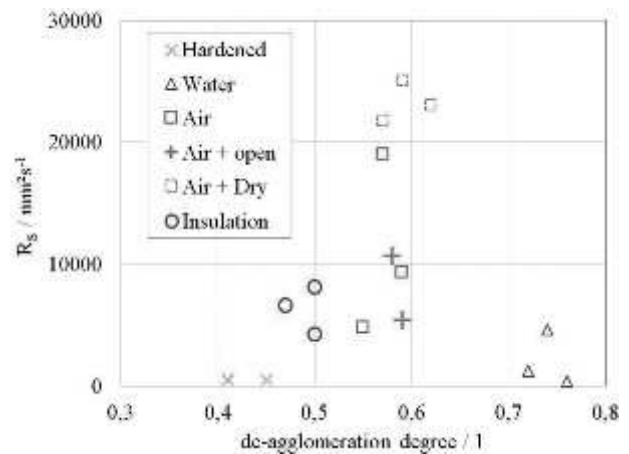


Fig. 12. De-agglomeration rate over de-agglomeration degree for different investigated thermal exposure conditions of investigated sand cores.

parameter combination for the silica raw sand.

A pronounced minimum is present, with $d_p = 0,331$ mm and $k = 4,178$ and a minimum standard deviation $\sqrt{s^2} = 1,68\%$. Standard deviation was below 2 % for all evaluated particle size distribution curves. The measured and modelled retained mass fraction results for the raw sand are documented in Table 2.

RRSB particle size distribution curves for raw sand and the removed core sand of all thermal exposure variants are shown in Fig. 11.

The removed core sand generally shows a shift towards higher particle sizes, indicating the presence of sand agglomerates. The highest lump mass fraction (above 50 %) was found for the hardened condition, followed by the insulated and air-cooled cases. Interestingly, the lump mass fraction was very low for the water-cooled case.

3.3. De-agglomeration behaviour

In Table 3, all results are summarised, while a graphical summary of the de-agglomeration properties of all samples is shown in Fig. 12. The degree of de-agglomeration for the different thermal sample conditions occurs in a typical range for each thermal exposure.

The data reveal that the de-agglomeration rate is direct proportional to the minimum shake-out mass rate and de-agglomeration degree is

Table 3

Shake-out results of all tested samples. The shake-out mass rate, RRSB parameters, evaluated diameter, de-agglomeration degree, and evaluated de-agglomeration rate are documented.

Condition	sample #	Particle size distribution parameters for RRSB fit		Shake-out quarter mass rate R_{25} in gs^{-1}	De-agg.- rate $R_S / mm^2 s^{-1}$	Lump mass fraction m_l in %	De-agg.- degree in %
		Grain size parameter d' in mm	Distribution parameter k				
pure	H32	0,331	4,178	–	–	–	100
Hardened	59	0,412	3,986	0,15	481	50	41
	60	0,394	3,781	0,14	460	52	41
	61	0,386	3,661	0,12	426	49	45
Water	50	0,429	5,609	0,21	1236	2	72
	51	0,415	5,175	0,06	343	2	76
	52	0,421	5,344	0,77	4594	2	74
Air	56	0,417	4,075	1,08	4779	31	55
	57	0,421	4,037	4,16	19008	29	57
	58	0,426	4,328	1,94	9292	23	59
Air + open	75	0,431	4,603	1,13	5390	22	59
	76	0,421	4,405	2,29	10681	26	58
Air + Dry	79	0,427	4,689	4,63	23082	19	62
	82	0,416	4,182	5,30	25080	26	59
	83	0,427	4,207	4,70	21796	26	57
Insulation	53	0,414	4,287	1,05	4221	38	50
	54	0,409	4,196	1,99	8091	38	50
	55	0,398	4,166	1,75	6605	44	47

inversely proportional to the lump mass fraction. Thus, applied for quality control purposes these primarily measured characteristics can be evaluated without full grain size analysis already.

The lowest de-agglomeration rate and –degree were observed for the hardened condition. The initial core strength is non-deteriorated by any overlaid loading.

The cast-in samples all exhibited a higher de-agglomeration rate. As previously discussed, this rate was potentially decreased by the influence of ambient air humidity, as different examples with air-cooled samples clearly show. Interestingly, for a longer thermal exposure time (e.g. during insulated cooling), a lower degree of de-agglomeration and higher de-agglomeration rate were found, relative to the water-cooled condition. This may be attributed to thermally induced sand core damage, which can cause binder embrittlement by de-hydration and micro-cracking caused by sand grain expansion.

The major process difference between the externally hardened sample and cast-in and water-cooled samples is the missing casting-core interaction for the hardened sample. This led to the early release of large core lump pieces, and the consequent observed low degree of de-agglomeration. In contrast, the core in the water-cooled sample suffered only minor damage during the casting process, but may have been intensively exposed to hydrostatic pressure from the rapidly contracting quenched casting as the core expanded, because of the low thermal conductivity of the core. These thermomechanical stress conditions could have prevented the early release of the cast-in core during the vibration-induced core removal process.

4. Conclusions

- Sand core disintegration at core removal from cast parts was quantified with a de-agglomeration rate criterion. Two main elements required are the minimum core removal mass rate, which is reflecting the kinetics, and the specific surface area of the removed core sand compared to the initial one of the raw sand.
- The core lump mass constituted a significant fraction of the removed cores sand. The observed core lump disintegration was depending on the casting parameters.
- Particle size measurement of the removed core sand required specifically adjusted parameters. The resulting size distribution was modelled with good accuracy using an approach adopted from the field of mineral processing. This allowed the subsequent calculation of the specific surface area.
- The de-agglomeration rate of non-cast in reference core samples was the lowest. Cast-in cores show higher de-agglomeration rate with increased thermal exposure. Specifically, samples stored without ambient air exchange exhibited the highest de-agglomeration rate.
- Implementation of the method is possible for whichever casting

geometry and core removal technology. For intricately shaped cores a complex transient process load overlay could be hindering to access the exact kinetics in experiments. Modelling of local core properties influenced the thermal and mechanical interaction with the cast part might be required.

Acknowledgements

The support from company Nematik Linz for this study by enabling the extensive use of production and engineering facilities is highly acknowledged.

References

- Bayat, H., Rastgo, M., Zadeh, M., Mansouri, Vereecken, H., 2015. Particle size distribution models, their characteristics and fitting capability. *J. Hydrol.* 529, 872–889. <http://dx.doi.org/10.1016/j.jhydrol.2015.08.067>.
- Brown, W.K., Wohletz, K.H., 1995. Derivation of the Weibull distribution based on physical principles and its connection to the Rossin-Rammler and lognormal distributions. *J. Appl. Phys.* 78, 2758–2763. <http://dx.doi.org/10.1063/1.360073>.
- Czerwinski, F., Mir, M., Kasprzak, W., 2015. Application of cores and binders in metalcasting. *Int. J. Cast Met. Res.* 28, 129–139. <http://dx.doi.org/10.1179/1743133614Y.0000000140>.
- Fennell, T., Crandell, G., 2008. Inorganic Binder Properties Study. 1413–145 NA. Principles of Mineral Processing. In: Fuerstenau, M.C., Han, K.N. (Eds.), Society for Mining, Metallurgy, and Exploration, Inc. (SME) (Littleton, Colorado, USA 80127).
- Gamisch, M., 2002. Mechanisches Entkernen von Al-Gussteilen mit geringer Beanspruchung des Gussteils. *Giesserei-Rundschau* 49, 43–45.
- Henry (Ashland), C., Showman (Ashland), R., Wandtke (Ashland), G., 1999. Core and foundry process variables affecting aluminum casting shakeout of cold box cores. *Trans. Am. Foundry Soc.* 107, 99–115.
- ISO, 2016. 3310-1:2016-08 2016–08 (E) Test Sieves – Technical Requirements and Testing – Part 1: Test Sieves of Metal Wire Cloth Standard. Beuth Verlag GmbH.
- Izdebska-Szanda, I., Angrecki, M., Matuszewski, S., 2012. Investigating of the knocking out properties of moulding sands with new inorganic binders used for castings of non-ferrous metal alloys in comparison with the previously used. *Arch. Foundry Eng.* 12, 117–120.
- Major-Gabryś, K., Dobosz, S.M., Jelinek, P., Jakubski, J., Beno, J., 2014. The measurement of high-temperature expansion as the standard of estimation the knock-out properties of moulding sands with hydrated sodium silicate. *Arch. Metall. Mater.* 59, 739–742. <http://dx.doi.org/10.2478/amm-2014-0123>.
- PN-85/H-11005, 1985. Moulding and Core Sands Technological Knockout Properties Test (No. PN-85/H-11005). Polish Standards Institute – Polski Komitet Normalizacji, Miar I Jakosci, Poland.
- Paluszny, A., Tang, X., Nejati, M., Zimmerman, R.W., 2016. A direct fragmentation method with Weibull function distribution of sizes based on finite- and discrete element simulations. *Int. J. Solids Struct.* 80, 38–51. <http://dx.doi.org/10.1016/j.ijsolstr.2015.10.019>.
- Quarzwerte, 2009. Quarzsand Haltern H 31 bis H 35, Quarzwerte Stoffdaten. (D-50207 Frechen).
- Rosin, P.O., Rammler, E.J., 1933. The Laws Governing the Fitness of Powdered Coal. Weibull, W., 1951. A statistical distribution function of wide applicability. *J. Appl. Mech.* 8491543.
- Zogg, M., 1993. In: Teubner, B.G. (Ed.), Einführung in die mechanische Verfahrenstechnik, 3rd ed. Burgdorf, Stuttgart.

4.4 Specific fracture energy and de-agglomeration rate of silicate-bonded foundry sand cores

Authors	B.J. Stauder (Nemak Linz); D. Gruber (MUL); P. Schumacher (MUL)
Journal	Springer - Journal of Production Engineering DOI: 10.1007/s11740-018-0854-8 © 2018 Springer. All rights reserved.
Individual author contributions	60 %: B.J. Stauder: sample planning and production; evaluation and interpretation; corresponding author. 30 %: D. Gruber: Wedge splitting testing evaluation, interpretation. 10 %: P. Schumacher: Casting process related scientific context.

Abstract

Inorganic binder systems have found increasing applications, driven by environmental and legal regulatory requirements. As a consequence of their thermal stability, the mechanical core removal process is challenging and not fully predictable, owing to a lack of mechanical fracture energy data.

In the present work, the wedge splitting test method was utilised to determine the specific fracture energy of sand cores, which was related to the strength and de-agglomeration rate results from the core samples before and after thermal exposure.

Silica sand (quartz) and a synthetic sintered mullite, bonded with a water glass binder, were investigated. Following thermal exposure up to 400°C, mullite-based cores retained a high strength without apparent bonding damage, an increased brittleness, and lower specific fracture energy. Following the same thermal exposure, quartz sand samples show decreased strength, Young's modulus and brittleness, but retained a high specific fracture energy. The characteristic differences were caused by micro-cracks in the intergranular silicate bonds.

Overall, an inverse relationship between the specific fracture energy and the de-agglomeration rate was found. In contrast to non-cast reference samples, shrinkage strain and thermal loading influences from the casting process resulted in much higher de-agglomeration rates for the cast-in samples.

In summary, the wedge splitting test data provided relevant improvements for the description of de-agglomeration mechanics. Future research should cover the effects of brittleness and mechanical load intensity.



Specific fracture energy and de-agglomeration rate of silicate-bonded foundry sand cores

Bernhard J. Stauder¹ · Dietmar Gruber² · Peter Schumacher²

Received: 10 July 2018 / Accepted: 11 October 2018
© German Academic Society for Production Engineering (WGP) 2018

Abstract

Inorganic binder systems have found increasing applications, driven by environmental and legal regulatory requirements. As a consequence of their thermal stability, the mechanical core removal process is challenging and not fully predictable, owing to a lack of mechanical fracture energy data. In the present work, the wedge splitting test method was utilised to determine the specific fracture energy of sand cores, which was related to the strength and de-agglomeration rate results from the core samples before and after thermal exposure. Silica sand (quartz) and a synthetic sintered mullite, bonded with a water glass binder, were investigated. Following thermal exposure up to 400 °C, mullite-based cores retained a high strength without apparent bonding damage, an increased brittleness, and lower specific fracture energy. Following the same thermal exposure, quartz sand samples show decreased strength, Young's modulus and brittleness, but retained a high specific fracture energy. The characteristic differences were caused by micro-cracks in the intergranular silicate bonds. Overall, an inverse relationship between the specific fracture energy and the de-agglomeration rate was found. In contrast to non-cast reference samples, shrinkage strain and thermal loading influences from the casting process resulted in much higher de-agglomeration rates for the cast-in samples. In summary, the wedge splitting test data provided relevant improvements for the description of de-agglomeration mechanics. Future research should cover the effects of brittleness and mechanical load intensity.

Keywords Casting · Sand core · Core removal · Specific fracture energy · Material testing

1 Introduction

Complex, undercut, and hollow cast metal shapes can be most economically realised using sand cores. Following the casting process, a fragmentation of the cast-in cores into pieces sufficiently small for their removal from the cast cavities is crucial. During the past decade, the share of sand cores using inorganic binders for aluminium castings has steadily increased [1, 2], and they are replacing organic binder systems for largely ecological reasons. Mechanical core removal is done by hammering and vibration of the castings [3].

Less favourable sand core de-composition must be expected, when inorganic cores with increased thermal stability are used. Precise adjustments of binder type and

addition are practised to achieve sufficient strength and satisfy the core removal. Moreover, according to Zaretskiy [2], inorganic binders applied for light metal casting volume production all contain additives to improve the casting surface quality and the core removal properties. These are frequently evaluated from the retained mechanical strength of thermally pre-conditioned core samples [2, 4–6]. Thermo-gravimetric or thermal analysis methods allow precise determination of the temperature-, atmosphere- and heating-rate-dependent de-composition behaviour of binder systems, as demonstrated in previous investigations [7–10]. Stauder et al. [11] introduced a de-agglomeration rate criterion evaluated from cast-in core samples with a defined mechanical agitation intensity. These results reflected the significant influences of the casting process history, such as cooling intensity, ambient conditions, and physical core material properties. The effective vibration load transfer during a core removal process from the metal casting walls to the cast-in core sections is highly variable over time. An intensive wall contact between the casting and the core can be initially present, when the core surface layer is not degraded. As soon as parts

✉ Bernhard J. Stauder
bernhard.stauder@nemak.com

¹ Nemak Linz GmbH, 4030 Linz, Austria

² Montanuniversität, 8700 Leoben, Austria

of the cores are loosened, a multi-body situation between the core fragments and the casting occurs, which is consequently dependent on the geometry and agitation parameters. The de-agglomeration rate constitutes a measurable reaction of the sand core specimens during a defined casting agitation.

An analytical prediction of core de-agglomeration is very complex because of the transient overlay of thermal and mechanical loads, resulting in locally altered core properties. Core sections after contact with melt, owing to their low thermal conductivity, heat up non-uniformly. During solidification, the metal shrinkage counteracts the core expansion, and increasing strains are exerted on the cast-in core sections. Castings with an increased volume of cavities formed by sand cores exhibit less casting shrinkage, as Campbell [13] documented referring to the dimensional accuracy of castings.

Only a few investigations concerning material models for foundry sand cores are available in the literature, e.g. [14–17]. In these specific case studies, not all transient and localised effects and structural binder changes were evaluated.

The assumed key characteristics for the description of a mechanical core removal step at the end of the casting process are the mechanical properties of the core and the specific fracture energy required during their comminution. The main intention of this study was to evaluate the applicability of wedge splitting testing for foundry sand cores and to relate the results to de-agglomeration tests.

2 Experimental background

The materials used for the core samples, their production and thermal exposure conditions, and the applied testing methods are described in the following.

2.1 Investigated materials

Silica sand type ‘H32’ (quartz), according to [18], termed ‘Q’, and sintered spray-compacted synthetic mullite [19], termed ‘M’, were used as granular materials for the core samples. As binder a sodium -silicate solution with a molar SiO₂:Na₂O ratio of 3:25 and 36% solid fraction (water glass) [20] was used, added by 2.5 mass% to the sand. The sample cores were produced using electrically heated core boxes on a manually operated ‘Roepert H1’ (1 l sand volume) core blowing machine. The cores were hardened in the core box according to the parameters given in Table 1.

Hot air gassing was not available. Therefore, after take-out from the core box, the samples were dried in a chamber furnace for another 10 min at 120 °C to evaporate residual water. After cooling, the sand cores were sealed in polypropylene foil to avoid air exchange and humidity take-up

Table 1 Core box hardening parameters for sand core samples

Core type	Core box temperature and hardening time of the sample in the core box
Bending test bars	160 °C/1 min
Core removal test cores	160 °C/1 min
Wedge splitting samples	150 °C/2 min

during storage. Storage time of bending test bars and core removal test cores was 1 day, whereas it was 3 weeks for the wedge splitting specimens.

The microstructure of the granular materials and cores was investigated using a light-optical stereo microscope (Zeiss ‘SteREO Discovery’) and a scanning electron microscope (SEM; Jeol ‘JSM-IT300 LV’) utilising a low vacuum modus.

2.2 Wedge splitting tests

The wedge splitting test was introduced by Tschegg [21]. Further developments for ceramic materials were developed and implemented, as documented from others [22–25]. From these tests the specific fracture energy, nominal notch tensile strength, and brittleness parameters can be evaluated. The sample dimensions, testing setup, and evaluation scheme are illustrated in Fig. 1.

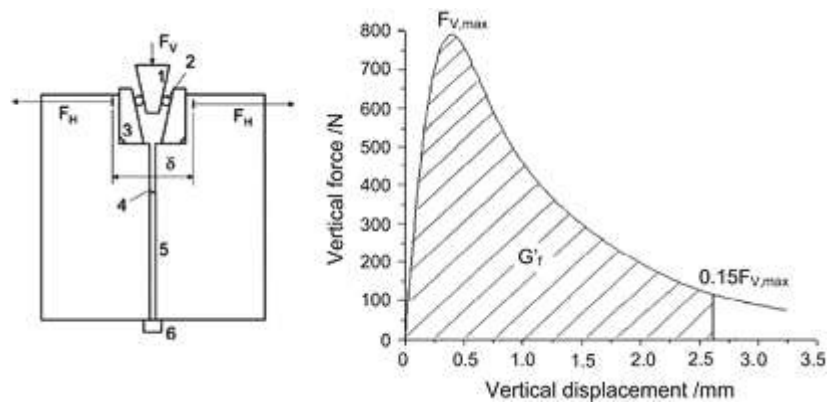
A load was introduced by a wedge (1) and laterally transferred via rolls (2) and load-transmission pieces with a defined wedge angle (3) onto the sample. During testing of the samples, as shown in Fig. 1 (left and centre), the load and displacement data, as shown in Fig. 1 (right), were recorded. A fracture was initiated at a starter notch (4) and a planar fracture growth was supported by optional side grooves (5). The whole setup was positioned on a narrow bar (6).

The mechanical fracture energy is defined by the load–displacement integral from the load F and displacement δ , evaluated both in either the vertical or horizontal directions until δ_U at fracture (Eq. (1)):

$$G_F = \frac{1}{A} \int_0^{\delta_U} F d\delta. \quad (1)$$

Load and displacement in the vertical direction, F_V and δ_V , respectively, can be directly obtained from the testing machine, whereas F_H in the horizontal direction is calculated using the wedge angle α with $F_H = F_V / (2 \cdot \tan(\alpha/2))$ and δ_H acquired on the sample using a separate (here optical) measurement system. In this work, we evaluated the horizontal load–deflection signals with the advantage that the

Fig. 1 Left picture: Wedge splitting testing setup and an example of a load–displacement curve of a refractory material [24]



potential settling effects between the load transmission elements and the core samples were eliminated.

With the maximum horizontal load, $F_{H, \max}$, the nominal notch tensile strength can be evaluated according to Eq. (2) as follows:

$$\sigma_{NT} = \frac{F_{H, \max}}{bh} \left(1 + \frac{6y}{h} \right). \quad (2)$$

Symbol b is the fracture ligament width, h is the height, and y is the vertical distance between the load vector and the ligament centre.

The load–displacement curves were generally recorded until a decline to 15% of the maximum load to avoid potential wedge collision (which is possible for less brittle samples), which allows the evaluation of the specific fracture energy G_f^* . Furthermore, an inverse evaluation of the load curve shape, described by Jin et al. [24], delivers the tensile strength σ_f and the characteristic length l_{ch} according to Hillerborg et al. [26]. The characteristic length is a material property and represents the relationship between the specific fracture energy and elastically stored energy, provided in Eq. (3) as follows:

$$l_{ch} = \frac{G_f E}{\sigma_f^2}. \quad (3)$$

The required Young's modulus E was evaluated using ultrasonic measurements using the Ultrasonic Tester BP-700 from the company Ultra test.

2.2.1 Wedge-splitting test samples

Test cores were produced according to Table 1 and the cores pre-conditioned at 300 °C were prepared for wedge-splitting tests. During the pre-conditioning operation, the fracture area of the core samples was shielded with Al-foil to avoid

overheating. The sample front ends remained uncovered to allow for potentially evolving steam to escape. Pre-conditioning batches were temperature-surveyed using an additional instrumented sample. As shown in Fig. 2a an as-produced sample and in Fig. 2b samples in the pre-conditioning furnace were developed.

Figure 3 shows a typical temperature profile during thermal pre-conditioning of the wedge splitting test samples.

In contrast to the cast-in cores, wedge splitting test samples were heated in a furnace with a limited heating rate to avoid cracking due to thermo-mechanical stresses of the sand core samples.

2.3 Bending tests

Three-point bending test evaluations of strength and stiffness development according to the method of Stauder et al. [27] were conducted. The elastic modulus was evaluated from the maximum stiffness of the recorded load–deflection curve using a linear-elastic continuum-mechanical approach. The bending strength was calculated from the maximum load and the total test bar cross-section. Produced samples according to Table 1 and in addition, samples after thermal pre-conditioning according to Table 2, were evaluated.

2.4 De-agglomeration rate evaluation

Test cores produced according to Table 1 were cast with alloy Al – 7% Si – 0.5% Cu – 0.3% Mg at 745 ± 10 °C. The castings subsequently cooled in ambient air, as documented in [11]. In the cast-in cores, a peak temperature of 400 °C and an exposure for approximately 20 min above 300 °C occurred. Figure 4 shows an overview of the de-agglomeration test procedure.

In addition to the cast-in cores, reference samples were provided. To produce these, mixed core sand was filled into sand-free test castings, which were pre-heated to

Fig. 2 **a** As-produced wedge splitting test sample. **b** Wedge splitting test sample batch in the furnace chamber prior to thermal pre-conditioning

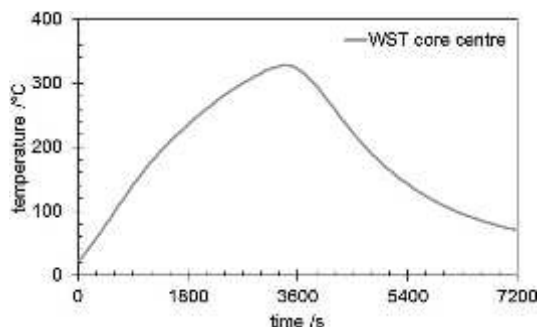
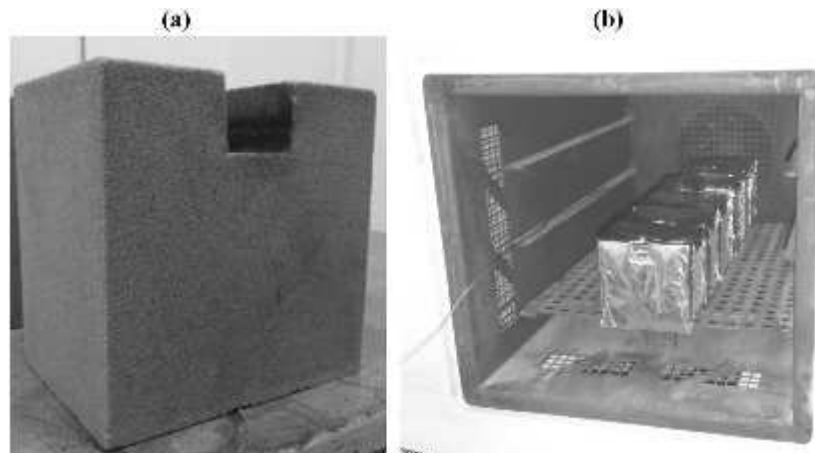


Fig. 3 Temperature profile during thermal pre-conditioning of an instrumented wedge splitting test sample, measured in the centre of the fracture ligament area

Table 2 Defined isothermal holding time for thermal pre-conditioning of the sand core samples

Temperature/ °C	Hold- ing time (min)
200 (±5)	60
300 (±5)	30
400 (±5)	10

200 °C. There, the core sand hardened via the heat transfer from the pre-heated casting, which was a comparable situation to the core sand hardening in a heated core box. As the same material conditioning was intended for the wedge splitting, bending and de-agglomeration tests, some of these reference specimens were preconditioned at 300 °C.

In summary, the de-agglomeration rates were evaluated for the following conditions:

1. Reference samples (not cast-in) in an as-produced condition;
2. Reference samples (not cast-in) pre-conditioned at 300 °C;
3. Cast-in samples with ambient air cooling;

3 Results

3.1 Bending tests

Under the as-produced condition, similar elastic moduli and a lower strength for synthetic mullite samples compared to that of the silica samples were evaluated. However, the temperature-dependent strength and elastic modulus development was very different for the water-glass-bonded silica and the synthetic mullite cores, as shown in Fig. 5.

After pre-conditioning at 200 °C, both core types showed increased elastic moduli, owing to a complete de-hydration of the water glass binder. The test results of the synthetic mullite samples remained similar even after being subject to higher applied pre-conditioning temperatures. In contrast, the silica samples after pre-conditioning at 300 and 400 °C showed significantly diminished strength and elastic moduli results. Therefore, the microstructure of the core samples was investigated for apparent damage after the 400 °C pre-conditioning. SEM-investigations showed micro-cracks in the bonds of the silica sand cores. In contrast, no damage was visible in the synthetic sintered mullite core bonds. The typical appearance of a granular particle bond is shown in Fig. 6 for both core types.

Thermal expansion data from Recknagel and Dahlmann [28] in the range from 20 to 600 °C show significantly different characteristics for both granular materials. Silica sand

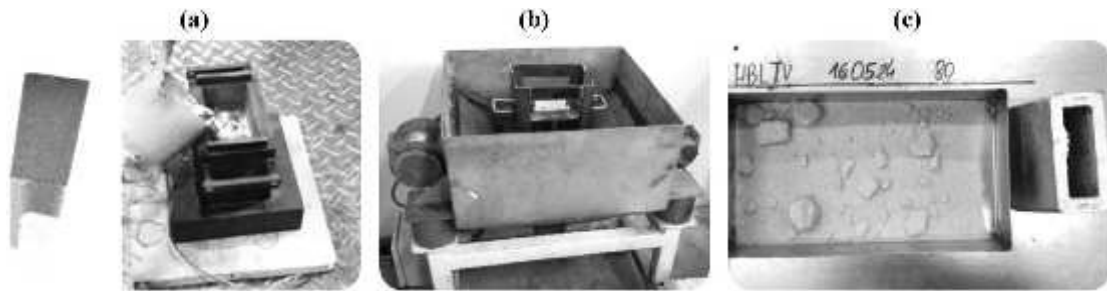


Fig. 4 Experimental setup for the de-agglomeration rate evaluation of the core samples cast with aluminium alloy (a). Core removal with mass acquisition (b) and subsequent core sand characterisation (c) are shown [11]

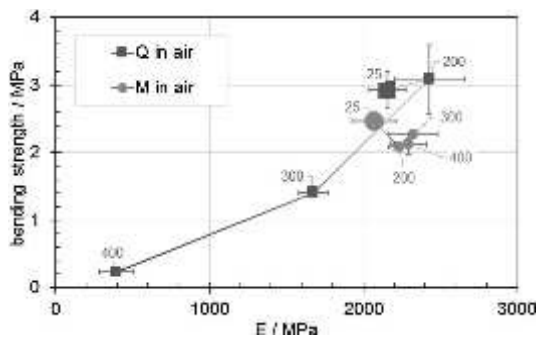


Fig. 5 Bending strength and elastic modulus of the water-glass-bonded silica (Q) and synthetic mullite (M) samples. The corresponding in-air pre-conditioning temperatures (°C) are shown

has an average thermal expansion coefficient of $23 \times 10^{-6}/K$ compared to $4 \times 10^{-6}/K$ for synthetic mullite. Hence, the much higher thermal strain of the silica grains appeared as

the most likely root cause for the formation of micro-cracks in their binder bridges.

The grain surface of the synthetic mullite (Fig. 6b) was highly irregular. This might have supported binder adhesion, but also increases the surface-related binder consumption, which could explain the lower initial strength achieved compared to the silica sand samples.

3.2 Wedge splitting test results of the sand core samples

For the as-produced condition, both materials showed a typically shaped load–displacement curve, as shown in Fig. 7.

The stiffness until the maximum load was similar for all samples, except for one synthetic mullite specimen with a deeper initial notch, which consequently showed a higher compliance. Higher and wider peaks, meaning higher absorbed energy, were apparent in the silica samples. Examples of the fractured wedge splitting test samples are shown in Fig. 8.

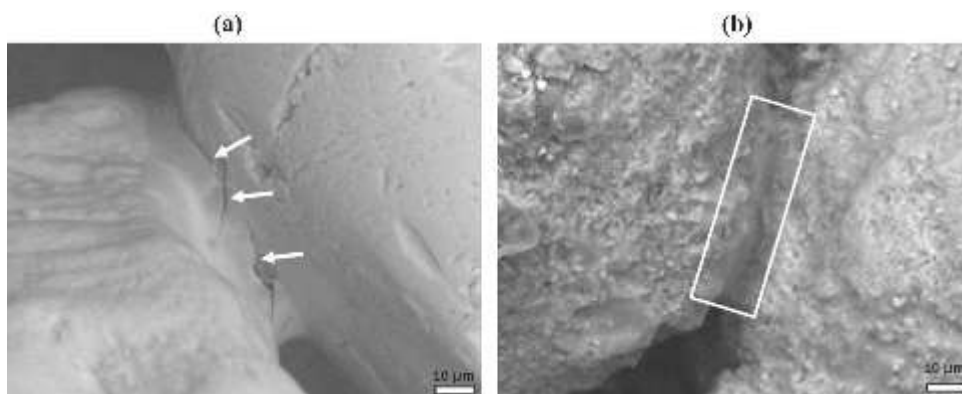


Fig. 6 Na-silicate binder bridge between silica sand particles (a) and synthetic sintered mullite granulate particles (b) after thermal exposure at 400 °C in air. Arrows indicate the micro-cracks in the binder bridges

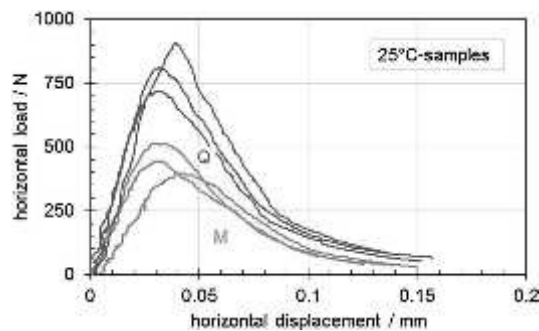


Fig. 7 Wedge splitting test results of the water-glass-bonded silica (Q) and synthetic mullite (M) core samples under the as-produced condition (without thermal exposure) before testing

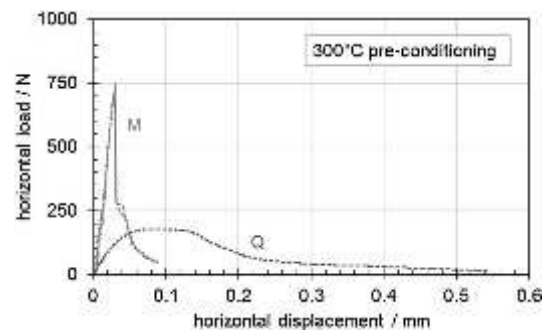


Fig. 9 Wedge splitting test results of water-glass-bonded silica (Q) and synthetic mullite (M) core samples after thermal pre-conditioning at 300 °C

The initial starter notch on top of the sample ligament area and the laterally glued on marks for displacement measurement are easily recognised. Within the fracture areas, an irregular sub-structure was present, which was more pronounced for the silica samples. Most likely, the more angular grain shape of the silica compared to that of the synthetic sintered mullite caused increased intergranular friction and hooking effects. This effect can also explain the larger peak area exposed by the silica sand samples.

The lower strength after the thermal exposure affected material property changes, which rendered the manipulation of the pre-conditioned silica samples difficult, and as consequence, only 1 of the 3 samples fractured in the correct area. Testing of the synthetic sintered mullite samples was also delicate because of the exposed brittle behaviour, such that only two samples could be evaluated. The wedge splitting load curves after thermal exposure at 300 °C are shown in Fig. 9.

The load curve of the silica sample after thermal exposure was characterised by a high compliance and a plateau-shaped load peak with a low maximum load. The synthetic mullite samples compared to the as-produced condition (Fig. 8) showed a higher stiffness and maximum load and unstable crack propagation at maximum load, resulting in a relatively low maximum displacement.

3.3 De-agglomeration rate

The evaluated de-agglomeration rates for the reference samples were lower than 10^3 mm²/s and in contrast higher than 10^4 mm²/s for the cast-in samples. The synthetic mullite samples showed the highest evaluated values, as illustrated in Fig. 10.

For the as-produced ‘RT’ condition, the lower de-agglomeration rate for the silica samples compared to the synthetic mullite ‘RT’ condition was associated with their higher initial strength and specific fracture energy.

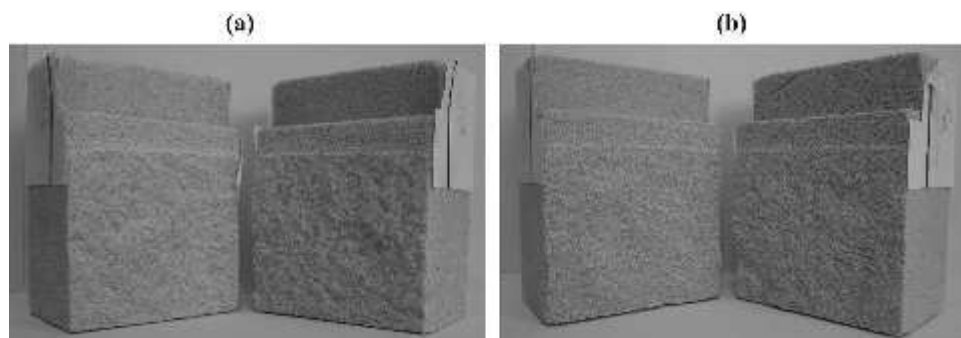


Fig. 8 Fractured wedge splitting test specimens (sample height 100 mm, ligament width 75 mm). **a** silica sand sample; **b** synthetic sintered mullite

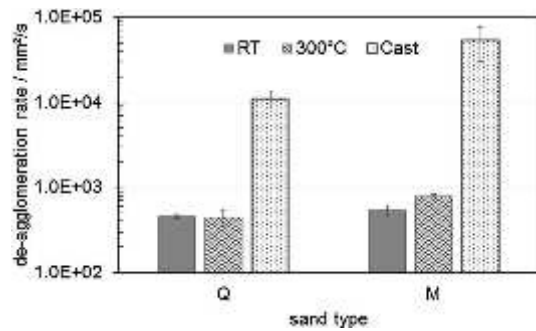


Fig. 10 De-agglomeration rate of the reference (RT: as produced; 300 °C: thermally pre-conditioned) and cast-in samples. Three samples per condition were tested. The mean value and standard deviation are shown

After thermal exposure at 300 °C, the de-agglomeration rate of the quartz sand samples changed but insignificantly. The results for the synthetic mullite samples showed an

increase in the de-agglomeration rate of 50%. These samples showed a high retained strength and brittleness, as was evaluated by the aforementioned testing results.

The retained particle size fraction from 0.7 to 1 mm was chosen for consecutive microscopy analysis, because this size was greater than the maximum grain size of the pure granulates. The agglomerate appearance is shown in Fig. 11.

Based on the agglomerate size distribution, the specific surface of the removed core sand was evaluated, assuming a spherical agglomerate shape. Apparently a significantly higher specific surface was created compared to the assumption of spherical particles for calculation.

Results from the bending, wedge splitting, and de-agglomeration tests are summarised in Table 3. For better comparability, the elastic modulus from the bending and ultrasonic measurements, and the strength from the bending and wedge splitting tests, are grouped.

Ultrasonic measurements showed higher elastic modulus results compared to those of the bending test evaluation. Ultrasonic measurements introduce very low strain amplitudes and do not cause serious bonding damage.

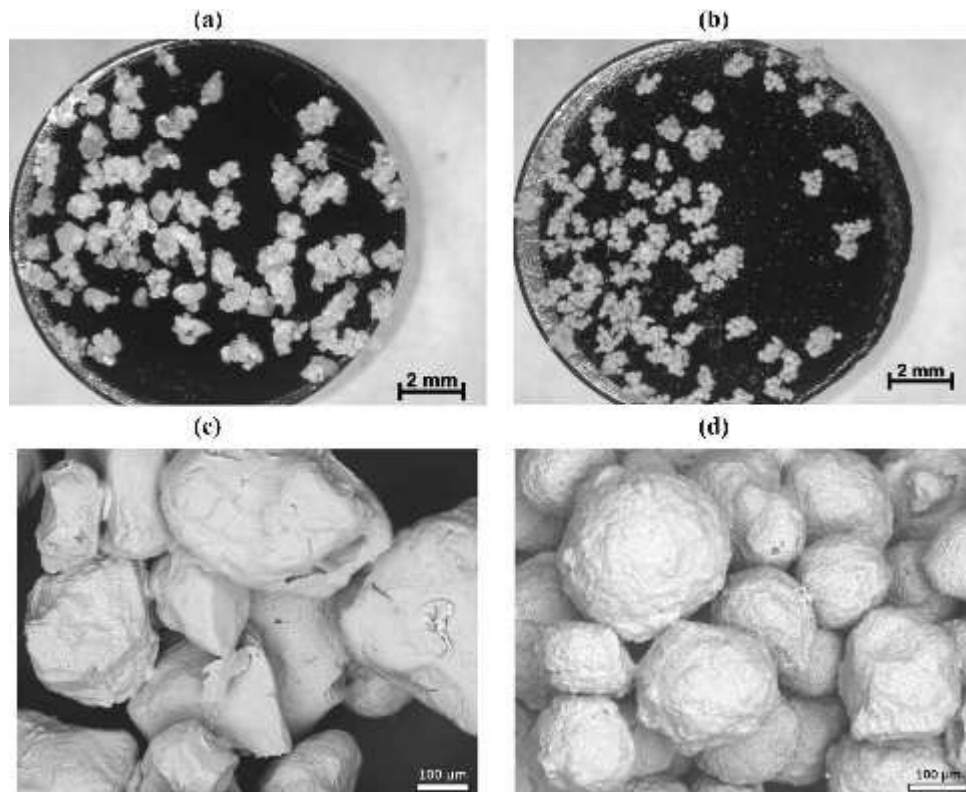


Fig. 11 Agglomerates from silica sand (left) and mullite granulate (right) from the 0.7 to 1 mm sieve fraction. Stereo microscope pictures are shown in **a** and **b** and SEM images in **c** and **d**

Table 3 Results for different sample conditions for silica (Q) and synthetic sintered mullite (M) core samples

Core type	Sample condition	E (3PBT/US) (GPa)	σ_B (MPa)	σ_f (MPa)	G_f^* (N/m)	l_{ch} (mm)	R_S (mm ² /s)
Q	As-produced	2.16/5.08	2.93	1.95	11.8	16	455
Q	300 °C	1.68/3.94	1.41	0.47	12.9	230	446
Q	Cast-in	–	–	–	–	–	11,026
M	As-produced	2.07/5.03	2.47	0.84	6.8	48	530
M	300 °C	2.32/4.74	2.26	2.57	4.2	3	782
M	Cast-in	–	–	–	–	–	54,109

Symbol designations used: E elastic modulus, evaluated using a three-point bending test (3PBT) and ultrasonic measurements (US). σ_B bending strength; σ_f tensile strength; G_f^* specific fracture energy; l_{ch} characteristic length; R_S de-agglomeration rate

In contrast to that, during bending tests stress distribution is not uniform and parts of the sample volume undergo higher strains. Thus, introduced local degradation decreases the evaluated Young's modulus. Schneider et al. [29] described the elastic modulus of inorganically bonded sand cores based on granular material and binder properties and pointed out the effects of different measurement techniques.

Bending test evaluations were based on the simplified continuum-mechanical isotropic material behaviour, assuming a linear stress distribution and crack initiation at maximum load. In reality the behaviour is much more complex due to the strain softening behaviour of the material [26]. The inversely evaluated tensile strength from wedge splitting test evaluation gives a more realistic value, as several material parameters were considered, including the effect of the strain softening behaviour [24]. Between the bending strength and the inversely determined tensile strength a factor of approximately 1.5–3 was observed. An exception were the thermally pre-conditioned sintered mullite cores, which showed very similar bending and tensile strength results. With a characteristic length of 3 mm the behaviour was relatively brittle, and consequently the deviation between three-point bending test results and the evaluated tensile strength showed the smallest difference, as thermal strain-induced damage was diminished.

It was expected to find a relation between the de-agglomeration rate R_S and the specific fracture energy G_f^* , because both depend on the energy consuming processes during disintegration. The results where fit with the empirically found equation (Eq. (4)):

$$R_S = \frac{2070}{G_f^*} + 270. \quad (4)$$

For this function, a standard deviation s of 25 mm² s⁻¹ with the single data points was determined. The result including the $\pm 3s$ -boundaries is shown in Fig. 12.

Equation (4) is valid in the range of the evaluated data and for the chosen settings for the de-agglomeration tests. A comparison of the energy consumption determined from

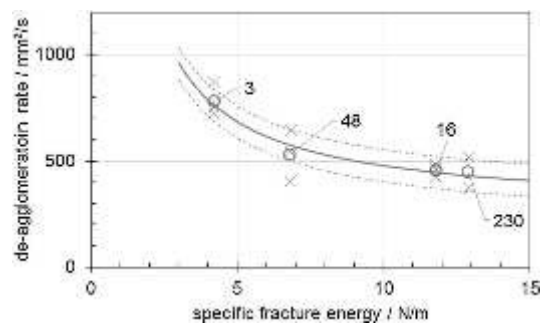


Fig. 12 De-agglomeration rate over the specific fracture energy. The dashed lines show the $\pm 3s$ -boundaries. 'X' indicates individual measurement results and the circles the mean values with the characteristic length assigned in/mm

the wedge splitting test and from the de-agglomeration test is difficult because from the latter the evaluation of the produced surface is extremely challenging.

An evaluation of the influence of the characteristic length as an indicator of the brittleness on the de-agglomeration rate gave no reliable result due to the not adequate data base.

4 Discussion

Bending and wedge splitting tests showed coincident relative changes in the strength and stiffness before and after thermal exposure. In contrast to the water-glass bonded silica sand cores, the synthetic sintered mullite cores retained their high strength after thermal exposure and presented much higher de-agglomeration rates for the cast-in core samples. The results demonstrated that the prediction of core removal properties from retained strength results is not reliable.

The decrease in the strength and elastic modulus of the silica sand cores resulted from the evolved micro-cracks in the sand particle bonds after thermal exposure (Fig. 6a), which also allowed the achievement of a high total deformation at the end of the test. A continuous fracture energy

consumption was possible because of crack branching due to micro-cracks, which could grow continually. Also in the de-agglomeration test this behaviour leads to a higher energy consumption.

In contrast to the silica sand cores, the sintered mullite cores showed pre-dominantly linear elastic behaviour, owing to the drying and lack of crack formation in the bonds. Therefore, the strength and brittleness increased and, most importantly, these cores provided no energy-absorbing deformation mechanisms. Consequently, stresses from shrinkage and vibration in the de-agglomeration tests increased without significant energy absorption unless brittle fracture occurred.

In particular, for the cast-in situation, mechanical interaction is defined by the difference in casting shrinkage strain and core expansion, as documented by Stauder et al. [30]. During the common cooling phase of the casting and the cast-in core to room temperature, a much higher strain difference was found for the synthetic mullite cores compared to the silica cores. In summary, high shrinkage strain was exerted from the casting together with the low fracture energy or high brittleness were responsible for the observed de-agglomeration rate of the cast-in water-glass-bonded sintered mullite cores.

For further research work a focus may be put on the nature of the foundry cores as bonded granular materials with separate consideration of granular material and binder properties, e.g. as published in [29], to which evidence was provided by this work. To enhance the predictability of the core removal behaviour, further research is proposed as follows:

1. Enhance the variety of core sample conditions with respect to specific fracture energy, strength, and brittleness by choice of sand and binder types and thermal loading.
2. Evaluation of the effects of different mechanical agitation intensities on the core removal velocity and the resulting de-agglomeration rate for cores with different brittleness, strength and specific fracture energy.
3. Evaluation of the effectively created specific surface of the de-agglomerated material based upon the consideration of fractured particle bonds to assign specific fracture energies thereon.

5 Conclusions

Experimental work with water-glass-bonded silica sand and synthetic mullite granulate was conducted. Reference variants with and without thermal exposure were evaluated by bending and wedge splitting tests. These results were related

to results from de-agglomeration tests of non-cast and cast-in samples.

- Wedge splitting tests were carried out on sand core samples. The specific fracture energy, tensile strength, and characteristic length of the core samples was obtained.
- The strength is not a meaningful measure for the de-agglomeration rate.
- The de-agglomeration rate of the different thermally pre-conditioned samples showed an inverse proportionality with the specific fracture energy.
- Cast-in samples were more rapidly de-agglomerated than thermally pre-conditioned samples, because of the exerted casting shrinkage strain in the cores.
- After thermal exposure, the silica sand cores showed a micro-crack network, resulting in a lower strength and Young' modulus, low brittleness, and a high specific fracture energy.
- Cast-in synthetic sintered mullite cores showed the highest de-agglomeration rate. These samples showed high strength, stiffness, and brittleness after thermal exposure and were subject to a high shrinkage strain during casting cooling.
- Future research should incorporate the role of materials brittleness using the material property of the characteristic length and enhance the evaluation of the effectively created specific core surface in de-agglomeration tests.

Acknowledgements The authors acknowledge the Austrian Research Promotion Agency (FFG) for supporting the projects *FFG 844552* and *FFG 849486*. We furthermore appreciate the support provided by the Austrian Foundry Research Institute, the Institute for Ceramic Materials at the University of Leoben for testing and evaluation, and Nematik Linz for the substantial financial support.

Compliance with ethical standards

Conflict of interest The authors declare that they have no conflict of interest.

References

1. Czerwinski F, Mir M, Kasprzak W (2015) Application of cores and binders in metalcasting. *Int J Cast Met Res* 28:129–139. <http://www.maneyonline.com/doi/10.1179/1743133614Y.0000000140> (**Internet**)
2. Zaretsky L (2015) Modified silicate binders new developments and applications. *Int J Met.* <http://link.springer.com/10.1007/s40962-015-0005-3> (**Internet; Springer International Publishing**)
3. Gamisch M (2002) Mechanisches Entkernen von Al-Gussteilen mit geringer Beanspruchung des Gussteils. *Giesserei Rundschau* 49:43–45
4. Döpp R, Deike R, Gettwert G (1985) Beitrag zum Wasserglas-CO₂-Verfahren. *Giesserei Düsseldorf* 72:626–635

5. Flemming E, Tilch W (1993) Formstoffe und Formverfahren, 1st edn. Deutscher Verlag für Grundstoffindustrie, Leipzig
6. Izdebska-Szanda I, Angrecki M, Matuszewski S (2012) Investigating of the knocking out properties of moulding sands with new inorganic binders used for castings of non-ferrous metal alloys in comparison with the previously used. *Arch Found Eng* 12:117–120
7. Lucarz M, Grabowska B, Grabowski G (2014) Determination of parameters of the moulding sand reclamation process, on the thermal analysis bases. *Arch Metall Mater* 59:1023–1027
8. Dobosz SM, Drożyński D, Jakubski J, Major-Gabryś K (2014) The influence of the content of furfuryl alcohol monomer on the process of moulding sand's thermal destruction. *Arch Metall Mater* 59:10–13. <http://www.degruyter.com/view/j/amm.2014.59.issue-3/amm-2014-0188/amm-2014-0188.xml>
9. Kmita A, Fischer C, Hodor K, Holtzer M, Rocznik A (2016) Thermal decomposition of foundry resins: a determination of organic products by thermogravimetry-gas chromatography-mass spectrometry (TG-GC-MS). *Arab J Chem*. <https://doi.org/10.1016/j.arabjc.2016.11.003>
10. Bargaoui H, Azzouz F, Thibault D, Cailletaud G (2017) Thermomechanical behavior of resin bonded foundry sand cores during casting. *J Mater Process Tech* 246:30–41. <https://doi.org/10.1016/j.jmatprotec.2017.03.002>
11. Stauder BJ, Harmuth H, Schumacher P (2018) De-agglomeration rate of silicate bonded sand cores during core removal. *J Mater Process Technol* 252:652–658. <https://www.sciencedirect.com/science/article/pii/S0924013617304764?via%3Dihub> (**cited 2018 May 13**)
12. Campbell J (2011) Complete casting handbook metal casting processes, metallurgy, techniques and design, 1st edn. Elsevier, Amsterdam
13. Campbell J (2011) Molds and cores. *Compleat. Cast. Handb*
14. Dong S, Iwata Y, Hohjo H, Iwahori H, Yamashita T, Hirano H (2010) Shell mold cracking and its prediction during casting of AC4C aluminum alloy. *Mater Trans* 51:1420–1427
15. Galles D, Beckermann C (2017) Effect of sand dilation on distortions and pattern allowances during steel sand casting. *Int J Cast Met Res* 30:257–275. <https://doi.org/10.1080/13640461.2017.1290909>
16. Motoyama Y, Inoue Y, Saito G, Yoshida M (2013) A verification of the thermal stress analysis, including the furan sand mold, used to predict the thermal stress in castings. *J Mater Process Technol* 213:2270–2277. <http://linkinghub.elsevier.com/retrieve/pii/S092401361300215X>
17. Thole J, Beckermann C (2009) Measurement of elastic modulus of PUNB bonded sand as a function of temperature. 63rd SFSA Tech Oper Conf. Steel Founders Society of America, Chicago, p 22
18. Quarzwerke (2009) Quarzsand Haltern H 31 bis H 35. D-50207 Frechen
19. Itochu (2010) Spherical Ceramic Sand for Foundry Naigai CERA-BEADS 60 for Any Kind of Metal. Itochu Ceratech Corporation, pp 1–7. <http://www.ite-cera.co.jp/english/prod/pdf/naigai.pdf>
20. Wöllner (2010) Betol 39 T. D-67065 Ludwigshafen: Wöllner GmbH&Co KG, p 2
21. Tschegg EK (1986) Equipment and appropriate specimen shapes for tests to measure fracture values (Prüfeinrichtung zur Ermittlung von bruchmechanischen Kennwerten sowie hiefür geeignete Prüfkörper). Austrian Patent Office, Vienna
22. Dai Y, Gruber D, Harmuth H (2017) Determination of the fracture behaviour of MgO-refractories using multi-cycle wedge splitting test and digital image correlation. *J Eur Ceram Soc* 37:5035–5043. <https://doi.org/10.1016/j.jeurceramsoc.2017.07.015>
23. Harmuth H (1995) Stability of crack propagation associated with fracture energy determined by wedge splitting specimen. *Theor Appl Fract Mech* 23:103–108
24. Jin S, Gruber D, Harmuth H (2014) Determination of Young's modulus, fracture energy and tensile strength of refractories by inverse estimation of a wedge splitting procedure. *Eng Fract Mech* 116:228–236. <https://doi.org/10.1016/j.engfracmech.2013.11.010>
25. Lackner S (2007) Anwendung eines Inversenverfahrens zur Auswertung eines Keilspalttests für die bruchmechanische Charakterisierung von Feuerfestbaustoffen Magisterarbeit am Lehrstuhl für Gesteinshüttenkunde. Montanuniversität Leoben
26. Hillerborg A, Modéer M, Petersson P-E (1976) Analysis of crack formation and crack growth in concrete by means of fracture mechanics and finite elements. *Cem Concr Res* 6:773–781. <http://www.sciencedirect.com/science/article/pii/0008884676900077#aep-abstract-id5> (**Internet; Pergamon; cited 2017 Oct 29**)
27. Stauder BJ, Kerber H, Schumacher P (2016) Foundry sand core property assessment by 3-point bending test evaluation. *J Mater Process Technol* 237:188–196. <http://www.sciencedirect.com/science/article/pii/S0924013616301819> (**Internet; cited 2016 Jun 24**)
28. Recknagel U, Dahlmann M (2009) Spezialsande—Formgrundstoffe für die moderne Kern- und Formherstellung/Special Sands - Base Materials for modern Core and Mould Making. *Giesserei Rundschau* 56:6–17
29. Schneider M, Hofmann T, Andrä H, Lechner P, Etemeyer F, Volk W et al (2018) Modelling the microstructure and computing effective elastic properties of sand core materials. *Int J Solids Struct*. <http://linkinghub.elsevier.com/retrieve/pii/S0020768318300556> (**Internet; Elsevier Ltd**)
30. Stauder BJ, Schumacher P, Harmuth H (2017) Core removal behaviour of silicate bonded foundry sand cores. *Int Conf Front Mater Process Appl Res Technol—FIMPART'17*. Springer, Bordeaux, p 5

4.5 Core removal behaviour of silicate bonded foundry sand cores

Presentation title	Quantitative shakeout behaviour determination of cast-in foundry sand cores.
Authors	B.J. Stauder (Nemak Linz); P. Schumacher (MUL); H. Harmuth (MUL)
Journal	Proceedings of <i>Frontiers in Materials Processing, Applications, Research and Technology; FiMPART 2017</i> , Bordeaux, July 9-12, 2017. Oral presentation at session ‘Materials processing- A3’, July 11, 13:00. © Springer (2017); Publication pending.
Individual author contributions	50 %: B.J. Stauder: Experiments and evaluation, preparation, presentation. 30 % : P. Schumacher: Casting related scientific context. 20 %: H. Harmuth: Mechanical response of sand cores.

Abstract

A high mechanical and thermal stability of cores is required for manipulation and during the casting process. In contrast to that a good decomposition behaviour of the sand core is favoured for the shakeout process of the cooled casting. The casting process imposes a complex overlay of thermal, mechanical and chemical loads on the sand cores. Core removal studies require consideration of applied casting process conditions.

The production of complex cast-Al cylinder heads is the motivation for this study. Adequate thermal and atmospheric pre-treatments were applied prior to mechanical property evaluation of foundry sand core specimens. Retained strength measurements and specific fracture energy determination by wedge splitting tests have been performed for several sand core types. A novel instrumented shakeout testing method served to deliver quantitative results for cast-in and, alternatively, thermally pre-conditioned sand cores. Retained strength and sand core brittleness were found to be important factors influencing core removal in the complex thermal and mechanical interaction between casting and core.

The obtained data are suitable for simulation purposes and improve the understanding of relevant foundry sand cores properties.

Core removal behaviour of silicate bonded foundry sand cores

Bernhard J. Stauder^{a,*}, Peter Schumacher^b, Harald Harmuth^c

^a *Nemak Linz GmbH; A-4030 Linz*

^b *Chair of Casting Research, Montanuniversitaet Leoben; A-8700 Leoben;*

^c *Chair of Ceramics, Montanuniversitaet Leoben; A-8700 Leoben*

Communication address of corresponding author

* *Email: bernhard.stauder@nemak.com*

Abstract

A high mechanical and thermal stability of cores is required for manipulation and during the casting process. In contrast to that a good decomposition behaviour of the sand core is favoured for the shakeout process of the cooled casting. The casting process imposes a complex overlay of thermal, mechanical and chemical loads on the sand cores. Core removal studies require consideration of applied casting process conditions.

The production of complex cast-Al cylinder heads is the motivation for this study. Adequate thermal and atmospheric pre-treatments were applied prior to mechanical property evaluation of foundry sand core specimens. Retained strength measurements and specific fracture energy determination by wedge splitting tests have been performed for several sand core types. A novel instrumented shakeout testing method served to deliver quantitative results for cast-in and, alternatively, thermally pre-conditioned sand cores. Retained strength and sand core brittleness were found to be important factors influencing core removal in the complex thermal and mechanical interaction between casting and core.

The obtained data are suitable for simulation purposes and improve the understanding of relevant foundry sand cores properties.

Keywords:

Casting; Sand Core; Testing; Thermal expansion;

Introduction

Sand cores are used at numerous metal casting technologies to shape complex contours and undercut sections. Subsequent to solidification and cooling of the casting a core removal process is required to obtain a sand-free cast metal part. Czerwinski et al., (2015) recently reviewed the state of the art in sand core technology (1). To foster high productivity with complex cores, demanded by the automotive casting industry in the past century, inorganic binders have been replaced by organic binders. Nowadays, inorganic core production technologies are implemented again, driven by more restrictive health and safety guidelines and emission regulations, since these are odourless and near emission free. Important is to highlight the given thermal impact on the cores by the casting and cooling process prior to core removal. The secondary strength maximum of silicate binders above 700 °C is limiting silicate binder application for heavy metal, iron and steel castings (2). Several additional investigations of retained strength results by Izdebska-Szanda and Baliński, (2011) and Izdebska-Szanda et al., (2012) confirmed this behaviour (3,4). According to them, applying inorganic core binder systems requires special attention to the core removal properties.

Methods to evaluate core removal properties of cast-in sand core samples quantitatively, evaluating core removal time and mass rate, were presented in (5,6). Industrially applied solutions for core removal have been reviewed in (7).

Recknagel and Tilch, (2000) characterized thermal expansion properties for various relevant granular materials used in foundry application and effects on casting quality (8). Thiel et al., (2007) have evaluated the impact of silica sand types, grain size parameters, binder types and additives on thermal expansion (9).

During own developments using silicate bonded silica sand cores for cast-Al cylinder heads and applying mechanical core removal processes, debilitated core removal properties compared to castings with organically bonded cores were confirmed. However, when granulates are used with low thermal expansion, conditions are obtained favourable for sand core decomposition during the cooling phase of castings (10). As explanation of that behaviour it was postulated, that due to a minimized thermal sand core expansion the casting shrinkage is causing higher effective stresses acting on cast-in sand cores, which help their mechanical decomposition.

This observation will be evaluated in the present article. Relevant mechanisms and conditions to achieve this effect will be analysed and experimentally validated.

Experimental methods

Core removal experiments in the field of foundry technology and quantitative property evaluations of the applied sand core types are presented.

Material characterization

Silica sand and synthetic mullite sand (11), bonded with Sodium-silicate binder (molar $\text{SiO}_2:\text{Na}_2\text{O}$ ratio of 3,25) were used. Both granulates have been characterized by micrographs and SEM (Figure 1).

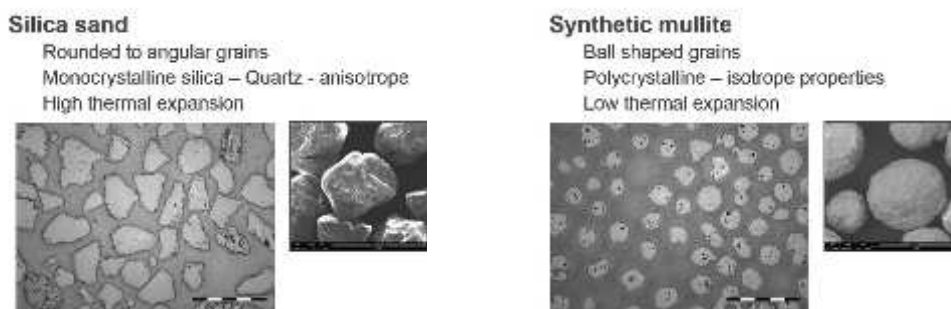


Figure 1: Light-optical and SEM characterization of the used granulates.

Thermal expansion was characterized upon sand core samples with 5 mm diameter and a length of 50 mm using a “Netzsch 402E” dilatometer applying a heating rate of 0,05 K/s.

Specific fracture energy was evaluated on sand core samples with a wedge splitting test method according to (12), with further developments described by (13–16).

Bending strength of thermally pre-conditioned test bars served as reference, applying the setup described in (17). Thermal conditioning was performed with bending test bars in air and under reducing conditions, similar to internal conditions in castings. Those were realized by sealing samples with Al-foil and embedding them in pre-heated sand.

Thermal conditioning was based upon evaluation of cast Al cylinder head sand cores applying the Rotacast process (18). From different sand core positions typical exposure times for temperature levels of 200 to 500 °C were obtained. Very thin sand core sections (thickness 3 – 8 mm) even might reach a maximum temperature of above 500 °C, which may lead to severe thermal expansion effects when silica sand is used. In addition to sand core properties

mechanical alloy property measurements were performed using a deformation dilatometer. Aluminium test bars were quenched from a temperature of 530 °C with 30 K/s until the test temperature and immediately tested with a strain rate of 10^{-3} 1/s.

Core removal experiments were conducted using castings with their cavities filled with test core sand and tempered at different temperature levels. Their results were compared to those of samples with cast-in sand cores and subsequent air cooling. For core removal a vibration unit equipped with two electrically driven imbalance drives was used. The shaken out sand was directly funnelled onto a balance tray recording the mass increase with 1 Hz resolution. The resulting peak acceleration in vertical direction measured on a test casting was 965 m/s², with a spectrum of 99 % of the values below 394 m/s² and 90 % below 190 m/s².

Results

In this section the experimental results including interpretation are documented, starting with the applied tempering profiles (Figure 2) and retained bending strength results after thermal pre-conditioning of both sand core types for oxidizing and reducing conditions (Figure 3).

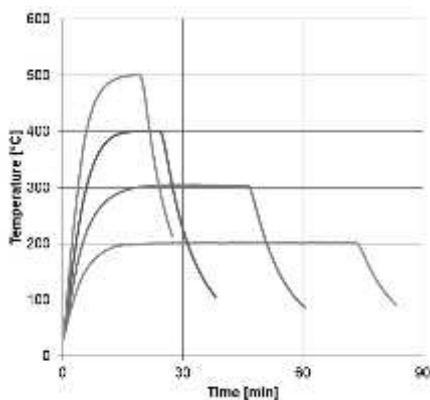


Figure 2: Applied temperature time profiles for thermal sample conditioning, realized using furnaces.

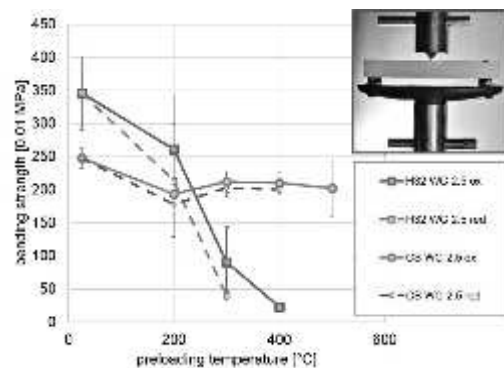


Figure 3: Retained bending strength of silica (H32) and synthetic mullite (CB) cores over pre-treatment temperature for oxidizing and reducing conditions.

Silica sand samples exhibited a significant mechanical property drop over temperature with the consequence, that samples tempered at 500 °C were not transferable to the bending test measurement. In contrast the synthetic mullite samples showed no significant temperature dependence and kept their strength with a maximum decrease of 20 % of the initial value.

The core removal samples with different tempering behaved in a similar way. A higher core removal mass rate was observed for a lower retained strength at a given temperature level which is more relevant for silica sand. A different behaviour was found for cast-in samples. Those samples containing silica sand showed core removal properties similar to samples conditioned at 300 – 500 °C. The cast-in synthetic mullite samples exhibit a much higher core removal mass rate compared to any of the tempered samples. Core removal results of silica and synthetic mullite samples are shown by Figure 4.

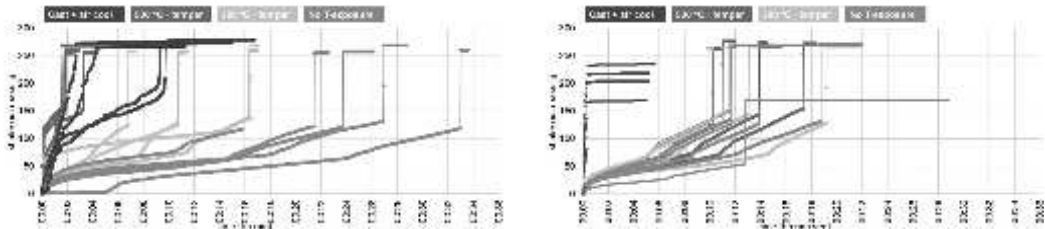


Figure 4: Mass-over time curves at core removal of silica (left) and synthetic mullite (right) samples.

For synthetic mullite no thermally induced decrease in strength was observed, however a potential mechanical interaction between casting and core was further analysed. Temperature data and relevant material properties are shown in Figure 5.

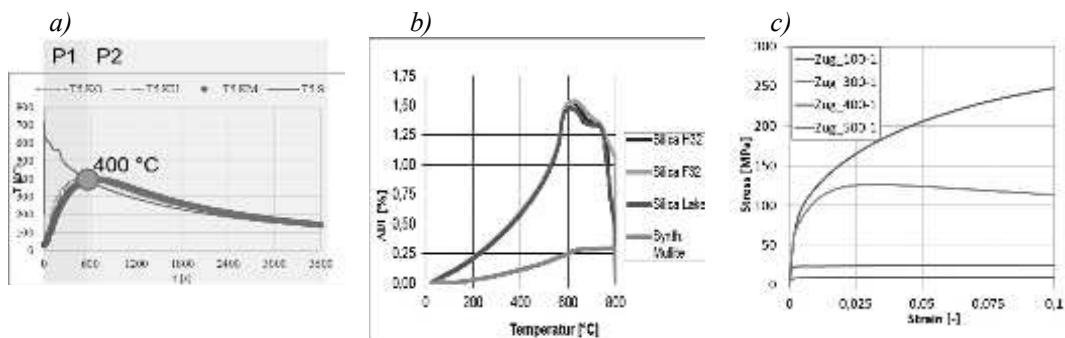


Figure 5: Experimental data used for thermo-mechanical evaluation of core-casting interaction. a) casting ($T5 S$) and core temperatures ($T5 K$); b) thermal expansion of sand cores and c) stress-strain curves of cast Al during cooling at different temperatures.

Generally, the casting contraction acts against the expanding sand core. Due to low thermal conductivity of sand cores, they heat up with a significant delay after the metal being cast-into the mould. Thermal expansion of sand cores is mainly controlled by the granular material and binder decomposition or plasticisation. The here used silicate binder is forming a brittle Nasilicate glass phase, which is stable until at least 500 °C before starting first crystallization. Cast Al develops a resistance against deformations of 5-10 MPa when cooled to 500 °C and 15 to 30 MPa at 400 °C, significantly increasing to above 100 MPa at 300 °C. Typically the strength of sand cores is one to two orders of magnitude below that of the cast metal at a given temperature. Therefore an Al casting during shrinking onto a sand core could be plastically deformed due to core resistance mainly at high metal temperatures. This effect is depending on the casting and core wall thickness relations and can be solved by computational simulation for complex geometries.

With this background, the common cooling of sand core and casting is analysed more deeply with respect to the contraction difference between sand core and casting. Cooling from 400 °C to 50 °C according to Figure 5 will be considered, using the measured thermal expansion results obtained for both core materials and $24 \cdot 10^{-6}$ 1/K for Al. For silica sand cores the contraction difference is low, whereas it is high for the synthetic mullite cores. The contraction stress transfer from the casting onto the core is best supported by the high retained strength of the synthetic mullite cores. Silicate bonded cores are assumed to be brittle and no binder plasticisation or decomposition can be expected at all. To verify this, sand core brittleness was investigated by wedge splitting tests. Results for non-conditioned and pre-conditioned samples at 300 °C are shown by Figure 6.

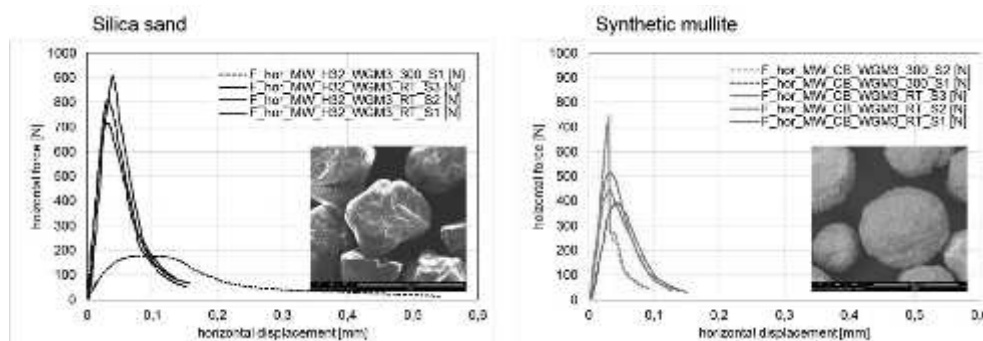


Figure 6 left: Load-deflection results from wedge splitting tests at room temperature and pre-conditioned at 300 °C. Left: silica (H32). Right: synthetic mullite (CB).

Wedge splitting tests of silica bonded sand cores at room temperature show a higher and wider peak compared to the samples of synthetic mullite. The decreased peak incline and low maximum peak value of thermally pre-conditioned silica sand samples indicate a high pre-damage of the binder. Those samples were highly fragile and difficult to handle with the present measurement setup.

The synthetic mullite samples with thermal pre-treatment exhibited a distinct and high peak, even above that of the non-conditioned samples, followed by brittle fracture. This indicates that the binder is not damaged. Intensified drying of the sand core due to thermal exposure resulted in increased strength and embrittlement.

Conclusions

A comparison of thermally pre-conditioned samples and cast-in samples bonded with silicate binder has demonstrated, that for core removal from Al-castings the analysis of retained sand core strength is not fully predictive for the core removal properties:

- Silica sand causes thermally induced damage of silicate binder. Applying synthetic mullite, no relevant temperature dependency on retained strength was found.
- Synthetic mullite enables to outperform full strength evolution of silicate binders by thermal conditioning, due to the low thermal expansion of mullite.
- Wedge splitting tests are an appropriate method to qualify foundry sand core properties.
- A high retained strength and a high brittleness in combination are the enablers for the mechanically induced destruction of cast-in sand cores by shrinkage of Al-castings during the cooling phase.

References:

1. Czerwinski F, Mir M, Kasprzak W. Application of cores and binders in metalcasting. *Int J Cast Met Res* [Internet]. 2015;28(3):129–39. Available from: <http://www.maneyonline.com/doi/10.1179/1743133614Y.0000000140>
2. Flemming E, Tilch W. *Formstoffe und Formverfahren*. 1st ed. Leipzig, Stuttgart: Deutscher Verlag für Grundstoffindustrie; 1993. 448 p.
3. Izdebska-Szanda I, Baliński A. New generation of ecological silicate binders. *Procedia Eng*. 2011;10:887–93.
4. Izdebska-Szanda I, Angrecki M, Matuszewski S. Investigating of the Knocking Out Properties of Moulding Sands with New Inorganic Binders Used for Castings of Non-ferrous Metal Alloys in Comparison with the Previously Used. *Arch Foundry Eng*. 2012;12(2):117–20.

5. Henry C (Ashland), Showman R (Ashland), Wandtke G (Ashland). Core and Foundry Process Variables Affecting Aluminum Casting Shakeout of Cold Box Cores. *Trans Am Foundry Soc.* 1999;107:99–115.
6. Fennell T, Crandell G. Inorganic Binder Properties Study - 1413-145 NA [Internet]. 2008. Available from: www.cerp-us.org
7. Gamisch M. Mechanisches Entkernen von Al-Gussteilen mit geringer Beanspruchung des Gussteils. *Giesserei-Rundschau.* 2002;49(3/4):43–5.
8. Recknagel U, Tilch W. Untersuchungen zum Ausdehnungsverhalten von Formstoffen im Hinblick auf die Vermeidung typischer Gußfehler. Sonderdruck aus *Giesserei-Praxis.* 2000;8+9:9.
9. Thiel J, Ziegler M, Dziekonski P, Joyce S. Investigation into the Technical Limitations of Silica Sand Due to Thermal Expansion. *AFS Trans* [Internet]. 2007;07–145(4):18. Available from: <http://prod.afsinc.rd.net/files/20072646a.pdf%5Cpapers3://publication/uuid/DBB37047-8901-4292-9AE2-B1952B1D5ADF>
10. Stauder BJ, Gintner W. Method for producing castings, molding sand and its use for carrying out said method [Internet]. WO; WO 2003/024642 A1, 2003. p. 29. Available from: <https://www.google.com/patents/WO2003024642A1?cl=de>
11. Spherical Ceramic Sand for Foundry Naigai CERABEADS 60 for Any Kind of Metal [Internet]. Itochu Ceratech Corporation; 2010. p. 1–7. Available from: <http://www.itc-cera.co.jp/english/prod/pdf/naigai.pdf>
12. Tschegg EK, Linsbauer HN. Prüfeinrichtung zur Ermittlung von bruchmechanischen Kennwerten (Testing procedure for determination of fracture mechanics parameters). Österreichisches Patentamt; A-233/86, 1986.
13. Harmuth H. Stability of crack propagation associated with fracture energy determined by wedge splitting specimen. *Theor Appl Fract Mech.* 1995;23(1):103–8.
14. Harmuth H, Rieder K, Krobath M, Tschegg E. Investigation of the nonlinear fracture behaviour of ordinary ceramic refractory materials. *Mater Sci Eng A.* 1996;214(1–2):53–61.
15. Lackner S. Anwendung eines Inversenverfahrens zur Auswertung eines Keilspalttests für die bruchmechanische Charakterisierung von Feuerfestbaustoffen Magisterarbeit am Lehrstuhl für Gesteinshüttenkunde Inhaltsverzeichnis. Montanuniversität Leoben; 2007.
16. Tschegg EK, Fendt KT, Manhart C, Harmuth H. Uniaxial and biaxial fracture behaviour of refractory materials. *Eng Fract Mech* [Internet]. Elsevier Ltd; 2009;76(14):2249–59. Available from: <http://dx.doi.org/10.1016/j.engfracmech.2009.07.011>
17. Stauder BJ, Kerber H, Schumacher P. Foundry sand core property assessment by 3-point bending test evaluation. *J Mater Process Technol* [Internet]. 2016 Nov [cited 2016 Jun 24];237:188–96. Available from: <http://www.sciencedirect.com/science/article/pii/S0924013616301819>
18. Gosch R, Stika P. Das ROTACAST-Gießverfahren - millionenfach für Aluminiumzylinderköpfe in der Serie bewährt. *Giesserei-Rundschau.* 2005;52(7/8):170–3.

5 Summary and discussion

In this chapter the resulting publications, which were re-printed in chapter 4, are summarised and linked to each other. A fundamental understanding of the decomposition behaviour of cast-in sand cores was developed. The research was triggered by the initially observed good disintegration of waterglass-bonded cast-in synthetic sintered mullite-based cores compared to quartz-based cores.

5.1 Mechanical properties of sand cores

Mechanical properties of sand cores were investigated in more details in the papers on bending test evaluation, mechanical properties after thermal exposure and specific fracture energy, which are documented in the sections 4.1 to 4.4. Generally the evaluation of mechanical testing was following continuum mechanical relationships. Cores show specific behaviour, which is summarised here:

- Foundry cores represent bonded granular material type with a high free volume of approximately 40-50%.
- Strength and durability of foundry cores is designed to achieve the minimally required level for a safe handling and casting process result, and to achieve a complete core removal after the casting process.
- Fracture occurs at low load levels compared to building, refractory or ceramic materials.

One of the most commonly used testing methods are bending tests. An enhanced testing concept was developed (section 4.1). The method is illustrated in Figure 5-1.

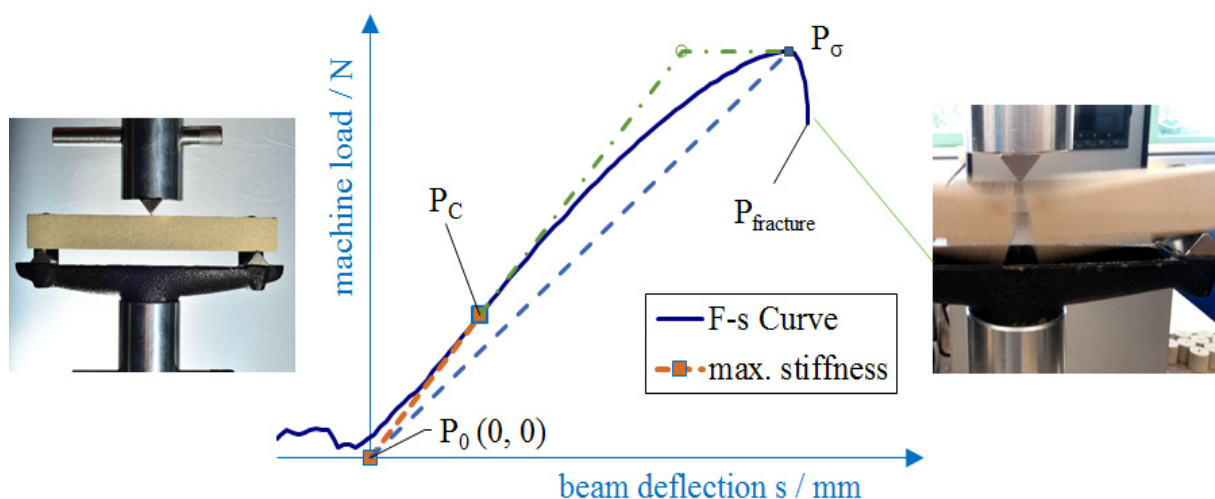


Figure 5-1: Bending test evaluation based on load curve evaluation (from section 4.1).

Influences from the initial sample settling towards the load supports, and their elimination, were highly important for a correct load curve evaluation. The elastic modulus was evaluated from the maximum stiffness. A brittleness index was proposed by separation of the work integral into purely elastic and irreversible work portions until the maximum load. Similar brittleness indices were obtained by the alternatively proposed secant to tangent modulus ratio. From these tests no specific fracture energy evaluation was possible due to spontaneous fracture of the samples in most cases. For the initially investigated organic binder systems bending test results over the first 24 hours are shown by Figure 5-2.

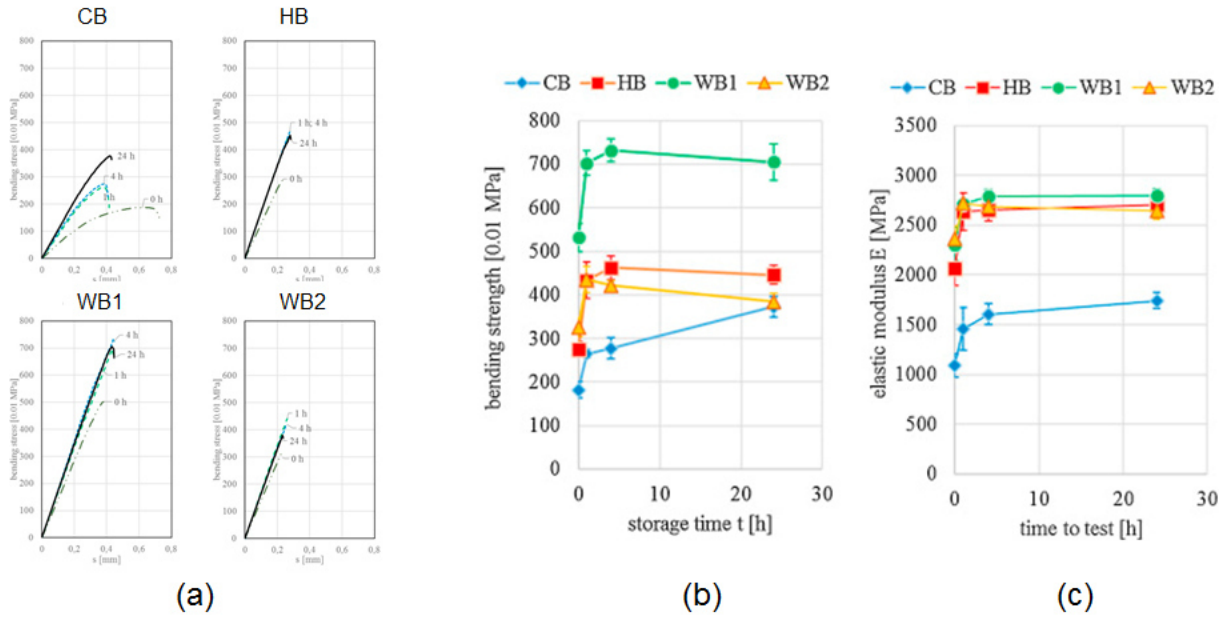


Figure 5-2: Results from three-point bending test evaluation based upon load curves. Load curves for PU-Coldbox (CB), urea-furanic hotbox (HB) and two furanic Warmbox binders (WB1 and WB2) after sample storage time of 0, 1, 4 and 24 hours are shown in (a). In (b) the bending strength and in (c) the elastic modulus of these cores are graphically shown.

PU-Coldbox cores revealed a distinct time dependency, whereas the hot-setting binder types after cooling presented stable properties. In addition the impact of the loading velocity on the results for PU-Coldbox cores was demonstrated, as shown in Figure 5-3.

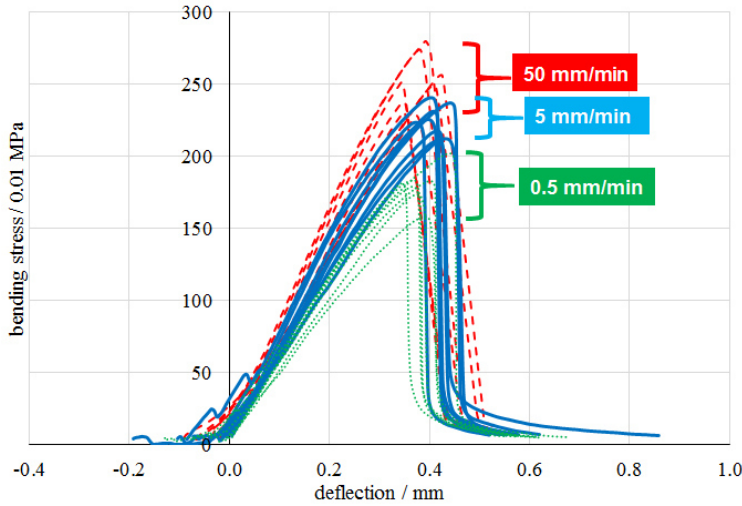


Figure 5-3: Testing of PU-Coldbox cores after 1 hour storage with three load velocities of: 0,5; 5 and 50 mm/min (presented at the 54th Int. Slovenian foundry conference in Portoroz).

Mechanical properties after the completed casting process were most relevant for the evaluation of core removal properties. Typical relations for car engine cylinder head sand cores served as a basis to derive thermal exposure parameters. From a verified simulation model of a cylinder head casting process virtual measurement points were evaluated, which were chosen from thin and thick core parts from central and peripheral positions, exemplarily shown by Figure 5-4.

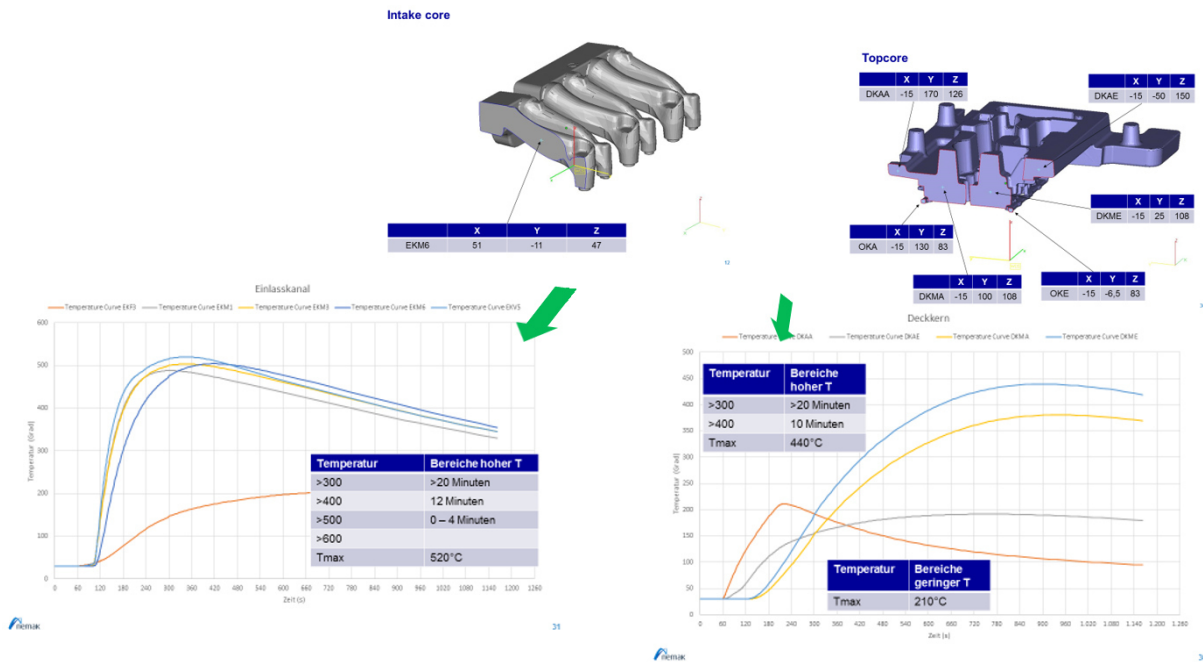


Figure 5-4: Examples for core temperature evaluation from casting simulation to derive heating profiles and typical exposure time at certain temperature regimes from 200 – 500 °C.

Evidently within cast-in cores location dependent heating rates and consequently no isothermal situation is given. Thermal stresses and various, location dependent property changes occur. For more detailed investigations a set of thermal exposure profiles for the temperature range from 200-500 °C, were defined, based upon the sample exposure time above the temperature steps shown in Figure 5-5.

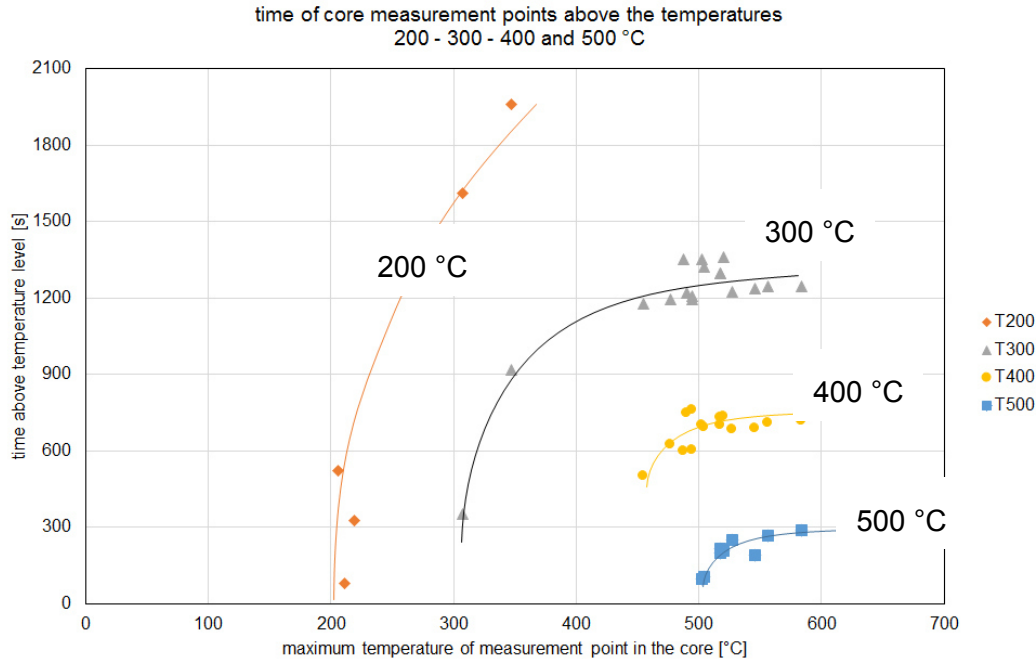


Figure 5-5: Dwell time of simulated temperature measurement points in sand cores of a cylinder head casting model above their individually reached maximum temperature from 200 – 500 °C in 100 °C steps.

The thermal exposure profiles were ranging from 5 min at 500 °C to 60 min at 200 °C, as documented in Table 3-3, and Figure 3-5. In casting practise and due to heating, cast-in cores evolve gases, which create an overpressure preventing the contact with surrounding air. Therefore, core pre-conditioning was evaluated with and without air exchange (sealed) conditions.

As expected, the sealed condition revealed higher thermal stability for organic cores, but slightly decreased properties for silicate bonded cores, which was explained by less possibility for evaporation of released water from the silica binder and therefore less embrittlement of the silicate structure, which is reported in details in section 4.2.

Bending tests of thermally pre-conditioned cores were conducted for silicate-bonded quartz and synthetic sintered mullite cores (details see section 4.4). Results after 24 hours without thermal exposure and after thermal pre-conditioning to 200, 300 and 400 °C are shown by Figure 5-6.

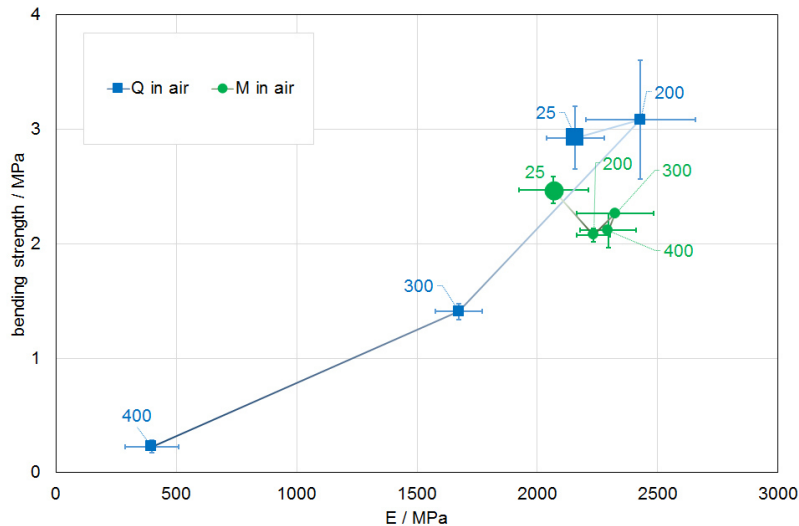


Figure 5-6: Bending strength over the elastic modulus for the core materials silica 'Q' and synthetic sintered mullite 'M'. The exposure temperatures / °C, for sample pre-conditioning in air are indicated.

The bending elastic modulus of silicate bonded cores is approximately 10 % lower compared to hot-setting organic cores. Figure 5-6 shows a high thermal stability of synthetic sintered mullite. From these data it was obvious, that in this case the high retained strength could not explain the extra-ordinary good core removal ability of these cores.

Foundry core sands can show a high variety of physical properties. Silica sand cores reveal a typically high thermal expansion, other than alumina silicate based materials, like mullite. The observed temperature dependent strength and elastic modulus decrease for the silica samples were owed to formation of micro-cracks in the silicate binder bridges, caused by the thermal expansion of the silica sand grains.

The temperature dependent behaviour of sand cores was verified by tensile, shear and uniaxial compression tests. These tests were also required to define a Mohr-Coulomb failure criterion, as documented in section 4.2, with the goal to assign material properties to the core sections after their maximum thermal exposure. The temperature-dependent properties were evaluated after in-air and sealed exposure conditions. The definition of the Mohr-Coulomb failure criterion is schematically shown, including the relevant test types by Figure 5-7.

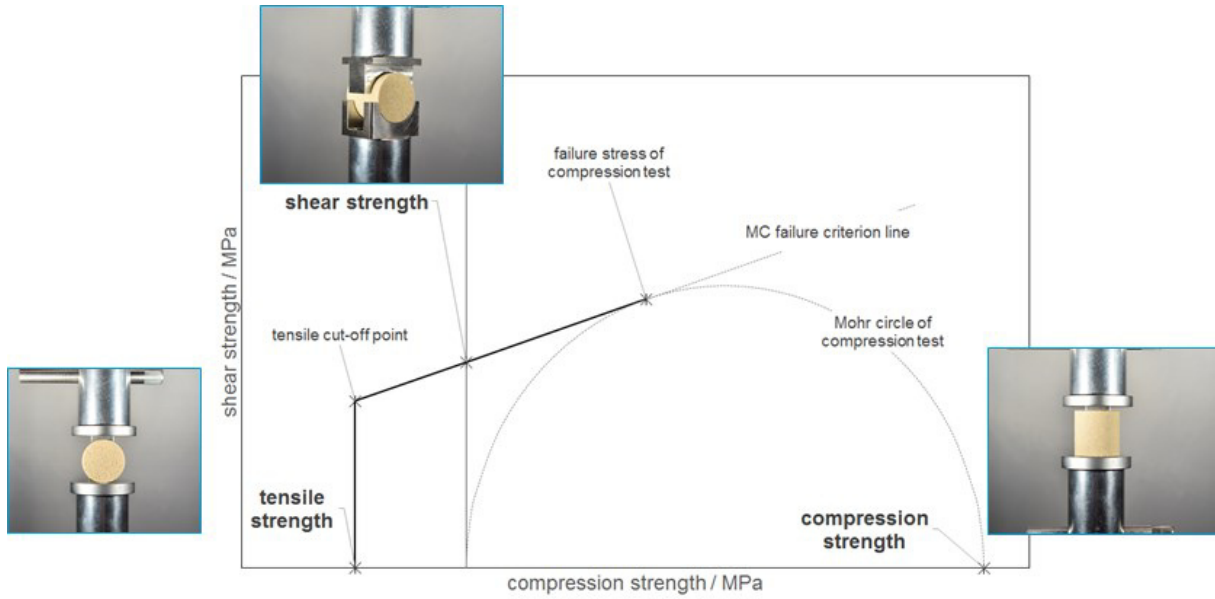


Figure 5-7: Mohr-Coulomb failure criterion function design of sand core samples after thermal exposure.

Silica sand (type H32) was used for core samples bonded with PU-Coldbox (Si-CB), furanic Warmbox (Si-FW) and waterglass (Si-WG). Additionally, a synthetic sintered mullite granulate with waterglass binder (Ce-WG) was evaluated. The initial situation and the situation after 300 °C in-air exposure are exemplarily shown in Figure 5-8.

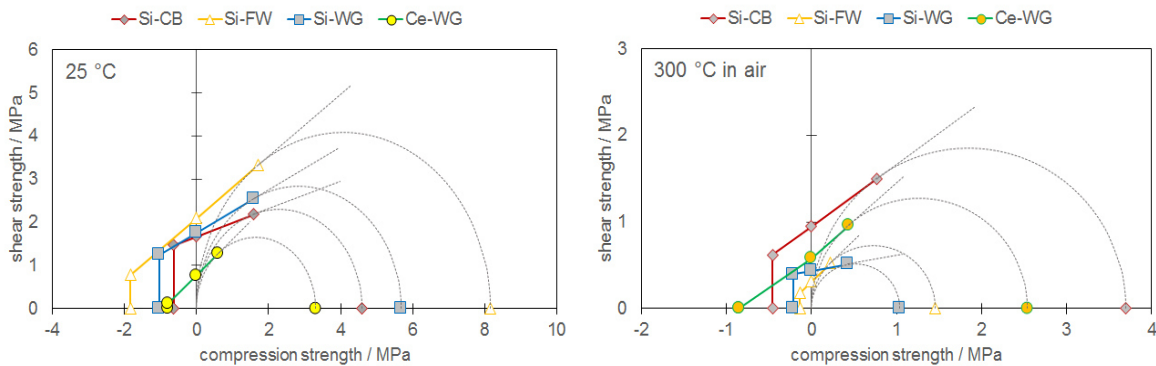


Figure 5-8: Comparison of Mohr-Coulomb criteria functions of samples tested without thermal exposure (left) and after 300 °C pre-conditioning (right).

The examples for waterglass-bonded silica and synthetic sintered mullite cores are shown by Figure 5-9. The changes relative to the initial values after 24 hours at room temperature are illustrated there.

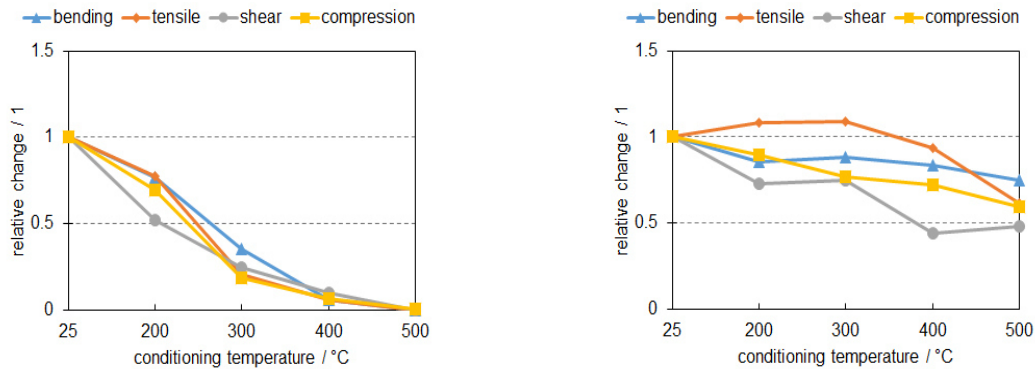


Figure 5-9: Mechanical properties of waterglass bonded sand core samples after thermal exposure. Left: silica sand; right: synthetic sintered mullite.

A similar relative development for the different test types was found within a certain band-width. The main parameters of an initial Mohr-Coulomb figure are tensile and compression strength and an internal friction angle. The similar behaviour of the different properties consequently allows a temperature dependent scaling of the initial failure criterion function. Hence, a first approximated material law describing core failure is available and prepared for future simulation purposes.

Some limitations might be given for deformable cores, due to possible viscous flow. The least error is made for rigid and brittle cores, without irreversible deformation (plastic binder flow, micro-crack development and growth). An anisotropy is given by the different intensity of grain contact pressure between tensile, shear and compression mode, which must be investigated in more detail in the future.

5.2 Fracture and de-agglomeration of foundry sand cores

The prediction of mechanical work required for core destruction is unknown, even if though it is possible to predict mechanical core properties for local core volumes. During a mechanical core removal process the volume of core sand in a casting cores and the contact condition of cores with the cast wall underlies a permanent change.

To approach the surface specific fracture energy wedge splitting tests were conducted. Thereby a sample is split into two halves and the load-displacement data are acquired during the complete sample fracture. A detailed description was given in section 4.4, [176]. This method was firstly applied with foundry core samples in the frame of this thesis, in thermally unconditioned and after a 300 °C pre-conditioning. An overview about the testing principle is illustrated in Figure 5-10.

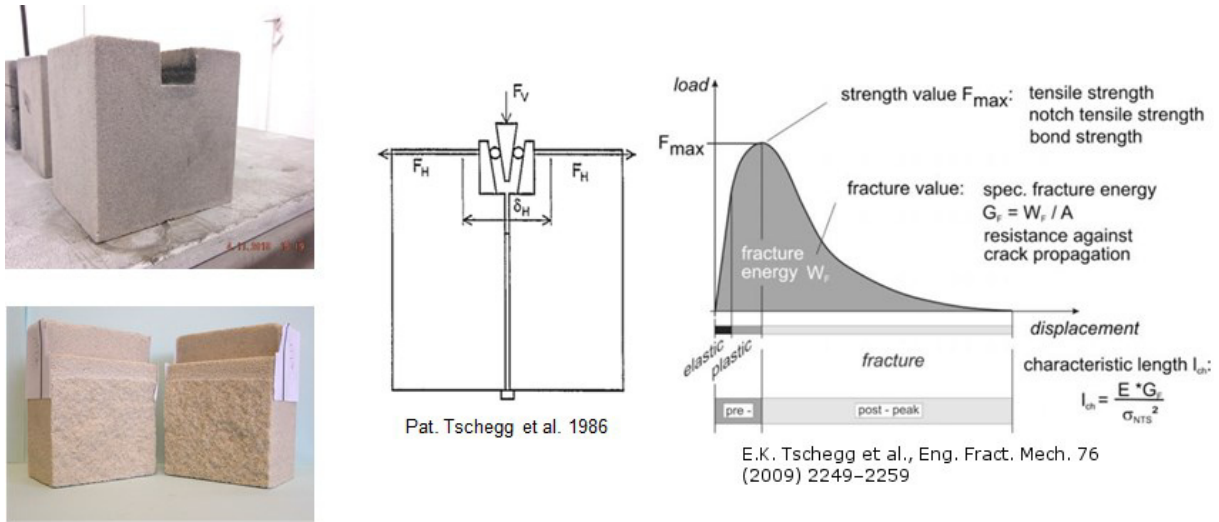


Figure 5-10: Core samples before and after a wedge splitting test (left) schematically shown (centre) and the principle of load curve evaluation for relevant material parameters (right).

From the wedge splitting tests the surface specific fracture energy, tensile strength and the characteristic length can be obtained. Brittleness of a sample is the higher, the lower the characteristic length is. The characteristic results of waterglass- bonded silica sand and mullite-granulate samples before and after a thermal exposure are overviewed in Figure 5-11.

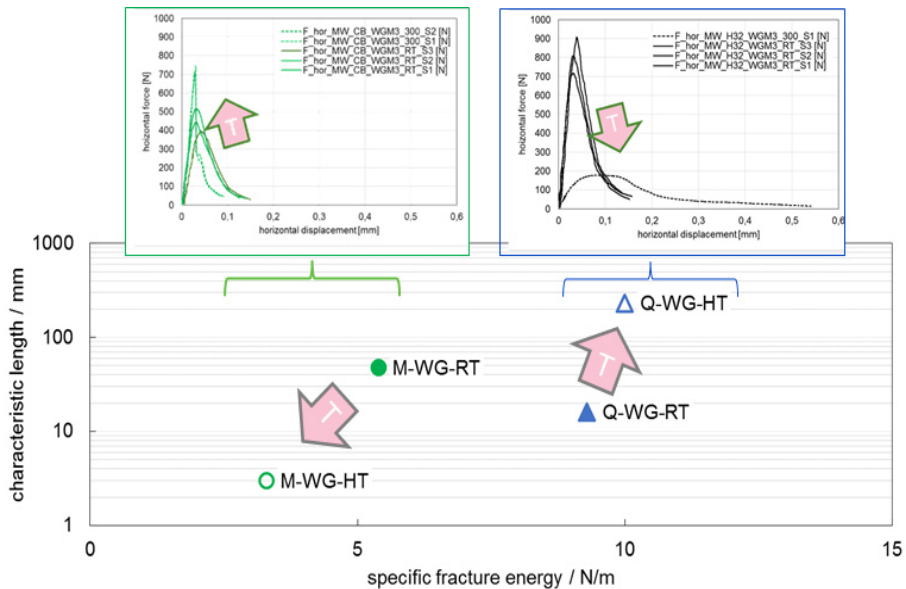


Figure 5-11: Characteristic length and specific fracture energy from wedge splitting tests of silicate bonded quartz (Q-WG) and mullite-based core samples (M-WG). The influence of thermal exposure at 300 °C compared to unconditioned samples is indicated by arrows.

Both the load displacement curve and the evaluated characteristics rendered obvious a significant impact of the granular material type on the fracture behaviour. After thermal exposure, the silica sand samples decreased in brittleness and even revealed a slight increase of the specific fracture energy, whereas the mullite based cores decreased significantly the specific fracture energy and embrittled.

These observations of the strength evolution after thermal exposure were in line with previous standard testing results. The root cause therefore was identified by the formation of micro-cracks only in the waterglass bonds of the quartz sand samples, which were presumably promoted by the high thermal expansion of the quartz, as these could not be observed for mullite based samples.

The de-agglomeration rate criterion, described in section 4.3 in detail, was developed during this thesis to allow a quantitative result verification. This criterion is based on the evaluation of the minimum mass rate during a core removal and on the achieved sand fineness, respectively the remaining agglomeration degree, of the removed core sand. It was investigated, whether strength, specific fracture energy or brittleness were the most dominating factors to influence core removal.

The used core and casting samples and the sand removed from a casting are shown in Figure 5-12 (a). De-agglomeration rate results for different sample conditions are illustrated in Figure 5-12 (b).

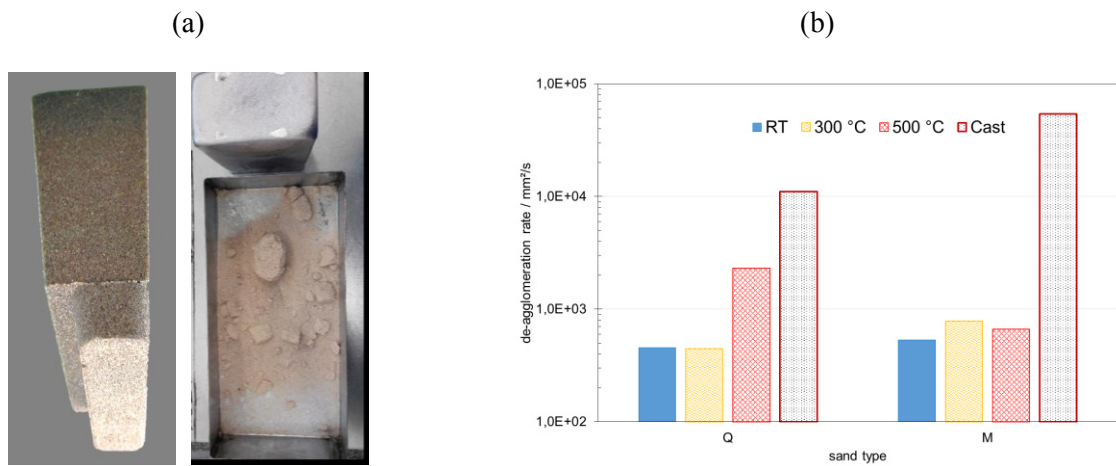


Figure 5-12: Overview about the determination of the de-agglomeration rate. (a) collected removed core sand; (b): de-agglomeration rate results for different sands (Q: silica; M: mullite) and conditions: non-cast hardened reference core samples at RT, 300 °C and 500 °C pre-conditioning and a cast-in sand core.

The indicated reference core samples were produced by hardening of core sand in pre-heated empty test castings, exposed to RT and thermal load at 300 °C and 500 °C. By this method mechanical constraints from casting shrinkage were avoided and the pure thermal influence on core de-agglomeration could be evaluated. The results were increasing according to the previously shown mechanical property decrease, hence, more for silica sand samples and nearly not for mullite-granulate samples.

In comparison to non-cast reference samples, the cast-in cores revealed multiply higher de-agglomeration rates. Interestingly the observed increase was significantly higher for the mullite-based samples, which had a high retained strength, but also high brittleness and lower specific work of fracture compared to the silica sand core samples. The specific work of fracture data were evaluation for their correlation with the de-agglomeration rate, with the result presented in Figure 5-13.

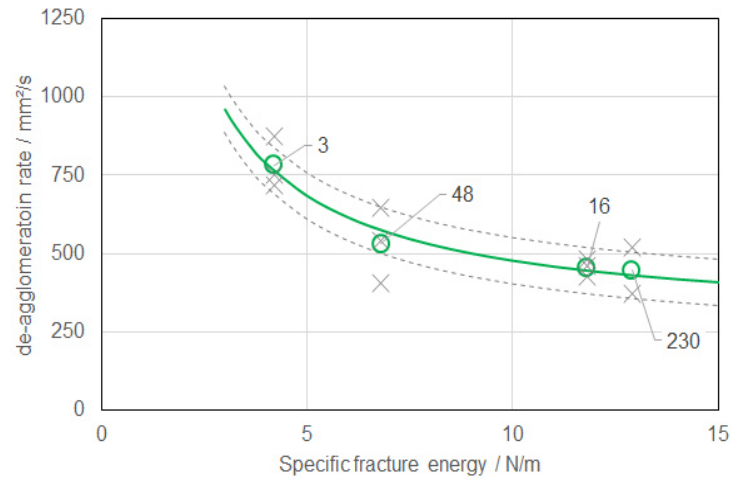


Figure 5-13: De-agglomeration rate of reference samples as function of the specific fracture energy and with indication of the characteristic length in /mm, which is an inverse measure for the brittleness (section 4.4).

In practise, core removal processes differ in impulse and vibration energy input, as well as various core materials and location dependent thermal exposure conditions are present. For future research the impact of brittleness and the effect of external energy input on the core removal remain to be evaluated and offer the potential to enhance this model.

5.3 Casting and core interaction

The experimentally achieved heating and cooling profile of casting and core were documented in details in section 4.4. The key results from this experiment are shown in Figure 5-14. The left picture shows temperature profiles and the right one thermal expansion of quartz and synthetic sintered mullite.

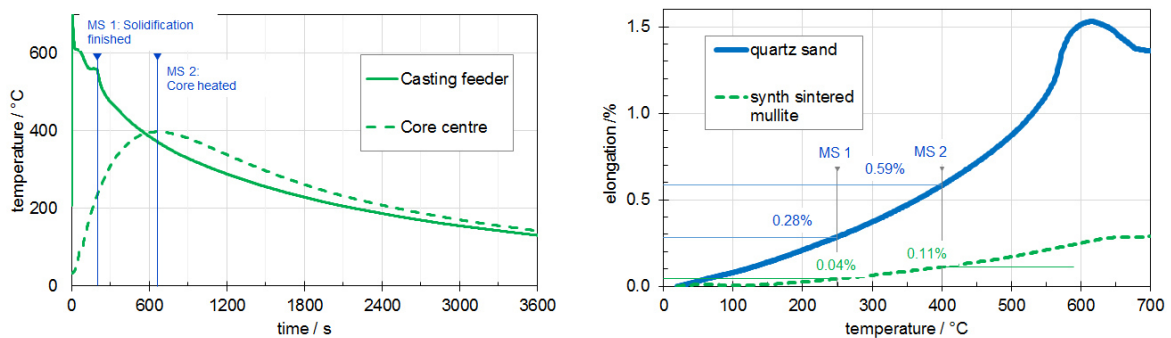


Figure 5-14: Left: Temperature curve in core and casting cooled in ambient calm air. Right: Dilatometer measurements of silicate bonded quartz and synthetic mullite samples. Indicated milestones are the completed solidification (MS 1) and the peak temperature of the core (MS 2).

The cast aluminium part completely solidified at time ‘MS 1’ after pouring, whereas the cast-in sand cores heated up more slowly and achieved their maximum temperature at time ‘MS 2’. Latest after

finished solidification casting shrinkage acted counter the expansion of the cores, hence between MS 1 and MS 2. The core centre temperature at time MS 1 was 250 °C in this experiment and the maximum core temperature at MS 2 was 400 °C. After that time core and casting cooled with a similar cooling rate, when ambient air cooling was applied.

Shrinkage of aluminium is governed by a thermal expansion coefficient of about $24 \cdot 10^{-6} \text{ K}^{-1}$, causing high strain. Thermal strain and strain difference between casting and both core materials were estimated based on the data shown in Figure 5-14 (right). In Table 5-1 the results are overviewed for the heating and the cooling phase, separately.

Table 5-1: Calculated unrestricted thermal strain for the phase from end of casting solidification until the maximum temperature of the core centre (MS 1 – MS 2) and during the cooling phase of the core until room temperature (MS 2 – RT). The differences between the casting and the cores (for every type) and the summed up total strain values are shown.

Strain in %	Casting	Quartz core		Mullite core	
	T-strain	T-strain	Difference	T-strain	Difference
MS 1 – MS 2 (core heating phase)	-0.46 %	0.31%	0.77%	0.07%	0.53%
MS 2 – RT (core cooling phase)	-0.85%	-0.59%	0.26%	-0.11%	0.74%
Total	- 1.31 %		1.03%		1.27%

From Table 5-1 the thermal strain difference during the core heating phase (MS 1 – MS 2) was dominated by the metal shrinkage. As aluminium above 300 °C has a low flow stress, the cast part can be easily strained by the resistance of cores, especially when thin-walled castings and thick-walled cores are present. In the phase of common cooling of casting and core from ~400 °C to room temperature (MS 2 - RT), the shrinkage difference was dominated by the physical properties of the sand core, which was largely different for both core types. Due to the high thermal expansion coefficient of silica sand, these consequently exhibited a low strain difference toward the surrounding aluminium casting. In contrast to that, the strain difference of the mullite-based cores towards the casting was about three times higher, with the consequence of significantly higher transferred mechanical strain.

6 Conclusions

Mechanical properties of sand cores are depending on the used sand and binder and the thermal history. Up to 200 °C the silicate-based binder revealed some structural changes and hardening by drying effects. Due to the evolution of micro-cracks in the silicate-binder bridges between sand grains, decreased retained strength after thermal exposure was achieved, when silica sand was used. For inorganically bonded sand cores it was shown, that their temperature-dependent mechanical properties between 200 and 500 °C were mainly depending on the thermal expansion of the used sand.

In contrast to silica sand, a high retained strength, hence, no temperature-induced damage, tested up to 500 °C was demonstrated with cores made from synthetic sintered mullite granulate. In addition to retained strength, the evaluation of retained stiffness reflected structural changes well. Both, secondary hardening effects and damages by micro-cracks in the binder were reflected.

However, even if absolute strain of cast-in cores is below one per-cent, a stress concentration at the binder bridges, due to the granular structure of sand cores, is present. Finally, depending on the elastic-plastic properties of a binder and the adhesion on the sand grains, a changed mechanical reaction of a core can be expected.

Therefore, additionally to strength, from wedge splitting tests the specific fracture energy and brittleness, evaluated from the characteristic length, were evaluated for foundry sand cores firstly in this work. Interestingly after thermal exposure of samples, a much decreased brittleness for silica sand cores was revealed, which was owed to evolving micro-cracks in the silicate-bonds, whereas increased brittleness for silicate-bonded mullite-based cores was encountered.

For different sand types used, the present study demonstrated, that retained strength of sand core samples after thermal exposure is insufficient to predict the core removal behaviour of cast-in cores. It remains open, if this is also valid for varied grades of chemically the same sand types (e.g. different quartz sand types). Both, the mechanical inter-action of a cast-in sand core with the casting due to shrinkage and the thermal expansion of the sand cores are contributing to the achievable de-agglomeration rates at core removal.

The mullite cores revealed also a high retained strength and, hence, could absorb higher elastic strain energy from casting shrinkage. With that granulate, a high de-agglomeration rate was observed only for cast-in samples. For those, a three-times higher accumulated mechanical strain was evaluated to act compared to silica-based cores. Due to the retained strength, the fracture energy was provided from transferred casting shrinkage strain, which then, owed to the brittleness, can explain the high de-agglomeration rates of such cast-in cores, which was the initially described starting point of this thesis.

7 Outlook

The applicability of failure criterion functions was demonstrated for foundry cores during this thesis, and data for low isostatic pressures are available for several core types. Assumptions were made, that due to the high free volume of sand cores, no significant increase of isostatic pressures might be possible. Future research might apply increased testing effort and evaluate the failure criterion function until high isostatic pressure region, e.g. applying tri-axial testing.

Based on the results of this thesis it is possible to implement failure criterion models at numerical simulation of foundry cores in inter-action with castings. For a system of a casting and a cast-in core, local properties can be assigned and failure evaluated applying the here described Mohr-Coulomb failure criterion. Further enhancements of modelling are possible, if mechanical properties and failure criterion data of cores for elevated temperatures are available. This could serve for higher precision in the prediction of casting shrinkage as the above proposed core failure simulations.

To refine the presented approach of mechanical inter-action of cores with the casting still surface inter-action effects are an issue to be considered in separate studies. For thin-walled cores a significant contribution of the core surface layer having inter-action with the casting at least by roughness, but eventually also by adherence might influence the core removal ability significantly. Consequently, the view onto a sand core from a solid body with certain assigned mechanical properties must be changed into that of a bonded granular material, hence, at least a two-component composite. It remained open, whether the characteristic length parameter from wedge splitting tests could be coupled with typical size of core sections and their reaction on kinetic agitation by hammering impulses. Otherwise also the application of bonded particle models with realistically mirrored particle size distributions and individual properties for granulate and binder has high potential for furtherly improved predictions.

The testing of sand cores after thermal exposure was delicate due to their low strength and high sensitivity during manipulation. Mainly for the positively evaluated wedge splitting testing method, adaptations to a reduced sample thickness allowing for higher heating rates and pre-conditioning temperatures are recommended. In general, automated testing procedures to precisely determine specific fracture energy at low load levels are desired at future implementations.

To enhance the evaluation of real cast-in cores and their local condition it was preliminarily studied, whether instrumented machining operations for core de-fragmentation may deliver specific fracture energy data. As some potential was found based upon drilling trials, the development of practical examinations on any cast-in core – similarly to machining energy of rock diminution energy investigations – is proposed for further investigations.

8 References

- [1] J. Campbell, "The concept of net shape for castings," *Materials & Design*, vol. 21, no. 4, pp. 373–380, 2000.
- [2] M. A. A. Khan, A. K. Sheikh, and B. S. Al-Shaer, *Evolution of Metal Casting Technologies - A Historical Perspective*. 2017.
- [3] J. Campbell, "Casting," in *Complete Casting Handbook Metal Casting Processes, Metallurgy, Techniques and Design*, Butterworth-Heinemann, 2011, pp. 939–1011.
- [4] C. M. Dunks, "Cores and Coremaking," in *Castings*, J. D. Beadle, Ed. Macmillan Publishers Limited, 1971, pp. 49–62.
- [5] E. Flemming and W. Tilch, "Grundeigenschaften der Formstoffkomponenten und ihre gießereitechnologische Bewertung," in *Formstoffe und Formverfahren*, 1st ed., Leipzig, Stuttgart: Deutscher Verlag für Grundstoffindustrie, 1993, pp. 37–104.
- [6] F. Czerwinski, M. Mir, and W. Kasprzak, "Application of cores and binders in metalcasting," *International Journal of Cast Metals Research*, vol. 28, no. 3, pp. 129–139, 2015.
- [7] H. Polzin, "Untersuchungen zur Mikrowellenverfestigung von wasserglasgebundenen Gießereiformstoffen," Dissertation, TU Bergakademie Freiberg, 2000.
- [8] H. Hänsel, "Method and device for removing the core of water-soluble casting cores," Patent US 2004/0195713 A1, 2001.
- [9] F. U. Bischoff, "Untersuchungen zum Einsatz eines wasserlöslichen, anorganischen Kernbinders auf Basis von Magnesiumsulfat in einer Aluminium-Leichtmetallgießerei," Dissertation, TU BA Freiberg, 2003.
- [10] M. Sobczyk, "Untersuchung zur Nutzung der Vakuumtrocknungshärtung für die Herstellung und den Einsatz magnesiumsulfatgebundener Kerne für den Leichtmetallguss," Dissertation, Otto-von-Guericke-Universität Magdeburg, 2008.
- [11] R. Böhm, J. Asal, and B. Münker, "Der Weg zu einer wirtschaftlichen und emissionsfreien Gießerei," *Giesserei-Rundschau*, vol. 60, no. 3/4, pp. 75–77, 2013.
- [12] U. Bischoff and P. Voigt, "Mit neuen anorganischen Formstoffbindern auf dem Weg zur Serienreife im Aluminiumguss," *Giesserei-Rundschau*, vol. 53, no. 9/10, pp. 191–193, 2006.
- [13] T. Pabel, C. Kneißl, J. Brotzki, and J. Müller, "Anorganisches Bindersystem - Einsatz von INOTEC®-Kernen für deutlich verbesserte mechanische Eigenschaften von Al-Gussteilen," *Giesserei-Praxis*, vol. 11, no. Sonderdruck, pp. 1–8, 2009.
- [14] E. Weissenbek, J. Willimayer, J. Wolf, and W. Blümlhuber, "Die Umstellung einer Leichtmetallgießerei auf anorganische Kernfertigung," *Giesserei-Rundschau*, vol. 55, no. 7/8, pp. 136–138, 2008.
- [15] J. Müller *et al.*, "Geht nicht , gibt ' s nicht – Weiterentwicklungen im Bereich anorganischer Bindersysteme," *Giesserei-Praxis*, no. 1–2, pp. 20–25, 2014.
- [16] J. Danko, M. Holtzer, and R. Danko, "Criteria of an Advanced Assessment of the Reclamation Process Products," *Archives of Foundry Engineering*, vol. 10, no. 3, pp. 25–28, 2010.
- [17] H. Schwickal, M. Becker, and S. Magerl, "Qualitative und wirtschaftliche Bewertung eines neuartigen Regenerationsverfahrens für anorganische Bindersysteme," *Abschlussbericht zu Aktenzeichen 26819-21/2*. Deutsche Bundesstiftung Umwelt, D-49090 Osnabrück, pp. 1–58, 2011.

- [18] R. Böhm, "Erfahrungen bei der Regenerierung neuer anorganischer Binder." Hüttenes-Albertus Chemische Werke GmbH, Düsseldorf, pp. 1–4, 2008.
- [19] T. Steinhäuser and B. Wehren, "Regenerierung von anorganisch gebundenen Kernsandten," *Giesserei*, vol. 99, no. 03, pp. 58–61, 2012.
- [20] J. L. Jorstad, "Expendable-mold casting processes with permanent patterns," in *ASM Handbook Vol. 15 Casting*, 10th ed., ASM International, 2008, pp. 523–634.
- [21] H. W. Dietert, "Core knock-out," in *Foundry Core Practice*, 2nd ed., Chicago, IL: American Foundrymen's Society, 1950, pp. 473–478.
- [22] "Photo of the month," *Giesserei*, vol. 102, no. 06, pp. 6–7, 2015.
- [23] "Swingmaster 315 R," *Datenblatt Entkernmaschine*, 2015. [Online]. Available: www.fill.co.at. [Accessed: 15-Jun-2015].
- [24] M. Gamisch, "Mechanisches Entkernen von Al-Gussteilen mit geringer Beanspruchung des Gussteils," *Giesserei-Rundschau*, vol. 49, no. 3/4, pp. 43–45, 2002.
- [25] R. Thewes, "Cerabite Technology," *Produktbeschreibung Klein Stoßwellentechnik*, 2015. [Online]. Available: <http://www.stoßwellentechnik.de/index.php/home.html>. [Accessed: 28-Nov-2015].
- [26] C. Konzack, "Entkernen von Gussprototypen mit Stoßwellen," *Giesserei*, vol. 100, no. 11, pp. 62–63, 2013.
- [27] L. Zaretskiy, "Modified Silicate Binders New Developments and Applications," *International Journal of Metalcasting*, p. 12, 2015.
- [28] J. Grassi, J. Campbell, and G. Kuhlman, "Chemically bonded aggregate mold," Patent US 7,165,600 B2, 2007.
- [29] P. Jelinek, T. Miksovsky, J. Beno, and E. Adamkova, "Development of foundry cores based on inorganic salts," *Materials and Technology*, vol. 47, no. 6, pp. 689–693, 2013.
- [30] E. Adamkova, P. Jelinek, F. Miksovsky, and J. Beňo, "Technology of Water Soluble Cores for Foundry Applications," in *XX International Student's Day of Metallurgy*, 2013, pp. 1–8.
- [31] J. Campbell, "Molding," in *Complete Casting Handbook*, Elsevier Ltd, 2011, pp. 911–938.
- [32] F. L. Le Serve, "Castings," in *Castings*, J. D. Beadle, Ed. Hampshire UK: The Macmillan Press Limited, 1971, pp. 35–48.
- [33] B. Stauder and W. Gintner, "Formgrundstoff, Formstoff und Formteil für eine Gießform," Patent DE 101 45 417 A 1, 2001.
- [34] X. Wang, "Thermal physical and mechanical properties of raw sands and sand cores for aluminum casting," Master thesis, Montanuniversität Leoben, 2014.
- [35] M. Aslanowicz, A. Fedoryszyn, T. Fulko, and A. Ościłowski, "Aspects of Quality Assurance in Mechanization of Core Making Process," *Archives of Foundry Engineering*, vol. 14, no. Special Issue 1/2014, pp. 43–46, 2014.
- [36] B. Stauder, "Formstoff für die Herstellung von Gießformteilen," Patent DE 102 09 183 A 1, 2002.
- [37] C. Klimesch, S. Bechtle, O. Vogt, S. Ziegler, S. Röpke, and A. Schüller, "Herausforderungen bei hoch beanspruchbaren Zylinderköpfen," *Giesserei*, vol. 98, no. 6, pp. 60–66, 2011.
- [38] I. Wagner and M. Schneider, "Kernsimulation - Effiziente Prozessoptimierung in der Gießerei," *Giesserei-Rundschau*, vol. 58, no. 9/10, pp. 224–228, 2011.

- [39] M. Pelzer, "Optimierung der Kernherstellung durch Numerische Simulation," Dissertation, RWTH Aachen, 2000.
- [40] B. Winartomo, U. Vroomen, A. Bührig-Polaczek, and M. Pelzer, "Multiphase modelling of core shooting process," *International Journal of Cast Metals Research*, vol. 18, no. 1, pp. 13–20, 2005.
- [41] S. I. Bakhtiyarov and R. a. Overfelt, "CFD modeling and experimental study of resin-bonded sand/air two-phase flow in sand coremaking process," *Powder Technology*, vol. 133, no. 1–3, pp. 68–78, 2003.
- [42] A. Mehta, "Computer simulation approaches - an overview," in *Granular physics*, Cambridge university press, 2007, pp. 18–26.
- [43] U. C. Nwaogu, "New Sol-Gel Coatings to Improve Casting Quality," PhD Thesis, Technical University of Denmark, 2011.
- [44] N. J. Brown, J. F. Chen, and J. Y. Ooi, "A bond model for DEM simulation of cementitious materials and deformable structures," *Granular Matter*, vol. 16, no. 3, pp. 299–311, 2014.
- [45] Minelco, "MinSand for stronger cores and smoother surfaces.," *Product brochure*, 2011. [Online]. Available: www.minelco.com. [Accessed: 01-Aug-2011].
- [46] M. Hoyos-Lopez, N. V. Perez-Aguilar, and J. E. Hernandez-Chavero, "Imaging of silica sand to evaluate its quality to use it as foundry core sand," *International Journal of Metalcasting*, vol. 11, no. 2, pp. 340–346, 2017.
- [47] S. T. Krukowski, "Foundry Sands," in *Industrial Minerals and Rocks*, 7th ed., J. E. Kogel, N. C. Trivedi, J. M. Barker, and S. T. Krukowski, Eds. Littleton, Colorado, USA 80127: Society for Mining, Metallurgy, and Exploration, Inc. (SME), 2006, pp. 1433–1440.
- [48] U. C. Nwaogu and N. S. Tiedje, "Foundry Coating Technology: A Review," *Materials Sciences and Applications*, vol. 02, no. 08, pp. 1143–1160, 2011.
- [49] J. R. Brown, Ed., *Foseco Ferrous Foundryman 's Handbook*, 1st ed. Oxford Auckland Boston Johannesburg Melbourne New Delhi: Butterworth-Heinemann, 2000.
- [50] J. R. Brown, Ed., *Foseco Non-Ferrous Foundryman's Handbook*, 11th ed. Butterworth-Heinemann, 1999.
- [51] I. Bindernagel, *Formstoffe und Formverfahren in der Gießereitechnik*, vol. 12. Düsseldorf: Verein Deutscher Gießereifachleute; Giesserei-Verlag GmbH, 1983.
- [52] U. Recknagel and W. Tilch, "Untersuchungen zum Ausdehnungsverhalten von Formstoffen im Hinblick auf die Vermeidung typischer Gußfehler," *Sonderdruck aus Giesserei-Praxis*, vol. 8+9, p. 9, 2000.
- [53] J. Campbell, *Castings*, 2nd ed. Oxford: Butterworth-Heinemann, 2003.
- [54] A. A. Langroudi, I. Jefferson, K. O'hara-Dhand, and I. Smalley, "Micromechanics of quartz sand breakage in a fractal context," *Geomorphology*, vol. 211, pp. 1–10, 2014.
- [55] V. Dargai, H. Polzin, and L. Varga, "Die Bestimmung der granulometrischen Eigenschaften von Gießereisanden mittels dynamischer Bildanalyse," *Giesserei Praxis*, no. 4, pp. 19–22, 2018.
- [56] H. Bayat, M. Rastgo, M. Mansouri Zadeh, and H. Vereecken, "Particle size distribution models, their characteristics and fitting capability," *Journal of Hydrology*, vol. 529, pp. 872–889, 2015.
- [57] M. T. Bui, "Influence of some particle characteristics on the small strain response of granular materials," PhD Thesis, University of Southampton, 2009.
- [58] M. Diepenbroek, "Die Beschreibung der Korngestalt mit Hilfe Eigenschaften von

- Sedimentpartikeln / The characterization of grain shape using Parameterization of morphological properties of sedimentary particles,” *Ber. Polarforsch.*, vol. 122, p. 95, 1993.
- [59] B. Belhadj, M. Bederina, K. Benguettache, and M. Queneudec, “Effect of the type of sand on the fracture and mechanical properties of sand concrete,” *Advances in Concrete Construction*, vol. 2, no. 1, pp. 13–27, 2014.
- [60] J. Beno, F. Miksovsky, P. Jelinek, K. Konecna, and P. Smysl, “Alternative evaluation of the properties of the silica sand,” *Archives of Metallurgy and Materials*, vol. 59, no. 2, pp. 15–18, 2014.
- [61] H. Salmang and H. Scholze, “Oberflächencharakterisierung,” in *Keramik*, 7th ed., R. Telle, Ed. Springer Berlin Heidelberg, 2007, pp. 121–127.
- [62] R. Brinschwitz, “Untersuchungen zur Einflussnahme alternativer Formgrundstoffe auf die form- und gießtechnologischen Eigenschaften,” Diplomarbeit, Technische Universität Bergakademie Freiberg Fakultät, 2005.
- [63] F. Ostermann, “Märkte und Anwendungen,” in *Anwendungstechnologie Aluminium*, 2nd ed., Springer Berlin Heidelberg, 2007, pp. 9–78.
- [64] C. Oberschelp, H. Kirchmeir, G. Huber, A. Wagner, J. Huber, and P. Stika, “Einsatz dynamischer Gießverfahren bei der Herstellung hoch belasteter Zylinderköpfe,” *Giesserei*, vol. 98, no. 12, pp. 26–35, 2011.
- [65] U. Recknagel and M. Dahlmann, “Spezialsande - Formgrundstoffe für die moderne Kern- und Formherstellung / Special Sands - Base Materials for modern Core and Mould Making,” *Giesserei-Rundschau*, vol. 56, no. 1/2, pp. 6–17, 2009.
- [66] J. Bast, A. Kadauw, and A. Malaschkin, “Optimising of moulding parameters for green sand compaction by computer simulation and a new compaction measuring device,” *International Journal of Metalcasting*, vol. Spring 09, pp. 55–65, 2009.
- [67] J. Campbell, “Molds and cores,” in *Complete Casting Handbook*, Elsevier Ltd, 2011, pp. 155–186.
- [68] S. Neves, W. Schäfer, and P. N. Hansen, “The Sensibility of Thermophysical Property Data for Simulating Casting Processes,” *International Journal of Thermophysics*, vol. 23, no. 5, pp. 1391–1399, 2002.
- [69] G. Solenicki, I. Budic, I. Kladaric, and D. Novoselovic, “Compressive stresses of mould mixture,” *Metalurgija*, vol. 53, no. 4, pp. 591–593, 2014.
- [70] G. Solenicki, “Istraživanje mehanizma nastanka odlupljivanja u kalupu / Research of scabbing defects mechanism,” Doktorski Rad, Sveuciliste u Zagrebu, 2006.
- [71] J. Thiel, M. Ziegler, P. Dziekonski, and S. Joyce, “Investigation into the Technical Limitations of Silica Sand Due to Thermal Expansion,” *AFS Transactions*, vol. 115, pp. 383–400, 2007.
- [72] J. Svidró, A. Diószegi, L. Tóth, and J. T. Svidró, “The Influence of Thermal Expansion of Unbonded Foundry Sands on the Deformation of Resin Bonded Cores,” *Archives of Metallurgy and Materials*, vol. 62, no. 2, pp. 795–798, 2017.
- [73] J. T. Svidro, A. Dioszegi, and J. Toth, “The novel application of Fourier thermal analysis in foundry technologies - Examination of degradation characteristics in resin-bound moulding materials,” *J Therm Anal Calorim*, vol. 115, pp. 331–338, 2014.
- [74] R. Siddique, “Foundry sand,” in *Waste Materials and By-Products in Concrete*, 2008, pp. 381–406.
- [75] M. Holtzer, M. Górný, and R. Daňko, “Microstructure and Properties of Ductile Iron and

- Compacted Graphite Iron Castings,” in *SpringerBriefs in Materials*, 2015, pp. 27–43.
- [76] P. W. Kopf, “Phenolic Resins,” in *Encyclopedia of Polymer Science and Technology*, vol. 7, John Wiley & Sons, Inc., 2002, pp. 322–368.
- [77] D. M. Trinowski, “Phenolic resins: A century of progress,” in *Phenolic Resins: A Century of Progress*, Luis Pilato, Ed. Berlin Heidelberg: Springer, 2010, pp. 451–502.
- [78] M. Holtzer, M. Górný, and R. Dańko, “The Effects of Mold Sand/Metal Interface phenomena,” in *Microstructure and Properties of Ductile Iron and Compacted Graphite Iron Castings*, Springer, 2015, pp. 27–43.
- [79] W. Tilch and H. Polzin, “Anwendung und Eigenschaften innovativer anorganischer Binder für die Kernherstellung,” *Archives of Foundry*, vol. 4, no. 13, pp. 219–224, 2004.
- [80] E. Lange, “Innovativer 3-D-Druck in Gießereien,” *Giesserei*, vol. 101, no. 10, pp. 74–77, 2014.
- [81] C. A. Lytle, W. Bertsch, and M. D. McKinley, “Determination of thermal decomposition products from a phenolic urethane resin by pyrolysis gas chromatography mass spectrometry,” *Hrc-Journal of High Resolution Chromatography*, vol. 21, no. 2, pp. 128–132, 1998.
- [82] H. Bargaoui, F. Azzouz, D. Thibault, and G. Cailletaud, “Thermomechanical behavior of resin bonded foundry sand cores during casting,” *Journal of Materials Processing Tech.*, vol. 246, pp. 30–41, 2017.
- [83] M. Holtzer, A. Bobrowski, R. Dańko, S. Żymankowska-Kumon, and J. Kolczyk, “Influence of a Liquid Metal Temperature on a Thermal Decomposition of a Phenolic Resin,” *Archives of Foundry Engineering*, vol. 13, no. 2, pp. 3–5, 2013.
- [84] H. Renhe, G. Hongmei, T. Yaoji, and L. Qingyun, “Curing mechanism of furan resin modified with different agents and their thermal strength,” *China Foundry*, vol. 8, no. 2, pp. 161–165, 2011.
- [85] M. Lucarz, B. Grabowska, and G. Grabowski, “Determination of parameters of the moulding sand reclamation process, on the thermal analysis bases,” *Archives of Metallurgy and Materials*, vol. 59, no. 3, pp. 1023–1027, 2014.
- [86] M. Kubecki, M. Holtzer, B. Grabowska, and A. Bobrowski, “Development of method for identification of compounds emitted during thermal degradation of binders used in foundry,” *Archives of Foundry*, vol. 11, no. Special Issue 3, pp. 125–130, 2011.
- [87] L. Nastac, S. Jia, M. N. Nastac, and R. Wood, “A Numerical Model for Predicting the Gas Evolution in Silica Sand (Furan Binder) Mold Castings,” in *Advances in the Science and Engineering of Casting Solidification*, 2015, pp. 363–370.
- [88] D. Khale and R. Chaudhary, “Mechanism of geopolymerization and factors influencing its development: A review,” *Journal of Materials Science*, vol. 42, no. 3, pp. 729–746, 2007.
- [89] D. Drozynski, A. Bobrowski, and M. Holtzer, “Influence of the Reclaim Addition on Properties of Moulding Sands with the Geopol Binder,” *Archives of Foundry Engineering*, vol. 15, no. 1, pp. 138–142, 2015.
- [90] M. T. Tognonvi, J. Soro, J. L. Gelet, and S. Rossignol, “Physico-chemistry of silica / Na silicate interactions during consolidation. Part 2: Effect of pH,” *Journal of Non-Crystalline Solids*, vol. 358, no. 3, pp. 492–501, 2012.
- [91] R. Döpp, R. Deike, and G. Gettwert, “Beitrag zum Wasserglas-CO₂-Verfahren,” *Giesserei*, vol. 72, no. 22, pp. 626–635, 1985.
- [92] G. Brümmer and R. Döpp, “Trocken statt Begasen mit CO₂ beim Wasserglasverfahren - neue Ansätze bei alten Bindemitteln,” *Giesserei*, vol. 84, no. 13, pp. 12–14, 1997.

- [93] I. Bindernagel, *Formstoffe und Formverfahren*. VDG, 1983.
- [94] M. Weider, H. Polzin, M. Göttert, K. Eigenfeld, and W. Schärfl, “Thermische Wechselwirkungen zwischen hochlegiertem TRIP- Stahlguss und wasserglasgebundenen Formstoffsystemen,” *Giesserei Praxis*, vol. 5, pp. 187–191, 2012.
- [95] K. Granat, D. Nowak, M. Stachowicz, and M. Pigieli, “Possibilities of utilizing used moulding and core sands by microwave treatment,” *Archives of Foundry Engineering*, vol. 11, no. 1, pp. 35–38, 2011.
- [96] M. Stachowicz, Ł. Pałyga, and K. Granat, “Prediction of Properties of Microwave- Hardened Sandmixes Containing Water-Glass with Use of Neural Networks,” *Archives of Foundry Engineering*, vol. 15, no. 2, pp. 99–104, 2015.
- [97] A. Wolff and T. Steinhäuser, “AWB — ein umweltverträgliches Kernherstellverfahren,” *Giesserei*, vol. 91, no. 6, pp. 80–84, 2004.
- [98] A. Sáenz, A. Velasco, J. Talamantes, and R. Colás, “Development of inorganic binders for the manufacture of sand cores used in the automotive casting industry,” in *70th World Foundry Congress*, 2012, pp. 255–260.
- [99] P. Jelínek, H. Polzin, and R. Škuta, “Utilization of physical dehydradion for hardening of cores bonded with colloidal solutions of alkaline silicates,” *Acta Metallurgica Slovaca*, vol. 1, no. 10, pp. 10–23, 2004.
- [100] A. Fedoryszyn, J. Dańko, R. Dańko, M. Aslanowicz, T. Fulko, and A. Ościłowski, “Characteristic of Core Manufacturing Process with Use of Sand, Bonded by Ecological Friendly Nonorganic Binders,” *Archives of Foundry Engineering*, vol. 13, no. 3, pp. 19–24, 2013.
- [101] J. Wang, Z. Fan, X. Zan, and Di Pan, “Propertis of sodium silicate bonded sand hardened by microwave heating,” *China Foundry*, vol. 6, no. 3, pp. 191–196, 2009.
- [102] I. Izdebska-Szanda, A. Baliński, M. Angrecki, and A. Palma, “The effect of nanostructure modification on the silicate binder on its binding characteristics and functional properties,” *Archives of Metallurgy and Materials*, vol. 59, no. 3, pp. 2–5, 2014.
- [103] I. Izdebska-Szanda, M. Angrecki, and S. Matuszewski, “Investigating of the knocking out properties of moulding sands with new inorganic binders used for castings of non-ferrous metal alloys in comparison with the previously used,” *Archives of Foundry Engineering*, vol. 12, no. 2, pp. 117–120, 2012.
- [104] I. Izdebska-Szanda, A. Palma, M. Angrecki, and M. Żmudzińska, “Environmentally friendly mould technology,” *Archives of Foundry Engineering*, vol. 13, no. 3, pp. 37–42, 2013.
- [105] K. Major-Gabryś and S. M. Dobosz, “High-temperature expansion and knock-out properties of moulding sands with water glass,” *Archives of Foundry Engineering*, vol. 7, no. 1, pp. 127–130, 2007.
- [106] S. M. Dobosz and K. Major-Gabryś, “The mechanism of improving the knock-out properties of moulding sands with water glass,” *Archives of Foundry Engineering*, vol. 8, no. 1, pp. 37–42, 2008.
- [107] K. Major-Gabryś, S. M. Dobosz, P. Jelinek, J. Jakubski, and J. Beno, “The measurement of high-temperature expansion as the standard of estimation the knock-out properties of moulding sands with hydrated sodium silicate,” *Archives of Metallurgy and Materials*, vol. 59, no. 2, pp. 739–742, 2014.
- [108] C. Menet, P. Reynaud, G. Fantozzi, D. Thibault, and A. Laforêt, “Thermomechanical properties and fracture of resin-bonded-sand cores – Experimental study and application in aluminium foundry,” in *Powders and Grains 2017 – 8th International Conference on Micromechanics on*

- Granular Media*, 2017, vol. 08006, pp. 8–11.
- [109] J. Jungwirth and A. Muttoni, “Teil 1 - Tragversuche. Projekt 00.02, Bericht 00.02.R3,” in *Versuche zum Tragverhalten von ultra hochfestem Beton*, Lausanne: EPFL, Institut de structures – Construction en béton, 2004, pp. 1–69.
- [110] D. M. Cole and J. F. Peters, “A physically based approach to granular media mechanics: Grain-scale experiments, initial results and implications to numerical modeling,” *Granular Matter*, vol. 9, no. 5, pp. 309–321, 2007.
- [111] Y. Dai, D. Gruber, and H. Harmuth, “Determination of the fracture behaviour of MgO-refractories using multi-cycle wedge splitting test and digital image correlation,” *Journal of the European Ceramic Society*, vol. 37, no. 15, pp. 5035–5043, 2017.
- [112] M. Conev, I. Vaskova, M. Hrubovcakova, and P. Hajdich, “Decorating behaviour of chosen moulding materials with alkali silicate based inorganic binders,” *Archives of Metallurgy and Materials*, vol. 62, no. 2, pp. 703–706, 2017.
- [113] A. P. Popoola and O. S. Fayomi, “Assessing the performance of binders on core strength in metal casting,” *International Journal of the Physical Sciences*, vol. 6, no. 34, pp. 7805–7810, 2011.
- [114] J. M. Denis and A. Schrey, “Ausgereifte Polyurethan-Cold-Box-Binder für Aluminiumguss mit verbessertem Zerfallsverhalten und geringerer Umweltbelastung,” *Giesserei-Rundschau*, vol. 53, no. 1/2, pp. 14–17, 2006.
- [115] J. M. Denis and A. Schrey, “Fortschrittliche Polyurethan-Cold-Box- Binder für Aluminiumguss mit verbessertem thermischen Zerfall und geringerer Umweltbelastung (Progressive PU Cold box binder for aluminum casting with improved thermal decay and of smaller environmental impact),” *Giesserei*, vol. 93, no. 01, pp. 26–31, 2006.
- [116] E. Flemming and W. Tilch, “Auspackverhalten,” in *Formstoffe und Formverfahren*, 1st ed., Leipzig, Stuttgart: Deutscher Verlag für Grundstoffindustrie, 1993, pp. 230–233.
- [117] Polish Standard PN-85/H-11005, “Moulding and core sands technological knockout properties test,” Polish Standards Institute - Polski Komitet Normalizacji, Miar I Jakosci, Poland, PN-85/H-11005, 1985.
- [118] W. L. Tordoff and R. D. Tenaglia, “Test casting evaluation of chemical binder systems,” *AFS Transactions*, vol. 80, no. 74, 1980.
- [119] W. L. Tordoff, “Test casting evaluation of chemical binder systems,” *AFS Transactions*, no. Silver Anniversary, Division 4, p. 16, 2006.
- [120] Y. M. Yunovich, R. A. Dudenhoefer, and H. J. Langer, “Inorganic foundry binder systems and their uses,” Patent US 5279665A, 1994.
- [121] C. Chen and J. T. Schneider, “Polyurethane-forming cold-box binders and their uses,” Patent US 5688857A, 1997.
- [122] C. Henry, R. Showman, and G. Wandtke, “Core and Foundry Process Variables Affecting Aluminum Casting Shakeout of Cold Box Cores,” *Transactions of American Foundry Society*, vol. 107, pp. 99–115, 1999.
- [123] M. Stancliffe, “Phenolic urethane cold-box binders - A study of global properties, variables, causes and effects,” *67th World Foundry Congress, wfc06*, vol. 1, pp. 483–492, 2006.
- [124] T. Fennell and G. Crandell, “Inorganic Binder Properties Study,” in *Casting Emission Reduction Program*, US Army Contract W15QKN-D-0030 FY2006 Tasks WBS # 1.4.5, 2008, p. 41.
- [125] M. Zogg, “Zerkleinern,” in *Einführung in die mechanische Verfahrenstechnik*, 3rd ed., M. Zogg, Ed. Burgdorf: B.G. Teubner Stuttgart, 1993, pp. 51–77.

- [126] H. Schubert, *Aufbereitung fester mineralischer Rohstoffe - Band I*, 2nd ed. Leipzig: VEB Deutscher Verlag für Grundstoffindustrie, 1983.
- [127] H. Schubert, *Handbuch der mechanischen Verfahrenstechnik*. D-09596 Freiberg: Wiley-VCH, 2003.
- [128] I. Einav, "Fracture propagation in brittle granular matter," *Proceedings of the Royal Society A: Mathematical, Physical and Engineering Sciences*, vol. 463, no. 2087, pp. 3021–3035, 2007.
- [129] C. Ovalle, E. Frossard, C. Dano, W. Hu, S. Maiolino, and P. Y. Hicher, "The effect of size on the strength of coarse rock aggregates and large rockfill samples through experimental data," *Acta Mechanica*, vol. 225, no. 8, pp. 2199–2216, 2014.
- [130] W. Weibull, "A statistical distribution function of wide applicability," *Journal of applied mechanics*, vol. 18, pp. 293–297, 1951.
- [131] Z. P. Bažant, "Concrete fracture models: Testing and practice," *Engineering Fracture Mechanics*, vol. 69, no. 2, pp. 165–205, 2002.
- [132] M. A. Mullier, J. P. K. Seville, and M. J. Adams, "A fracture mechanics approach to the breakage of particle agglomerates," *Chemical Engineering Science*, vol. 42, no. 4, pp. 667–677, 1987.
- [133] D. A. Jones, S. W. Kingman, D. N. Whittles, and I. S. Lowndes, "The influence of microwave energy delivery method on strength reduction in ore samples," *Chemical Engineering and Processing: Process Intensification*, vol. 46, no. 4, pp. 291–299, 2007.
- [134] E. Eberhardt, "The Hoek–Brown Failure Criterion," *Rock Mechanics and Rock Engineering*, vol. 45, no. 6, pp. 981–988, 2012.
- [135] L. R. Alejano and A. Bobet, "Drucker-Prager criterion," *Rock Mechanics and Rock Engineering*, vol. 45, no. 6, pp. 995–999, 2012.
- [136] N. Mitarai and F. Nori, "Wet granular materials," *Advances in Physics*, vol. 55, no. 1–2, pp. 1–45, 2006.
- [137] E. Dahlem, D. Gruber, T. Auer, H. Harmuth, M. Huger, and T. Chotard, "Evaluation of the Drucker-Prager parameters at elevated temperature for two refractories," in *Conference of the 12th Conference of the European Ceramic Society – ECerS XII*, 2011, vol. 1, no. 4, pp. 1–4.
- [138] E. Dahlem, "Characterisation of refractory failure under combined hydrostatic and shear loading at elevated temperatures," Dissertation, Montanuniversität Leoben, 2011.
- [139] E. K. Tschegg, "Equipment and appropriate specimen shapes for tests to measure fracture values (Prüfeinrichtung zur Ermittlung von bruchmechanischen Kennwerten sowie hierfür geeignete Prüfkörper)," Patent AT no. 390328, 1986.
- [140] H. Harmuth, "Stability of crack propagation associated with fracture energy determined by wedge splitting specimen," *Theoretical and Applied Fracture Mechanics*, vol. 23, no. 1, pp. 103–108, 1995.
- [141] S. Jin, D. Gruber, and H. Harmuth, "Determination of Young's modulus, fracture energy and tensile strength of refractories by inverse estimation of a wedge splitting procedure," *Engineering Fracture Mechanics*, vol. 116, pp. 228–236, 2014.
- [142] S. Lackner, "Anwendung eines Inversenverfahrens zur Auswertung eines Keilspalttests für die bruchmechanische Charakterisierung von Feuerfestbaustoffen," Magisterarbeit, Montanuniversität Leoben, 2007.
- [143] A. Hillerborg, M. Modéer, and P.-E. Petersson, "Analysis of crack formation and crack growth in concrete by means of fracture mechanics and finite elements," *Cement and Concrete Research*, vol. 6, no. 6, pp. 773–781, Nov. 1976.

- [144] Y. Dai, D. Gruber, S. Jin, and H. Harmuth, "Modelling and inverse investigation of the fracture process for a magnesia spinel refractory using a heterogeneous continuum model," *Engineering Fracture Mechanics*, vol. 182, pp. 438–448, 2017.
- [145] D. O. Potyondy and P. A. Cundall, "A bonded-particle model for rock," *International Journal of Rock Mechanics & Mining Sciences*, vol. 41, pp. 1329–1364, 2004.
- [146] J. Subero, Z. Ning, M. Ghadiri, and C. Thornton, "Effect of interface energy on the impact strength of agglomerates," *Powder Technol.*, vol. 105, pp. 66–73, 1999.
- [147] V. Topin, J. Y. Delenne, F. Radjai, L. Brendel, and F. Mabilie, "Strength and failure of cemented granular matter," *European Physical Journal E*, vol. 23, no. 4, pp. 413–429, 2007.
- [148] J. Y. Delenne, V. Topin, and F. Radjai, "Failure of cemented granular materials under simple compression: Experiments and numerical simulations," *Acta Mechanica*, vol. 205, no. 1–4, pp. 9–21, 2009.
- [149] R. Affes, J. Y. Delenne, Y. Monerie, F. Radjaï, and V. Topin, "Tensile strength and fracture of cemented granular aggregates," *European Physical Journal E*, vol. 35, no. 11, p. 15, 2012.
- [150] S. Antonyuk, "Deformations- und Bruchverhalten von kugelförmigen Granulaten bei Druck- und Stoßbeanspruchung," Dissertation, Otto-von-Guericke-Universität Magdeburg, 2006.
- [151] S. Antonyuk, J. Tomas, S. Heinrich, and L. Mörl, "Breakage behaviour of spherical granulates by compression," *Chemical Engineering Science*, vol. 60, no. 14, pp. 4031–4044, 2005.
- [152] A. Spetl, M. Dosta, S. Antonyuk, S. Heinrich, and V. Schmidt, "Statistical investigation of agglomerate breakage based on combined stochastic microstructure modeling and DEM simulations," *Advanced Powder Technology*, vol. 26, no. 3, pp. 1021–1030, 2015.
- [153] S. Antonyuk, S. Palis, and S. Heinrich, "Breakage behaviour of agglomerates and crystals by static loading and impact," *Powder Technology*, vol. 206, no. 1–2, pp. 88–98, 2011.
- [154] Quarzwerke, "Stoffdaten Quarzsand Haltern H 31 bis H 35." Quarzwerke GmbH, D-50207 Frechen, p. 2, 2009.
- [155] ASK, "Sicherheitsdatenblatt Askocure 355 Hydro Teil 1." Ashland-Südchemie-Kernfest GmbH, D-40721 Hilden, p. 8, 2005.
- [156] ASK, "Sicherheitsdatenblatt Askocure 655 Hydro Teil 2." Ashland-Südchemie-Kernfest GmbH, D-40721 Hilden, p. 7, 2003.
- [157] TRG, "Sicherheitsdatenblatt Dimethylethylamin DMEA." TRG Cyclamin GmbH, D-39218 Schönebeck, p. 6, 2006.
- [158] Furtenbach, "Sicherheitsdatenblatt Thermophen 2143." Furtenbach GmbH, A-2700 Wiener Neustadt, p. 4, 2001.
- [159] Furtenbach, "Sicherheitsdatenblatt Härter MBT." Furtenbach GmbH, A-2700 Wiener Neustadt, p. 4, 2002.
- [160] HA, "Sicherheitsdatenblatt Furesan 7022/1." Hüttenes-Albertus Chemische Werke GmbH, D-40549 Düsseldorf, p. 6, 2010.
- [161] HA, "Sicherheitsdatenblatt Furedur 8154." Hüttenes-Albertus Chemische Werke GmbH, D-40549 Düsseldorf, p. 5, 2006.
- [162] HA, "Sicherheitsdatenblatt Furesan 8885." Hüttenes-Albertus Chemische Werke GmbH, D-40549 Düsseldorf, p. 7, 2012.
- [163] HA, "Sicherheitsdatenblatt Furedur 8099." Hüttenes-Albertus Chemische Werke GmbH, D-40549 Düsseldorf, p. 1, 2009.

-
- [164] Wöllner, “Sicherheitsdatenblatt Betol 39 T.” Wöllner GmbH&Co KG, D-67065 Ludwigshafen, p. 2, 2010.
- [165] Itochu, “Naigai Cerabeads 60.” Itochu Ceratech Corp., pp. 1–4, 2003.
- [166] Damrec, “Kerphalite KF Foundry sand.” Damrec, F-75007 Paris, p. 1, 2007.
- [167] M. Berbic, “Untersuchungen zur thermischen Degradation von Kernformstoffen,” Diplomarbeit, Montanuniversität Leoben, 2017.
- [168] R. Gosch and P. Stika, “Das ROTACAST-Gießverfahren - millionenfach für Aluminiumzylinderköpfe in der Serie bewährt,” *Giesserei-Rundschau*, vol. 52, no. 7/8, pp. 170–173, 2005.
- [169] G. Schindelbacher, H. Kerber, M. Riegler, and M. Berbic, “Umfassende Charakterisierung von Formstoffen mit einer neuen Prüfmethode,” *Giesserei-Rundschau*, vol. 60, no. 3/4, pp. 58–66, 2013.
- [170] H. Kerber, M. Riegler, G. Schindelbacher, and P. Schumacher, “New possibilities with improved green sand testing facilities,” in *54th International Foundry Conference*, 2014, p. 10.
- [171] B. J. Stauder, H. Kerber, and P. Schumacher, “Foundry sand core property assessment by 3-point bending test evaluation,” *Journal of Materials Processing Technology*, vol. 237, pp. 188–196, Nov. 2016.
- [172] B. J. Stauder, M. Berbic, and P. Schumacher, “Mechanische Eigenschaften von Sandkernen nach thermischer Beanspruchung mit und ohne Luftaustausch,” 2017.
- [173] D. Gruber, “Miniaturized wedge split test specimen.” Personal communication, Montanuniversität Leoben, 2017.
- [174] P. Wurm, “Erfassen der Entkernbarkeit bei anorganischen Kernen,” Bachelorarbeit, FH OÖ - Wels, 2016.
- [175] B. J. Stauder, H. Harmuth, and P. Schumacher, “De-agglomeration rate of silicate bonded sand cores during core removal,” *Journal of Materials Processing Technology*, vol. 252, pp. 652–658, 2018.
- [176] B. J. Stauder, D. Gruber, and P. Schumacher, “Specific fracture energy and de-agglomeration rate of silicate-bonded foundry sand cores,” *Production Engineering*, p. 10, 2018.
- [177] B. J. Stauder, P. Schumacher, and H. Harmuth, “Core removal behaviour of silicate bonded foundry sand cores,” in *International Conference on Frontiers in Materials Processing, Applications, Research & Technology - FIMPART'17*, 2017, p. 6.

9 Appendices

9.1 Abbreviations

Abbreviation	Full text
3D	Three Dimensional
AFS	American Foundrymen Society
ASM	American Society for Metallurgy
AWB	Anorganisches Warm Box Verfahren
BS	British Standards
BCC	Body Cube Centred
BET	Brunauer–Emmett–Teller gas adsorption measurement method
CB	Coldbox
CN	Coordination Number
CSF	Corey’s Shape Factor
CTE	Coefficient of Thermal Expansion
CPS®	Core Package System
DEM	Discrete Element Method
DMEA	Di-Methyl-Ethyl-Amine
DTA	Differential Thermal Analysis
DTG	Differential Thermo Gravimetry
EK	Eckigkeitskoeffizient
FCC	Face Cube Centred

FE	Finite Element
FNB	Furan No-bake
GIFA	Gießerei-Fachausstellung / Fair on Foundry Technology
HB	Hotbox
HPDC	High pressure die casting
ISO	International Standardisation Organisation
NMR	Nuclear Magnetic Resonance
OGI	Austrian Foundry Research Institute; “Österreichisches Gießerei-Institut”
PP	Poly-Propylene
PU	Poly-Urethane
SEM	Scanning Electron Microscope
SPM	Semi-Permanent-Mould
TA	Thermal Analysis
TG	Thermo-gravimetry
WB	Warmbox
WST	Wedge Splitting Tests

9.2 List of Figures

- Figure 1-1: Material flow of metal and sand core at the production process chain of cast-Al cylinder heads. - 1 -
- Figure 1-2 (a): Example of a sand core package to shape complex internal cavities of a car engine cylinder head prepared to be placed in a steel mould. (b): Cylinder head with cast-in sand cores during hammering for core removal (Nemak, 2005). - 2 -
- Figure 1-3: Examples of state-of-the-art mechanical core removal equipment applied for cast-Al parts. (a): Pneumatic hammer [20]; (b): Hammering station with a clamped casting containing sand cores, as exhibited on the ‘GIFA’ 2015 fair [22]; (c): Vibration shake-out unit with clamped cylinder heads [23]. - 3 -
- Figure 1-4: Picture sequence taken in 10 minute-steps starting after casting extraction from the mould (Picture 1) showing increasing, shell-wise core destruction with increasing time (Pictures 2-4) and the resulting channel after approximately 50 minutes from de-moulding..... - 4 -
- Figure 2-1: Factors influencing the achievable sand core strength in general, after Flemming & Tilch (1993), [5]. The inserts are showing inorganically bonded car-engine cylinder head sand cores at different magnifications, illustrating the granular nature of the solid core. - 6 -
- Figure 2-2: Sand core fracture surface illustrating the grains and the bonding binder patches. Silica sand and a urea-furanic based, Warmbox bonded resin were used. The sample was taken from a cast-in sand core [34]. - 7 -
- Figure 2-3 left: Cross section through a core blowing machine [40]. Right: Core blowing simulation result showing the sand volume fraction during the sand transport through the blowing nozzles on top into the core box cavity [37]. - 8 -
- Figure 2-4: DEM-simulated cylindrical body built from a granulate with uniform spherical particle size distribution ranging from 1,15 to 2,71 mm particle radius and the evaluated coordination number distribution according to [44]. Mean coordination number is 8,2..... - 10 -
- Figure 2-5: Comparison of the free expansion of non-siliceous refractory sands with high silica sand [53, Ch. 8]. In addition, a typical average thermal expansion of cast aluminium alloys of $24 \cdot 10^{-6} \text{ K}^{-1}$ is indicated ‘Al-av. CTE’..... - 11 -
- Figure 2-6: Example for applied particle shape terminology modified after *Barrett, 1980*, acc. to [57]. The particle roughness is schematically shown as magnified property, which demonstrates the potential to apply a fractal description concept..... - 14 -

- Figure 2-7: Examples for foundry base forming materials with different roundness [34]. Min-sand is a spherically shaped due to spray compaction process, silica sand H32 is sub-angular rounded, due to its natural source and andalusite is faceted due to the crushing process for sand generation..... - 14 -
- Figure 2-8: Visual grain shape classification by sphericity and angularity of individual grains [50, Ch. 12]. Sphericity is defined by the ratio of maximum to minimum projected diameter and angularity is evaluated by visual examination with low magnification microscopy in comparison to reference charts. - 15 -
- Figure 2-9: Different surface qualities of silica sands [5]. Left: sand grain with smooth surface; Right: rough and fissured sand grain surface in more detail. - 15 -
- Figure 2-10: Temperature indications for a gravity cast Al-cylinder head at the end of filling. (a): Casting with filling system and feeder. (b): Cross section through the casting centre plane. (c): Water jacket core positioned in the lower casting section at the end of filling [64]. - 17 -
- Figure 2-11: Thermal diffusivity of different granulates bonded with PU-Coldbox binder, evaluated from Brinschwitz (2005). Sand denominations are according to Table 2-5. Mineral types of additional abbreviations: J-Sand: quartz-feldspar; LD 30, LD 50 and ID 40 are sintered aluminosilicates; M-sand is molten mullite [62]. - 18 -
- Figure 2-12: Thermal conductivity of several granular materials over temperature, evaluated by the stationary heated wire and tube - method [62]. - 19 -
- Figure 2-13: Specific true heat capacity over the temperature for a heating and cooling cycle of a clay bonded moulding sand, used for casting simulation [68]. Latent heat of evaporation at the heating cycle and a lower specific heat for the cooling cycle due to occurred irreversible effects are incorporated. - 20 -
- Figure 2-14: Dilatometer study (sample 50 mm length) with different amounts of a fine and a coarse grain type [69]. Samples G1-G4 are illustrated on the left hand picture and the dilatometer results are shown in the graph at the right hand side. - 22 -
- Figure 2-15: Thermal expansion of high purity silica sand samples (HSSA: sub-angular; HSR: rounded) with PUCB binder (a), FNB – Furan No-bake (b) and waterglass-CO₂-hardened – sodium silicate (c) [71]. Note relevant temperatures in °C converted from °F are: 246 °C – 500 °F; 300 °C – 512 °F; 523 °C – 1000 °F; 573 °C – 1064 °F; 600 °C – 1112 °F; 1079 °C – 2000 °F. - 23 -

Figure 2-16: Evaluated heating time of sand spheres with PU-CB and furan no-bake hardened silica sand samples until the quartz transformation temperature, when immersed in 660 °C molten Al as function of the radius [73].	- 24 -
Figure 2-17: Schematic view of organic binder decomposition depending on local temperature and the core wall thickness for iron- and aluminium-based castings, redrawn from Bindernagel (1983)-fig.39, [51, Ch. 3].	- 26 -
Figure 2-18: PU no-bake cold-box process – general reaction equation [81].	- 27 -
Figure 2-19: DTG analysis of a PU-Coldbox bonded sand core (with 150 °C/min), [81].	- 27 -
Figure 2-20 (a): DTG analysis of PU-bonded core samples. (b) Thermal analysis of the same sample types. All measurements were executed with different heating rates, according to [82].	- 28 -
Figure 2-21: Polymerization of furfuryl alcohol monomers triggered by acid environment. A furan resin and water are formed, under generation of heat [78].	- 29 -
Figure 2-22: Thermogravimetric (TG and DTG) analysis of a furanic bonded moulding material in oxygen-free atmosphere (Ar) and on oxygen (air), acquired with 10 °Cs ⁻¹ . Redrawn from Lucarz (2014), [85].	- 29 -
Figure 2-23: Distribution after 1000 s of a cylinder geometry cast in Aluminium, with the radius (horizontal axis) and the height indicated in mm. <i>Left</i> : temperature in °C, <i>Centre</i> : local rate of hazardous products generated in weight portion w_g of the total amount w_{tot} and <i>Right</i> : simulated hazardous product concentration c_g in kg of gas per kg of sand around a cast cylinder specimen ($x=r$; $y=height$) within a printed mould [87].	- 30 -
Figure 2-24: Phase diagram SiO ₂ -Na ₂ O from 40 to 100 % SiO ₂ -content, from [19]. Technically applied water glass binders are within a range of 66 to 77 % SiO ₂ -content, which is corresponding to a molar SiO ₂ /Na ₂ O-ratio of 2 to 3,5.	- 32 -
Figure 2-25: Secondary bending strength of sodium silicate bonded core samples after thermal exposure. I: primary maximum; II: secondary maximum; III: secondary minimum; A: light metal castings; B: copper based; C: Cast iron; D: Steel. [5]	- 32 -
Figure 2-26: Influence of silicate modulus and binder amount in the mixture on bending strength of cores hardened by Hot-Box process (210°C, 70 sec.), [99].	- 34 -
Figure 2-27: Test results for samples with Cordis binder [100].	- 35 -
Figure 2-28: Comparison of modified (designated M1, C1, C2) and unmodified (designated N1, N2) silicate binders. Sand core retained strength [27]. Organic additives can enhance core breakdown. Inorganic additives are preferred from an ecological point of view.	- 37 -

Figure 2-29: Cyclic loading and unloading during compression test of a PU-CB bonded sample in steps of 50 μm compression deformation [108].....	- 38 -
Figure 2-30: Hot distortion tests of silica (QS) and Cerabeads (Ce) samples bonded with a) Resol-CO ₂ ; b) shell moulding material and c) PU-Coldbox [52]. x-axis: time in s and y-axis: dilatation in mm.	- 39 -
Figure 2-31: Sand core specimens after dipping in melt (left) and carefully released from the aluminium-skin before weighing (right), [115].....	- 40 -
Figure 2-32: Results for absorbed heat rate from dipping trials into Al-melt of 660 °C. Spherical sand cores with diameters 40, 50 and 60 mm bonded with PU-Coldbox (left) and a furan no-bake system (right) were compared [73].	- 40 -
Figure 2-33: Testing device to evaluate knock-out work type LUW-C1 [116]. 1: falling mass; 2: ramming geometry; 3: test core; 4: test casting; 5: sample holder.	- 41 -
Figure 2-34: Falling mass for knock out testing device according to a polish norm [117].	- 41 -
Figure 2-35: Test parts of cast-in dog bone tensile samples (1 square-inch cross-section) with chaplet support to hold constant wall thickness around the sample, gating and feeder system indicated (left) and disk test part with a mould drawing for sample production (right), [119].	- 42 -
Figure 2-36 left: A cut test specimen after initial hammering, showing the fractured core [122]. Right: shake-out tests system with hammer and an in-line scale for sand collection [124].	- 42 -
Figure 2-37: Particle fracturing model in initial state (upper left) and after being pressurized (upper right) with indicated breakage ratio 'B', respectively increment ' δ_B '. Right: Particle size distribution function during comminution process of particle agglomerates are moving towards an ultimate distribution. B_t is the breakage fraction at time t and B_p is the breakage potential of a particle mixture, leading to the ultimate distribution F_u , where B is equal to unity [128].	- 44 -
Figure 2-38: Comparison of Mohr-Coulomb versus the Hoek-Brown criterion [134].	- 45 -
Figure 2-39: Tomography across a compression test sample showing a clear shear plane leading to failure. Sample dimensions are diameter 30 mm and height 45 mm. Loading direction was vertical [108]	- 46 -
Figure 2-40: Schematic diagrams (a): tri-axial test system and (b): direct shear test system [136]. ..	- 47 -
Figure 2-41: Modified shear test [137]. FE-models of applied geometries with 60° and 80° notch angle, indicating the van-Mises stress field under compression load.	- 47 -

- Figure 2-42: Schematic representation of the wedge splitting test (a) and a typical load/displacement curve (b), [144]. F_V : vertical load; F_H : horizontal load; a_0 : initial notch depth; ZOI: zone of interest; G_f' : specific work of fracture. - 48 -
- Figure 2-43: A schematic representation of cracking regimes with the ratio of particle-matrix strength related to the particle strength over the matrix volume [147]. - 49 -
- Figure 2-44: Diminution of a ball depending on the loading intensity, scheme according to Schubert (2003), [127]. Elastic-plastic and elastic-brittle fracture lead to different typical grain size distributions, also depending on the loading intensity [150]. - 49 -
- Figure 2-45: Principal illustration of the granulate grain size distribution change due to abrasion and fracture of the test body. The particle size of an initial body, after abrasion, an elastic-plastic and an elastic-brittle fracture is indicated [150]. - 49 -
- Figure 2-46: Illustration of a primary particle de-bonding and fracture of a bonded agglomerated body after multiple loading [150, Fig. 6.53] - 50 -
- Figure 3-1: Cumulative grain size distribution arriving at a sieve of the indicated lower mesh size for the basic forming materials silica H32, Cerabeads 650 and Kerphalite. Kerphalite exhibits a high fines content of 10 % passing the 90 μm mesh. Average grain size is in the range from 125 – 200 μm . Upper grain size is limited by 0,5 mm. - 52 -
- Figure 3-2: Core blowing machine of the type Röper H5 situated at the ÖGI in Leoben. (1) is a core box mounted on the machine table, (2) the gassing unit for Coldbox production and (3) a hydraulic unit for tool clamping. - 53 -
- Figure 3-3: (a) shows the core box used for cylindrical samples and (b) the core box for bending test bars mounted on the core blowing machine [167]. - 53 -
- Figure 3-4: Sand core used for the upper part of a cylinder head casting with six analysed measurement positions, denominated with “In” for inner and “Out” for outer regions and “-fine” for thin and “-thick” for thick core sections (a) and the evaluated temperature profiles from the local virtual thermo-couples (b), based upon casting process simulation. - 54 -
- Figure 3-5: Temperature profiles applied for the sand core tempering measured in test cores [167]. - 55 -
- Figure 3-6: Thermal pre-conditioning of bending test samples. (a): oxidizing condition, (b): preparation of sealed samples for reducing condition and (c): prepared treatment batch for reducing condition with samples embedded in pre-heated sand; [167]. - 55 -
- Figure 3-7: Test types applied for mechanical property assessment [167]. - 56 -

- Figure 3-8 left: 3D design of the wedge split test sample core box in top view. On top of this tool is the blowing plate, which is part of the core blowing machine. Right: Sand core sample for wedge split testing. - 57 -
- Figure 3-9: Drawing for miniaturized wedge split test specimen [173] and a first realized test core. - 57 -
- Figure 3-10: (a): Test core main dimensions. The asymmetric core print allows wall thickness variation in the mould by rotation of the core. The increase of width and core thickness along the core height is 14 mm. - 58 -
- Figure 3-11: The core box for the core removal test cores with opened side parts (left) and a therewith realized sand core (right)..... - 59 -
- Figure 3-12 left: Schematic cross section through the mould setup consisting of (1) a base plate, (2) a core, and (3) the upper mould part. The casting is formed in the cavity (4). The thermocouple positions are: T_M in the mould, T_C in the core centre, and T_F in the feeder centre. Right: Casting of a test part..... - 59 -
- Figure 3-13: temperature curves of the cast in cores and the feeder temperatures with the cooling methods on air, in water and insulated (without core temperature), starting 100 s after pouring start. The simple wedge shaped cast part is shown to the right hand side. - 60 -
- Figure 3-14: Top view on test casting clamped in the sliding sample holder with attached vibration measurement sensors [174]. The sample holder guidance and the base grid of the vibration device can be seen, also. - 61 -
- Figure 3-15: Schematic description of the pneumatic hammer used for core removal [174]. The PP-sample holder and upper part of test casting are put on the core removal station. Below the sample holder the sand collecting tray is positioned..... - 61 -
- Figure 3-16: Vertical acceleration measured on the sample positioned in the vibration device and in the hammer station including a rubber damping on the hammer head [174] measured over a period of 0,25 s..... - 62 -
- Figure 5-1: Bending test evaluation based on load curve evaluation (from section 4.1). - 125 -
- Figure 5-2: Results from three-point bending test evaluation based upon load curves. Load curves for PU-Coldbox (CB), urea-furanic hotbox (HB) and two furanic Warmbox binders (WB1 and WB2) after sample storage time of 0, 1, 4 and 24 hours are shown in (a). In (b) the bending strength and in (c) the elastic modulus of these cores are graphically shown..... - 126 -

- Figure 5-3: Testing of PU-Coldbox cores after 1 hour storage with three load velocities of: 0,5; 5 and 50 mm/min (presented at the 54th Int. Slovenian foundry conference in Portoroz). - 127 -
- Figure 5-4: Examples for core temperature evaluation from casting simulation to derive heating profiles and typical exposure time at certain temperature regimes from 200 – 500 °C. - 127 -
- Figure 5-5: Dwell time of simulated temperature measurement points in sand cores of a cylinder head casting model above their individually reached maximum temperature from 200 – 500 °C in 100 °C steps. - 128 -
- Figure 5-6: Bending strength over the elastic modulus for the core materials silica ‘Q’ and synthetic sintered mullite ‘M’. The exposure temperatures / °C, for sample pre-conditioning in air are indicated. - 129 -
- Figure 5-7: Mohr-Coulomb failure criterion function design of sand core samples after thermal exposure. - 130 -
- Figure 5-8: Comparison of Mohr-Coulomb criteria functions of samples tested without thermal exposure (left) and after 300 °C pre-conditioning (right). - 130 -
- Figure 5-9: Mechanical properties of waterglass bonded sand core samples after thermal exposure. Left: silica sand; right: synthetic sintered mullite. - 131 -
- Figure 5-10: Core samples before and after a wedge splitting test (left) schematically shown (centre) and the principle of load curve evaluation for relevant material parameters (right). - 132 -
- Figure 5-11: Characteristic length and specific fracture energy from wedge splitting tests of silicate bonded quartz (Q-WG) and mullite-based core samples (M-WG). The influence of thermal exposure at 300 °C compared to unconditioned samples is indicated by arrows..... - 132 -
- Figure 5-12: Overview about the determination of the de-agglomeration rate. (a) collected removed core sand; (b): de-agglomeration rate results for different sands (Q: silica; M: mullite) and conditions: non-cast hardened reference core samples at RT, 300 °C and 500 °C pre-conditioning and a cast-in sand core. - 133 -
- Figure 5-13: De-agglomeration rate of reference samples as function of the specific fracture energy and with indication of the characteristic length in /mm, which is an inverse measure for the brittleness (section 4.4). - 134 -
- Figure 5-14: Left: Temperature curve in core and casting cooled in ambient calm air. Right: Dilatometer measurements of silicate bonded quartz and synthetic mullite samples. Indicated milestones are the completed solidification (MS 1) and the peak temperature of the core (MS 2). - 134 -

9.3 List of tables

Table 2-1: Properties to evaluate technological applicability of basic forming materials [5].	- 7 -
Table 2-2: Coordination number for various regular packings of monodisperse spheres.	- 9 -
Table 2-3: A comparison of silica and non-silica sand properties [47].	- 11 -
Table 2-4: Typical UK and German foundry sands with sieve analysis [50, Ch. 12].	- 13 -
Table 2-5: Angularity coefficient, visually evaluated angularity and surface condition and water absorption of different granulates investigated by Brinschwitz (2005), [62]. The angularity coefficient is defined by the ratio between physically measured and theoretical specific surface calculated from grain size analysis.	- 16 -
Table 2-6: Averaged thermal expansion coefficients of forming materials for temperature ranges 20 to 300 / 20 to 600 and 20 to 800 °C [65].	- 21 -
Table 2-7: History of core and mould processes using synthetic resins as binders [77].	- 25 -
Table 2-8: Organic compounds generated as a result of selected temperature impact on furan resin [86]. Sand cores used for Al-castings show little portions exceeding 500 °C at casting. For them still a less complex de-composition product mix and incomplete degradation must be expected.	- 30 -
Table 3-1: Sand core sample mixtures applied for experiments.	- 51 -
Table 3-2: Hardening parameters for mechanical test core samples.	- 54 -
Table 3-3: Defined isothermal holding time for sand core sample thermal pre-conditioning.	- 55 -
Table 4-1: List of resulting publications from this thesis.	- 63 -
Table 5-1: Calculated unrestricted thermal strain for the phase from end of casting solidification until the maximum temperature of the core centre (MS 1 – MS 2) and during the cooling phase of the core until room temperature (MS 2 – RT). The differences between the casting and the cores (for every type) and the summed up total strain values are shown.	- 135 -